43461

NAME OF AUTHOR/NOM DE L'AUTEUR_____YAN KUI LAU

TITLE OF THESIS/TITRE DE LA THÈSE____STUDIES OF THERMAL ION-MOLECULE

____EQUILIBRIA — DETERMINATIONS OF GAS PHASE

____BASICITIES AND PROTON AFFINITIES BY HIGH
    PRESSURE MASS SPECTROMETRY

UNIVERSITY/UNIVERSITÉ____UNIVERSITY OF ALBERTA

DEGREE FOR WHICH THESIS WAS PRESENTED/
GRADE POUR LEQUEL CETTE THÈSE FUT PRÉSENTÉE____PH.D

YEAR THIS DEGREE CONFERRED/ANNÉE D'OBTENTION DE CE GRADE____1979

NAME OF SUPERVISOR/NOM DU DIRECTEUR DE THÈSE____PAUL KEBARLE

Permission is hereby granted to the NATIONAL LIBRARY OF CANADA to microfilm this thesis and to lend or sell copies of the film.

The author reserves other publication rights, and neither the thesis nor extensive extracts from it may be printed or otherwise reproduced without the author's written permission.

L'autorisation est, par la présente, accordée à la BIBLIOTHÈ-QUE NATIONALE DU CANADA de microfilmer cette thèse et de prêter ou de vendre des exemplaires du film.

L'auteur se réserve les autres droits de publication; ni la thèse ni de longs extraits de celle-ci ne doivent être imprimés ou autrement reproduits sans l'autorisation écrite de l'auteur.

DATED/DATÉ____Aug. 8 1979____SIGNED/SIGNÉ____Yan Kui Lau

PERMANENT ADDRESS/RÉSIDENCE FIXÉ____11626 - 89th Street

____Edmonton, Alberta T5B 3N2

NL-91 (3-74)

NOTICE

AVIS

THE UNIVERISTY OF ALBERTA

STUDIES OF THERMAL ION-MOLECULE EQUILIBRIA-DETERMINATIONS
OF GAS-PHASE BASICITIES AND PROTON AFFINITIES BY HIGH
PRESSURE MASS SPECTROMETRY

BY

© YAN KUI LAU

A THESIS

SUBMITTED TO THE FACULTY OF GRADUATE STUDIES AND RESEARCH
IN PARTIAL FULFILMENT OF THE REQUIREMENTS FOR THE DEGREE
OF
DOCTOR OF PHILOSOPHY

DEPARTMENT OF CHEMISTRY

EDMONTON, ALBERTA

FALL, 1979

THE UNIVERSITY OF ALBERTA

FACULTY OF GRADUATE STUDIES AND RESEARCH

The undersigned certify that they have read, and
recommend to the Faculty of Graduate Studies and
Research for acceptance, a thesis entitled

"STUDIES OF THERMAL ION-MOLECULE EQUILIBRIA-DETER-
MINATIONS OF GAS-PHASE BASICITIES AND PROTON
AFFINITIES BY HIGH PRESSURE MASS SPECTROMETRY"

submitted by YAN KUI LAU in partial fulfilment of
the requirements for the degree of Doctor of
Philosophy.

....
Supervisor

....

........Byron Kratochvil........

....

....
External Examiner

Date........July 23, 1979........

TO LUC

A B S T R A C T

A pulsed electron beam, high-pressure-quadrupole mass spectrometer which was constructed for the study of ion-molecule equilibria is described. The mass spectrometer can be operated with ion source pressures up to 10 torr. The equilibrium constants for the proton transfer reactions: $B_1H^+ + B_2 = B_1 + B_2H^+$ involving some 50 bases B whose gas-phase basicities are between water and 1,8-bis-(dimethylamino)naphthalene were measured at 600°K. This allowed the evaluation of ΔG^o_{600} for the proton transfer reactions. A complete ladder of equilibria connecting these compounds was obtained. The temperature dependence of equilibrium constant was studied for two proton transfer reactions involving benzene and halobenzenes (fluoro- and chlorobenzene). The results showed that ΔS^o for proton transfer reactions can be estimated by considering the rotational symmetry numbers. The estimation of ΔS^o permitted the evaluation of ΔH^o from ΔG^o for proton transfer reactions. Using the external standard proton affinity, PA(isobutene) = 198.2 kcal/mole (Beauchamp, Tsang), the absolute proton affinities of different compounds were obtained. These include: water 171.7, benzene 185.4, methanol 186.2, acetone 198.6, ketene 199.2, benzoic acid 200.2, ammonia 207.6, DMSO 214.4, methylamine 217.3 and 1,8-bis(dimethylamino)naphthalene 245.1 kcal/mole.

The substituent effects on the intrinsic basicity of benzene were considered. It was observed that all mono-

substituted benzenes have proton affinities higher than that
of benzene. From the correlations of proton affinities with
Hammett type σ_p^+ substituent constants and STO-3G calculated
results, it is suggested that protonation for anisole, phen-
ol, ethylbenzene, toluene, fluoro- and chlorobenzene occurs
at the ring. Substituent protonation is energetically more
favorable for acetophenone, benzaldehyde, benzoic acid,
benzonitrile and nitrobenzene. The proton affinity for N-
protonated aniline is very close to that for ring protona-
tion.

The gas-phase basicities of N-methyl substituted 1,8-
diaminonaphthalenes and several related compounds were
studied. The results indicated that ring protonation
yields more stable ion for 1-aminonaphthalene and m-phenyl-
enediamine than N-protonation. All 1,8-diaminonaphthalenes
are N-protonated. N-methyl substitution enhances the
basicity of 1,8-diaminonaphthalene, but strong attenuation
of the effects was observed in solution except for the fully
N-methylated base. The high gas-phase basicity of 1,8-bis-
(dimethylamino)naphthalene obtained in the present study is
in agreement with the suggested explanation for its high
aqueous basicity, namely, the effective removal of steric
strain in the neutral base on protonation.

The solvation of the proton by dimethyl sulfoxide mole-
cules: $H^+(DMSO)_{n-1} + DMSO = H^+(DMSO)_n$, was studied for n =
2,3. The (n-1,n) interactions for DMSO were compared with
those for water and dimethyl ether. The results showed that

the ion-dipolar interactions in $H^+(DMSO)_3$ is as strong as hydrogen bonding in the stabilization of the $H^+(H_2O)_3$ cluster.

ACKNOWLEDGEMENTS

TABLE OF CONTENTS

ix

xiv

xv

LIST OF FIGURES

xviii

xix

CHAPTER I

INTRODUCTION

1.1 The Present Work

The present work is directed toward the determination of gas-phase basicities of various organic compounds such as benzenes, alcohols and amines. In the latter part of the study, the clustering of dimethyl sulfoxide molecules around the proton in the gas phase is also being examined.

The study of gas-phase basicities is a continuation of work performed in this laboratory (1-3). The classical acid-base thermodynamics studied in solution is always complicated by the presence of the solvent. As a result, the energy involved in a reaction is always composed of solvation terms and internal energy terms. In order to study the effect of structural changes on reactivity, one must be able to eliminate the solvation effects. The gas-phase study is most desirable for this purpose because a given reaction can be examined without solvent interferences. An understanding of structural effects on the intrinsic basicity of molecules enables the evaluation of the role of solvation terms in solution chemistry. In this work it was also intended to examine enough compounds of a wide range of basic strength so that a comprehensive scale of relative gas-phase basicities can be constructed from water to compounds with as high basic strength as possible.

1

The gas-phase basicities are obtained from studies of ion-molecule reaction equilibria. The studies are made with mass spectrometers, specially designed for ion-molecule reaction studies.

1.2 Development of Ion-Molecule Reaction Studies

Since ion-molecule reactions are observed with mass spectrometers, there has been an intimate relationship between the development of ion-molecule reaction studies and mass spectrometry. Early in 1912, J. J. Thompson (4) reported the observation of ions of m/e = 3 in experiments with H_2 in the cathode-ray-tube apparatus. The observation was later confirmed by Dempster who correctly identified the ion as H_3^+ (5). The ion-molecule reaction that leads to the formation of H_3^+ was established subsequently as reaction 1.1 (6,7). After Thompson, the

$$H_2^+ + H_2 \longrightarrow H_3^+ + H \qquad (1.1)$$
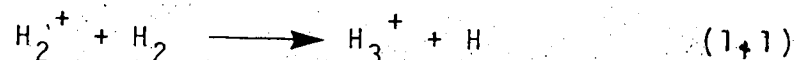
development of mass spectrometry was directed toward determinations of isotopic abundances and later on toward determinations of ionization potentials, appearance potentials and bond dissociation energies. For these purposes, the occurrence of reactions between primary ions and neutral molecules were undesirable. Therefore, conventional mass spectrometers were designed in such a way that the operating ion source pressure is as low

as possible so that collisions between primary ions and neutral molecules do not occur. With the advances in vacuum technology, conventional mass spectrometers can easily be operated at a pressure below 10^{-5} torr where the interference by ion-molecule reactions is eliminated.

Interest in ion-molecule reactions was rekindled in the early 1950's by radiation chemistry. Elementary reactions between ions and molecules are generally an important component in the reaction mechanisms occurring in irradiated systems. Early systematic studies of ion-molecule reactions by Stevenson and Schissler (8,9), Tal'roze and Lyubimova (10) and Field, Franklin and Lampe (11,12) were carried out with conventional mass spectrometers in which the ion source pressure was raised to the range $10^{-4} - 10^{-3}$ torr. A schematic of the experimental arrangement is shown in Figure 1.1. A repeller voltage of about 1-10 volt was used to push the ion out of the ion source and into the mass analyser section of the instrument. Under these conditions a small fraction of primary ions P^+ formed by electron impact would collide with neutral molecules M, and undergo ion-molecule reaction 1.2 on their way out of the ion

$$P^+ + M \longrightarrow S^+ + N \qquad (1.2)$$
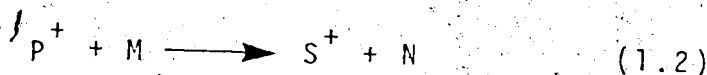
source. The intensities of the primary ions P^+ and the secondary ions follow the relationship 1.3 (8,9), where I_p and I_s are the intensities of the primary and second-

gas
inlet

Repeller

Focus
Plates

Ion source

Electron
trap

Electron
Filament

ℓ

E_R

electron
beam

Ion
accelerating
electrodes

Ion path

Magnetic
field

Ion
detector
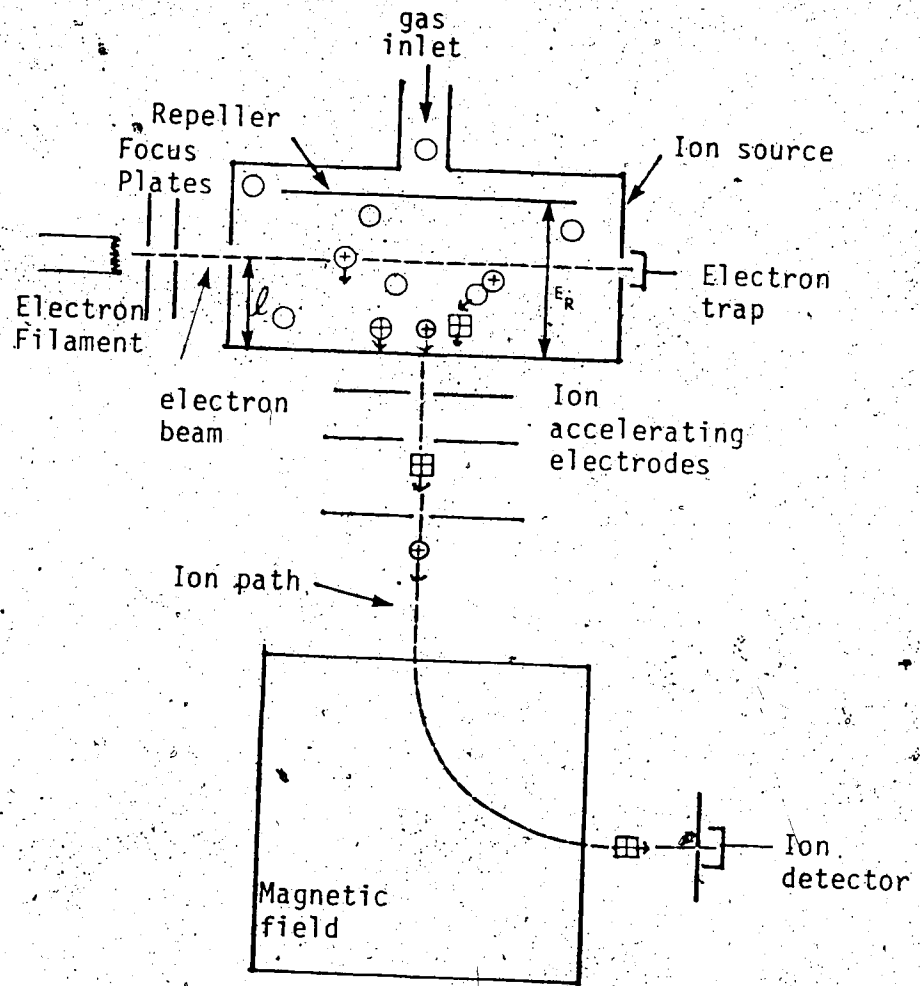
○ — gas molecule

⊕ — primary ion

⊞ — secondary ion

ℓ — path length for
primary ions

E_R — repeller voltage

FIGURE 1.1   Schematic Diagram of a Mass Spectrometer

$$I_s = I_p Q \ell n \qquad (1.3)$$

ary ions, Q is the cross-section of the ion-molecule re-
action, ℓ is the path length of the primary ion (see
Figure 1.1) and n is the number density of the neutral
molecule in the ion source. Stevenson and Schissler (8,9)
studied the cross-sections for several ion-molecule re-
actions. They observed that the reaction cross-sections
for many exothermic ion-molecule reactions are about 100
times larger than those of the fastest neutral reactions,
which are the free radical recombination reactions.
Gioumousis and Stevenson (13) were able to derive equa-
tions relating to the cross-sections observed in the ion
source of Figure 1.1 where the ion is continuously accel-
erated by the repeller field. They were also able to
derive an expression for the reaction rate constants of
thermal ions reacting with thermal molecules. The treat-
ment depended on an earlier equation by Langevin which
gave the trajectory of an ion attracted to a molecule by
the ion induced-dipole on the molecule. Gioumousis and
Stevenson (13) assumed that all trajectories which lead
to orbiting of the ion-molecule pair, lead to reaction.
For a given relative velocity v between the ion-molecule
pair, all trajectories which bring the ion and the
molecule within less than a critical distance b_0, lead to
orbiting. The expression 1.4 was obtained by Stevenson

and Gioumousis for the orbiting cross-section $Q_c = \pi b_o^2$, where q is the electronic charge, α the polarizability of the molecule and μ the reduced mass of the ion-molecule pair. Since the experiments were carried out under an

$$Q_c(v) = \frac{2\pi q}{v}\left(\frac{\alpha}{\mu}\right)^{\frac{1}{2}} \tag{1.4}$$

electric field (see Figure 1.1), the variable velocities of ions due to the repeller field had to be taken into account. The neutrals were taken to have Maxwell velocity distribution. The treatment led to the expression 1.5, where Q_c is the phenomenological i.e. observed, cross-

$$Q_c = 2\pi q\left(\frac{\alpha}{\mu}\right)^{\frac{1}{2}}\left(\frac{2m_p}{qE_r \ell}\right)^{\frac{1}{2}} \tag{1.5}$$

section, m_p is the mass of the ion, E_r is the voltage of the repeller and ℓ is the path length of the primary ion. Equation 1.5 was found to be in good agreement with several experimentally measured Q_{expt} observed for simple and exothermic ion-molecule reactions. Maintaining the assumption that orbiting leads to reaction, Gioumousis and Stevenson (13) also derived an expression for the thermal rate constant for ion-molecule reactions where both ions and molecules move with thermal (Maxwell) velocities. The expression is given in equation 1.6.

$$k_c(\text{thermal}) = 2\pi q\left(\frac{\alpha}{\mu}\right)^{\frac{1}{2}} \tag{1.6}$$

Introducing α and μ for various ion-molecule pairs, $k_c(\text{thermal})$ is generally found to be in the vicinity of

10^{-9} cm^3 molecule^{-1} sec^{-1}. By comparing equations 1.6 and 1.5, k_c may be evaluated from the Q_{expt}, determined experimentally under the presence of a repeller field, by assuming $Q_{expt} = Q_c$. This resulting relationship is given in equation 1.7. The validity of equation 1.7 depends on the

$$k_c(thermal) = (\frac{qE_r\ell}{2m_p})^{\frac{1}{2}} Q_c$$

$$= (\frac{qE_r\ell}{2m_p})^{\frac{1}{2}} Q_{expt}$$

(1.7)

assumption $Q_{expt} = Q_c$, which implies that $Q_{expt} \propto E_r^{\frac{1}{2}}$. However, many ion-molecule reactions were observed in which the relationship $Q_{expt} \propto E_r^{\frac{1}{2}}$ was not followed.

A pulsing technique was introduced by Tal'roze (14,15) which allows a direct measurement of thermal rate constants for ion-molecule reactions. In this method, ions are formed by allowing electrons to pass into the ionization chamber for a very brief period of time ($\sim 10^{-7}$ sec). After cutting off the electron beam, the ion source is maintained at equipotential conditions from zero to several microseconds. A short pulse is then applied to extract ions from the ion source. The rate constant of an ion-molecule reaction can therefore be evaluated in a conventional way by measuring the change of the ion intensity with time. Tal'roze (14) showed that under the conditions of constant electron pulse width and constant repeller pulse width, the rate constant k of an ion-molecule reaction may be evaluated

from the measured ratio of secondary and primary ion intensities (I_s/I_p) with the use of equation 1.8. n is the

$$I_s/I_p = nkt + \text{constant} \qquad (1.8)$$

number density of the neutral under reaction and t is the time period during which ions are at equipotential conditions. Equation 1.8 is equivalent to the second-order rate equation $\Delta I/\Delta t = kIn$, where $\Delta I = I_s$ and $I = I_p$. The constant in equation 1.8 is a correction for the fact that the reaction is also taking place during the electron pulse and the repeller pulse. The technique has since been used by many other workers notably Futrell et al. (16,17) and Harrison et al. (18) to measure rate constants of ion-molecule reactions at thermal energies.

The use of conventional low pressure mass spectrometers places limitations on the types of ion-molecule reactions that can be studied. Even with a pressure of 10^{-3} to 10^{-4} torr in the ion source, only a small fraction of the primary ions may be expected to undergo collision with neutrals in the ion source. The short ion-residence time together with the low pressure limits the observations to only second-order ion-molecule reactions with large rate constants. Field (19) circumvented the problem by increasing the ion source pressure to enhance the ion-molecule collision frequency. By narrowing down the ion source exit slit and installing better differential pumping

system, Field and coworkers (19-21) were able to study higher kinetic order ion-molecule reactions at an ion source pressure of 0.1 - 2 torr while still maintaining a pressure of about 10^{-4} torr outside the ion source. Low pressure outside the ion source is essential in mass spectrometric studies for minimizing collisions between ions and neutrals in passing through the mass analysing section of the instrument. By operating at higher ion source pressure, the residence time of ions is much longer because the diffusion of ions to the wall is slowed down by an increased number of collisions with neutral molecules. The rate of the reaction is also faster because of the increased concentration of the reacting neutrals. With the progress in the design of instruments, high pressure mass spectrometers could be constructed to operate at ion source pressures of up to 1 atmosphere (22).

The first ion-molecule reactions studied under the high pressure condition were those of methane. The following major reactions were observed by Field, Franklin and Munson (20):

Primary ions formation:

$$CH_4 + e \longrightarrow CH_4^+, CH_3^+, CH_2^+, CH^+, C^+, H_2^+, H^+ \quad (1.9)$$

Major ion-molecule reactions:

$$CH_4^+ + CH_4 \longrightarrow CH_5^+ + CH_3 \quad (1.10)$$

$$CH_3^+ + CH_4 \longrightarrow C_2H_5^+ + H_2 \quad (1.11)$$
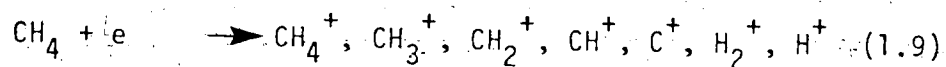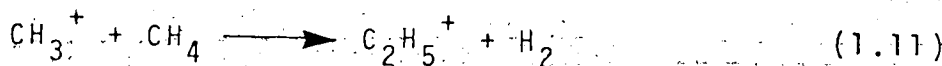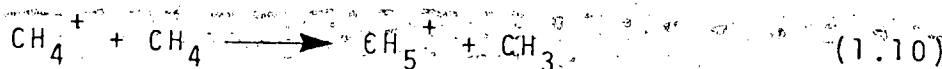
These authors (20) also observed that the relative abundance of the major product ions, CH_5^+ and $C_2H_5^+$, did not change at ion source pressures above 0.2 torr. They concluded that these ions are inert to further reactions with methane. Further experiments on the study of ion-molecule reactions of methane with a trace of additive (e.g. ethane or propane) under high ion source pressures showed that CH_5^+ and $C_2H_5^+$ react rapidly with the additive (23). The formation of resulting ions by ion-molecule reactions is called chemical ionization. The results from these studies led to the development of chemical ionization mass spectrometry (24-26).

A modification of the chemical ionization tehcnique has to be made for the study of thermal ion-molecule reactions. This is the removal of the repeller voltage from the ion source. One obtains in this manner field-free conditions, where the energies of the ions should depend solely on the temperature of the ion source. If the reactant ions are not excited when they enter into reactive collisions with neutrals, the reactions are truly thermal. With sufficiently high pressure and long ion-retention time in the ion source, it is possible to observe the thermal equilibrium for certain ion-molecule reactions and to determine the thermal equilibrium constants. Following the development of high pressure mass spectrometry, other methods like ion cyclotron resonance

and flowing afterglow method were also developed for the study of thermal ion-molecule reactions and thermal ion equilibria. These will be described in the next section.

1.3 Types of Apparatus Used for Thermal Ion Equilibria Measurements.

Several criteria must be met for thermal ion-molecule equilibria measurements. First, the reactants and products must be in thermal equilibrium with the surroundings. Excess energies present in the reactants and products have to be removed prior to the occurrence of the equilibrium reaction. Therefore, the reaction chamber should be at equipotential conditions. Secondly, sufficient residence time must be allowed for the system to reach equilibrium. Thirdly, the forward and backward interconverting rates at equilibrium must be faster than other competitive reactions, if any, involving the ionic reactants and products.

Three types of instruments are currently actively in use in the study of ion-molecule equilibria. These are the high pressure mass spectrometer with a pulse electron beam; the low pressure pulsed electron beam ion cyclotron resonance spectrometer and the flowing after-glow apparatus.

A. The Pulsed High Pressure Mass Spectrometry

This is the method used in the present study. A brief description of the method follows, a detailed description

of the apparatus and experimental procedures will be given in the following chapter. A suitable reaction mixture is allowed to flow in and out of the field-free ionization chamber which is maintained at a constant pressure of 1-10 torr. Ionization is achieved by irradiating the mixture with a short electron beam pulse ($\sim 10^{-5}$ sec/pulse). Ions that are formed in a pulse enter in reactions and may even reach an equilibrium as they diffuse in all directions. Some ions will diffuse toward the small ion exit slit (~ 0.015 mm x 1 mm) and escape to the evacuated region. They are then accelerated by an electric field to the mass analysing region and mass analysed. The variation of intensities of ions with time after the electron pulse is followed by collecting ion signals in a multichannel scaler. After the equilibrium is reached, the ratio of intensities of the reactant ion and the product ion will be constant with time since the concentrations of neutrals may be taken as constant throughout the reaction. By using a high inert gas to neutral reactant ratio ($\sim 100:1$), ion-thermalization would be achieved, since one may expect that the excess internal energy in an ion will be quenched by the ~ 100 collisions occurring with the inert gas before the ion enters in a reactive collision with the reactant molecule. The ion-residence time in the reaction chamber is in the millisecond range. This is a result of the absence of electric fields and the slowness of ion diffusion to the wall at the pressures employed. This method

has been used successfully in this laboratory for the last ten years. A similar pulsed apparatus was put into operation in Field's laboratory a few years ago (27).

B. The Low-Pressure, Trapped Ion, Pulsed Ion Cyclotron Resonance (ICR) Spectrometry.

The electron pulsing technique was employed by McIver (28) in the ion cyclotron resonance spectrometer developed earlier by Baldeschwieler (29). Since the ICR spectrometer can only be operated at low pressures where ion-molecule collisions are not too frequent, a trapped ion analyser is used. This lengthens the time that the ions spend in the cell. Ions are produced in a small rectangular cell by a short electron pulse ($\sim 10^{-4}$ sec). A typical gas pressure in the cell is around 10^{-6} torr. The movements of ions in the x and y directions of the cell are restricted by the presence of a magnetic field H which is in the z direction. The trapping of ions in the z direction is achieved by the presence of a small potential ($\sim 1 V$) on the side plates in the z direction of the cell. The ions with mass m and charge q circle in the xy plane with their cyclotron frequencies, $\omega = qH/mc$, where c is the speed of light. Ion-molecule collisions occur during the ion retention period. Detection of an ion is obtained by pulsing the magnetic field to make the cyclotron frequency of the ion of a given m/q equal to an applied marginal oscil-

lator frequency. The intensity of ions is determined by the energy absorption that can be detected in the marginal oscillator. The ions can be trapped in the cells for seconds. This time is often sufficient for the reaction system to reach equilibrium even at pressures in the 10^{-6} torr range. For fast ion-molecule reactions, studies using ICR spectrometers have the advantage that the ion concentrations are measured _in situ_. This eliminates the dependence on a sampling leak and removes problems with sampling discrimination that occurs with high pressure apparatus. On the other hand the ICR technique does not lend itself easily to measurements involving equilibria of very slow ion-molecule reactions such as third-order clustering reactions or hydride transfer reactions. The ICR spectrometric method has been used very successfully in studying ion equilibria of proton-transfer reactions by the groups of Aue, Bowers, Beauchamp, McIver and Taft (30,31).

C.   The Flowing Afterglow Method.

The flowing afterglow method was developed by Ferguson, Fehsenfeld and Schmeltekoff (32). In this technique, the reactor is a cylindrical tube of some 8 cm diameter. A carrier gas (usually He) flowing down the tube at a pressure of about 0.5 torr is ionized by a heated filament. Suitable reactant gas is admitted downstream from the excitation region through inlet nozzles. Helium ions or He metastables ionize some of the reactant gas molecules.

Further downstream of the tube, a second reactant gas whose reactions with the reactant ions are to be studied is admitted to the reactor. The reactions proceed over a distance of some 50 cm down the tube. At an elbow of the tube, the ions are sampled by bleeding a small part of the gas through a small leak into the evacuated region where mass analysis is obtained with a quadrupole mass spectrometer. The reaction time ($\sim 10^{-3}$ sec) depends on the distance between the entrance of the second gas and the exit orifice of the tube, and on the velocity of the gas flow. The reaction time and the rate constant can be calculated from the knowledge of the fluid dynamics of the flow. The equilibrium constants can be calculated from separate determinations of the forward and backward reaction rate constants. It is also possible to increase the reactants concentrations up to the point where equilibria are achieved within the reaction time and then measure the equilibrium ion concentration ratio directly. The flowing afterglow method is best noted for the determination of rate constants of bimolecular reactions. It appears that the study of ion equilibria is somewhat less convenient. One disadvantage of the method is the difficulty of changing the temperature of the fast flowing reaction system. This method has the advantage of being capable to study even reactions involving unstable neutrals such as reactive atoms. Bohme and his coworkers (33) have very

successfully used this technique to determine the rate con-
stants of a large number of proton transfer reactions. They
have also been able to measure the equilibrium constants of
several proton transfer reactions.

1.4 Ion-Molecule Reactions of Importance to Present Work

There are two types of ion-molecule reactions which
are of importance to the present work. They are proton
transfer and attachment reactions.

A. Proton Transfer Reactions

Proton transfer reactions are used for the determina-
tion of the gas-phase basicities of different compounds.
The proton affinity of a base B is defined as the enthalpy
change of reaction 1.12. Since the proton affinities of

$$BH^+ = B + H^+ \quad \Delta H = PA(B) \qquad (1.12)$$

ordinary bases are in the order of 100-250 kcal/mole and
the bond dissociation energies are only in the order of 100
kcal/mole, it is impossible to observe the thermal equilib-
rium of reaction 1.12 directly. Instead, the proton
transfer reaction 1.13 between two bases B_1 and B_2 must
be used to measure the relative proton affinities of bases
involved. The equilibrium constant of reaction 1.13 is
given by equation 1.14. The pressure ratio of the

$$B_1H^+ + B_2 = B_1 + B_2H^+ \qquad (1.13)$$
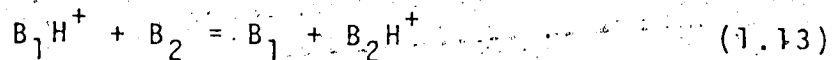
$$K = \frac{P_{B_1}}{P_{B_2}} \times \frac{P_{B_2H^+}}{P_{B_1H^+}} \qquad (1.14)$$

neutrals, P_{B_1}/P_{B_2}, is obtained from the known composition of the reaction mixture. In the experiments, the percentage of neutrals being converted to ions are negligibly small and the concentrations of neutrals remains constant throughout the reaction. The equilibrium concentration ratio of ions $P_{B_2H^+}/P_{B_1H^+}$ is measured with a high pressure mass spectrometer (see preceding section).

The standard free energy change ΔG^O of the reaction 1.13 is calculated from K using equation 1.15. The standard enthalpy change ΔH^O of the reaction may be obtained from the study of temperature dependence of the equilibrium constant. With the assumption that ΔH^O is essentially temperature-independent, equation 1.16 holds. Based on equation 1.16, a van't Hoff plot of ln K vs 1/T gives a

$$\Delta G^O = -RT \ln K \qquad (1.15)$$

$$\ln K = -\frac{\Delta H^O}{RT} + \text{constant} \qquad (1.16)$$

slope which is equal to $-\Delta H^O/R$. The enthalpy change of the reaction can also be calculated from the thermodynamic relationship 1.17. For the proton transfer reaction 1.13, the standard entropy change ΔS^O may be estimated by

$$\Delta G^O = \Delta H^O - T\Delta S^O \qquad (1.17)$$

assuming that the only contribution to ΔS^O is the

als, P_{B_1}/P_{B_2}, is obtained from the known composition of

reaction mixture. In the experiments, the percentage of

als being converted to ions are negligibly small and

concentrations of neutrals remains constant throughout

reaction. The equilibrium concentration ratio of ions

$/P_{B_1H^+}$ is measured with a high pressure mass spectro-

(see preceding section).

The standard free energy change ΔG^0 of the reaction

is calculated from K using equation 1.15. The stand-

nthalpy change ΔH^0 of the reaction may be obtained

the study of temperature dependence of the equilibrium

ant. With the assumption that ΔH^0 is essentially

rature-independent, equation 1.16 holds. Based on

ion 1.16, a van't Hoff plot of ln K vs 1/T gives a

$$\Delta G^0 = -RT \ln K \qquad (1.15)$$

$$\ln K = -\frac{\Delta H^0}{RT} + \text{constant} \qquad (1.16)$$

which is equal to $-\Delta H^0/R$. The enthalpy change of

eaction can also be calculated from the thermodynamic

ionship 1.17. For the proton transfer reaction 1.13,

tandard entropy change ΔS^0 may be estimated by

$$\Delta G^0 = \Delta H^0 - T\Delta S^0 \qquad (1.17)$$

ing that the only contribution to ΔS^0 is the

$$\Delta H^{O} = PA(B_1) - PA(B_2) \qquad\qquad (1.20)$$

exothermic, B_2 has a higher proton affinity than B_1. Proton transfer reactions in general are found to proceed at a very fast rate ($k \sim 10^{-9}$ cm^3 molecule^{-1} sec^{-1}) if the reaction is exothermic (33).

Before the introduction of the high pressure mass spectrometry, the study of ion equilibria was not possible and "bracketing technique" was used to qualitatively determine the order of basicities of various organic compounds. In this method (35), only the sign of ΔG^{O} for the proton transfer reaction 1.13 was measured. For example, from the observation that the proton transfer reactions 1.13 and 1.21 occurred in the mass spectrometer, it was assumed

$$B_1H^{+} + B_2 = B_1 + B_2H^{+} \qquad\qquad (1.13)$$

$$B_2H^{+} + B_3 = B_2 + B_3H^{+} \qquad\qquad (1.21)$$
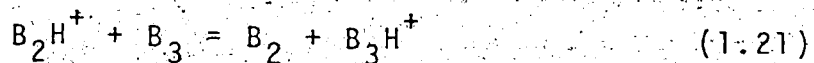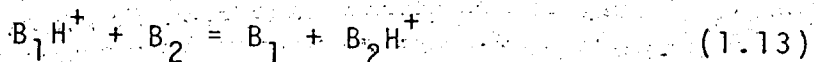
that $\Delta G^{O} \simeq \Delta H^{O} \leq 0$ for both reactions 1.13 and 1.20. This led to the conclusion that $PA(B_1) \leq PA(B_2) \leq PA(B_3)$.

The advances in experimental techniques enable one to observe the equilibria and to measure the equilibrium constants for the proton transfer reaction 1.13. This allows direct quantitative comparison of proton affinity values. The first report on the relative proton affinities from ion equilibria measurements was due to Bowers, Aue, Webb and McIver (36). Equilibrium constants for proton trans-

fer reactions involving amines were measured with the ion
cyclotron resonance spectrometer at room temperature.
Relative proton affinities accurate to ± 0.3 kcal/mole were
reported. Similar measurements were carried out at about
the same time by Kebarle and his coworkers in this laborat-
ory (1). A high pressure mass spectrometer was used to
measure the equilibrium constants of the proton transfer
reactions. Absolute proton affinities can be obtained
from the relative values if the proton affinity of at least
one of the bases has been determined by other methods.
The principles of these methods are discussed in a sub-
sequent section.

Since the introduction of proton transfer equilibria
measurements, proton affinity data have been accumulating at
an extremely rapid rate. The majority of the data were ob-
tained by one of the three types of apparatus described in
section 1.3. Bohme and his associates using the flowing
afterglow method have been mostly engaged in the determina-
tions of relative proton affinities of simple molecules such
as H_2 and O_2 (37), N_2, CO_2 and CH_4 (38,39), and the rare
gases (40). The groups of Aue, Bowers, Beauchamp, McIver and
Taft using an ion cyclotron resonance spectrometer (38) and
this laboratory (41) using high pressure mass spectrometers
are engaged in the determination of relative proton affinit-
ies of various organic compounds. The agreement in values is
not always within the precision ($\sim \pm 0.3$ kcal/mole) reported
by different groups, but it is surprisingly good consider-
ing the wide differences among different methods.

B. Attachment Reactions

Successive additions of neutral molecule B to an ion A^+ can be studied in the gas phase. These reactions are represented by equation 1.22. Attachment reactions in the

$$[A(B)_{n-1}]^+ + B = [A(B)_n]^+ \tag{1.22}$$
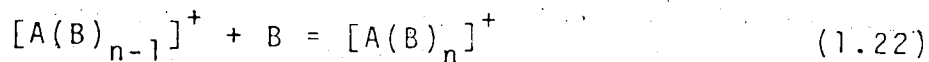
gas phase are usually third-order reactions as shown in equation 1.23 (42). Since the attachment reactions are

$$[A(B)_{n-1}]^+ + B + M \underset{k_b}{\overset{k_f}{\rightleftharpoons}} [A(B)_n]^+ + M \tag{1.23}$$
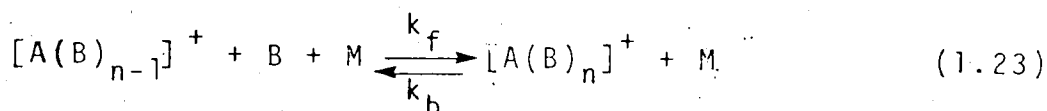
exothermic, a third body M is required to remove the excess energy and stabilize the initially excited association product, $[A(B)_n]^{+*}$. The forward reaction 1.23 can be written as reaction 1.24, where k_c and k_d are the rate

$$[A(B)_{n-1}]^+ + B \underset{k_d}{\overset{k_c}{\rightleftharpoons}} [A(B)_n]^{+*} \overset{k_s}{\underset{M}{\longrightarrow}} [A(B)_n]^+ \tag{1.24}$$
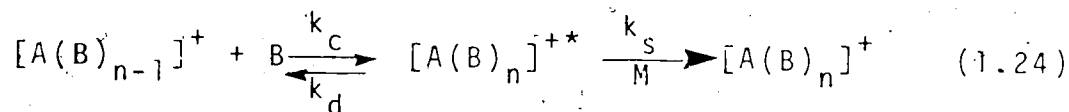
constants for the formation and the decomposition of the activated ion complex, respectively, and k_s is the rate constant for the stabilization of the activated intermediate by a third body M. The stable ion complex could be formed only if the lifetime of the activated intermediate is longer than the time required for the collisional stabilization, otherwise decomposition of the activated intermediate back to reactants would result. Applying the steady state assumption on the concentration of the activated intermediate, i.e. $\dfrac{[A(B)_n]^{+*}}{dt} = 0$, the overall

forward rate constant for reaction 1.24 is given by (43):

$$k_f = \frac{k_c k_s}{k_d + k_s[M]} \qquad (1.25)$$

Under the condition of low pressure of M ($< \sim 10$ torr) $k_d \gg k_s[M]$, the forward rate constant k_f may be simplified to the form given in 1.26. The typical magnitude of the

$$k_f = \frac{k_c k_s}{k_d} \qquad (1.26)$$

forward rate constant for attachment reactions is in the order of 10^{-26} to 10^{-29} cm^6 $molecule^{-2}$ sec^{-1} (44). The reverse reaction 1.23 is then a second-order reaction. The presence of the third-body activates the breaking up of the association cluster.

The thermochemical properties of the attachment or association reaction 1.22 can be studied through the determination of the equilibrium constant which is expressed in equation 1.27. The pressure of the neutral

$$[A(B)_{n-1}]^+ + B = [A(B)_n]^+ \qquad (1.22)$$
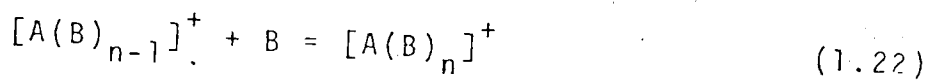
$$K = \frac{P_{[A(B)_n]^+}}{P_{[A(B)_{n-1}]^+}} \times \frac{1}{P_B} \qquad (1.27)$$

B is known from the composition of reactant gases. The equilibrium ion ratio is determined with the high pressure mass spectrometer. The equilibrium constant obtained can be used to calculate ΔG^0 of the reaction by the equation

$\Delta G^O = \Delta H^O - T\Delta S^O$. It is important to observe that the concentration of B should be expressed in the unit of atmospheric pressure so as to agree with the standard state for free energies. From the temperature dependent study of equilibrium constants, ΔH^O and ΔS^O may also be obtained through equations 1.16 and 1.17. Unlike proton transfer reactions, ΔS^O of an attachment reaction cannot be estimated by only considering the rotational entropy changes, contributions from translational and vibrational entropy changes must also be considered. Because the reaction involves a change in the number of molecules in going from reactants to products, the translational entropy changes are the major contribution to the ΔS^O for the attachment reactions.

Thermodynamic data obtained from the reaction 1.22 give intrinsic solvation energies for stepwise additions of molecule B to the ion.[a] This is useful in providing information on ion-molecule interactions involving single solvent molecules. Ion-solvation in solution involves ions that are not isolated from the bulk of solvent molecules. The interactions in the second case are much more difficult to unravel.

The solvation of the hydrogen ion by different molecules B as shown in reaction 1.27 have been studied

$$H^+(B)_{n-1} + B = H^+B_n \tag{1.27}$$

extensively in this laboratory (45-47). The solvation

energies for the reaction 1.27 with B = H_2O (n up to 8)
(45), B = NH_3 (n up to 5) (46), B = CH_3OH (n up to 8) (47)
and B = CH_3OCH_3 (n up to 3) (47) have been determined. The
importance of the hydrogen bonding in the ion-solvation
reactions has been shown by Kebarle and coworkers (47) by
comparing the following reactions:

$$H^+(H_2O)_{n-1} + H_2O = H^+(H_2O)_n \qquad (1.28)$$

$$H^+(CH_3OH)_{n-1} + CH_3OH = H^+(CH_3OH)_n \qquad (1.29)$$

$$H^+(CH_3OCH_3)_{n-1} + CH_3OCH_3 = H^+(CH_3OCH_3)_n \qquad (1.30)$$
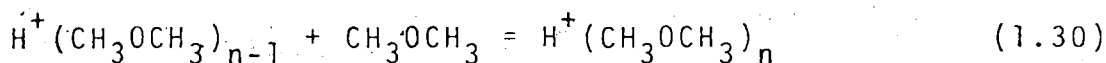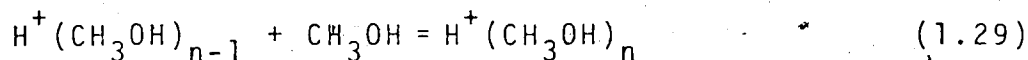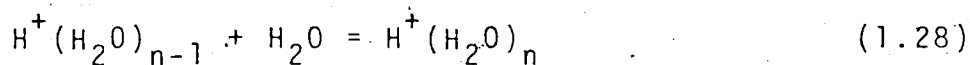
The water and methanol form stable ion clusters with the
proton readily even when n is greater than 2. However,
the dimethyl ether only produces stable clusters up to n = 2.
When n is equal to or greater than 3, the resulting pro-
tonated dimethyl ether cluster is quite unstable. This is
thought to be due to the lack of available site in the
$H^+(CH_3OCH_3)_n$ ion with n $\geq$ 2 for further hydrogen bonding
with dimethyl ether molecules. This rationalization was
confirmed by further studies of ion equilibria of the
hydrogen ion in water-dimethyl ether and methanol-di-
methyl ether mixtures (48).

1.5   Determination of Proton Affinities by Appearance
       Potential Measurements.

The proton affinity of a compound B, PA(B), was

defined in equation 1.12. If the value of $\Delta H_f^0(BH^+)$ can be determined experimentally, it can be combined with literature values of $\Delta H_f^0(H^+)$ and $\Delta H_f^0(B)$ to give PA(B) according to equation 1.31. The heat of formation of the protonated species BH^+ may be determined from its appearance potential

$$BH^+ = B + H^+ \qquad \Delta H^0 = PA(B) \qquad (1.12)$$
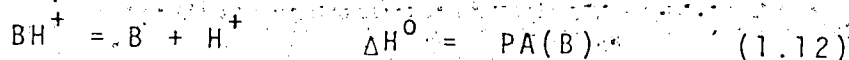
$$PA(B) = \Delta H_f^0(H^+) + \Delta H_f^0(B) = \Delta H_f^0(BH^+) \qquad (1.31)$$

as a fragment ion. For example, the proton affinity of NH_3 can be determined from the appearance potential of NH_4^+ in the mass spectrum of $C_2H_5NH_2$ as shown below:

$$e + C_2H_5NH_2 \longrightarrow NH_4^+ + C_2H_2 + H + 2e \qquad (1.32)$$
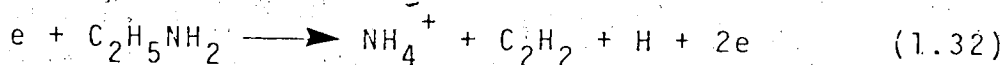
The experimentally measured appearance potential, $AP(NH_4^+, C_2H_5NH_2)$, corresponds to the energy required to produce the molecular ion $M^+ = C_2H_5NH_2^+$ that decomposes to the fragment ion NH_4^+ within the residence time of the ions in the ion source. If one assumes that there is no excess energy in the ion fragment and the neutrals, the appearance potential of NH_4^+ may be written as in equation 1.33. Generally the ΔH_f^0 values for the neutrals are

$$AP(BH^+, M) = \Delta H_f^0(BH^+) + \Delta H_f^0(\text{neutral products}) - \Delta H_f^0(M)$$

$$\left. \begin{array}{l} AP(NH_4^+, C_2H_5NH_2) = \Delta H_f^0(NH_4^+) + \Delta H_f^0(C_2H_2) + \Delta H_f^0(H) - \\ \Delta H_f^0(C_2H_5NH_2) \end{array} \right\} \qquad (1.33)$$

available from the literature, so that the ΔH_f^0 of the fragment ion, $\Delta H_f^0(NH_4^+)$ may be calculated. Substituting $\Delta H_f^0(NH_4^+)$ into equation 1.31 one obtains the $P.A.(NH_3)$. The proton affinities of some olefins and carbonyl compounds have also been determined in this manner using either the electron-impact ionization method (49,50) or the photo-ionization method (51) to measure the appearance potentials of the corresponding ions. One drawback of the method is the fact that the protonated species BH^+ of many molecules B do not occur as fragment ions. As evidenced from example 1.32, BH^+ is generally formed by a rearrangement process and such rearrangements are of low probability. Moreover, even if BH^+ is present as a fragment ion the identification of the other neutral products from the fragmentation process is not always certain (i.e. is the neutral C_2H_2 + H or C_2H_3 in reaction 1.32). In some cases the observed ion of mass equal to BH^+ may not necessarily have the same structure as the protonated ion of B. The major drawback of the method is the fact that excess energy is very often present in the fragments so that equation 1.33 does not hold. Haney and Franklin (52,53) developed a semi-empirical equation relating internal energy of the fragments to the translational energy of the product ion. The translational energy of the product ion was determined experimentally. From this energy the average translational energy $\bar{\epsilon}_t$ present in the two fragments can be evaluated.

The total excess energy E* was then obtained from the semi-empirical equation 1.34, where N is the degrees of freedom

$$E^* = 0.44 \; N\bar{\varepsilon}_t \tag{1.34}$$

for vibrations in the parent molecule. By measuring the translational energy of the product ion mass spectrometrically, the excess energy can be estimated and included in equation 1.33. The simple relationship 1.34 for energy partitioning cannot be expected to hold rigorously, and such quantitative corrections should be treated with caution. By using the above approach Haney and Franklin (53) reported $\Delta H_f^O(NH_4^+) = 148$ kcal/mole and $\Delta H_f^O(H_3O^+) = 143$ kcal/mole which lead to $PA(NH_3) = 207$ kcal/mole and $PA(H_2O) = 165$ kcal/mole.

E X P E R I M E N T A L

CHAPTER II

2.1   General

Measurements of equilibrium constants of ion-molecule reactions in this study were carried out using a high pressure mass spectrometer similar to the one described previously by Cunningham, Payzant and Kebarle in this laboratory (8). The design of the high pressure mass spectrometer for this purpose is considerably different from that of a conventional mass spectrometer. The ion source must be able to operate at a constant and accurately known pressure in torr range for the duration of a measurement. To obtain thermal equilibrium, the temperature of the ion source must be uniform and the measured temperature must reflect the true temperature of the ion source and the reacting species. High energy (2000 eV) electrons are needed to penetrate the gaseous sample in torr range so as to effect primary ionization. The design of the ion source should be such that the conductance from the ion source to the vacuum chamber is very low. With the installation of the high efficiency pumping system to the instrument, the vacuum chamber should be at a very low pressure (around 10^{-4} torr) even when the ion source is at a pressure of several torrs. The low pressure in the vacuum chamber is necessary to ensure that ions which are at thermal equilibrium in the ion source would not undergo further collisions with neutral

molecules once they diffuse out from the ion source. Since the sample detection is done outside the ion source, it is very important that the ratio of ion intensities sampled is a true representation of the ratio of ion concentrations in the reaction chamber. Since at a pressure of 10^{-4} torr, the mean free path is longer than the distance between the ion source and the detector, no collisions occur for the average ion travelling from the ion source to the detector.

The high pressure mass spectrometer could be split into three major components: the electron gun which generates high voltage electrons to effect ionization; the ion source which serves as the reaction chamber for thermal equilibrium; the detection unit which mass-analyses all ions and measures their intensities quantitatively. It is found from experience that it is best to mount them separately on individual flanges which are attached to the vacuum chamber. This makes trouble-shootings and routine maintenance much easier.

The investigations described in this thesis were conducted with a high pressure mass spectrometer equipped with a quadrupole mass analyser (Granville-Phillips Spectroscan 750). The mass spectrometer was designed and assembled by J. P. Briggs and R. Yamdagni of this laboratory. Some modifications were made to suit particular requirements for the present study. The features of the instrument along with modifications are described in this chapter. A second high pressure mass spectrometer was also assembled by this author. It was modified from

the mass spectrometer designed and assembled by D. A. Durden
(54). A new quadrupole mass analyser (Extranuclear #4-324-9)
was installed in the instrument. The special features of
the second high pressure mass spectrometer and its opera-
tional mode are also described in the latter part of this
chapter.

2.2 Overall Description of the System

A block diagram of the pulsed electron beam, high
pressure mass spectrometer is shown in Figure 2.1. The
electron gun, the ion source, the quadrupole mass filter
and the detector were housed in the vacuum chamber which
was pumped by a high capacity diffusion pump. The puls-
ing of the electron beam was effected by the master pulse
generator and the pulse amplifier [1]. Ions which re-
mained in the ion source could be removed before the start
of a new electron pulse with the aid of a pulse generator
and the pulse amplifier [2]. Sample preparations were
carried out in the gas handling plant which provided
sample to the ion source. Ions coming out from the ion
source were mass analysed by the quadrupole mass analyser
according to their m/e ratios. They were then detected by
a secondary electron multiplier. The signal from the
detector could be measured by an electrometer and dis-
played on an oscilloscope or a recorder. But in this
study, the ion counting technique was preferred. The

FIGURE 2.1   Block Diagram of the System
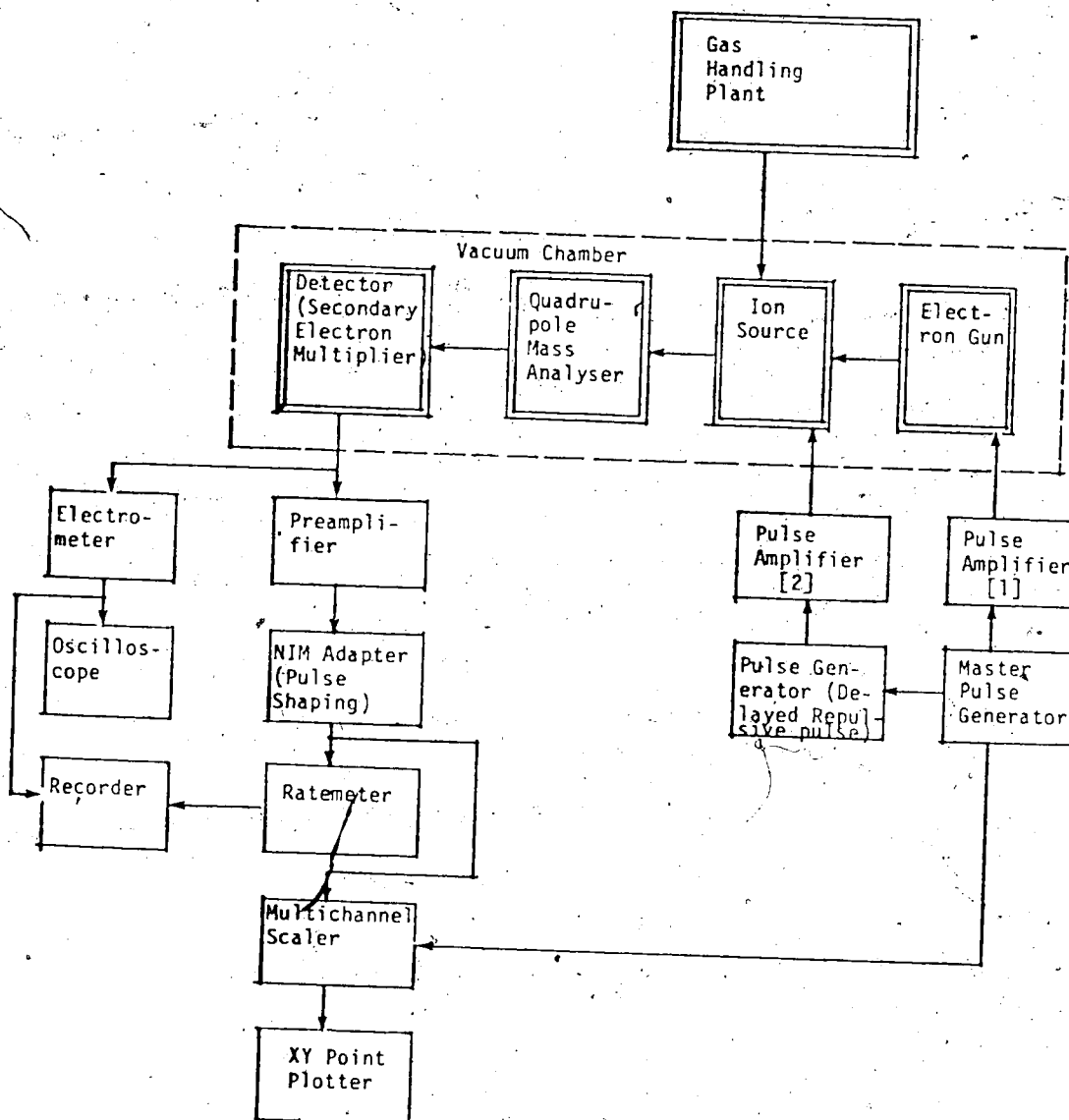
signal from the detector was amplified and individual pulses were counted by the ratemeter and the multichannel scaler. The time dependence of the ion intensity after the electron pulse was obtained by synchronizing the sweep of the multichannel scaler with the start of an electron pulse.

Individual components of the mass spectrometer are described in the following sections.

2.3 The Vacuum Chamber

A schematic diagram of the mass spectrometer is shown in Figure 2.2. The basic components of the apparatus were made by the machine shop at the University of Alberta. Only the quadrupole mass analyser was bought commercially. The main vacuum chamber was machined from an 8 inch outer diameter stainless steel tube, about 10 inches long. The inside diameter of the tube was 7½ inches. This tube supported four ports at right angles to each other. Two opposite ports carried the ion source and the ion detection system. A third port at right angles to the first two ports carried the electron gun assembly. The fourth port was used for the installation of an ionization gauge. The top of the vacuum chamber was sealed by a stainless steel flange which had a 2 inch diameter hole sealed by a transparent plexiglass flange. The transparent flange was needed for observing the electron beam. This facilitated focussing of the electron beam into the ion source. The

1.   Filament
2.   Drawout electrode
3.   Extractor
4,5,6   Focussing lenses
7,8   Deflection plates
9.   Shielding cylinder
10.   Heating mantle
11.   Electrostatic shield
12.   Electron entrance slit
13.   Electron trap
14.   Ion exit slit
15.   Gas inlet
16.   Kovar seal flange
17.   Stainless steel support
18.   Ceramic support
19.   Gas inlet heater
20.   Cone
21.   Focussing lens
22.   Filament
23.   Auxiliary ion source
24.   Electron collector
25.   Ion focussing plate
26.   Quadrupole entrance
27.   Quadrupole rods
28.   Quadrupole exit
29.   Channeltron electron multiplier
30.   Manifold of mass spectrometer.

FIGURE 2.2. Cross-sectional view of the mass
spectrometer.
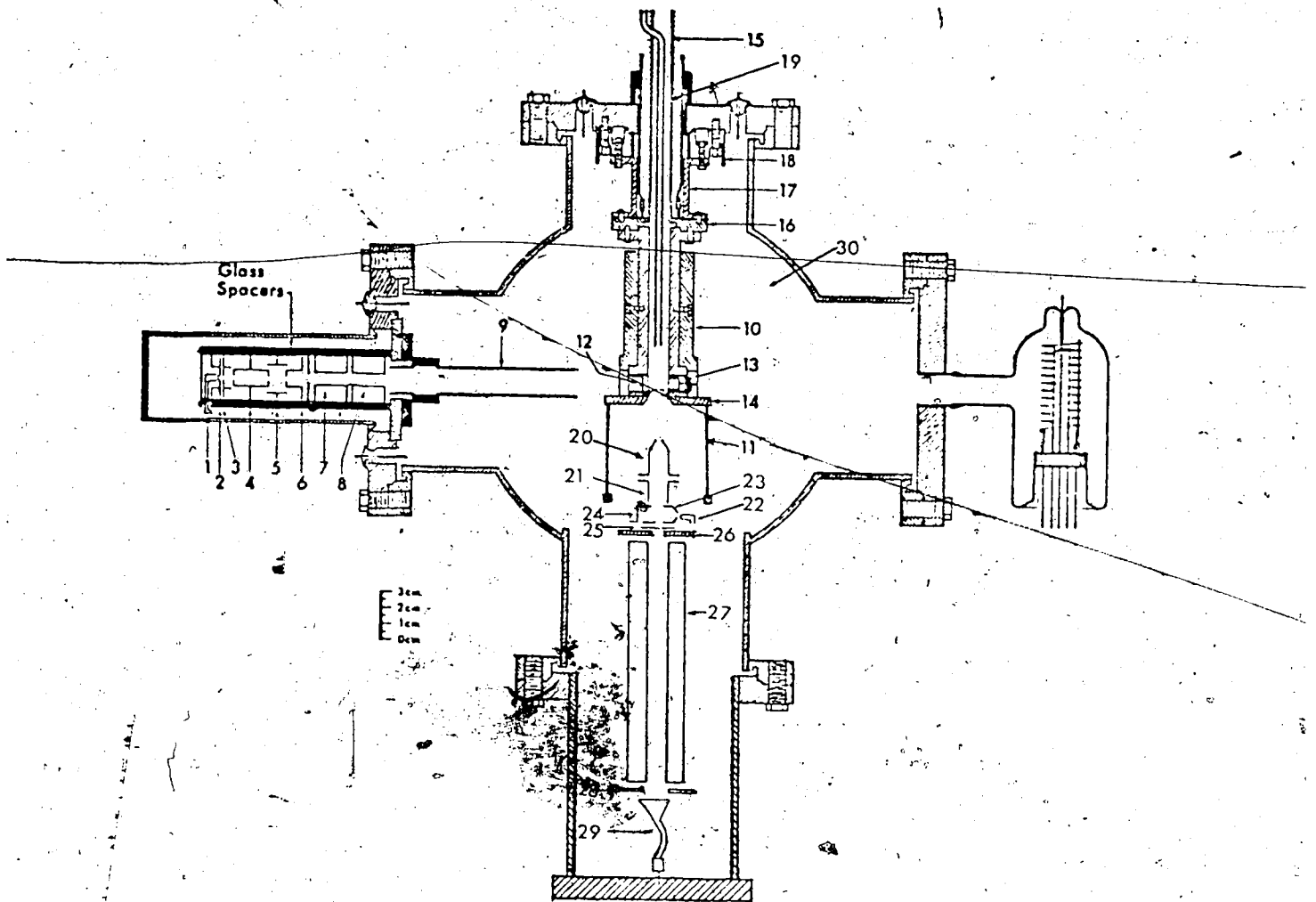
vacuum chamber was pumped through its bottom opening by a 2400 ℓ/second 6 inch oil diffusion pump (National Research, Corporation VHS-6) backed by a 375 ℓ/minute mechanical forepump (Welch Duo-Seal Pump #1397). In between the vacuum chamber and the diffusion pump was mounted a 6 inch water cooled baffle. The pumping speed at the top of the baffle was quoted to be 1000 ℓ/second. The pumping speed at the exit of the ion source can be calculated from equation 2.1 if the conductance of the tube is known.

$$\frac{1}{S} = \frac{1}{S_p} + \frac{1}{F}$$ (2.1)

S is the pumping speed at the exit of the ion source. S_p is the pumping speed at the top of the baffle (1000 ℓ/second) and F is the conductance of the tube from the baffle to the ion source (~5 inch). The conductance of a tube can be estimated by using the equation 2.2 (see Dushman (55, p.96)):

$$F = 2638 K' A \sqrt{\frac{T}{M}} \ cm^3 \ sec^{-1}$$

$$\text{where } K' = \frac{1}{1 + \frac{3}{8}\frac{\ell}{a}}$$ (2.2)

A is the cross-sectional area of the tube in cm^2, ℓ is the length of the tube in cm, a is the radius of the tube in cm , T is the temperature in °K and M is the molecular weight of the gas. A lead of 7.5 inch diameter and 5 inch long has a conductance of 2260 ℓ/second for air at

300°K. Substituting the values of F and S_p into equation 2.1 gives a pumping speed of 690 ℓ/sec at the exit of the ion source.

The only leaks from the ion source to the vacuum chamber were the ion source exit slit (0.015 mm x 1 mm) and the electron gun entrance slit (0.020 mm x 2 mm). The conductance of the slits was very low. The conductance, F_ℓ, of a very thin aperture under molecular flow conditions is given by equation 2.3 (55, p.91),

$$F_\ell = \frac{1}{4}\bar{v}A \qquad (2.3)$$

where A is the cross-sectional area of the aperture and $\bar{v}$ is the average velocity of the molecule. The average velocity of the molecule can be calculated from equation 2.4,

$$\bar{v} = \left(\frac{8RT}{M\pi}\right)^{\frac{1}{2}} \qquad (2.4)$$

where M is the molecular weight of the molecule, R is the ideal gas constant and other symbols are as previously defined. At 300°K, the average velocity of CH_4 is 6.3×10^4 cm/sec. Using this value in equation 2.3, the conductances of the ion source exit slit and the electron gun entrance slit are 2.4 cm^3/sec and 6.3 cm^3/sec, respectively.

The combined calculated conductance is 8.7 cm^3/sec. By measuring the time dependence of the pressure drop in the gas handling plant reservoir when gas was bled

through the ion source, an experimental conductance about 9 cm^3/sec was obtained. The agreement showed that the gas flow from the ion source through the slits are near molecular. The expected pressure in the vacuum system can be calculated by comparing the net flow Q using equation 2.5,

$$Q = P_{ion\ source}\ F_{slits} = P_{vacuum\ chamber}\ S \qquad (2.5)$$

where P is the pressure in the corrsponding system, F_{slits} the conductance of the slits and S the pumping speed outside the ion source. With F_{slit} = 8.7 cm^3/sec and S = 690 ℓ/sec, an ion source pressure of 4 torr will result in a pressure of 5 x 10^{-5} torr in the vacuum chamber. It was found that during normal operation, when the ion source was maintained at a pressure of 4 torr with CH_4, the vacuum chamber was typically at a pressure of ~1 x 10^{-4} torr, in fair agreement with the expected value. Ultimate vacuum of ~5 x 10^{-7} torr was attained in the vacuum chamber after letting the system pump overnight.

2.4   The Ion Source

A schematic diagram of the ion source is shown in Figure 2.3. The design of the ion source was very similar to those of other high pressure mass spectrometers used in our laboratory (56). The ion source was machined from a non-magnetic stainless steel tube 4½ inch long with an inner diameter of one-half inch. One end of the tube

[1]   High pressure ion source

[2]   Ion exit slit

[3]   Electron entrance slit

[4]   Electron trap

[5]   Repeller

[6]   High conductance grid for electric field
       shielding

[7]   Heating mantle

[8]   Base heater

[9]   Radiation heat shield

[10]   Gas inlet and outlet

[11]   Heater

[12]   Heat shield

FIGURE 2.3   The High Pressure Ion Source

Scale in cm
3
2
1
0
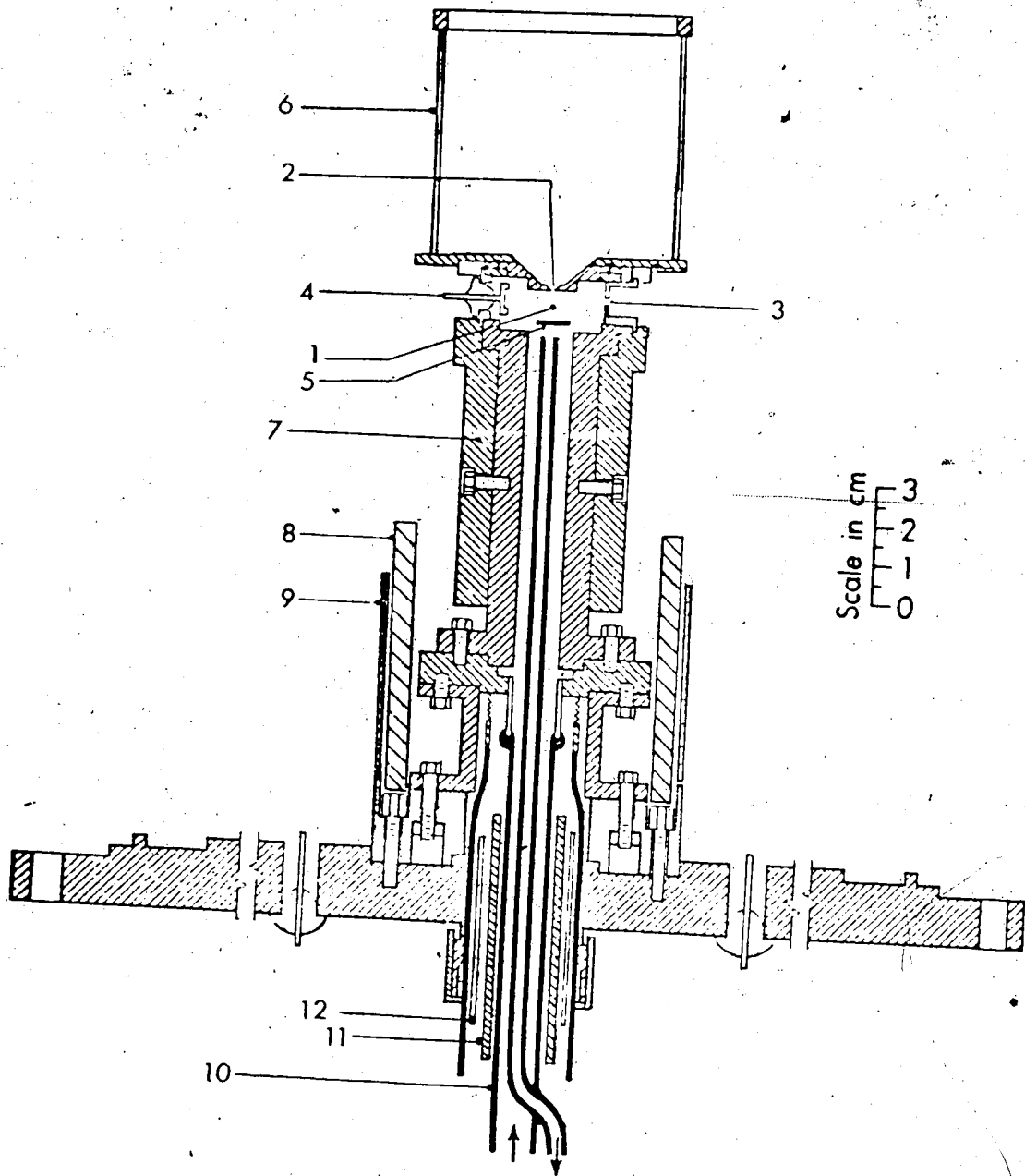
was attached to the base of the assembly. Three holes were bored on the other end of the tube perpendicular to the main axis. The three holes which were at right angles to each other were sealed by three small flanges which carried the electron entrance slit [3] and the electron trap [4] opposite to each other and the repeller plate [5]. The top of the ion source [1] was sealed by a small "hat shaped" flange which carried the ion exit slit [2]. "0"-rings made from 0.015 inch gold wire were used in sealing of flanges to the ion source. The volume of the ion source was about 1.5 cm^3. Both the ion exit slit and the electron entrance slit were made, by spot welding under microscope two small pieces of stainless steel razor blades onto the hole of the respective demountable flange. Typical dimensions of the ion exit slit and the electron entrance slit were 0.015 mm x 1 mm and 0.020 mm x 2 mm, respectively. An electrostatic shield [6] was mounted on top of the ion source. It was used to ensure a uniform field for ions which are to be accelerated from the ion exit slit to the acclerating cone. The shield was in a form of a cylindrical cage made from very fine wire gauze with high flow conductance. Eight stainless steel rods were used to support the wire gauze. High conductance was necessary so that the pumping efficiency within the cage was not impaired. The ion source was heated by a stainless steel heating mantle [7]. The heating mantle

was composed of two half-circular blocks with eight verti-
cal grooves in which heaters were embedded. The heaters
were made of 0.25 inch diameter ceramic rods 2.5 inch
long, with eight holes through which a 0.010 inch molyb-
denum wire was threaded. The heaters were held in
position by two half-circular stainless steel heat shields
which were screwed onto the heater mantle.

Gas flowed in and out the ion source through the gas
inlet and outlet tubes [10]. The concentric tubes which
were made of Pyrex glass were mounted to the base of the
assembly through a Kovar seal which was welded onto a
flange. Around the concentric tube was another glass
tube which was mounted to the base of the assembly on a
stainless steel bellow to allow flexibility. The outer
glass tube was sealed onto the main flange by a Viton
"O"-ring. It was used to hold heaters [11] around the
gas inlet and outlet tubes so that no condensation would
occur in this region. The heaters were made of eight 0.1
inch ceramic rods with four holes each through which a
0.010 inch molybdenum wire were threaded. A thin sheet
of stainless steel heat shield [12] was wrapped around
the heaters in order to achieve more uniform heating.

Six 100 watt Hotwatt "pencil" heaters [8] together
with a heat shield [9] were installed around the region
between heaters [7] and heaters [11]. It was used to
eliminate the presence of any cold spots along the gas

path to the ion source.

All electrical connections to the ion source were made through glass to metal feed-throughs which were silver-soldered onto the main flange carrying the ion source.

2.5 Temperature Control and Temperature Measurement of the Ion Source.

The ion source heater [7], the base heater [8] and the gas inlet heater [11] were controlled by individual trans-formers (Variac). Typically, some three amperes at fifty volts on the ion source heaters would produce a temperature of $600°K$ at the ion source. The exact tempera-ture of the ion source also depended on the setting of the base heaters. Even though the ion source was only at a small voltage (7 volt) above ground during operation, it was found that an isolation transformer put in between the ion source heaters and the Variac was necessary. The installation of which eliminated the disturbances on the measurements of electron current reaching the ion source when the resistance between the ion source and the heater wire was not exactly infinity. This happened when the surface of the insulating ceramics became dirty with fine deposits of conducting materials. A constant tem-perature could be reached in about four hours after a change in the settings of the Variac by allowing the temperature to reach a steady state. It was found (54) that this steady state method gave a much more constant

temperature than using an automatic temperature controller. The base heater and the gas inlet heaters were controlled in a similar manner. No isolation transformer was necessary for them because the heating elements were not in contact with the ion source.

The temperature of the ion source was monitored by an iron-constantan thermocouple. A small hole was drilled into the metal block housing the ion source. The hole was at a level in between the electron entrance slit and the ion source exit slit. The thermocouple was threaded through a small ceramic rod before silver-soldered at the tip. A stainless steel shim was used to press the thermocouple firmly into the hole and to make sure that the thermocouple had good thermal contact with the ion source.

A second thermocouple was installed at the base of ion source assembly. A hole was drilled through the center of a screw. The thermocouple was inserted into the hole and silver-soldered at the tip of the screw. The screw was then tightened onto a tapped hole in the assembly. The temperature of the base was kept close to that of the ion source.

A third thermocouple was inserted around the gas inlet and outlet tubes. The glass tubes that connected the inlet tube from the gas handling plant and the outlet tube to a mechanical pump through a capillary were also heated by electrical heating types. The temperatures of

all connecting tubes was kept close to that of the gas handling plant. The temperature of the gas handling plant was typically 150°C.

The voltage of the thermocouples relative to the reference thermocouple at ice-water temperature was measured by a potentiometer. The temperature was read from the EMF table in "CRC Handbook of Physics and Chemistry". The temperature could be read to within one degree centigrade.

2.6 The Gas Handling Plant

The gas handling plant was made from Pyrex glass with stainless steel valves. Six Granville-Phillips ultra high vacuum all-metal valves were mounted to the metal framework of the plant. A glass manifold, a 5 liter glass bulb and others were connected to the valves through 14 mm o.d. Pyrex tubings as shown in Figure 2.4. The complete system was enclosed in a box made of 1 inch thick asbestos boards. The box was heated by three heaters; one at the bottom of the box and the others on two sides of the box. The heaters were GE 100 watt oven-type heaters covered with metal shields to provide more uniform heating and prevent the possibility of thermal decompositions that might occur at some hot spots. The gas handling plant was usually kept at a temperature of about 150°C.
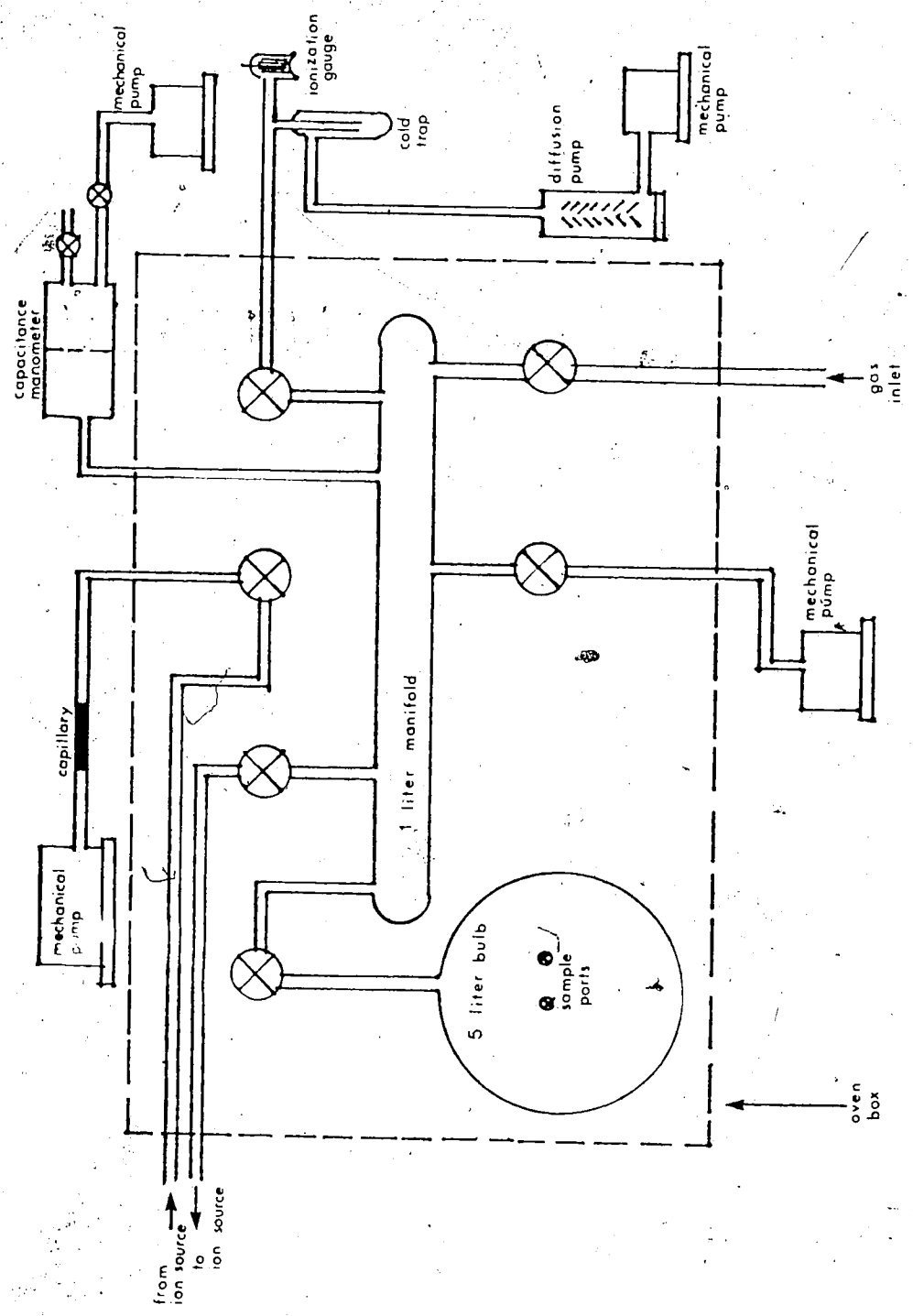
The Gas Handling Plant

FIGURE 2.4

The volumes of the manifold and the bulb were measured by expanding air from another bulb of known volume to the manifold and then to the complete system. The volume of the calibrated bulb was determined from the weight of water it could hold and the density of water. The volumes of manifold and the bulb were found to be 0.96 liter and 5.06 liter, respectively.

The complete system was pumped by a liquid nitrogen cold trap and an oil diffusion pump (Edward #E-02) backed by a mechanical pump. A roughing pump was also connected to the system. During evacuation the system was pumped down to below 1 torr by the roughing pump before it was exposed to the diffusion pump. This was to minimize the contamination of the diffusion pump oil by the condensable compounds present in the system.

The pressure of the manifold was monitored by an Atlas-Bremen MCT capacitance manometer. It was a differential capacitance manometer which could read pressure from 0.1 to 20 torr relative to that of the reference cavity. Normally, the reference cavity was pumped continuously by a mechanical pump and the reading gave the absolute pressure in the manifold. When a pressure of 1 atmosphere was required in the system, the reference cavity was open to the atmosphere and the gas was introduced to the system until the manometer gave a zero reading. The pressure of the system was then read from a

mercury barometer. The calibration of the capacitance mano-
meter was checked periodically against a McLeod gauge using
a non-condensable gas such as methane.

The 5 liter bulb had two ports: one was an injection
port for introducing liquid samples with a syringe; the
other port was for solid samples. Gaseous samples were
introduced into the bulb through the gas inlet and the
manifold. The sample was allowed to mix thoroughly and
stored in the bulb. The flow of the sample from the bulb
to the ion source was controlled by the metal valve con-
necting the bulb and the manifold. The ion source was
continuously pumped by an exhaust pump through a capillary.
This was to ensure the presence of a fresh and uniform
sample at all times during the experiment.

The pressure gradient between the manometer and the
ion source was negligible because the size of the connect-
ing glass tubes was large (1/2 inch i.d.). The pressure
gradient may be calculated from the Poiseville law (55,
p. 84):

$$n_M = \frac{\pi}{16\eta} \frac{a^4}{\ell} \frac{P_2^2 - P_1^2}{RT} \qquad (2.6)$$

where n_M is the rate of gas flow expressed in terms of
moles per second for a tube of length ℓ and radius a; R
is the gas constant; η is the coefficient of viscosity
of the gas at temperature T. P_2 and P_1 denote the pres-
sures at two ends of the tube. With a pressure of 4 torr
registered on the manometer, the flow rate was measured

to be about 18 cc atm min^{-1}. The length of the tube from the manifold to the ion source was about 200 cm. The viscosity of methane is 1.09×10^{-4} poise at 20°C (57). From equation 2.6, it was calculated that the pressure difference between the manometer and the ion source was about 0.5%. Since the difference was insignificant, the pressure reading in the manometer was taken as the pressure in the ion source.

2.7 The Electron Gun Assembly and the Pulsing Circuitry

A schematic diagram of the electron gun assembly is shown in Figure 2.2. Electrons emitted from the heated filament [1] were accelerated and focussed by various electrode plates and lenses [2-6] along the z axis towards the ion source. Two pairs of deflection plates [7,8] were used to deflect the electron beam in the x and y axes so as to position the electron beam right on the electron entrance slit. In order to produce high energy (2 kV) electrons for ionizing the gas sample in the high pressure ion source at +7V, the filament was kept at -2000 V. Typical voltage settings and control meter readings are given in Table 2.1. Two different types of filaments were used in the construction of the electron gun. Filaments made of thoriated iridium were found to be resistant to attack by most gases used in the present study except when hydrogen sulfide and amines were involved.

TABLE 2.1

Typical Operating Voltages for Electron Gun Assembly

	Electrode[a]	Voltage (volt)
1	Filament	-2000^b
2	Drawout	-1950
3	Extractor	-1800
4	Lens #1	-50^b
5	Lens #2 (focus)	-1650
6	Lens #3	-50^b
7	Deflection half-plates	
	X_1	-75
	X_2	-50^b
8	Deflection half-plates	
	Y_1	-35
	Y_2	-50^b
	Ion Source, Trap & Repeller	+7

Typical control meter readings under continuous electron irradiations:

> Emission Current: 1 mA
>
> Case current (from electrons hitting the ion source):   50 μA
>
> trap current (from electrons reaching the electron trap):   0.5 μA

[a] Number refers to Figure 2.2

[b] Fixed voltages on these electrodes. Others were adjustable.

In those cases, it was found that filaments made of 75/25 tungsten/rhenium were more satisfactory. The long distance separating the filament from the ion source meant that the filament was not exposed to the high pressure gas. This led to longer filament life. Also, a better ion source temperature control was achieved in this manner since the hot filament would not heat up the ion source, and the temperature of the ion source could be controlled solely by the ion source heaters.

Focussing of the electron beam was done with the system at vacuum. A small metal plate with a small hole in front of the electron entrance slit was mounted on the ion source assembly. The outer surface of the plate was coated with a phosphor (Type P-31 Sylvania) embedded in sodium silicate. The electron beam was first deflected onto the plate by varying the voltages on the deflection plates and focussed to give a sharp green spot. The focussed electron beam was then deflected onto the electron entrance slit. Final positioning was attained by adjusting the deflection until a maximum current was read on the electron trap current microammeter.

All experiments were performed with a pulsed electron gun. The pulsing was achieved by varying the potential of the drawout electrode at regulated intervals. Electrons could only pass into the ion source when the filament was at a higher negative potential than the

drawout electrode. In the pulsing mode, the drawout plate
was kept at some 40 volts negative to the filament. Upon
receiving a triggering pulse from the master pulse genera-
tor, the floating pulse amplifier would alter the potential
of the drawout plate to some 50 volts positive with res-
pect to the filament for a desirable period of time (6-
140 μsec). This allowed electrons to pass through the
drawout plate only for the preset period of time. Then
the drawout plate would return to the original potential
negative to the filament, and the electron beam would be
cut off until the next cycle was initiated by another
pulse from the master pulse generator. The duration of
the cycle (~4 msec/cycle) was controlled by the master
pulse generator whereas the duration of the "on" time
for the electron beam (10-20 μsec) was governed by the
pulse amplifier which also had the provision to adjust
the exact voltage of drawout plate to give the best in-
tensity of electron beam pulses.

The triggering pulse from the master pulse generator
also served two other purposes (see Figure 2.1). It was
used to send a delayed pulse to the repeller in the ion
source to sweep all positive ions to the wall of the
ion source and thus destroy the ions before the start of
the next fresh electron beam pulse. This was achieved
with another floating pulse amplifier together with a delay
pulse·generator externally triggered by the master pulse

generator. The repeller pulse was typically of 50 μsec duration and at some 40 volts positive to the ion source. The sweep of the multichannel scaler for data collection was also synchronized with the triggering pulse from the master pulse generator. In this manner, a time dependence of ion intensities after the ionizing pulse could be obtained. A schematic diagram of the pulsing sequence was shown in Figure 2.5.

When the electron gun was not pulsed, the intensity of the electron beam striking the ion source was around 50 microamperes. Only a small fraction of the electron beam passed through the electron entrance slit and reached the trap in the ion source. This trap current was normally about 0.5 microampere. It may be calculated that a 10 μsec electron pulse, followed by a no electron current period of 3 msec, will generate 3×10^7 electrons per pulse in the ion source.

2.8 Ion Acceleration from the Ion Source to the Mass Analyser.

Ions coming out from the ion exit slit were accelerated and focussed towards the quadrupole mass analyser (Figure 2.2). An entrance cone [20] and a focussing lens [21] were mounted on the existing quadrupole mass spectrometer auxialiary ion source [23]. It was found that satisfactory focussing of the ion beam could be

FIGURE 2:5 Pulsing Sequence with Typical Voltages and Durations

10 µs

voltage

Drawout
Plate in
Electron Gun
(filament at
-2000 V)

- 1950 V

-2140 V

4 ms

Repeller Plate
in Ion Source
(ion source at
+7 V)

50 µs

+ 40 V

+ 7 V

3 ms

Multichannel
Scaler
start (↑) and
stop (●) of
sweeping
sequences

2.56 ms
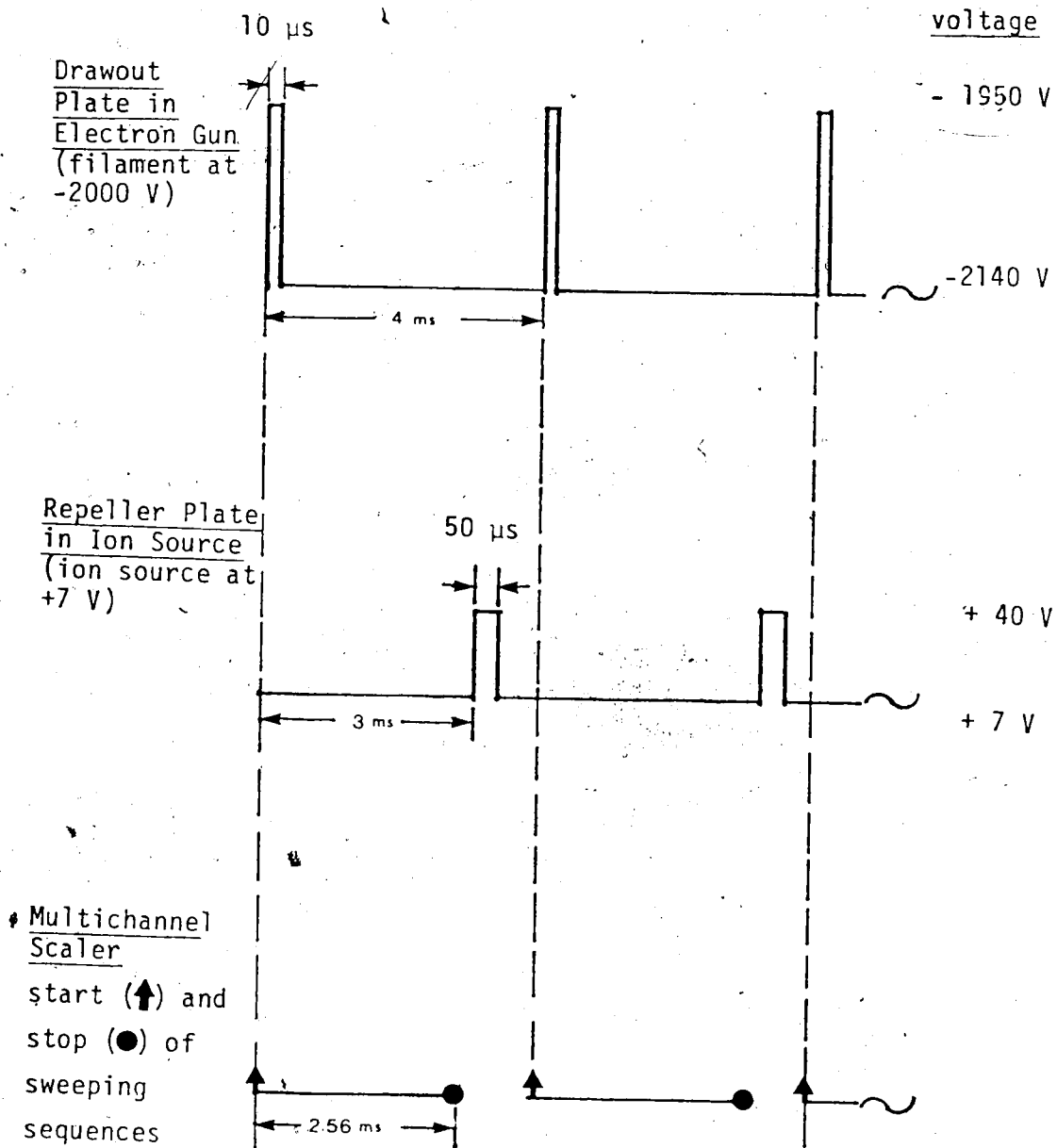
achieved with the cone and the lens at the same potential. In a typical run, the ion source and the ion exit slit were at +7V. The entrance cone and the focus lens were at a negative potential of -150V. The various plates [22-26] in front of the quadrupole rods were at ground potential. With this arrangement, ions coming out from the ion exit slit were accelerated towards the entrance cone. Once the ions were inside the cone, they would travel at constant velocity through the lens to the grounded plates [23-26] where they would slow down to 7 volts acceleration.

The time of flight for ions to travel from the ion source exit slit to quadrupole entrance slit can be estimated. It might be assumed that ions were accelerated under a uniform field from the ion exit slit to the entrance cone with a terminal velocity of v_t. The terminal velocity of an ion is given by equation 2.7,

$$v_t = \left(\frac{2eE}{m}\right)^{\frac{1}{2}} \tag{2.7}$$

where e is the electron charge and is equal to 1.6×10^{-12} g cm^2 s^{-2}, E is the potential of the field in volts and m is the mass of the ion in gram. The average velocity v_a would be half of the terminal velocity. The time required for ions to reach the cone is then calculated from equation 2.8,

$$t_1 = \frac{d_1}{v_a} = 2d_1\left(\frac{m}{2eE}\right)^{\frac{1}{2}} \tag{2.8}$$

where d_1 is the distance between the ion exit slit and the entrance cone. The time required for ions to travel through the cone and the lens (total length = d_2) under constant velocity, v_t, before they were stopped is given by equation 2.9.

$$t_2 = \frac{d_2}{v_t} = d_2 \left(\frac{m}{2eE}\right)^{\frac{1}{2}} \qquad (2.9)$$

After entering the auxiliary ion source assembly, ions would possess energy E_i. The time required for them to travel to the quadrupole entrance under constant velocity, v_i, will be:

$$t_3 = \frac{d_3}{v_i} = d_3 \left(\frac{m}{2eE_i}\right)^{\frac{1}{2}} \qquad (2.10)$$

where d_3 is the length of the auxiliary ion source assembly. The total flight time is given by equation 2.11.

$$t_{total} = t_1 + t_2 + t_3 \qquad (2.11)$$

The instrument was set up such that d_1 was 5 cm, d_2 was 4 cm and d_3 was 0.8 cm. For an ion with a molecular weight of 100 under an accelerating field of 157 V and having a final ion energy of 7V, the total flight time from the ion source to the quadrupole entrance was calculated to be about 10 μsec.

The assumption that the average velocity of an ion under acceleration is half of its terminal velocity is not exactly true. The potential gradient between the ion source exit slit and the entrance cone are not linearly

proportional to their distance because of their geometries. More elaborate calculations had shown that the assumption is good to within 10% (54), and it is therefore good enough for estimation purposes.

The auxiliary ion source assembly [22-25] in front of the quadrupole housing could be used to obtain conventional low pressure electron impact mass spectra on different compounds. It was used to check on the purity of compounds used.

2.9 Quadrupole Mass Analyser and Ion Detection System

A brief theory on the quadrupole mass analyser is given below, followed by a description of the quadrupole mass spectrometer used in the present system.

A. Theory of the Quadrupole Mass Analyser

The possibility of using an electrodynamic quadru-pole field to sort out ions of different m/e ratios was first recognized by Paul and co-workers (58) in 1953. This and the subsequent studies (59,60) resulted in the development and the construction of quadrupole mass analysers. A quadrupole mass analyser consists of four long parallel rods arranged as in Figure 2.6. Although the theory was developed assuming hyperbolic field-forming surfaces, circular rods are usually used because it is much easier to achieve the required dimensional precision with circularly cylindrical rods than

$+(U + V_0 \cos\omega t)$ $-(U + V_0 \cos\omega t)$
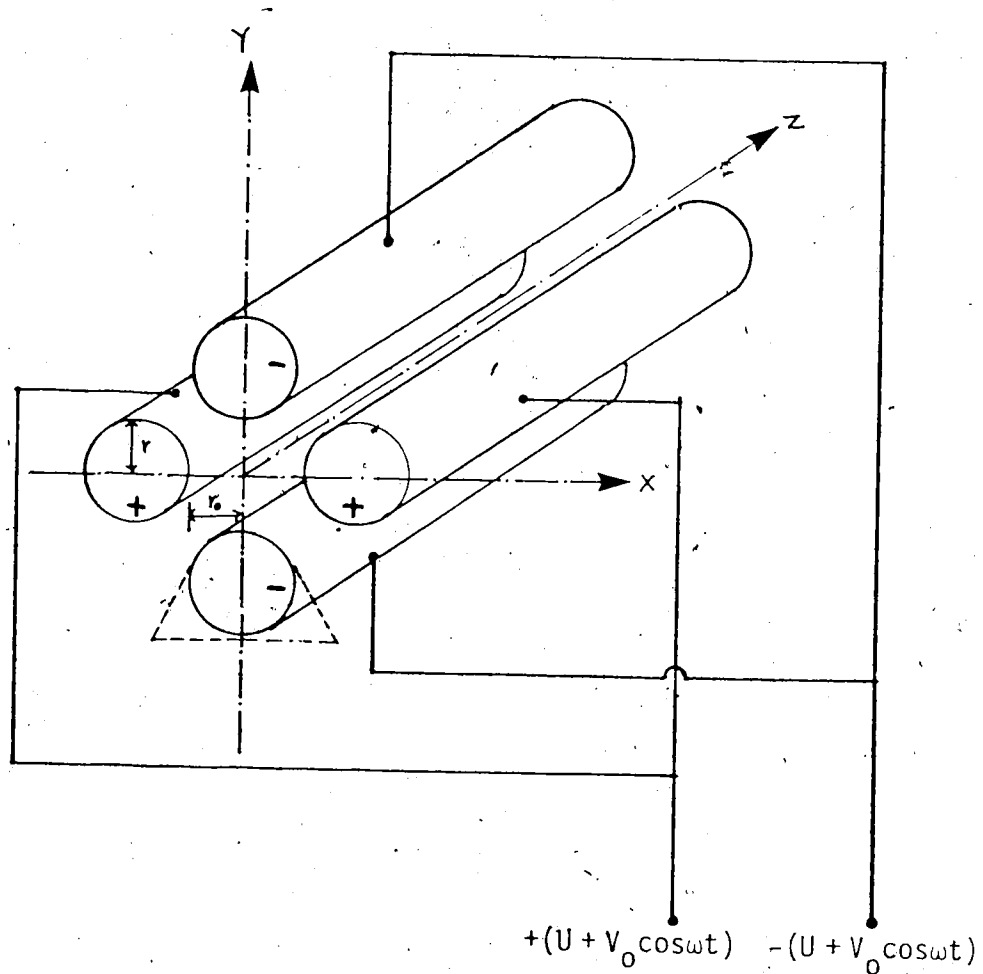
FIGURE 2.6 The Arrangement of Quadrupole Rods. The Hyper-
bolic Cross-section (dashed lines) is Approximated by the
circular cross-section with r = 1.16 r_0.

with hyperbolic cylinders. When the radius of the rods is 1.16 times the inscribed circle radius, the fields near the axis closely approximate the ideal hyperbolic field. The quadrupole field is created by the application of a dc voltage (U) and a superimposed rf voltage ($V_0 \cos \omega t$) on four hyperbolic electrodes so that two opposing electrodes will have a postive potential of +(U + $V_0 \cos \omega t$) while the other two opposing electrodes will have a negative potential of -(U + $V_0 \cos \omega t$). The electrostatic field potential, Φ, generated at any point within the field is given by equation 2.12,

$$\Phi = [U + V_0 \cos \omega t](x^2 - y^2)/r_0^2 \quad (2.12)$$

where $2r_0$ is the distance between two opposite pole surfaces, ω is the angular frequency of the rf with peak potential V_0 and U is the dc potential. The cartesian coordinates (see Figure 2-6) are arranged such that x is the direction of the positive poles, y is the direction of the negative poles and z is in the direction of the quadrupole axis. When a singly charged ion with mass m enters the mass filter, it is accelerated by the electrostatic field. The cartesian force components are given by equations 2.13 - 2.15,

$$m \frac{d^2 x}{dt^2} = -e \frac{\partial \Phi}{\partial x} \quad (2.13)$$

$$m \frac{d^2 y}{dt^2} = -e \frac{\partial \Phi}{\partial y} \quad (2.14)$$

$$m \frac{d^2 z}{dt^2} = -e \frac{\partial \Phi}{\partial z} \qquad (2.15)$$

where e is the electron charge. After obtaining the partial differentials from equation 2.12, the equations of motion of the ion can be rewritten as:

$$m \frac{d^2 x}{dt^2} + (\frac{2e}{r_o^2})(U + V_o \cos\omega t)x = 0 \qquad (2.16)$$

$$m \frac{d^2 y}{dt^2} - (\frac{2e}{r_o^2})(U + V_o \cos\omega t)y = 0 \qquad (2.17)$$

$$m \frac{d^2 z}{dt^2} = 0 \qquad (2.18)$$

Equation (2.18) can be easily integrated to give dz/dt = constant. This implies that the axial velocity of any ion is constant throughout the quadrupole rods and it is not affected by the voltages applied to the poles of the filter. The magnitude of axial velocity is equal to the initial velocity of the ion when entering the mass filter. It is governed by the potential difference between the ion source and the quadrupole axis.

The filtering action of the quadrupole results from the trajectory characteristics of equations 2.16 and 2.17. They can be solved by rearranging them into the canonical form of the Mathieu differential equation as shown in 2.19 and 2.20. Three dimensionless parameters have been introduced in equations 2.19 and 2.20. They are defined

in 2.21 - 2.23.

$$\frac{d^2x}{d\phi^2} + (a + 2q \cos2\phi)x = 0 \qquad (2.19)$$

$$\frac{d^2y}{d\phi^2} - (a + 2q \cos2\phi)y = 0 \qquad (2.20)$$

$$\phi = \frac{\omega t}{2} \qquad (2.21)$$

$$a = \frac{8eU}{mr_o^2\omega^2} \qquad (2.22)$$

$$q = \frac{-4eV_o}{mr_o^2\omega^2} \qquad (2.23)$$

The solutions for the Mathieu equations 2.19 and 2.20 give the amplitudes of x and y displacements with respect to the number of oscillations. Two groups of solutions exist for the equations 2.19 and 2.20. There are unstable solutions in which the amplitudes of oscillations increase without bound and there are stable solutions in which the amplitudes of oscillations do not exceed a given boundary. The ions with unstable trajectories collide with one of the rods and are removed from the ion beam. For a limited set of values of a and q, stable solutions exist. The trajectories of the ions under such conditions are stable oscillations which amplitudes remain less than $2r_o$. Conditions under which ions achieve a stable trajectory in the x and y directions can be obtained from the solutions of the Mathieu equations. They are represented in the so-called "stability diagram" (see Figure 2.7) which was developed by Paul and co-workers (60). The stability
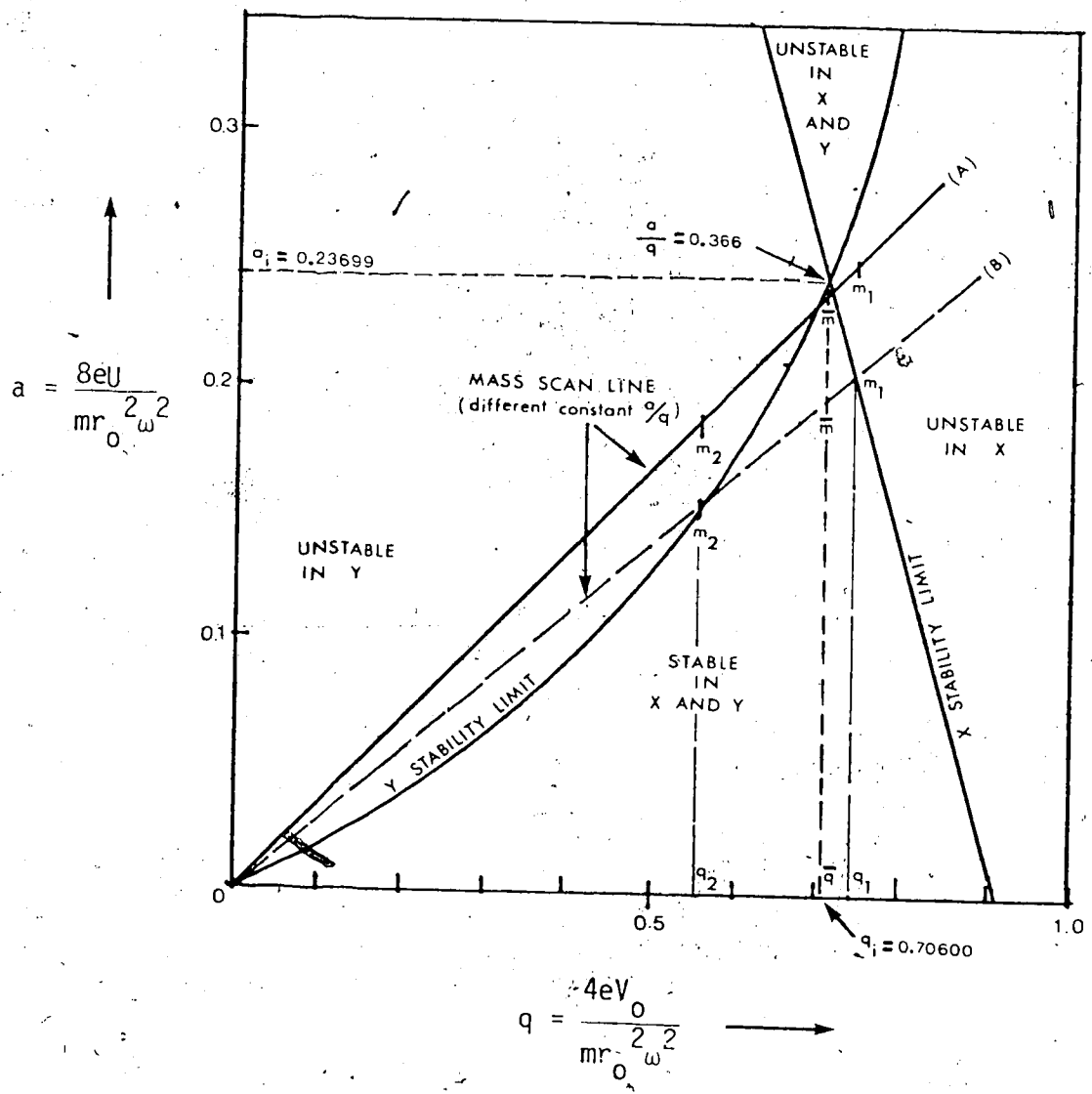
FIGURE 2.7   Stability Diagram.

diagram 2.7 is a plot of the parameters a and q for which stable solutions of the Mathieu equations are obtained. It is evident from equations 2.22 and 2.23 that the ratio of a/q is proportional to that of dc to rf voltages $(a/q = 2U/V_o)$. In Figure 2.7, it is shown that the number of different ion masses which have stable trajectories through the quadrupole depends on the ratio of a/q. If the ratio is small (dashed scan line in Figure 2.7), many ions of similar mass $(m_1, \ldots \bar{m}, \ldots m_2)$ can traverse the filter without hitting the rods. If the ratio is large enough (solid scan line in Figure 2.7), only ions of one mass $(\bar{m})$ can pass through the filter and be detected. The resolution of the mass filter therefore increases with the value of a/q, and it theoretically becomes infinity at the apex of the stability diagram with a/q = 0.336 (a_i = 0.23699 and q_i = 0.70600 in Figure 2.7). In practice, the working scan lines used are always in the region near the apex of the stability diagram. Mass scanning may be achieved in two ways. (a) At constant rf frequency, the dc and rf voltages (U and V_o) are varied in such a manner that the ratio of voltages, U/V_o, remains constant. Ions with different mass-to-charge ratio will be transmitted successively. (b) At constant U/V_o, the frequency is changed. Most commercial quadrupole mass filters operate in the former mode. The mass-to-charge ratio of ions transmitted can be obtained by rearranging equation 2.23 into 2.24. By

$$\frac{m}{e} = \frac{1}{q} \cdot \frac{4V_o}{r_o^2 \omega^2} \tag{2.24}$$

substituting $q_i = 0.706$ for q (at infinite resolution).
The mass of the singly charged ions which reach the detector
is given by equation 2.25, where V_o is in volts, r_o is

$$m = 0.138 \, V_b/r_o^2 f^2 \text{ amu at infinite resolution} \tag{2.25}$$

in cm and f is the frequency in megacycles per sec. It is
evident from equation 2.25 that the operating mass range
of a quadrupole analyser depends on the diameter of the
rods, the rf frequency and the maximum rf voltage.

The resolution, R, is a quantitative measure of the
mass separation achieved with the mass spectrometer. It
is usually defined as $R = \bar{m}/\Delta m$ where $\bar{m}$ is the molecular
weight of the ion and Δm is the peak width in amu for the
ion measured at 10% of the peak height. When Δm is 1,
two ions of masses differed by one are said to be resolved.
Since $m \propto 1/q$ from equation 2.23, the resolution may be
expressed in terms of q values as shown in equation 2.26,

$$R = \frac{\bar{m}}{\Delta \bar{m}} = \frac{\bar{m}}{m_1 - m_2} = \frac{1/\bar{q}}{\frac{1}{q_1} - \frac{1}{q_2}} = \frac{q_1 q_2}{\bar{q}(q_2 - q_1)} = \frac{q_1 q_2}{\bar{q}(\Delta q)} \tag{2.26}$$

where $\bar{q} = q_i = 0.706$, and $\Delta q = q_2 - q_1$ is the width of the
scan line within the stable region in the stability dia-
gram as illustrated in Figure 2.7. When the operating
scan line is closed to the apex of the stability diagram

as it is generally the case in practice, $q_1 \approx \bar{q} \approx q_2$. Equation 2.26 may be simplified into 2.27.

$$R \approx \frac{\bar{q}}{\Delta q} = \frac{0.706}{\Delta q} \qquad (2.27)$$

Under these conditions, the relationship 2.28 obtained

$$\Delta q \approx 4(0.236 - 1.410\frac{U}{V_o}) \qquad (2.28)$$

by Paul et al. (59) from a detail study of the geometry of the "stability tip" of the stability diagram 2.7 is valid. The combination of equation 2.27 and 2.28 leads to the expression 2.29 for resolution R in terms of U and V_o.

$$R = \frac{\bar{m}}{\Delta m} = \frac{0.125}{0.178 - U/V_o} \qquad (2.29)$$

The foregoing discussion on resolution based on the stability diagram 2.7 assumes that the ions have experienced an infinitely large number of oscillations in the quadrupole field. In practice, the number of oscillations that the ions would encounter is limited by the physical length of the quadrupole rods. It has been shown by Zahn (61,62) that under the condition that the ions spend relatively "few" oscillations in the quadrupole field, the maximum attainable resolution $(\frac{\bar{m}}{\Delta m})_{max}$ is related to the number of cycles of rf field, N, encountered by the ions. The relationship is given in equation 2.30

$$\left(\frac{\bar{m}}{\Delta m}\right)_{max} = \text{constant} \times N^2 \qquad (2.30)$$

where the constant depends on the instrumental design such as the instrument aperture and the field radius. For estimation purposes, the constant may be assumed to have a value of 20 (61). The number of rf cycles, N, may be expressed as in equation 2.31, where f is the rf frequency, ℓ is the

$$N = f\ell\left(\frac{\bar{m}}{2eE_z}\right)^{\frac{1}{2}} \qquad (2.31)$$

length of the rods, E_z is the ion energy in z direction, $\bar{m}$ is the mass of the ion, and e is the electron charge. On substituting equation 2.31 into equation 2.30, the expression for the maximum obtainable resolution becomes:

$$\left(\frac{\bar{m}}{\Delta m}\right)_{max} = \text{constant}\left[\frac{f^2\ell^2\bar{m}}{2eE_z}\right] \qquad (2.32)$$

The maximum resolution obtainable is therefore dependent on three operating parameters: the length of the rods, the rf frequency and the ion injection energy. It is interesting to note from equation 2.32 that the maximum resolution increases with the mass of the ion. In other words, the minimum attainable peak width is independent of ion mass in a given operation. In the present instrument, with a fixed operating resolution setting, Δm increases only very slightly with mass, and for all practical purposes, Δm is more or less constant over the mass range

of interest in a particular experiment. As evident from equation 2.32, the ion energy has an important bearing on the maximum resolution attained. For mass separation to occur, any ions of the incorrect m/e values must remain in the traverse field long enough so that they will be rejected. This means a maximum axial ion energy $E_z(max)$ exists for a filter of given length ℓ, operating at rf frequency f and a given resolution ($\frac{\bar{m}}{\Delta m}$). By substituting a value of 20 for the constant in equation 2.32, an approximate relationship between $E_z(max)$ and a given resolution ($\frac{\bar{m}}{\Delta m}$) is given by equation 2.33,

$$E_z(max) \approx \frac{f^2 \ell^2}{30} (\frac{\Delta m}{\bar{m}}) \bar{m}$$ (2.33)

where f is in megacycles per sec and ℓ in cm.

Another important assessment on the performance of any quadrupole mass spectrometer is its efficiency in the transmission of ions. It is highly desirable that the efficiency of transmission of the quadrupole mass filter should not be dependent upon the mass-to-charge ratio of the ions, i.e. there is no mass discrimination on ion transmission. Unfortunately, this is often difficult to achieve. One of the reasons for the mass dependence of the transmission arises from the effect of the injection aperture on resolution. It has been shown (83) that for ions injected parallel to the quadrupole axis, the radius of the maximum mass filter aperture, a, which

will ensure that none of the ions of the right m/e will strike the rods can be approximated by equation 2.34,

$$a \approx \frac{2}{3} r_0 \left(\frac{\Delta m}{m}\right)^{\frac{1}{2}}$$

(2.34)

where r_0 is the distance between the quadrupole axis and the pole surface. It is evident from equation 2.34 that the maximum mass filter aperture decreases with an increase in resolution. When the quadrupole mass spectrometer is operated with a constant Δm, over the mass range as in the present instrument, the maximum radius of injection of ions to be transmitted will diminish with ion mass. Since the transmitted ion signal is proportional to the area of the acceptance aperture, it would diminish as the inverse first power of ion mass.

The mass dependence of the transmission is further complicated by the presence of fringing fields near the entrance of the quadrupole rods. This occurs in practially all quadrupole mass spectrometers. With a fixed ion energy, the time that an ion spends in the fringing fields depends on its mass. The heavier the ion the longer the time it would spend in the fringing fields and, therefore, the greater the dispersion in the quadrupole field. As a result, there is always a tendency for the heavier ions to be transmitted less efficiently causing mass discrimination on transmission. Dawson (84) has shown by theoretical calculations that if an ion spends more than three rf cycles in the fringing fields, there is a large re-

duction in transmission because of the large reduction
in effective aperture of the instrument. The effects
of the fringing fields on ion trajectories were first
considered by Brubaker (65). He showed that when ions
are approaching the mass filter entrance, they are sub-
jected to weaker fields varying from zero to the full
potentials represented by the a and q values distributed
along the working scan line from the origin to the
stability tip (Figure 2.8). These lower a and q values
cause the instability for the ion trajectories in the
yz plane but not for the xz plane. As a result of this
consideration, Brubaker (65) suggested a modification in
the mode of operation of the quadrupole mass analyser
to minimize the effect of fringing fields on ion trans-
mission. If an ion approaching the mass filter is first
subjected only to rf excitation before it is subjected
to the normal dc and rf excitation, the "working point"
for the ion moves first along the q-axis (a = 0) in the
stability diagram (Figure 2.8) and only later does the a
value increase until the stability tip is reached when
the ion enters the full quadrupole field. In this manner,
the ion always remains in a condition that its traject-
ory is mathematically stable. The defocussing of ions
in the y direction when they are traversing the fringing
fields is thus minimized. Under such conditions, one
of the many paths the "working point" for the ion may

$$a = \frac{8eU}{mr_o^2\omega^2}$$

$$q = \frac{4eV_o}{mr_o^2\omega^2}$$
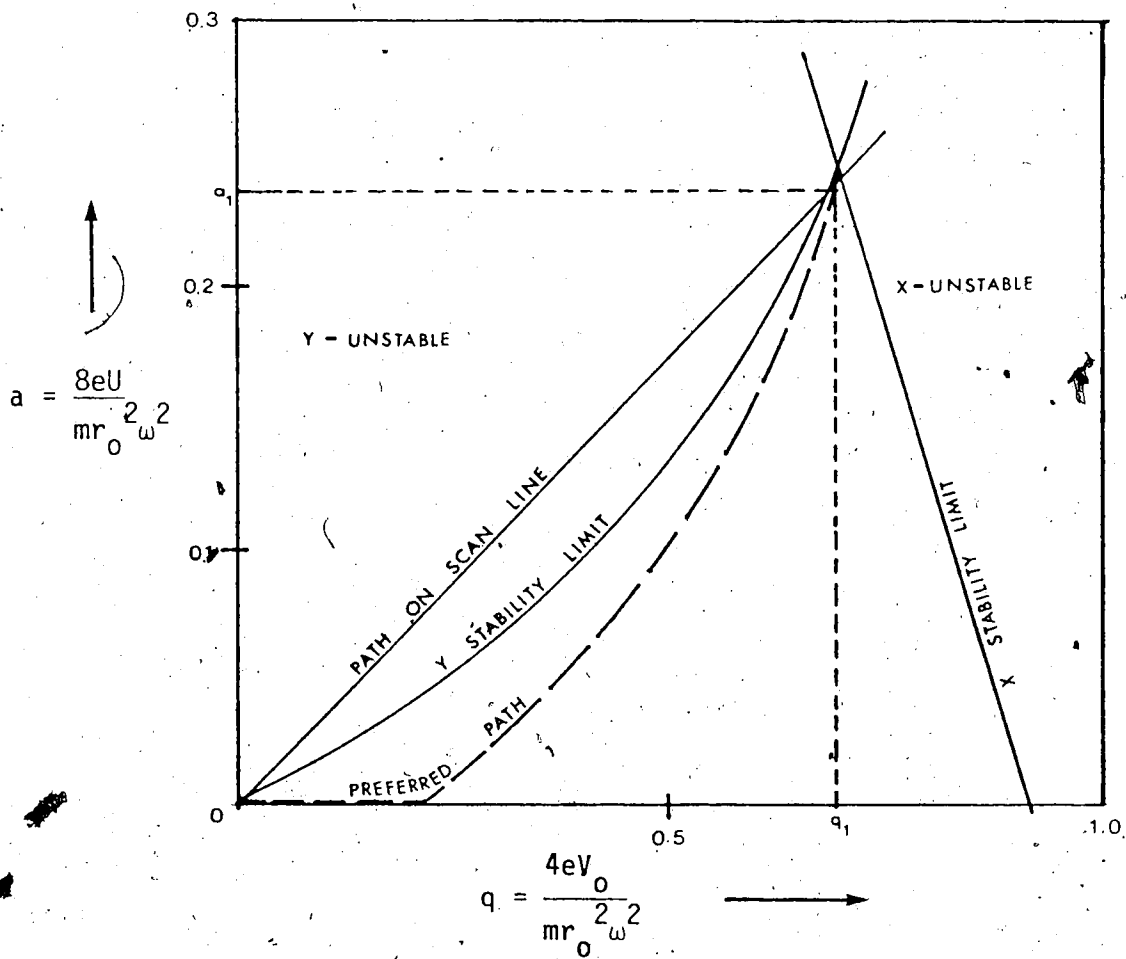
FIGURE 2.8   Stability diagram, showing a preferred path of working point for ions during transversal of fringing field.

take through the stability diagram during its traversal
of fringing fields is shown in Figure 2.8. 'The modifi-
cations in the apparatus were done by putting an addi-
tional set of four electrodes in a form of insulated rod
segments, one on each quadrupole rod, at the entrance
of the quadrupole. The short additional segments were
only supplied with rf voltages while dc and rf voltages
were applied to the quadrupole rods as shown in Figure
2.9. Because the dc fields are delayed along the in-
strument axis, this mode of operation is called "delayed
dc ramp" mode. For very slow ions, such as ions of high
mass and low ion energy, this mode of operation may be
very useful if high efficiency in transmission is de-
sired. Brubaker (65) compared the sensitivity of the
conventional and "delayed dc ramp" modes of operation
with his instrument. Krypton gas was used and Kr^+ (m/e =
84) was monitored. He reported that, typically, when
the "delay dc ramp" was used, the sensitivity for 15 eV
ions was increased by a factor of 6, for 8 eV ions by a
factor of 100 and for 4 eV ions by a factor of 200. The
improvement also depended to a small extent on the re-
solving power. Other workers (61) using this mode of
operation reported a much smaller improvement on sensi-
tivity (a factor of 6 for 4 eV ions). They argued that
it might be due to the more accurate construction and
alignment of the ion source that their sensitivity with
the conventional mode was much higher than that of

$+(V_0 \cos\omega t)$

$+(U+V_0 \cos\omega t)$

Instrument

axis (Z axis)

insulation separating additional electrode from rod

$-(U+V_0 \cos\omega t)$

$-(V_0 \cos\omega t)$
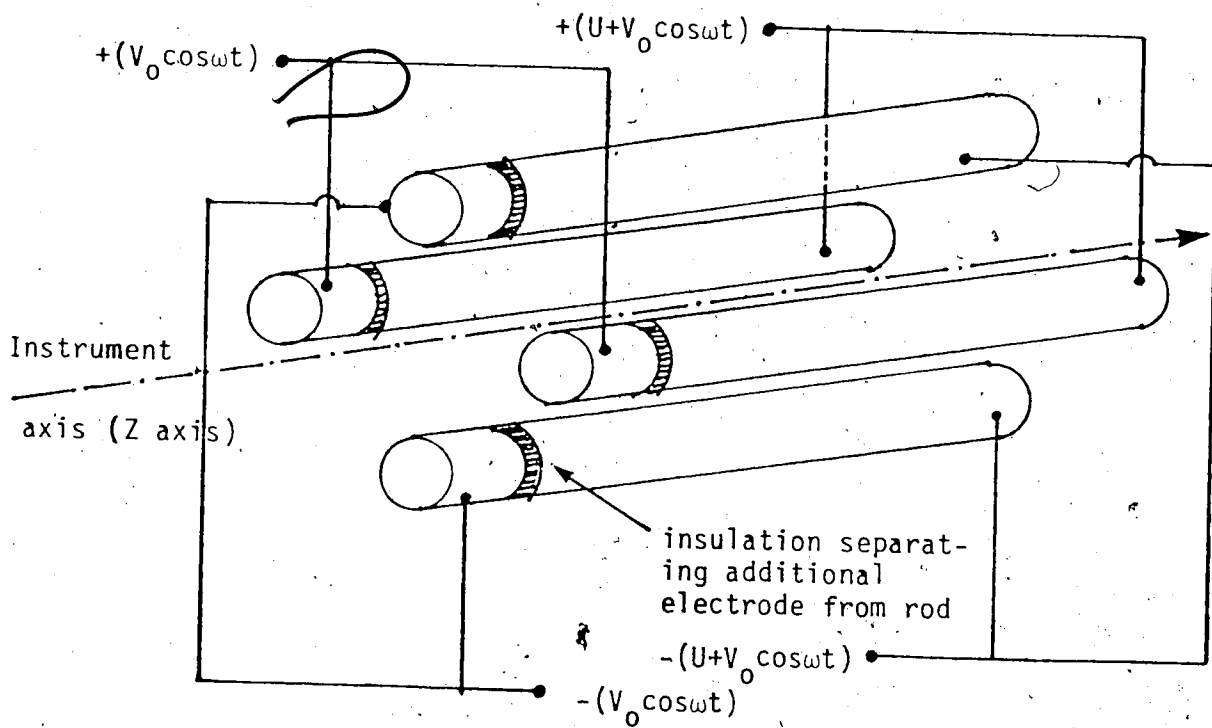
FIGURE 2.9 The quadrupole arrangement for "delayed DC ramp" mode of operation.

Brubaker's instrument. If that is the case, it would mean that the "delayed dc ramp" is of great value in remedying the misalignments in the source region.

Another later version of the "delayed dc ramp" mode which is easier to achieve experimentally was also suggested by Brubaker (66). In this modification, four small electrodes, one paired with each rod, were put ahead of the mass filter. Each electrode was supplied with an appropriate dc voltage of opposing polarity relative to its paired rod in order to partially nullify the dc field in the vicinity of the ion entrance aperture.

B. The Quadrupole Mass Analyser Used in the Present Study. The Measurement of Ion Transmission Efficiency of the Analyser.

There are several advantages in the quadrupole mass spectrometers over the conventional magnetic mass spectrometers. It is compact in size and less expensive. Its fast scanning speed and compatibility with computers make it an attractive analytical tool. Besides, it has no magnet, and consequently no stray magnetic fields which might interfere with adjacent apparatus is possible. Its main drawback is the susceptibility to the presence of fringing fields which would affect the ion transmission and the resolution attainable by the quadrupole mass spectrometer.

The quadrupole mass spectrometer used in the present system was a Granville-Phillips Spectrascan 750 Quadrupole mass filter. The quadrupole assembly consisted of four parallel cylindrical rods. The radius of the rods was 0.5 cm, their length 14 cm. The rods were arranged in such a way that the radius of the inscribed circle was 0.86 times the radius of the rods. This was done to approximate hyperbolic fields near the quadrupole axis with four circular rods. The quadrupole rods were housed in a grounded housing. The auxiliary (low pressure) ion source which came with the mass analyser was mounted in front of the housing. The quadrupole axis was always at ground potential. In general, an ion energy of 7 eV was used in the experiments. Mass scanning was achieved by varying the dc and rf voltages (U and V_0) at a fixed rf frequency, keeping the ratio U/V_0 constant. The resolution was adjusted by varying the U/V_0 ratio. Three mass ranges operating at three different frequencies were provided. They are: low mass (m/e : 1-50) at 5.5 megacycles per sec; medium mass (m/e: 10-250) at 2.6 megacycles per sec; and high mass (m/e: 100-750) at 1.5 megacycles per sec. As most ions investigated in this study had masses in between 15 amu and 250 amu, only the medium and the high mass ranges were used.

A special feature was incorporated in the quadrupole mass filter to allow ions of all masses to traverse

through the rods without mass separation. This was achieved
by switching off the dc voltage. Under this condition,
$a/q = 0$ (which is the ordinate in the stability diagram in
Figure 2.7), and ions of all masses will have stable tra-
jectories passing through the rods. A small rf voltage V_0,
is required to focus the ions into the quadrupole entrance.
All ions except those with masses much smaller than that
corresponding to the small value of V_0 are focussed into
the quadrupole aperture. Since the rf voltage V_0 required
is very small, essentially ions of all masses are trans-
mitted. This provision is useful in enhancing the sensi-
tivity if the quadrupole mass filter is used to monitor
the total pressure of a system.

Since no special modification was made on the present
quadrupole mass filter, discrimination against heavier
ions in transmission was expected. Therefore, the rela-
tive transmission efficiency for ions of different m/e
ratios had to be measured in order to correct for the
mass dependent transmission loss through the quadrupole
rods. The transmission factors were measured in the
following manner. Perfluorotributylamine, $((CF_3)_3C)_3N$
was used as a reference compound for calibration. It
was chosen because its major peaks spread over a wide
mass range. An electron impact mass spectrum for the
compound was run using the auxiliary low pressure ion
source with an electron energy of 70 eV. The typical

control settings used in the auxiliary ion source are shown in Table 2.2. The relative peak intensities (I_Q) of major peaks were measured as the percentage of the intensity of the most intense peak, CF_3^+ (m/e = 69). These were compared with the relative intensities (I_M) from the spectrum obtained from an A.E.I. MS-9 magnetic mass spectrometer operated with the same electron energy. The transmission factors, T.F., for different ion masses were expressed as:

$$T.F. = \frac{I_Q}{I_M} \qquad (2.35)$$

Since magnetic mass spectrometers have essentially no mass dependence on ion transmission within the mass range of interest, the transmission factors measured for different m/e values were the relative transmission efficiences for different ion masses. In the present experiments, only ratios of the intensity of the two ions participating in a reaction are of interest. The true ion intensity ratio may be calculated from the measured intensity ratio if the transmission factors for the corresponding ions are known. This is expressed in equation 2.36,

$$\left(\frac{I_1}{I_2}\right)_{true} = \left(\frac{I_1}{I_2}\right)_{measured} \times \frac{(T.F.)_2}{(T.F.)_1} \qquad (2.36)$$

where $\left(\frac{I_1}{I_2}\right)$ is the intensity ratio and the subscripts 1 and 2 indicate the two different ions. The transmission factors measured for different ions over a mass range was

TABLE 2.2

Typical Control Settings for Operating the Auxiliary Ion-Source

Ionizer Controls[b]	Settings	
Ionizing current	1mA	(Electron emission current)
Ionizing voltage	70V	(Potential difference between the filament [22][a] and the ion source [23][a])
Ion energy	7V	(Potential difference between the ion source [23][a] and the quadrupole [27][a])
Lens voltage	-98V	(Voltage of the lens [25][a])
Collector voltage	10V	(Voltage of the collectors [24][a])
Typical operating pressure	5×10^{-6} torr	
Resolution setting	460	

[a] Number refers to Figure 2.2. Cone [20] and focus lens [21] were grounded when the auxiliary ion source was used.

[b] When high pressure ion source was used, all electrodes in the auxiliary ion source were grounded.

joined by a smooth curve. From the transmission curve, transmission factors for ions of different m/e values may be obtained. The calibration procedure was done on the two operating (medium and high) mass ranges with different resolution settings. Typical transmission curves for the medium and the high mass range are shown in Figures 2.10 and 2.11. For the calibration of the medium mass range, trifluoroacetic acid (CF_3CO_2H) was also used as a secondary reference compound. It was used to check on the transmission factors in the lower mass scale. The transmission factors of ions from CF_3CO_2H obtained by comparing the quadrupole spectrum with the MS-9 spectrum were normalized to the factor obtained for CF_3^+ (m/e = 69) since it is a common ion in the spectra of CF_3CO_2H and $((CF_3)_3C)_3N$. Each transmission curve was obtained from the average of at least three runs. They were consistent to within 10%. Since the mass spectrum of a given compound may be fairly different when measured with different magnetic mass spectrometers due to different repeller fields and ion source extraction fields used, spectra of $((CF_3)_3C)_3N$ obtained from the A.E.I.MS-9 magnetic mass spectrometer and from the A.E.I. MS-2 magnetic mass spectrometer were compared. The agreement in the intensities of the major peaks among different spectra was in general within 30%. It is expected that the uncertainties in the transmission curves (Figures
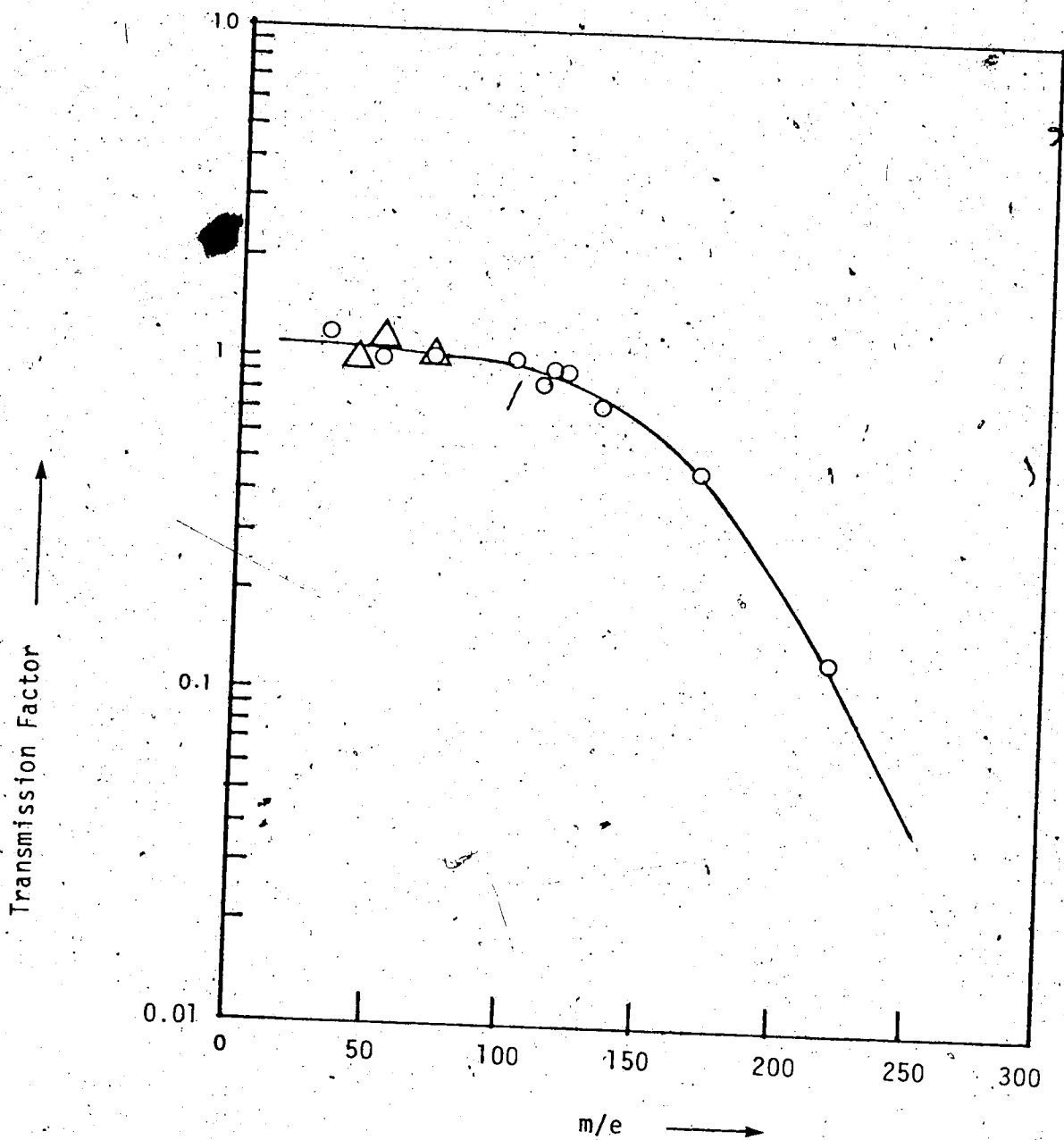
FIGURE 2.10 Transmission curve for the quadrupole mass analyser.
Medium mass range, resolution setting 460.
(O - ions from perfluorotributylamine,
 △ - ions from trifluoroacetic acid)
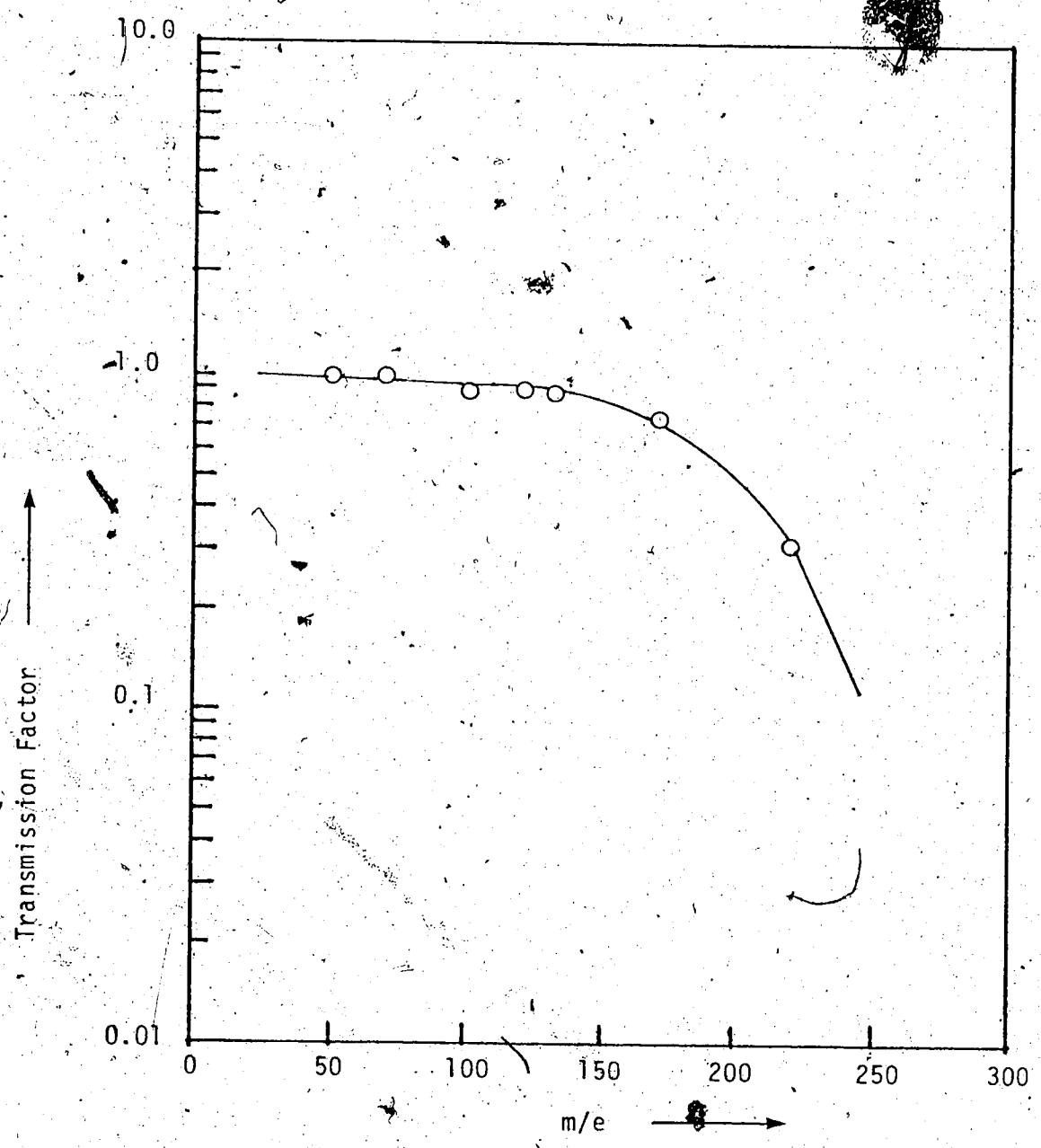
FIGURE 2.11   Transmission curve for the quadrupole mass
analyser. High mass range, resolution
setting 460. All ions from perfluorotri-
butylamine

2.10 and 2.11) are of similar magnitude. Since the masses
of ion pairs under study usually do not differ to a great
extent, the uncertainty on the ratios of transmission
factors used was estimated to be ±20%.

C. The Ion Detection System

The ions after mass analysis were detected by a Channel-
tron electron multiplier (CEM 4700) obtained from Galileo
Electro-Optics Corp. It consisted of a glass tube,the in-
side of which was coated with a high resistance film.
Comparing with the conventional multi-stage copper-beryl-
lium secondary electron multiplier, the Channeltron has
several advantages. It is insensitive to the exposure to
the air. It has a higher stability in the gain and the
gain dependency on ion mass is minimal (67). Furthermore,
the output pulses are of fairly uniform sizes. The uni-
formity in pulse heights allows one to set up a gate in
the amplifier discriminator such that only signal pulses
are accepted while the low level noises are rejected.
Typically, the Channeltron was operated with a gain of
10^6 which was obtained with an accelerating voltage of
2.5 kV across the two ends of the Channeltron. As the
Channeltron gets older, the gain attenuates and higher
accelerating voltages are required to achieve the same
gain. The Channeltron has to be replaced when its gain
drops below 10^4 with the maximum accelerating voltage of

3 kV.

The output negative pulses from the multiplier were amplified further by an amplfier before being counted. The pulse amplifier used was the SSR Model 1120 amplifier/discriminator from Princeton Research Corp. It had a rise time of 6×10^{-9} sec and a minimum gain of 2300. The amplifier/discriminator was designed to permit resolving electron pulses separated as little as 10^{-8} sec, with sufficient sensitivity to detect individual secondary pulses representing less than 10^{6} electron charges. The discriminator sensitivity had a range of 25 mV to 250 mV, and it allowed the setting of a gate level such that only the signal pulses were transmitted while the low level noise pulses were rejected. The amplifier/discriminator could be used for counting rates up to 10^{7} per second. This resolution was sufficient for the present system as the typical signal rate was only about 10^{4} per second. The output pulses from the amplifier/discriminator were fed into the SSR Model 1127 NIM adapter (from Princeton Research Corp.) which converted the discriminated pulses into uniform 5 volt, 10 nsec pulses. The uniform pulses were counted either with an Ortec Model 441 ratemeter and displayed on a chart recorder or with a multichannel scaler (Nuclear Data 2200). The typical noise level observed was about 10 counts per sec. The time dependence of the intensity

of an ion was observed with the multichannel scaler in the following manner. The start of the sweep of the multi-channel scaler was synchronized with the triggering pulse of the electron gun (Figure 2.5). In a typical experiment, the dwell time per channel of the multichannel was set to be 10 μsec, and 256 channels were used. The number of ions arriving at the detector in the first 10 μsec after the triggering pulse were stored in the first channel. The number of ions which arrived from 10 to 20 μsec were stored in the second channel and so on for 256 channels. In this way, the change in ion intensity was followed for 2.56 msec. After a period of 3 msec, the intensity of the ions had decayed by a factor of ~10^3. A positive repeller pulse relative to the ion source was applied in the ion source to remove all the remaining positive ions. The electron gun was then pulsed again and the whole process repeated. The content per channel was accumulated for the period of the collection time. It was found that a collection time of 60 second per ion would be enough to give a satisfactory temporal profile of the ion intensity.

2.10   Temporal Behavior of Ions and Treatments of Data

The temporal profile of positive ions involved in the ion-molecule equilibrium reaction 2.37 is shown in

$$H^+(benzene) + ethanol = benzene + H^+(ethanol) (2.37)$$
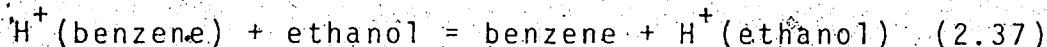
Figure 2:12, obtained with a mixture of 3.5 torr methane,
22.8 mtorr benzene and 1.75 mtorr ethanol in the ion source
at 327°C. Figure 2.12 gives a plot of the logarithm of
counts per channel against the time after the electron
pulse. The electron pulse width used was 20 μsec. The
primary ionization is expected to be mainly due to methane,
because this gas is present in much larger concentration.
As evident from Figure 2.12 both ethanol and benzene are
protonated by reactant ions from methane (CH_5^+, $C_2H_5^+$)
very shortly after the electron pulse. Proton transfer
between the protonated species and the neutrals then
follows. This kinetic stage is short ~100 μsec as is
evident from Figure 2.12. The relative intensities of
the two ions were treated as their relative concentrations
of the ions in the ion source. Since the concentrations
of the neutrals were constant in the ion source, the
establishment of equilibrium is indicated by the invari-
ance of relative ion intensities with time. This stage
is achieved after some 100 μsec in Figure 2.12 and
lasts over the remaining time of the observation. The
invariance of relative ion intensities between two ions
shows up as two parallel lines and the measured
equilibrium ion intensity ratio can be determined by
the vertical distance between the two lines.

The temporal profile of ions in Figure 12 deserves
some comments. The diffusion of ions to wall is the
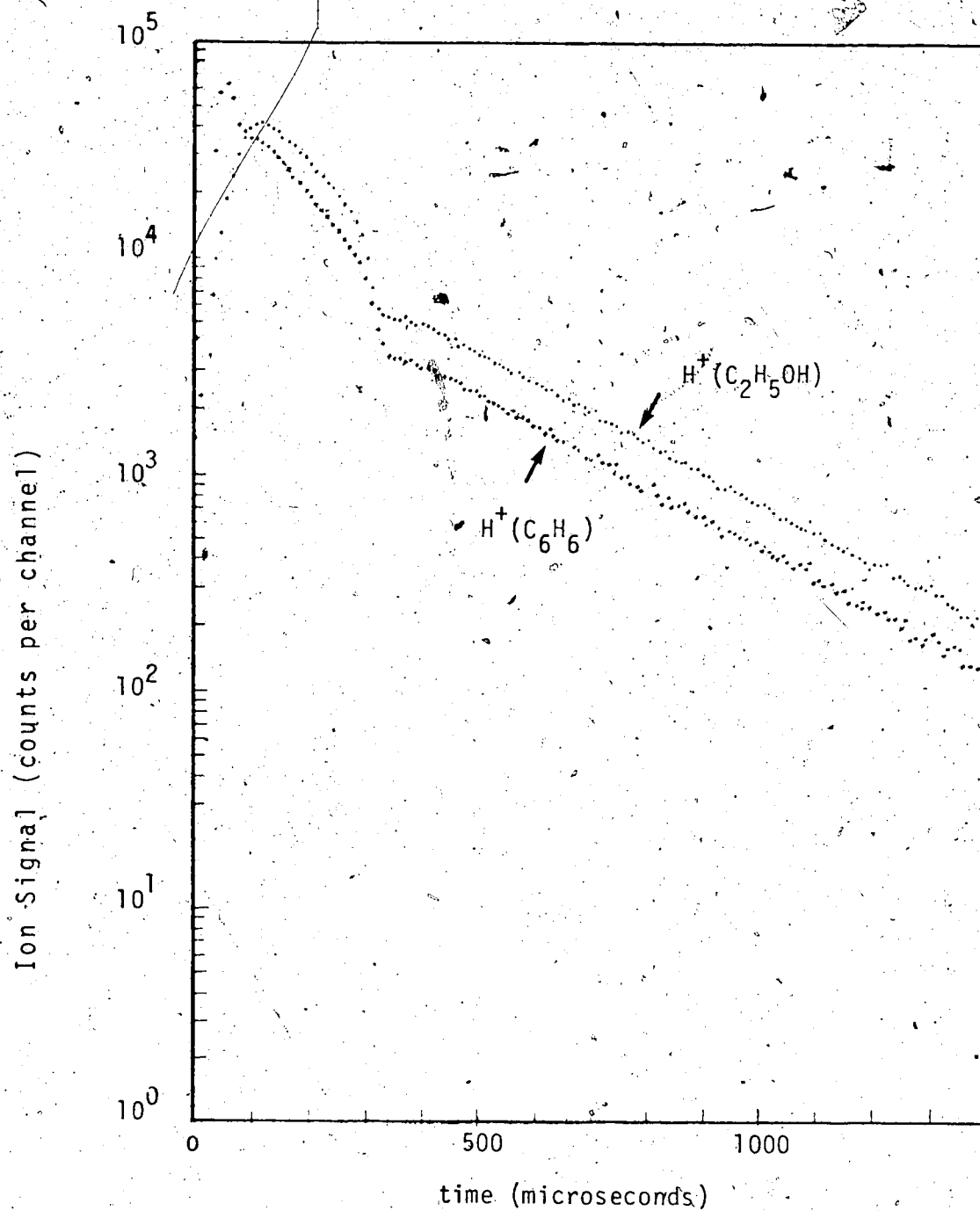
FIGURE 2.12. The time-dependence of ion intensities. Gaseous mixture in the ion source: CH_4 at 3.5 torr. C_6H_6 of 22.8 mtorr, C_2H_5OH at 1.75 mtorr. Temperature = 327°C.

major ion removal mechanism besides the ion loss due to ion molecule reactions. When equilibrium in reaction 2.37 is reached, there is no ion loss due to ion molecule reactions for $H^+(C_6H_6)$ and $H^+(C_2H_5OH)$. The ions are removed mainly by diffusion to the wall of the ion source. As it is shown in Figure 2.12, the decay of the positive ions may be broken into two stages. In the early stage, the ions are decaying a little faster. After about 0.3 msec, there is a sudden drop of ion intensities (by a factor of about 3). It is then followed by a slower ion decay. The rates of ion decay in the two stages are different by a factor of about 2. The observation can be qualitatively explained in the following manner: the high energy electron beam initially produces an equal number of positive ions and electrons. Any deviation from the charge equality will create an electric field as to oppose the charge separation and tend to restore the balance. Since the lighter electrons have a much higher diffusion coefficient than that of the ions (68, p.512), they will diffuse faster to the wall, leaving the positive ions behind. The resulting charge imbalance creates a "self field" which tends to cause the ions to diffuse with the electrons at a faster rate than they would in the absence of the field. Under this condition, both the ions and electrons diffuse at the same velocity and it is termed positive ion-electron ambipolar diffu-

sion. Ambipolar diffusion is important only when the charge density is higher than $10^7/cm^3$ (68, p.512). Below this level, the separations between charged particles are large enough that their interactions with each other are small compared with the thermal energy. The loss of electrons due to diffusion and formation of negative ions by electron capture finally causes the collapse of the "self field". It is observed as the transition point (at ~300 μsec) in Figure 2.12. The latter stage of the positive ion decay is due to the slower positive-negative ambipolar diffusion followed by free diffusion.

The coefficient of ambipolar diffusion D_a, is given (68, p.513) by the equation 2.38,

$$D_a = \frac{D^+ K^- + D^- K^+}{K^+ + K^-}$$

(2.38)

where D^+, D^- are the diffusion coefficients for the positively and negatively charged particles and K^+ and K^- are the mobilities of the corresponding species. In the case of positive ion and electron, $K^- \gg K^+$, equation 2.38 may then be approximated by equation 2.39.

$$D_a \approx \frac{1}{K^-} (D^+ K^- + D^- K^+)$$

(2.39)

Using the relationship 2.40 (68, p.491),

$$\frac{D}{K} = \frac{kT}{e}$$

(2.40)

where k is the Boltzmann constant, T is the temperature

in °K and e is the electronic charge, we may express the positive ion-electron ambipolar diffusion coefficient as:

$$D_a \approx 2D^+$$

when $T^+ = T^- = T_{gas}$. The diffusion coefficient for ions is of the same order of magnitude as that for the same neutral species in a given gas but lower by a factor of 3 to 5 due to the polarization effects (68, p.490), and it is inversely proportional to the square root of the reduced mass of the ion and the gas molecule (68, p.435). With methane as the gas medium which has a molecular weight of only 16, the diffusion coefficients of all ions studied in the present work are not significantly different. Under such conditions the positive-negative ion ambipolar diffusion coefficient could be assumed to be the same as the diffusion coefficient for free ions. As a result, the ion diffusion loss after the transition point is slower by a factor of two since $D_a \approx 2D^+$. This is in agreement with the temporal profile shown in Figure 2.12.

A further experimental confirmation of the analysis was done in the following manner. The identical gaseous mixture as in Figure 2.12 was used except that 2.0 mtorr of CCl_4 was added to the ion source. Other operating conditions were the same. The resulting temporal profile is shown in Figure 2.13. The addition of a small amount of CCl_4 induces the rapid conversion of electrons to
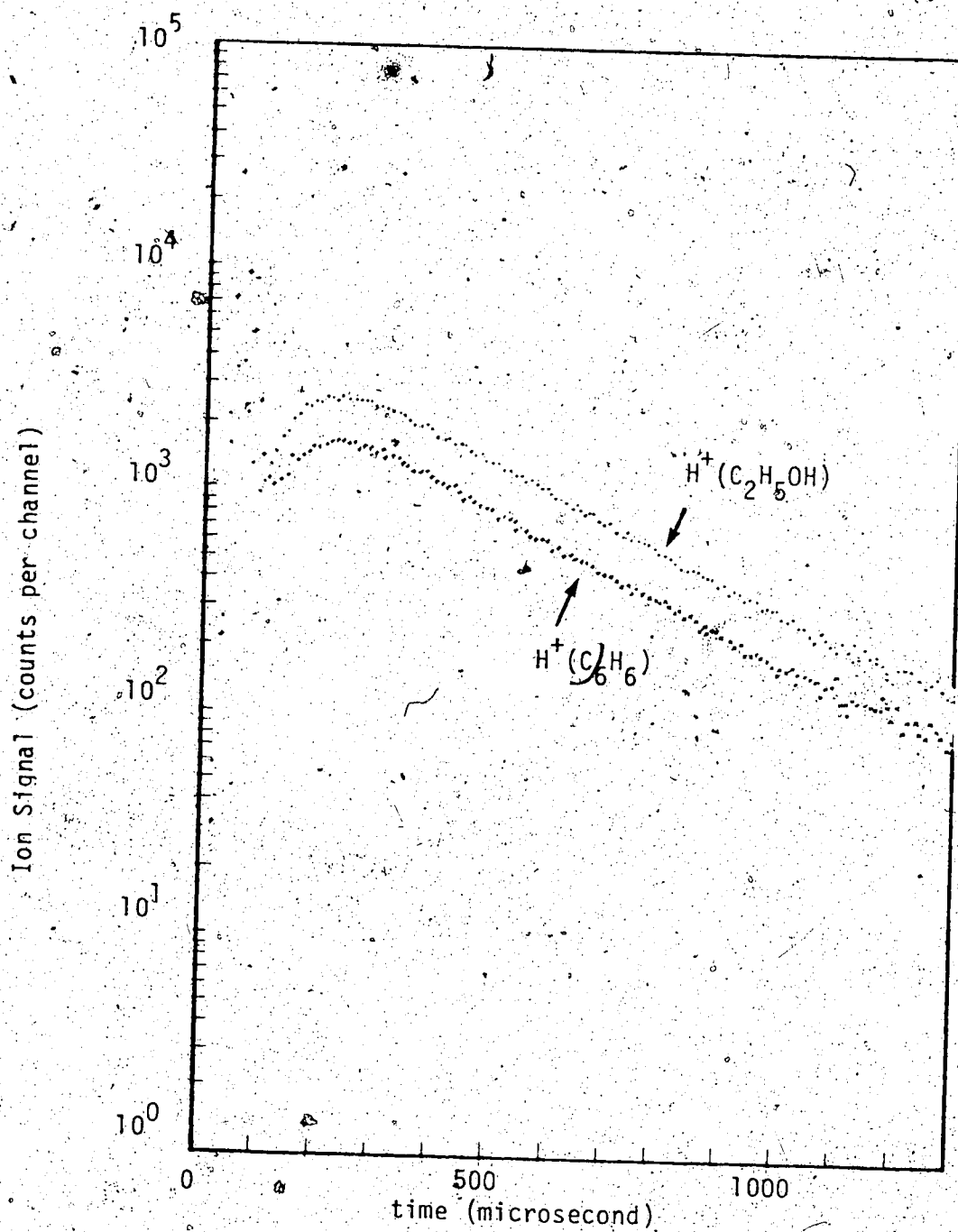
FIGURE 2.13. The time dependence of ion intensities. Gaseous mixture in the ion source: CH_4 at 3.5 torr, C_6H_6 at 22.8 mtorr, C_2H_5OH at 1.75 mtorr, CCl_4 at 2.0 mtorr. Temperature = 327°C.

negative ions by the dissociative electron capture
reaction 2.42.

$$e^- + CCl_4 = CCl_3 + Cl^- \qquad\qquad (2.42)$$
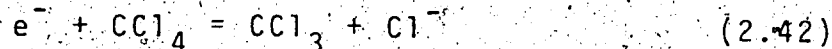
The rapid depletion of electrons quickly reduces the elect-
ron density in the ion source and eliminates the positive
ion-electron ambipolar diffusion stage. The slow and
uniform ion decays in Figure 2.13 indicates the absence
of ambipolar diffusion. The relative ion intensities of
the $H^+(C_6H_6)$ and $H^+(C_2H_5OH)$ after equilibrium is reached
in both experiments are the same as shown by the equal
spacings between the two ion decay lines in Figures 2.12
and 2.13. The equilibrium was attained in about 0.2 msec
after the electron pulse in both experiments. Since the
absence of the "self field" is more suitable in the study
of thermal equilibria, all measurements were carried out
in the presence of an efficient electron scavenger when
conditions permitted, i.e. when the presence of CCl_4 did
not lead to complicating positive ion-molecule reactions
involving CCl_4.

The equilibrium constant and the standard free energy
change for a proton transfer reaction were calculated from
concentration ratios of the neutrals and the ions. For
reaction 2.37 in the above experiment, the equilibrium
constant, K, is given by equation 2.43,

$$H^+(benzene) + ethanol = benzene + H^+(ethanol) \qquad (2.37)$$
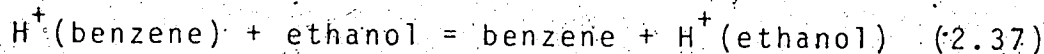
$$K = \frac{P_{benzene}}{P_{ethanol}} \times \frac{I_{H^+(ethanol)}}{I_{H^+(benzene)}} \qquad (2.43)$$

where the former term is the pressure ratio of the neutrals and the latter term is the intensity ratio of the ions. The pressure ratio of neutrals was 13.0. The ion intensity ratio was calculated from the measured ion intensity ratio in Figure 2.13 and the transmission factors obtained from Figure 2.10. Combining equation 2.43 and 2.36, we may write:

$$K = \frac{P_{benzene}}{P_{ethanol}} \times \left(\frac{I_{H^+(ethanol)}}{I_{H^+(benzene)}}\right)_{measured} \times \frac{(T.F.)_{H^+benzene}}{(T.F.)_{H^+ethanol}}$$

$$(2.44)$$

where T.F. is the transmission factor for the respective ions as defined in equation 2.35. Substituting numerical values into equation 2.44, the equilibrium constant was calculated to be:

$$K = 13.0 \times 1.63 \times \frac{1.0}{1.06} = 20.0$$

This is the equilibrium constant for the reaction at 327°C (600°K). The standard free energy change, ΔG_T^0, for the reaction is calculated by the equation $\Delta G^0 = -RT\ln K$:

$$\Delta G_{600}^0 = -\frac{1.987}{10^3} \times 600 \times \ln 20.0 \quad kcal/mole$$

$$= -3.57 \quad kcal/mole$$

The variation of ion intensities with time as shown

in Figures 2.12 and 2.13 is the result of ion-molecule re-
actions and other ion loss mechanisms. If we assume other
ion loss mechanisms affect all ions equally, the varia-
tion of ion intensities due to ion-molecule reactions
alone can be shown after "normalization". The normaliza-
tion procedure involves expressing the ion intensity of
a given ion at a given time, t, as the percentage of the
total ion intensity at time t. It represents the varia-
tion of ion intensities in the ion source in which the
total ionization is constant. Since ion diffusion to the
wall is the only major ion loss other than that due to
ion-molecule reactions and the diffusion coefficient for
ions does not differ significantly for the ions under
study, the assumption on normalization is approximately
valid. The temporal profile in Figure 2.13 after normal-
ization is shown in Figure 2.14. The attainment of
equilibrium is shown as the invariance of ion intensity
expressed in terms of the percentage total ionization.
The equilibrium ion ratio is the same as the one obtained
previously. Normalization is necessary if one wishes to
study the kinetics of ion-molecule reactions. It is not
necessary in the determination of equilibrium constants.
Most measurements in the present study were made without
normalization.

Some comments should be made on the very initial
part of the temporal profiles (Figures 2.12-2.13). No
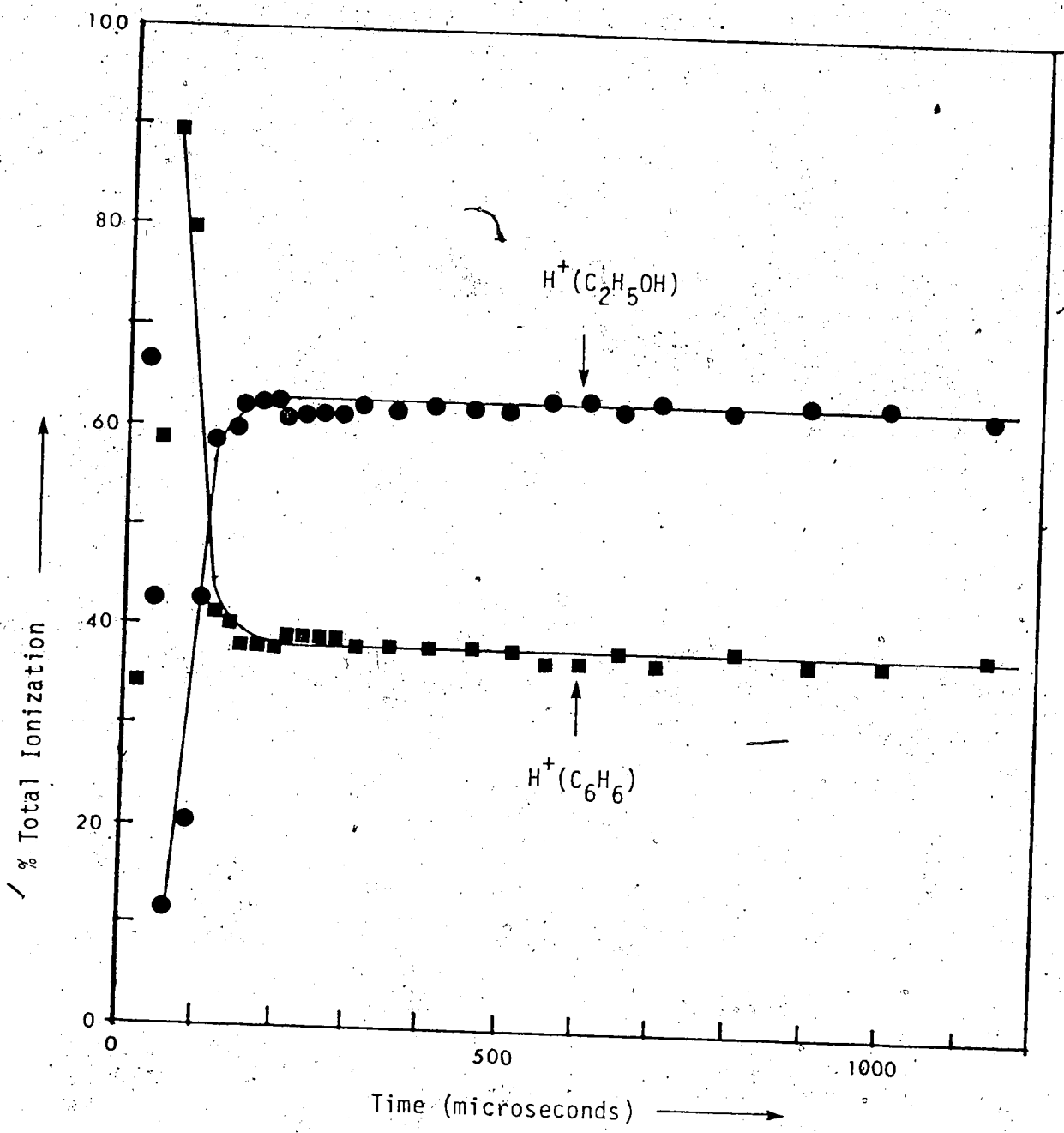
FIGURE 2.14. The time dependence of normalized ion intensities. Gaseous mixture in the ion source: CH_4 at 3.5 torr, C_6H_6 at 22.8 mtorr, C_2H_5OH at 1.75 mtorr, CCl_4 at 2.0 torr. Temperature = 327°C.

significance should be attached to the first some 50 μsec of the ion profiles. In this stage one observes effects which are due to the fact that the sweep of the multi-channel scaler was not delayed to make allowance for the electron pulse width and for the ion flight time from the ion source to the detector. The total ion flight time is the sum of the time required for the ion to travel from the ion source to the quadrupole and the time required for the ion to traverse the quadrupole rods. Both are mass dependent to a small extent. The flight time from the ion source to the mass analyser was estimated to be 1.0 $\sqrt{m}$ μsec (see section 2.9) where m is the molecular weight of the ion. The time an ion spent in the quadrupole can be calculated from the ion energy, the length of the rods and its molecular weight. With an ion energy of 7 volts and quadrupole rods of 14 cm, the flight time was calculated to be 3.8 $\sqrt{m}$ μsec. The total flight time is then 4.8 $\sqrt{m}$ μsec. For H^+(benzene) (m/e = 79) and H^+(ethanol) (m/e = 47), the total flight time is 43 μs and 33 μs, respectively. This implies that for the first some 30 μs, there should be no signal collected by the multichannel scaler. It is followed by 20 μs (electron pulse width) in which the electrons are entering the ion source causing the formation of ions all the time. Therefore, the ion intensities in the first 50-60 μsec are more complex and not useful for kinetic or equilibrium measurements. For some unknown reasons, small

signals are collected even as early as 10 μsec after the electron pulse (see Figures 2.12 and 2.13). The mass dependence on ion flight time is not significant in the present work as most ion pairs under study are within a limited range of molecular weights. The difference in their flight times is usually within 20 μsec. As it is shown in Figures 2.12 and 2.13 the variation of ion intensities within 20 μsec is insignificantly small after the equilibrium is reached. Therefore, no correction is made on the flight time for ions of different masses.

2.11 Experimental Procedures

The samples were prepared in the gas handling plant (see Figure 2.4). Typically, about 700 torr of methane was introduced into the 5 liter storage bulb. Liquid samples were mixed thoroughly, where permissible, before injection to the bulb. The ratio of the neutrals was calculated from weight measurements. Solid samples were introduced into the bulb through the solid inlet port. Whenever gaseous samples were used, they were introduced into the ballast bulb prior to the admission of methane gas. For equilibrium measurements on proton transfer reactions, the concentration ratios of the neutrals, B_1/B_2, were chosen so as to make the ion intensity ratio, B_1H^+/B_2H^+, not to exceed one order of magnitude if possible. The neutral ratio, B_1/B_2, was varied by a factor of 10

to 20 in different runs to ensure that the equilibrium
constants measured were invariant with the concentration
ratios of the two bases. For each individual neutral ratio,
equilibrium constants were determined at different ion
source pressures from 1 to 5 torr. The equilibrium con-
stants were also shown to be invariant with the changes
in ion source pressure. The typical concentrations of
the bases in the ion source were in the range of 1-200
mtorr depending on the volatilities of the bases.

The methane gas used was the ultrahigh purity grade
from Matheson. Other samples were from commercial sources
unless otherwise specified. Their purities were assessed
mass spectrometrically with the auxiliary ion source and
the quadrupole mass analyser. Further purification of
sample by distillation was done only when necessary.

2.12 Description of the Second High Pressure Mass Spectro-
meter.

The mass spectrometer described in the previous
sections was used for all measurements given in the
Results part of this thesis. Since that instrument had
been largely assembled by Dr. R. Yamdagni, the present
author, in order to obtain additional instrumental ex-
perience, was required to assemble a second mass spectro-
meter. The second high pressure mass spectrometer was
a modified version of the mass spectrometer designed and

used by Durden (54). A new Extranuclear Model #4-324-9

quadrupole mass filter was used as the mass analyser.

The quadrupole rods were larger in size than those of

the previous quadrupole mass analyser. Its attainable

resolution and sensitivity were superior. The design

of the second high pressure mass spectrometer was very

similar to the first one except for the electron gun

and the mass analyser. Therefore, only these two

components and the overall operation would be described

here.

The electron gun used in the second apparatus was

modified from Durden's design (54). A schematic diagram

of it is shown in Figure 2.15. The only modification

made was on its pulsing circuitry. The electron beam

was pulsed by varying the potential of the drawout

electrode as described in section 2.7 instead of varying

the potential of some deflection plates at the far end

of the electron gun as used by Durden. The major dif-

ference in the design of the first (see section 2.7)

and the present electron gun was in the focussing of the

electron beam. The electron beam in the first electron

gun was focussed by electrostatic fields whereas in the

present electron gun, it was focussed by electromagnetic

fields. Stronger focussing effects are acheived by

magnetic fields resulting in higher intensity of the

electron beam in the ion source.
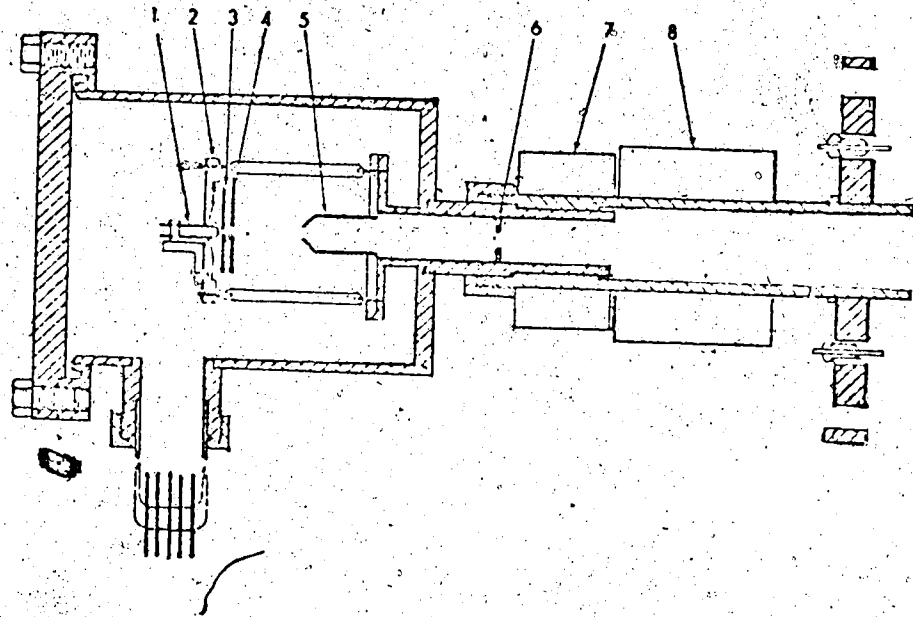
1. Electron filament
2. Filament support plate
3. Drawout electrode
4. Extractor electrode
5. Grounded cone (electron acceleration electrode)
6. Grounded collimating plate
7. Solenoid coil providing axial magnetic field for electron focussing
8. T.V. yoke for horizontal and vertical motion of the electron beam.

FIGURE 2.15 The electron gun for the second apparatus.

During the operation of the electron gun, the center of the filament [1] and the filament support plate [2] were at -2kV. Electrons from the heated filament were accelerated between the support plate [2] and the drawout electrode [3]. They were then slightly focussed by the extractor electrode [4] before being accelerated towards the grounded cone [5]. The electron beam was focussed by the solenoid coil [7] (1,000 turns of 22 AWG copper wire with 0.2 to 1.5 amps generally required for focussing). Horizontal and vertical positioning of the electron beam to the ion source was achieved by a television tube yoke. The solenoid of the yoke was controlled by a low voltage (7 volts) gas chromatograph dc supply modified to give two independent outputs. The solenoid coil [7] and the yoke [8] were put outside of the vacuum envelope. The vacuum envelope within them were made of brass to minimize the disturbance of the magnetic fields. The typical operating voltages of the electron gun are shown in Table 2.3.

The pulsing of the electron beam was achieved in the same way as described in section 2.7. The potential of the drawout plate was kept at some 45 volts negative with respect to the filament most of the time except in some regulated short periods of time (5-140 μsec) when its potential was brought to some 45 volts positive to that of the filament. The electron beam was allowed to pass through the drawout plate and be focussed into the ion

Table 2.3   Typical operating settings for the electron gun

Electrodes[a]	Voltage (volt)	Current
1. Filament	-2000^b	
2. Filament support plate	-2000^b	
3. Drawout	-1955	
4. Extractor	-1700	
5. Cone	0^b	
6. Collimator	0^b	
7. Solenoid choke (focussing)		1.0 A
8. T. V. yoke		
X deflection		3.3 mA
Y deflection		1.0 mA

Meters Readings		
Filament current	3.7 A	
Emission current	90 µA	
Case current	78 µA	
Trap current	1.4 µA	

[a] Numbers refer to Figure 2.15

[b] Fixed voltages on the electrodes. Others were variable.

source only when the drawout plate was at a positive potential with respect to the filament. The pulsing of the electron gun was synchronized with the sweep of the multichannel scaler.

The quadrupole mass analyser was from Extranuclear Laboratories. The mass filter composed of four circular rods, each with a diameter of 1.90 cm and a length of 22 cm. The distance, $(2r_0)$ between two opposing rods was 1.644 cm. The larger rod diameter used in the mass filter increases the ion entrance aperture and thereby enhances sensitivity. The longer rods used in the instrument result in better resolution and higher ion energy handling ability since the number of rf cycles the ions are exposed to increases proportionally with the rod length. The rf/dc supplied to the quadrupole rods were produced by the power source of the Quadrupole Control unit. A High-Q Head which is a tuned transformer was used to step up the rf voltage produced by the power source to a level suitable for driving the mass filter. The frequency of operation was 1.2 MHz. The maximum rf voltage output from the power source was 2.85 kV and the theoretical mass range spanned from 1 to 400 amu. A (low pressure) auxiliary ion source also came with the unit. It was mounted in front of the quadrupole rods. The auxiliary ion source was used to produce low pressure electron impact mass spectra and it was powered by an AEI ionizer power supply

together with some external voltage sources. An entrance cone was mounted in front of the auxiliary ion source for extracting ions from the high pressure ion source to the quadrupole mass analyser during the operation of the high pressure ion source. A schematic diagram of the quadru- pole is shown in Figure 2.16. Typical potentials on various ion accelerating plates for operations with the high pressure ion source and the auxiliary low pressure ion source are shown in Table 2.4.

The control of the resolution of the instrument was slightly different from the one described in the previous section. According to the stability diagram 2.7, resolution $\propto U/V_0$, and the dc and rf voltages (U and V_0) are linearly related for a fixed resolution setting. The resolution of a quadrupole mass filter may be varied in a more versatile mode by changing the linear proportion- ality between U and V_0 into a form as shown in equation 2.45, where γ and δ are constants. Since the resolution

$$U = \gamma V_0 - \delta \qquad (2.45)$$

R of a quadrupole mass filter operating near the tip of the stability diagram 2.7 was derived in section 2.9, as given in equation 2.29, on substituting equation 2.45 into 2.29, an expression for the resolution under this condition is obtained. This is given in equation 2.46. At constant
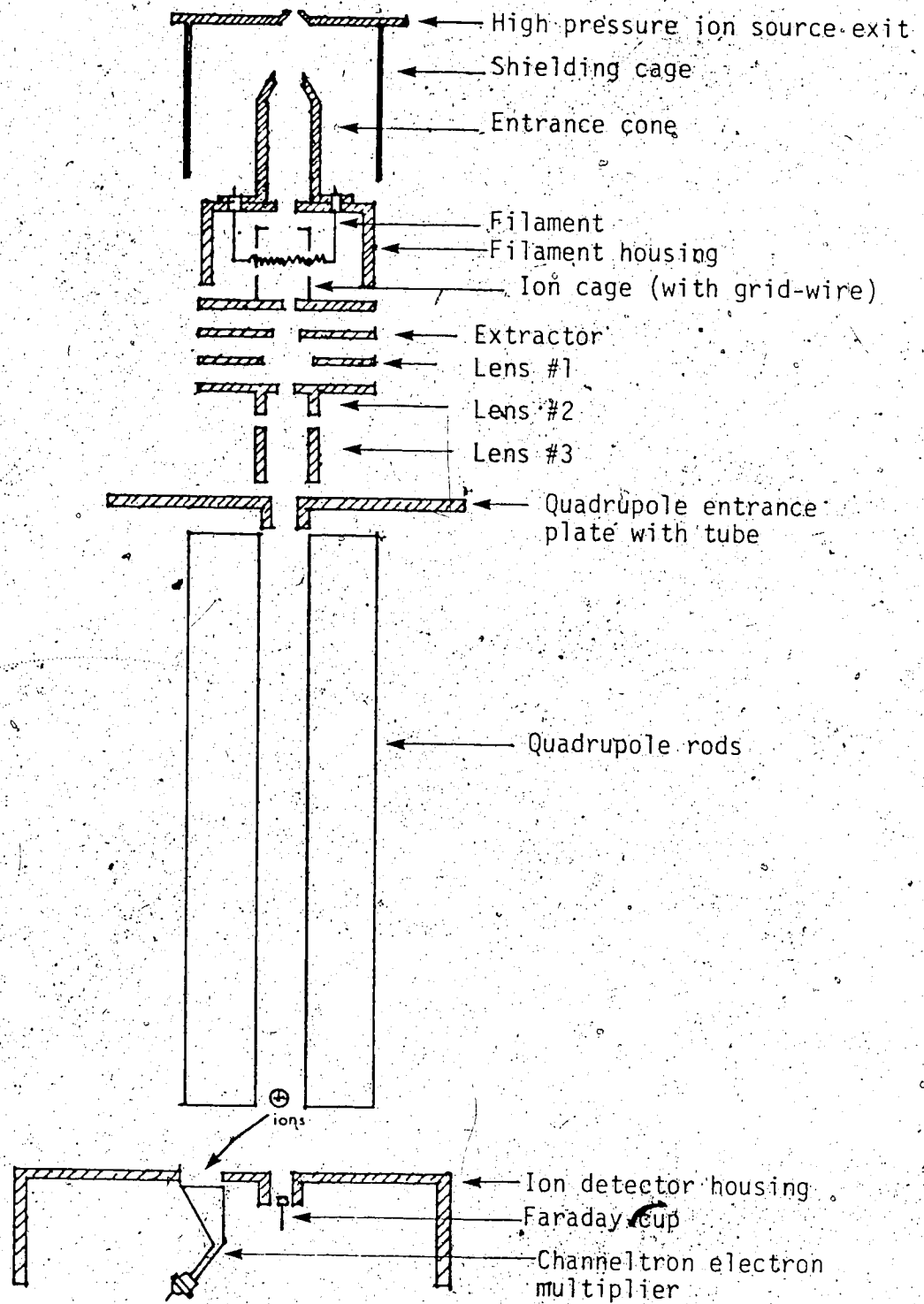
FIGURE 2.16   Quadrupole assembly

Table 2.4 Typical potentials on ion acclerating plates
during the operation with high pressure ion
source or auxiliary low pressure ion source

Electrodes	High pressure source in operation	Low pressure source in operation
High pressure source and shielding cage	+ 7 V	grounded
Entrance cone, filament and filament housing	-250 V	-63 V (provide 70 eV electrons)
Ion cage	grounded	+ 7 V
Extractor	grounded	+10 V
Lens #1	grounded	+ 3 V
Lens #2	grounded	0 V
Lens #3	-45 V	-60 V
Quadrupole entrance	grounded	grounded

Quadrupole power supply control (common to both operations)

Resolution	580 on dial	
ΔM	+1 volt	
Pole bias	0 — +3 on dial	

$$R = \frac{\bar{m}}{\Delta m} = \frac{0.125}{(0.168 - U/V_0)} \qquad (2.29)$$

$$R = \frac{\bar{m}}{\Delta m} = \frac{0.125}{(0.168 - \gamma) + \delta/V_0} \qquad (2.46)$$

U and V_0, two modes of operation are then possible. (a) If $\delta = 0$, U is proportional to V_0 and the normal constant $\bar{m}/\Delta m$ resolution mode is operative. (b) If γ is set to be 0.168 (U/V_0 ratio at infinite resolution on the stability diagram 2.7), $\bar{m}/\Delta m$ will be proportional to V_0 which in turn is proportional to $\bar{m}$. Under this condition, the mass filter is operating with a constant Δm mode. According to the definition of resolution $R = \frac{\bar{m}}{\Delta m}$, the resolution increases with mass. In the Extranuclear quadrupole mass analyser, provisions were given to vary the two parameters, γ and δ. The former parameter, γ, could be adjusted through the "Resolution Setting" dial and the latter, δ, through the "ΔM" dial. Theoretically, we could then vary the resolution mode between the two extremes. In practice, the constant $\bar{m}/\Delta m$ mode was not achieved due to field imperfections. The normal resolution mode chosen was closer to constant Δm mode with only slight increase of Δm with mass. It was to ensure that mass separations were similar over the whole mass range. With the typical settings as shown in Table 2.4, the Δm value increases from 0.3 amu to 0.6 amu in going from $\bar{m} = 10$ amu to $\bar{m} = 250$ amu.

The potential of the Extranuclear quadrupole axis was normally at ground but it could be adjusted positively or negatively. The provision of the "Pole Bias" control allowed the potential to which the poles were referenced to be varied between ±8 volts relative to ground. This small adjustment was useful in reducing the broad foot and asymmetric appearance of mass peaks in high resolution by suppressing the escape of scattered ions from the filter. It also permitted the establishment of dc fields to counteract the rejection of desired ions as they passed through the fringe fields in entering the mass filter. Examples of mass scans with different pole bias voltages are shown in Figure 2.17. As evidenced from the figure, a higher pole bias voltage improves the appearance of peak shape for the lower mass ion while a lower pole bias voltage enhances the sensitivity for the higher mass ion.

A Channeltron electron multiplier (CEM 4700) was used as the ion detector. The Channeltron was offset, but parallel to the line of exit of ions from the mass filter (see Figure 2.16). Since the surface of the Channeltron was maintained at a high negative potential (-2.5 kV) relative to the quadrupole axis, the ions coming out from the exit of the quadrupole were sucked into the multiplier. The "off axis" arrangement reduced the background noise level as all neutral species would

(i) m/e = 264

Pole bias = -2V   Pole Bias = 0V   Pole Bias = +2

(ii) m/e = 69

Pole Bias = -2V   Pole Bias = 0V   Pole Bias = +2V
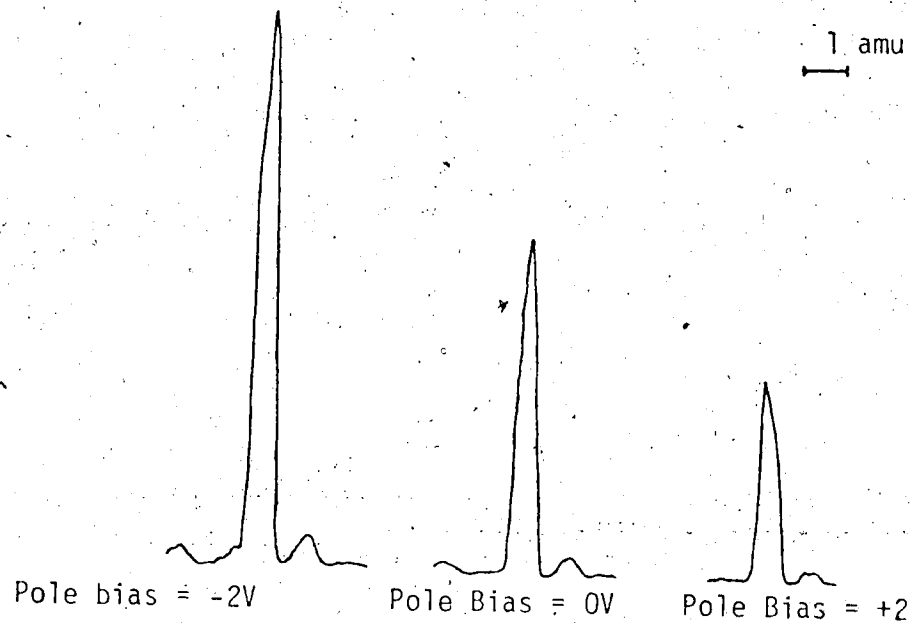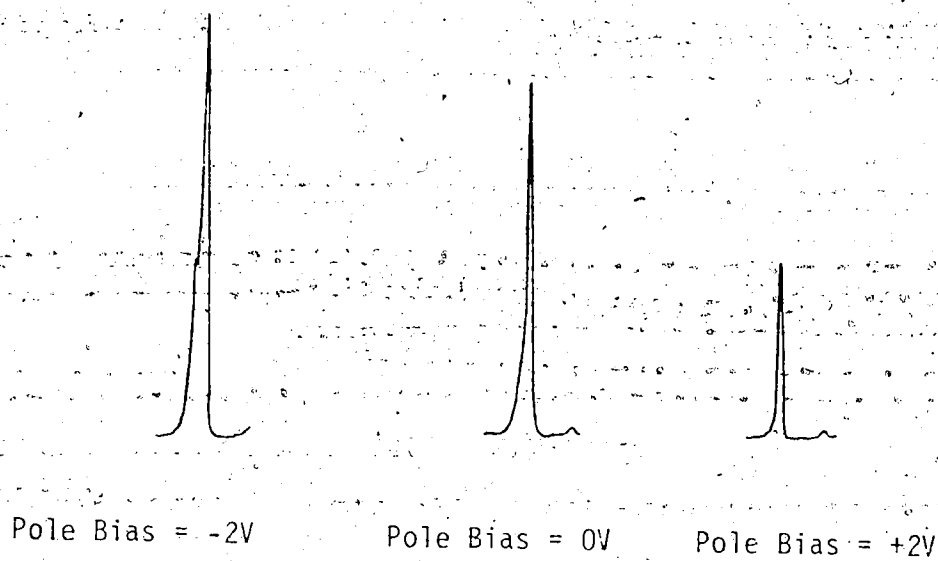
FIGURE 2.17 Effects of Pole Bias Voltage on Peak Shape. [(i)

$C_5F_{10}N^+$ (ii) CF_3^+ from perfluorotributylamine,

low pressure ion source was used, other operating

parameters as in table 2.4].

exit through the "on axis" hole without striking the elect-
ron multiplier.

The mass dependence on ion transmission through
the mass filter was determined in the same way as des-
cribed previously in section 2.9. Very large discrimina-
tion against heavier ions on transmission was observed.
With typical operating conditions as shown in Table 2.4,
the relative ion transmission dropped by about three
orders of magnitude going from m/e = 30 to m/e = 250 as
shown by the solid line in the transmission curve in
Figure 2.18. The large mass discrimination on ion trans-
mission is very undesirable in quantitative studies of
ion intensities as it imposes large uncertainties in
measurements. Mass discrimination on ion transmission
was expected as the instrument was operating in a mode
in which the resolution increased with the ion mass.
But the large difference in transmission efficiency
between heavier and lighter ions was also partly caused
by the difference in the time spent in the fringe fields
among ions in entering the mass filter. With a fixed
ion energy for all ions, the heavier ions will traverse
more slowly than the lighter ions along the quadrupole
axis, and they will spend longer time in the fringing
fields. A method to balance out this effect is to vary
the pole bias voltage with mass. If the quadrupole
poles are positively biased, positive ions entering the
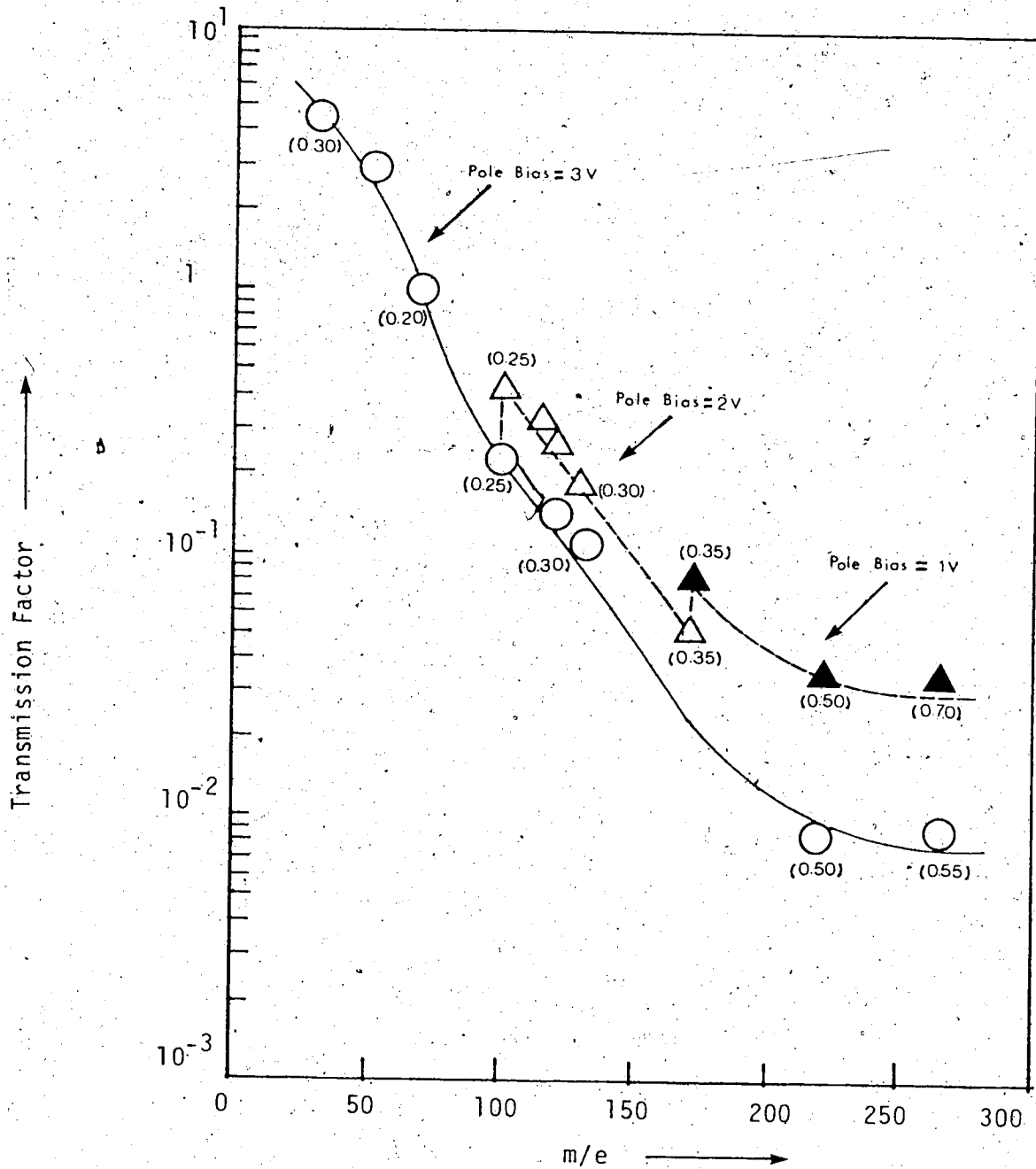
FIGURE 2.18   Transmission curves for Extranuclear quadrupole mass
filter.   Solid line: pole bias = +3V; dashed line:
pole bias varied as indicated; resolution setting: 580.
ΔM setting: + 1V; Δm in amu for mass peaks are shown
in parenthesis.

mass filter will be "retarded". By retarding the lighter ions to a higher degree, the difference in time spent in the fringe fields by all ions would be similar. Ions will then travel along the quadrupole axis with energies determined by the potential difference between the ion source and the pole axis. An experiment same as described in Section 2.9 was carried out to measure the transmission factor as defined by equation 2.35 for various m/e ratios. Increasing pole bias voltage was used for lighter ions. For convenience in operation, the mass scale of interest was divided in three ranges; m/e: 30-100, pole bias = +3V, m/e: 100-170, pole bias = +2V, m/e: 170-265, pole bias = +1V. The ion source voltage used was +9V so the ion energies vary from 6 - 8 eV for different ions. The normalized transmission curve obtained is shown by the dashed line in Figure 2.18 alongside with the resolution expressed in terms of Δm, the peak width measured at 10% of the maximum peak height. As it is shown in Figure 2.18, the mass discrimination on transmission is still considerable under such conditions, especially in the mass range between m/e 30-100. It is expected that if the lighter ions in that range were retarded more, the mass dependence on transmission would be less. Further reduction on the mass discrimination may be achieved if the pole bias voltage decreases continuously with the increase in ion mass instead of in stepwise variations,

but a better calibrated control must be installed for voltage variations if reproducible results are to be obtained.

An experimental confirmation of the above suggestion was carried out. Instead of varying the pole bias voltage, transmission factors were determined under the conditions that the ion source potential was varied with the ion mass while keeping the pole bias voltage at 0V. All other conditions were the same as before. The ion source voltages for different ion masses were chosen so that minimum transmission discrimination occurred but individual ions still had acceptable peak shapes. The resulting voltages for different ions are shown as triangles in Figure 2.19. The corresponding transmission factors are shown on the transmission curve in Figure 2.20. As evident from Figures 2.19 and 2.20, the mass discrimination on ion transmission can be corrected by increasing the ion source voltage with ion mass. Based on the above results, a scheme was set up, in which the transmission factors for different ions were measured at ion source voltages linearly proportional to their masses (45 mV/amu). The voltages used for different ions are shown as circles in Figure 2.19, and the resulting transmission curve in Figure 2.20. Under such conditions, the transmission efficiency varied by a factor of about 3 in a mass range of 40-250 amu. Although
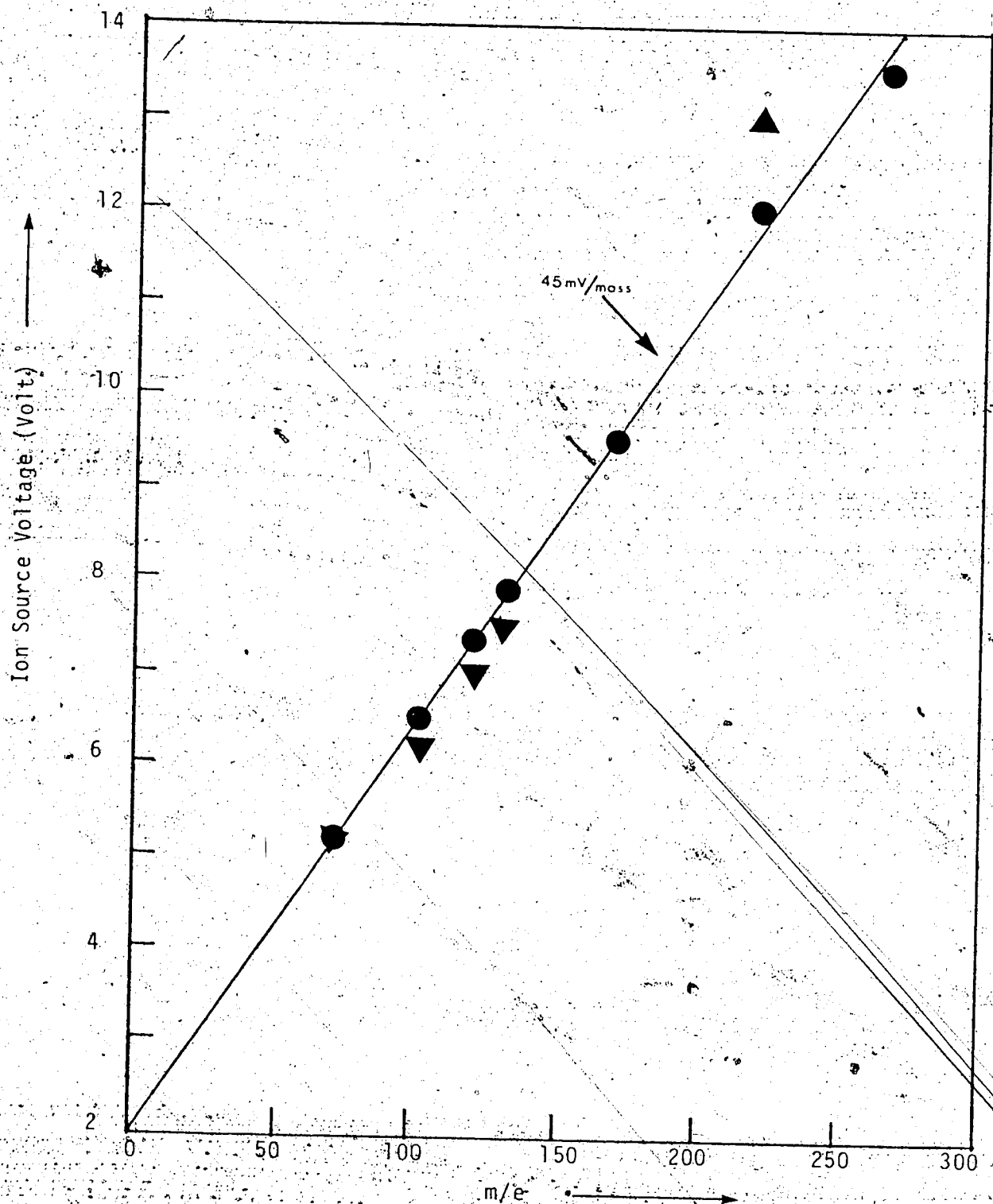
FIGURE 2.19   Optimum Ion Source Voltages for Ion Transmission.

Triangles: Optimum voltages

Circles: Optimum voltages by linear approximation
            between ion source voltage and ion mass

(Resolution: 580, △M: +1V, Pole bias: 0V)
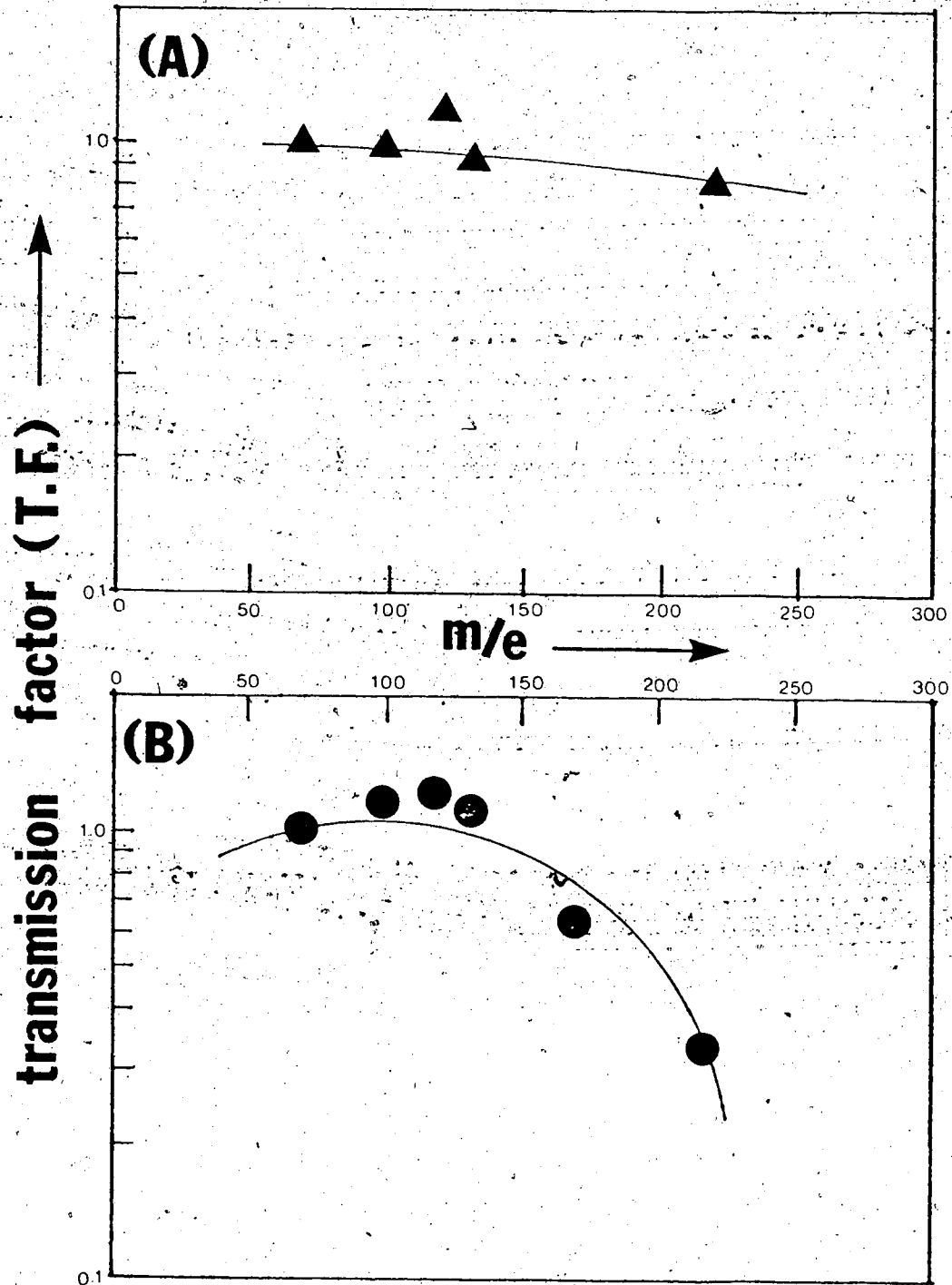
FIGURE 2.20 Transmission Curves with Optimum Ion Source Voltages.

(A) Optimum voltages

(B) Optimum voltages by linear approximation between ion source voltage and ion mass

(Resolution: 580, ΔM: + 1V, pole bias: 0V)

this magnitude of variation in transmission efficiency is similar to that of the previous quadrupole mass filter used in the present work, it would be much better to operate in a mode in which the mass discrimination on transmission is minimum. A plan is underway to design a voltage source by which the ion source voltage can be varied in a nonlinear fashion with ion mass as shown by the triangles in Figure 2.19.

As a comparison, the Extranuclear quadrupole mass analyser does provide better resolution and sensitivity than the Granville Phillips mass analyser. Its ability to handle high energy ions is superior. Its large mass dependence on transmission suggests the presence of sizable fringing fields near the entrance of the mass filter. A continuous variation of ion energy with ion mass could be used to minimize the variation of ion transmissivity. Another alternative would be to modify the quadrupole to operate in a "delayed dc ramp" mode (65,66) as suggested by Brubaker. It would remove the instability imposed on the ion trajectories due to the presence of fringing fields.

2.13 Assessments of the System

A. Number of Ion-Molecule Collisions in the Ion Source

Although the proton transfer equilibria were measured in a field-free ion source, there would still

be excess energy in the reaction products initially because of the exothermicity of the reaction 1.13.

$$B_1H^+ + B_2 = B_1 + B_2H^+ \qquad (1.13)$$

The excess energy in the reaction products B_1 and B_2H^+ have to be removed by molecular collisions before they engage in the backward reaction if the thermal equilibrium constant is to be obtained.

The number of collisions of a molecule per second, Z, is given by equation 2.47 (69, p.44),

$$Z = \sqrt{2} n \bar{v} \pi d^2 \qquad (2.47)$$

where n is the number density of the gas, $\bar{v}$ is the average gas velocity, and d is the diameter of the molecule. The quantity πd^2 is termed the collision cross-section of the molecule. For methane (d = 4.1 x 10^{-8} cm) at a pressure of 1 torr at 300°K, a molecule will undergo about 10^4 collisions in 1 millisecond.

A charged particle will suffer somewhat more collisions because of the long range interactions between the charged particle and the permanent dipole or induced dipole of the neutral molecules. By taking the thermal orbiting rate constant k = 10^{-9} cm^3 molecule^{-1} sec^{-1}, it may be calculated that an ion would undergo about 10^7 collisions per millisecond at a pressure of 1 torr.

The quenching of the excess energy depends mainly on the collisions between reactive collisions. As the

concentration of the buffer gas (methane) was higher than those of the reactants by a factor of more than 100, the ions would suffer more than 100 collisions before entering into a reactive collision. The present results shown in the next chapter suggested that thermalization of ions were established under such conditions.

B. Ion Sampling

In the present experiments, it was assumed that the ion population outside the ion source was a true representation of the ion population inside the ion source where the reactions actually took place. The assumption is valid only if two conditions are met. (a) The diffusion coefficients of the ions are the same. (b) The gas flow through the ion source exit slit is molecular. The first condition is required to ensure uniform ion population ratios throughout the ion source, as probably only the flux of ions (i.e. ions arriving per unit time) to a region near the ion exit slit was measured. The diffusion coefficient of an ion is inversely proportional to the square root of the reduced mass of the ion and the gas molecule. With methane (M.W. = 16) as the buffer gas, the differences in reduced masses for different ions, which are of considerably higher molecular weight are usually insignificantly small. The second condition requires molecular flow of gases from the ion source to

the evacuated chamber. Under molecular flow, the ions effuse through the ion exit slit without colliding with another molecule and therefore no serious distortion on the ion population would occur. Molecular flow occurs when the dimensions of an orifice are smaller than the mean free path of the gas molecule, that is, the average distance a molecule travels between collisions. The mean free path, λ, is given by equation 2.48,

$$\lambda = \frac{1}{\sqrt{2}\pi d^2 n} \qquad (2.48)$$

where d is the molecular diameter of the gas and n is the number density of the gas. The mean free path of methane at a pressure of 3 torr at 300°K is 1.4×10^{-4} cm. The ion source exit slit had the dimensions of 1.5×10^{-4} cm x 0.1 cm. Therefore the flow through the ion exit slit should be near molecular.

The conductance of an orifice by molecular flow is proportional to $\sqrt{T/M}$ where T is the temperature and M is the molecular weight of the molecule in question. The viscous flow of a gaseous mixture from the gas handling plant to the ion source does not fractionate the gaseous mixture. As the gaseous mixture diffuses through the ion source exit slit by molecular flow, the lighter gas molecules will escape faster and the ion source will be enriched in the heavier gas molecules. To avoid the

enrichment of heavier components in the gaseous mixture, the ion source was continuously being exhausted by a mechanical pump through a capillary. In doing so, the ion source was replenished by a fresh, uniform gaseous mixture at all times. The size of the capillary was chosen so that the flow through the capillary was at least three times faster than the flow through the ion exit slit and the electron gun entrance slit combined. The relative flow rates may be compared by monitoring the pressure drop with time in the manifold of the gas handling plant after it is filled with a gas at 10 torr and is open to the ion source. Typical relative rates of pressure drop in a normal flowing system (slits and capillary open) and that through slits only are shown in Figure 2.21. At a pressure of 3 torr, the relative rates of pressure drop with and without the capillary were in a ratio of 4:1. This was enough to prevent the accumulation of heavier components in the ion source. As the rate of pressure drop is first order with respect to the pressure, P, in the ion source for molecular flow and second order for viscous flow, the straight line in the plot of log P vs time in Figure 2.21 indicated that the flow through the slits was indeed near molecular.

C. Ion Removal

The positive ions in the ion source may be removed by diffusion to the wall or by ion-electron recombination.
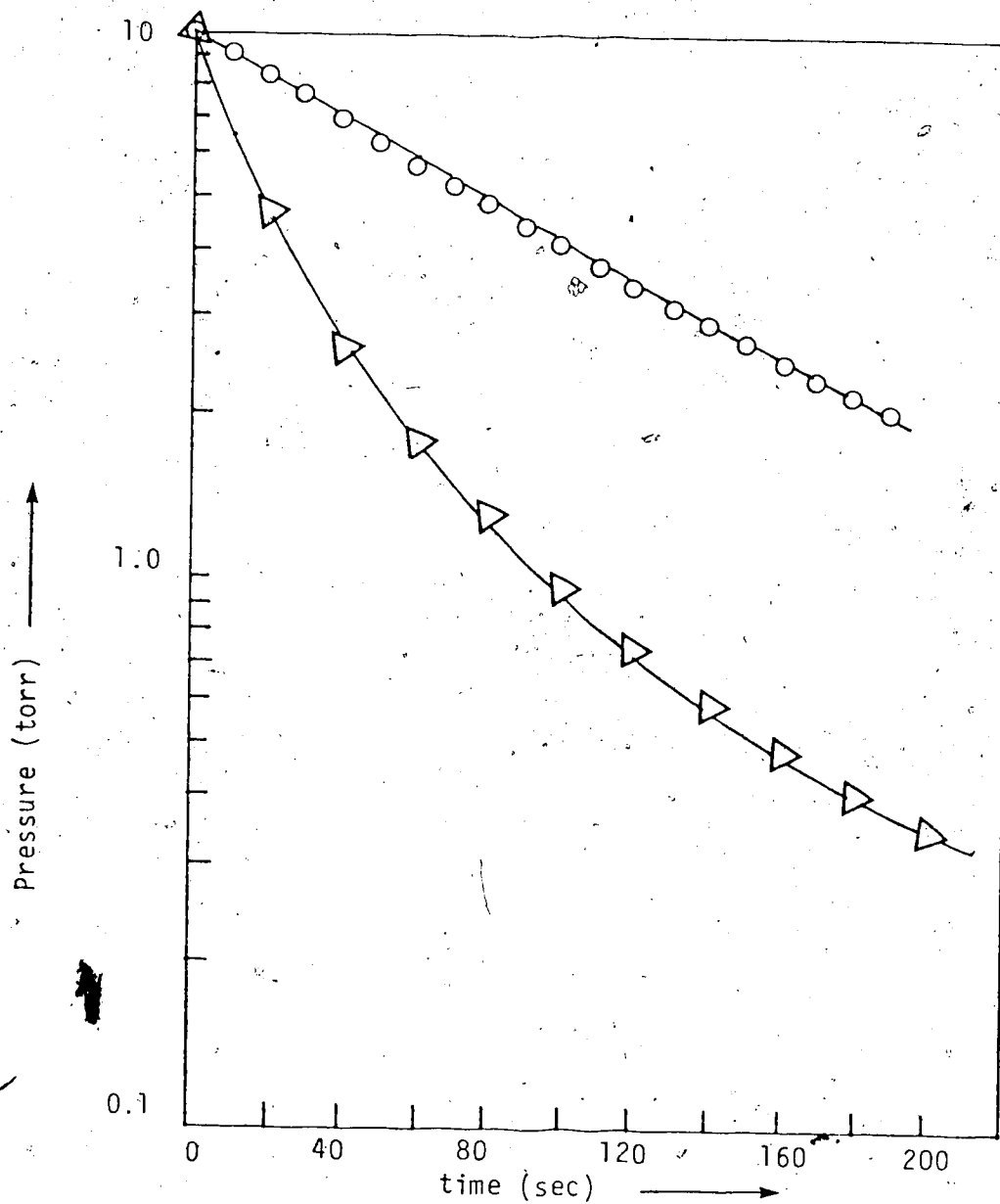
FIGURE 2.21 Rate of Pressure Drop in the Ion Source

O - flow through slits only

△ - flow through capillary and slits

The former is a first order ion loss mechanism and the latter is a second order process. Since the ion-molecule reactions studied are pseudo-first order, the kinetics of the reactions studied will be distorted if the second order ion electron recombination was important as an ion loss mechanism.

Treating the ion-electron recombination as a typical second order reaction and assuming that the initial number density of the positive ions and that of the electrons are the same, the half life of the reaction, $\tau_{\frac{1}{2}}$, is given by equation 2.49

$$\tau_{\frac{1}{2}} = [\alpha n_e]^{-1} \qquad\qquad (2.49)$$

where α is the recombination rate coefficient and n_e is the number density of the electrons. The values of α depend on the ionic species in question but is usually in the order of 10^{-6} cm^3 molecules^{-1} sec^{-1}. For CH_5^+ and $C_2H_5^+$ from methane, α has a value of 4.2×10^{-6} cm^3 molecule^{-1} sec^{-1} (70). The number density of electrons after each electron pulse is difficult to determine. Since the number densities of electrons and positive ions are the same, n_e may be estimated from the number of ions generated in one electron pulse and the ionizing volume. The number of positive ions generated per primary electron

in the ion source, I_p/I_e, is given by equation 2.50,

$$I_p/I_e = \alpha \ell n \qquad (2.50)$$

where α is the cross-section of ionization of the gas molecule, ℓ is the electron path length through the gas and n is the number density of gas molecules. The ionization cross-section of methane with 2kV electron is 2×10^{-17} cm^2 (71). The distance between the electron gun entrance slit and the electron trap was about 1 cm. At a pressure of 3 torr, the ratio of I_p/I_e was about 2. This implies that 2 ions were generated by every primary high energy electron. For each positive ion generated, a secondary electron is also formed. The average energy imparted on a secondary electron is about 70 eV (72). Assuming each of these electrons generated two extra ions before it was degraded to low energies (92), the number of ions produced by every high energy electron which entered the ion source was about 4. With a trap current of 0.5 μA, it may be calculated that in a 10 μsec electron pulse, about 3×10^7 electrons entered the ion source, therefore, about 1×10^8 ions were formed.

The volume of the ion source was about 1.5 cm^3. However, the ions were generated mainly along the electron path. Taking into consideration that the electron beam would spread on collisions with molecules once it entered the ion source and the secondary electrons might be

generated outside the electron beam, the ionization volume may be approximated to be 0.1 cm^2. The initial density of the ion was then about 1 x 10^9 cm^{-3}. Putting the values of α and n_e into equation 2.48, the half-life of the ion-electron recombination was about 0.2 msec. Since the half-life of the positive ion disappearance was about 0.1 msec (see Figure 2.14), one might suspect that the ion-molecule recombination was a significant loss mechanism in the system.

.A second look at the rate of diffusion of electrons would show that the average lifetime of electrons against collisions with the walls of the ion source was extremely short. The average time, τ, for a particle to diffuse to the wall of a container is given by equation 2.51 (68, p.493),

$$\tau \approx \frac{d^2}{D} \tag{2.51}$$

where d is the distance from the wall and D is the diffusion coefficient of the particle. The diffusion coefficient of electrons in methane at a pressure of 3 torr is about 10^4 cm^2 sec^{-1} (68, p.490). The distance between the ion source exit slit and the plane of the electron beam was about 0.1 cm which may be taken as d. The average lifetime of the electron was then calculated to be 1 μsec. This shows that the ion-electron recombination could only be significant in the inital few microseconds. The electron density dropped rapidly within

that period of time by diffusion to the wall. As the average lifetime of the electron against diffusion loss was shorter than the electron pulse width (~ 10 µsec), the presence of the second order ion-electron recombination in the initial period would not affect the kinetics of other first order processes after the electron pulse was "off". In a typical experiment, the kinetics and the equilibrium of a reaction were followed only some 20 µsec after the pulse, and more often after some 100 µsec.

The average lifetime of the ions against diffusion to the wall may be calculated using equation 2.49. Taking $D = 10$ cm sec^{-1} (68, p.490), a typical diffusion coefficient for ions under these conditions, the average lifetime of ions in the ion source was about 1 msec.

In conclusion, the ion diffusion to the wall is the only major ion loss mechanism in the present system. As the ion diffusion and the ion-molecule reaction are first order with respect to the ion intensity, they just have additional kinetic effects on each other. Assuming that the rate of diffusion is the same for all ions, the effect of ion diffusion on the variation of ion intensities can be removed by normalization as discussed in section 2.10, such that the kinetics of ion-molecule reactions may then be studied.

PRESENTATION OF RESULTS. THE GAS-PHASE BASICITY

LADDER AND THE PROTON AFFINITY SCALE

CHAPTER III

3.1 The Gas-Phase Basicity Ladder

The equilibrium constants for the proton transfer

reaction 1.13 involving amines, substituted benzenes,

$$B_1H^+ + B_2 = B_1 + B_2H^+ \qquad (1.13)$$
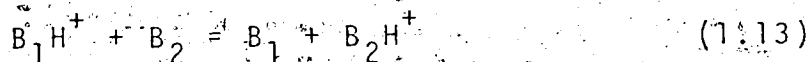
alcohols etc. as bases B were determined at 600°K. The

higher reaction temperature was chosen so as to avoid

the interference from the formation of protonated dimers

$(B)_2H^+$. These dimer ions can become the major ions at

lower temperature if the positive charge in BH^+ is loc-

alized in a few hydrogens as in the case of NH_4^+ or H_3O^+,

such that strong hydrogen bonding results. The experi-

mental results are summarized in Table 3.1 in which a

continuous ΔG° ladder of equilibria between water (low-

est basicity) and 1,8-bis(dimethylamino)naphthalene

(highest basicity) is shown. The ladder covers a span

of some 70 kcal/mole basicity difference and involves

some 50 bases. The ΔG°_{600} value for a given pair of

bases obtained by direct measurements is shown beside

the arrow linking the two bases. An average of three

thermodynamic cycles connect each compound to the

ladder. They are consistent to within ~0.3 kcal/mole.

123

Table 3.1. — Free Energy Changes of Proton Transfer Reactions[a]

Compound (B)	Directly Measured $-\Delta G^o_{600}$ [b]		($NH_4^+ + B = NH_3 + BH^+$) This work ΔG^{o}_{600} [c]	Literature ΔG^{o}_{600} [d]	ΔG^{o}_{300} [e]

Me₂N NMe₂ (structure)   -39.2

7.0*

Me₂N NHMe (structure)   -32.2

0.35*   4.35*

NMe₂ (structure)   -31.8

3.9*   6.0*

MeNH NHMe (structure)   -27.9

1.7*

NH₂(CH₂)₅NH₂   -26.2

3.1* 5.0* 4.7* 6.8*

Piperidine   -23.1   -23.7   -21.2

2.1* 3.5

H₂N NH₂ (structure)   -21.1

1.4*

NH₂ NH₂ (structure)   -19.7

2.1

Pyridine   -17.6   -17.8   -16.6

3.5   5.7

NH₂ (structure)   -14.0

4.0   7.7

o-Anisidine   -11.8   -14.3

1.7

Methylamine   -10.0   -10.8   -9.1

1.5

DMSO   -8.5   -7.2

1.6 3.0   4.3

Aniline   -6.9   -8.9   -6.7

1.3   2.9

Pyrrole   -5.6   -7.2

2.0 3.3   5.2

m-Chloroaniline   -3.6   -3.6

1.6   3.6

Acetophenone   -2.0   -0.8

2.0 3.6

Ammonia   0   0   0

2.3

n-Propyl acetate   2.3   2.2

Table 3.1 (continued)

125.

Compound			
n-Propyl acetate	2.3	2.2	
Anisole	2.7		
Diethyl ether	2.8	2.6	3.7
Benzaldehyde	3.0		7[f]
Benzoic Acid	5.5		
Methyl acetate	5.7	5.3	6.1
Ketene	6.3		6.7[g], 6.9[h]
Acetone	6.5	6.1	7.2
Benzonitrile	7.0		7[f]
Phenol	7.1		
Naphthalene	7.2		
Isobutene	8.1	7.7	8.6
t-Butanol	9.2		
n-Propyl formate	9.5	9.0	9.2
Nitrobenzene	9.5		
Ethyl formate	10.0	9.5	10.3
Ethylbenzene	11.1		11.6[i]
iso-Propanol	11.7		
Toluene	12.1		12.5[i]
Methyl formate	13.5	12.9	13.8
Acetonitrile	14.5	13.3	14.5
Ethanol	14.7	13.9	14.8
Acetaldehyde	16.1	15.3	16.5
Benzene	18.4	17.3	

Arrow labels (between columns): 0.35, 0.2, 0.25, 0.3, 3.6, 3.0, 3.2, 3.55, 2.7, 0.25, 0.9, 1.0, 1.5, 3.9, 0.2, 0.5, 1.4, 2.4, 3.6, 0.15, 2.5, 0.5, 1.6, 3.1, 3.0, 3.55, 1.7, 0.7, 0.9, 1.6, 1.1, 2.95, 0.55, 1.0, 2.3, 1.0, 2.2, 3.8, 0.45, 1.5, 0.8, 2.15, 0.4, 1.3, 4.25, 1.9, 2.55, 3.6

Table 3.1 (continued)

126

Compound							
Benzene						18.4	17.3
	0.8						
Fluorobenzene						19.2	18.2
	0.2	1.0		2.3			
Chlorobenzene						19.4	18.3
	0.3	0.5					
Methanol						19.7	18.6	19.3
		0.55					
m-Difluorobenzene						20.3	19.2
		0.3					
1,3,5-Trifluorobenzene						20.7	19.7
		2.9	3.5	5.3			
Formic acid						23.6	22.6	21.8
		2.5					
Malononitrile						26.1		24.2
	5.7	8.4		6.2			
Hydrogen sulfide						31.8	28.7	27.8
		0.9					
1,1,1-Trifluoroethanol						32.7		29.8
	0.2	1.85	2.9	1.1			
Trifluoroacetic acid						32.9	30.4	28.6
		1.8					
Water						34.7	31.8	31.4

a. All values in kcal/mole

b. Values with superscript (*) were done at 460°K, the rest at 600°K. $-\Delta G^o$ values refer to the reaction: $B_1H^+ + B_2 = B_1 + B_2H^+$ where B_1 is less basic (lower in the column) than B_2.

c. For the reaction: $NH_4^+ + B = NH_3 + BH^+$. Assume $\Delta G^o_{460} = \Delta G^o_{600}$.

d. From: (1) R. Yamdagni and P. Kebarle, J. Am. Chem. Soc., 95, 3504 (1973), based on the present value for methylamine. (2) R. Yamdagni and P. Kebarle, J. Am. Chem. Soc. 96, 1320 (1976).

e. Unless otherwise stated, all values are from: (1) Tabulations by R. W. Taft in "Proton Transfer Reactions" E. F. Caldin and V. Gold Ed., Chapman and Hall, London, 1975. (2) J. Wolf, R. H. Staley, I. Koppel, M. Taagepera, R. T. McIver, Jr., J. L. Beauchamp and R. W. Taft, J. Am. Chem. Soc., 99, 5417 (1977).

f. B. S. Freiser and J. L. Beauchamp, J. Am. Chem. Soc., 98, 265 (1976).

g. From ΔG^o_{300} measured relative to acetone. J. Vogt, A. D. Williamson and J. L. Beauchamp, J. Am. Chem. Soc., 100, 3478 (1978).

h. From ΔG^o_{350} measured relative to acetone. P. Ausloos and S. G. Lias, Chem. Phys. Lett., 51(1), 53 (1977).

i. From ΔG^o_{300} measured relative to methyl formate. W. J. Hehre, R. T. McIver, Jr., J. A. Pople and P.v.R. Schleyer, J. Am. Chem. Soc., 96, 7162 (1974).

The data based on which the ladder is constructed are tabulated in Tables 3.2 - 3.52. The partial pressures of B_1 and B_2 were varied in order to examine whether the equilibrium constant is independent of the concentrations. Representative plots of equilibrium constants <u>vs</u> ion source pressures and equilibrium constants <u>vs</u> concentration ratios of neutral P_{B_1}/P_{B_2} are shown in Figures 3.1 - 3.9 and Figures 3.10-3.17, respectively. The results indicate that the equilibrium constant is invariant with the partial pressures of the neutrals.

Since ammonia is usually chosen as the reference base in comparing gas-phase basicities, the ΔG^0_{600} for the reaction 3.1 are given for different bases B in

$$NH_4^+ + B = NH_3 + BH^+ \qquad (3.1)$$
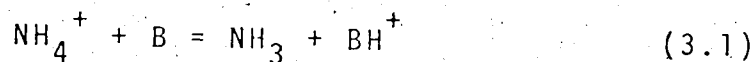
Table 3.1. Also given in Table 3.1 are the ΔG^0_{600} values reported previously from this laboratory (1-3) and the ΔG^0_{300} values obtained from ICR measurements (31,73-75). The present results, where overlapping with earlier measurements from our laboratory, are generally in agreement within ~0.5 kcal/mole.

The tendency of most of the protonated benzenes to form ring-protonated dimer ions is much lower even at lower temperatures. This allows the examination of the temperature dependence on the equilibrium constants of the proton transfer reaction 1.13 between benzene and

Table 3.2   Equilibrium Constants for the Proton Transfer Reaction:

$$H^+(water) + B_2 = water + B_2H^+$$

B_1	B_2	P_{B_1}/P_{B_2}	P_{CH_4} (torr)	P_{B_1} (mtorr)	P_{B_2} (mtorr)	K	$-\Delta G^o_{600}$ (kcal/mole)
water	trifluoro-acidic acid	4.13	2.70	53.2	12.9	3.92	
			3.60	70.9	17.2	4.13	
			4.50	88.7	21.5	4.55	
		8.25	1.75	63.5	7.70	3.77	
			2.80	101.6	12.3	4.40	
			3.40	123.4	15.0	4.84	
			3.60	130.6	15.8	4.52	
			4.30	156.0	18.9	5.04	
					Ave.	4.40	1.77
water	1,1,1-tri-fluoro-ethanol	0.447	2.45	2.94	6.58	4.08	
			3.20	3.84	8.59	4.28	
			4.80	5.75	12.9	4.31	
		0.796	2.00	13.2	16.6	4.72	
			3.60	23.8	29.9	5.08	
			4.40	29.0	36.5	5.26	
		4.02	1.70	33.5	8.33	4.27	
			3.00	59.1	14.7	4.17	
			3.90	76.8	19.1	4.27	
		7.99	1.75	63.5	7.95	4.34	
			2.80	101.6	12.7	5.06	
			3.40	123.4	15.4	5.62	
			3.60	130.6	16.4	5.20	
			4.30	150.6	19.5	5.69	
					Ave.	4.74	1.85

Table 3.2 (continued)

B_1	B_2	P_{B_1}/P_{B_2}	P_{CH_4}	P_{B_1}	P_{B_2}	K	$-\Delta G^o_{600}$
			(torr)	(mtorr)	(mtorr)		(kcal/mole)
water	hydrogen sulfide	2.00	1.20	11.8	5.88	10.0	
			1.70	16.7	8.33	10.0	
			2.60	25.5	12.7	11.2	
			3.50	34.3	17.2	12.0	
		4.00	1.10	43.3	10.8	10.0	
			1.80	70.9	17.7	10.8	
			2.50	98.5	24.6	12.0	
			3.30	130.0	32.5	12.0	
						Ave. 11.0	2.86

Table 3.3   Equilibrium Constants for the Proton Transfer Reaction:

H^+(trifluoroacetic acid) + B_2 = trifluoroacetic acid + B_2H^+
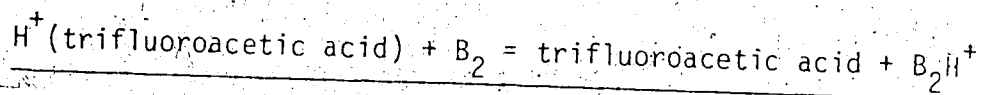
B_1	B_2	P_{B_1}/P_{B_2}	P_{CH_4} (torr)	P_{B_1} (mtorr)	P_{B_2} (mtorr)	K	$-\Delta G^o_{600}$ (kcal/mole)
trifluoro- acetic acid	1,1,1-tri- fluoro- ethanol	0.968	1.75	7.68	7.94	1.15	
			2.80	12.3	12.7	1.15	
			3.40	14.9	15.4	1.16	
			3.60	15.8	16.3	1.15	
			4.30	18.9	19.5	1.13	
		2.99	2.90	27.3	9.12	1.47	
			3.50	32.9	11.0	1.31	
			3.80	35.7	12.0	1.23	
						Ave. 1.22	0.24
trifluoro- acetic acid	hydrogen sulfide	1.32	1.35	12.7	9.61	2.54	
			2.40	22.6	17.1	2.54	
			3.70	34.8	26.4	2.54	
			4.70	44.2	33.5	2.44	
		3.25	1.50	42.0	12.9	2.42	
			2.70	75.6	23.3	2.38	
			3.50	98.0	30.2	2.46	
						Ave. 2.47	1.08

Table 3.4   Equilibrium Constants for the Proton Transfer Reaction:

$$H^+(1,1,1\text{-trifluoroethanol}) + B_2 = 1,1,1\text{-trifluoroethanol} + B_2H^+$$
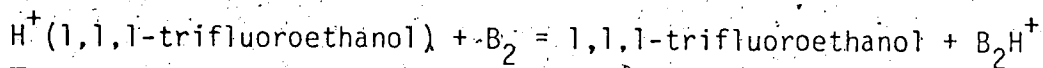
B_1	B_2	P_{B_1}/P_{B_2}	P_{CH_4} (torr)	P_{B_1} (mtorr)	P_{B_2} (mtorr)	K	$-\Delta G^0_{600}$ (kcal/mole)
1,1,1-tri-fluoro-ethanol	hydrogen sulfide	0.841	1.20	5.91	7.03	2.06	
			1.90	9.36	11.1	2.20	
			2.40	11.8	14.1	2.35	
			3.00	14.8	17.6	2.35	
			3.10	15.3	18.2	2.23	
			4.00	19.7	23.4	2.28	
		0.846	1.50	7.39	8.74	2.22	
			2.60	12.8	15.1	2.07	
			3.30	16.3	19.2	1.96	
		8.58	1.30	32.5	3.79	1.96	
			2.10	52.5	6.12	1.89	
			2.90	73.5	8.45	1.93	
					Ave.	2.13	0.90
1,1,1-tri-fluoro-ethanol	malono-nitrile	32.8	1.95	96.1	2.93	174.8	
			2.70	133.1	4.06	166.2	
			3.40	167.6	5.11	163.3	
			4.50	221.9	6.76	149.2	
		83.4	0.90	44.4	0.532	218.9	
			2.10	103.5	1.24	189.7	
			3.00	147.9	1.77	189.7	
			4.00	197.2	2.37	182.4	
					Ave.	179.3	0.19

Table 3.5   Equilibrium Constants for the Proton Transfer Reaction:

$$H^+(\text{hydrogen sulfide}) + B_2 = \text{hydrogen sulfide} + B_2H^+$$
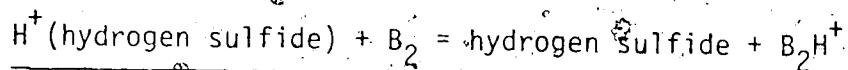
B_1	B_2	P_{B_1}/P_{B_2}	P_{CH_4} (torr)	P_{B_1} (mtorr)	P_{B_2} (mtorr)	K	$-\Delta G^0_{600}$ (kcal/mole)
hydrogen sulfide	malono- nitrile	19.6	2.00	57.2	2.92	127.4	
			2.60	74.4	3.79	125.4	
			3.00	85.8	4.38	125.4	
			3.20	91.5	4.67	117.6	
			4.20	120.1	6.13	125.4	
		29.9	1.35	38.6	1.29	128.6	
			2.25	64.4	2.15	128.6	
			3.10	88.7	2.97	134.6	
			4.20	120.1	4.02	130.1	
		117.6	2.00	328.0	2.79	114.7	
			2.10	344.4	2.93	111.7	
			3.10	508.4	4.32	113.1	
			4.00	556.0	5.58	118.8	
		295.8	0	1200	4.05	125.9	
			0	1700	5.75	125.9	
			0	2300	7.78	125.9	
			0	4000	13.5	128.6	
					Ave.	124.0	5.75
hydrogen sulfide	formic acid	86.0	1.50	223.5	2.60	1118	
			2.70	402.3	4.68	1161	
			2.70	402.3	4.68	120.	
			3.10	461.9	5.37	1161	
			3.85	573.7	6.67	1204	
		264.6	0	1600	6.05	1270	
			0	2600	9.87	1283	
			0	3500	13.2	1270	
			0	4000	15.1	1297	

Table 3.5 (continued)

B_1	B_2	P_{B_1}/P_{B_2}	P_{CH_4}	P_{B_1} (mtorr)	P_{B_2} (mtorr)	K	$-\Delta G^o_{600}$ (kcal/mole)
hydrogen sulfide	formic acid	268.7	0	1800	6.70	1048	
			0	2600	9.68	1129	
			0	3780	13.8	1263	
			0	4700	17.5	1263	
		533	0	800	1.50	1066	
			0	1200	2.25	1066	
			0	1800	3.38	1066	
			0	3000	5.63	1119	
			0	4700	8.82	1173	
					Ave.	1176	8.43

Table 3.6   Equilibrium Constants for the Proton Transfer Reaction:

$$H^+(malononitrile) + B_2 = malononitrile + B_2H^+$$
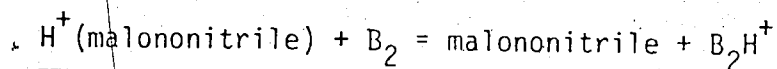
B_1	B_2	P_{B_1}/R_{B_2}	$P_{(CH_4)}$ (torr)	P_{B_1} (mtorr)	P_{B_2} (mtorr)	K	$-\Delta G^o_{600}$ (kcal/mole)
malono-nitrile	formic acid	0.905	1.40	4.76	5.26	7.60	
			1.60	5.44	6.01	8.33	
			2.00	6.80	7.51	7.96	
			2.40	8.16	9.02	7.87	
			3.50	11.9	13.2	7.96	
			4.30	14.6	16.2	7.60	
		1.90	1.05	7.46	3.92	7.79	
			1.25	8.88	4.67	7.79	
			1.70	12.1	6.35	7.98	
			2.00	14.2	7.47	7.79	
			3.60	25.6	13.5	8.17	
					Ave.	7.89	2.46
malono-nitrile	1,3,5-tri-fluoro-benzene	6.04	3.10	38.4	6.36	92.6	
			3.20	39.7	6.57	93.9	
			4.40	54.6	9.03	87.5	
			4.50	55.8	9.24	92.6	
		16.1	2.40	26.4	1.64	77.2	
			2.60	28.6	1.78	84.0	
			3.00	33.0	2.05	80.6	
			4.00	44.0	2.73	80.6	
					Ave.	86.1	5.31

Table 3.7 Equilibrium Constants for the Proton Transfer Reaction:

$$H^+(\text{formic acid}) + B_2 = \text{formic acid} + B_2H^+$$
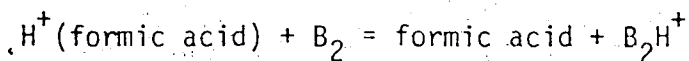
B_1	B_2	P_{B_1}/P_{B_2}	P_{CH_4} (torr)	P_{B_1} (mtorr)	P_{B_2} (mtorr)	K	$-\Delta G^o_{600}$ (kcal/mole)
formic acid	1,3,5-tri-fluoro-benzene	9.19	1.60	1.50	0.16	10.6	
			2.30	2.16	0.24	12.0	
			2.60	2.44	0.27	12.0	
			3.70	3.48	0.38	10.2	
			3.80	3.57	0.39	11.0	
			3.80	3.57	0.39	10.8	
		36.2	2.50	39.8	1.10	12.5	
			3.60	57.2	1.58	11.0	
			4.15	66.0	1.82	11.6	
					Ave.	11.3	2.89
formic acid	m-difluoro-benzene	2.61	2.50	85.8	32.9	21.7	
			3.10	106.3	40.7	21.4	
			3.60	123.5	47.3	21.7	
		5.37	2.50	88.0	16.4	19.2	
			2.95	103.8	19.3	16.9	
			4.00	140.8	26.2	16.2	
		25.8	2.35	123.1	4.77	20.6	
			3.30	172.9	6.70	18.9	
			3.40	178.2	6.91	18.8	
			3.80	199.1	7.72	18.0	
		52.4	2.75	144.1	2.75	17.4	
			3.60	188.6	3.60	16.5	
			3.90	204.4	3.90	16.1	
					Ave.	18.7	3.49

Table 3.8   Equilibrium Constants for the Proton Transfer Reaction:

H^+(1,3,5-trifluorobenzene) + B_2 = 1,3,5-trifluorobenzene + B_2H^+
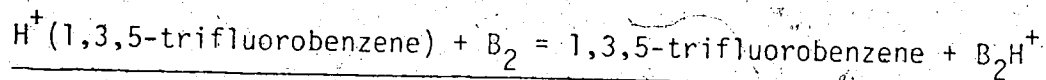
B_1	B_2	P_{B_1}/P_{B_2}	P_{CH_4} (torr)	P_{B_1} (mtorr)	P_{B_2} (mtorr)	K	$-\Delta G^o_{600}$ (kcal/mole)
1,3,5-tri-fluoro-benzene	m-difluoro-benzene	0.338	2.50	14.7	43.5	1.35	
			3.70	21.7	64.3	1.30	
			4.00	23.5	69.5	1.32	
		0.563	1.60	16.0	28.5	1.10	
			3.60	36.0	64.0	1.16	
			3.85	38.6	68.5	1.17	
		3.98	2.00	33.4	8.39	1.25	
			3.10	51.8	13.0	1.28	
			3.80	63.4	15.9	1.23	
					Ave:	1.24	0.26
1,3,5-tri-fluoro-benzene	benzene	1.67	3.40	40.8	24.4	8.10	
			3.70	44.4	26.6	7.74	
			4.00	48.0	28.7	7.04	
		3.49	2.20	19.5	5.60	6.78	
			3.85	34.2	9.80	6.96	
			3.90	34.6	9.92	6.96	
			4.20	37.3	10.7	6.59	
		4.11	3.00	25.5	6.20	6.69	
			3.40	28.9	7.03	6.58	
			4.20	35.7	8.69	6.69	
					Ave:	7.01	2.32

Table 3.9 · Equilibrium Constants for the Proton Transfer Reaction:

$$H^+(\text{m-difluorobenzene}) + B_2 = \text{m-difluorobenzene} + B_2H^+$$
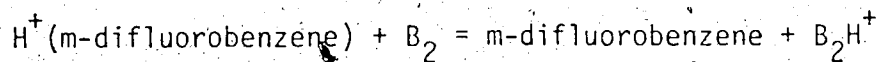
B_1	B_2	P_{B_1}/P_{B_2}	P_{CH_4} (torr)	P_{B_1} (mtorr)	P_{B_2} (mtorr)	K	$-\Delta G^O_{600}$ (kcal/mole)
m-difluoro-benzene	methanol	0.831	2.45	32.1	38.6	1.44	
			3.00	39.3	47.3	1.50	
			3.70	48.5	58.3	1.49	
		1.03	2.20	36.7	35.7	1.50	
			3.60	60.1	58.4	1.63	
			3.80	63.5	61.6	1.57	
		8.24	3.50	186.9	22.7	1.54	
			3.60	192.2	23.2	1.59	
			3.70	197.6	24.0	1.83	
			3.80	202.9	24.6	1.75	
					Ave:	1.58	0.55

Table 3.10 Equilibrium Constants of the Proton Transfer Reaction:

$$H^+(\text{methanol}) + B_2 = \text{methanol} + B_2H^+$$

B_1	B_2	P_{B_1}/P_{B_2}	P_{CH_4} (torr)	P_{B_1} (mtorr)	P_{B_2} (mtorr)	K	$-\Delta G^0_{600}$ (kcal/mole)
Methanol	Chlorobenzene	0.250	2.60	8.32	33.3	1.38	
			2.60	8.32	33.3	1.49	
			3.10	9.92	39.7	1.23	
			4.00	12.8	51.2	1.22	
			4.70	15.0	192	0.98	
		1.25	3.10	49.6	39.7	1.41	
			4.00	64.0	51.2	1.18	
		2.51	2.00	6.40	2.55	1.49	
			3.30	10.6	4.21	1.36	
			3.90	12.5	4.97	1.32	
			4.60	14.7	5.86	1.21	
						Ave. 1.30	0.31
Methanol	Fluorobenzene	0.232	2.30	7.36	31.7	1.61	
			3.70	11.8	13.7	1.52	
			4.30	13.8	59.3	1.52	
		0.465	2.70	17.3	37.2	1.64	
			3.50	22.4	48.2	1.48	
			4.10	26.2	56.4	1.48	
		0.775	3.20	51.2	66.1	1.46	
			3.80	60.8	78.5	1.40	
			4.20	67.2	86.7	1.45	
		2.32	2.40	19.2	8.28	1.64	
			3.70	29.6	12.8	1.66	
			4.00	32.0	13.8	1.50	
						Ave. 1.51	0.50

Table 3.11. Equilibrium Constants of the Proton Transfer Reaction:

$$H^+(\text{chlorobenzene}) + B_2 = \text{chlorobenzene} + B_2H^+$$
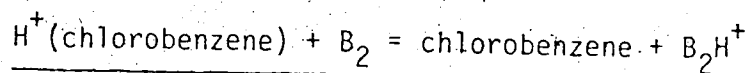
B_1	B_2	P_{B_1}/P_{B_2}	P_{CH_4} (torr)	P_{B_1} (mtorr)	P_{B_2} (mtorr)	K	$-\Delta G^o_{600}$ (kcal/mole)
chloro-benzene	fluoro-benzene	0.463	2.10	13.4	28.9	1.34	
			3.60	23.0	49.6	1.30	
			4.10	26.2	56.5	1.28	
		0.516	3.00	98.4	191	1.27	
			4.00	131	254	1.12	
			4.10	135	261	1.20	
		0.927	2.50	32.0	34.5	1.22	
			3.60	45.1	49.7	1.32	
			3.70	47.4	51.1	1.30	
			4.10	52.5	56.6	1.25	
		6.18	2.50	32.0	5.18	1.16	
			2.60	33.3	5.39	1.28	
			3.30	42.2	6.83	1.16	
			4.20	53.8	8.70	1.26	
						Ave. 1.24	0.25
chlorobenzene	benzene	0.881	1.40	12.7	14.4	2.50	
			2.50	22.7	25.7	2.50	
			2.70	24.5	27.8	2.37	
		8.76	2.60	46.8	5.34	2.28	
			3.40	61.2	6.99	2.35	
			4.40	79.2	9.04	2.55	
						Ave. 2.40	1.04

Table 3.12 Equilibrium Constants for the Proton Transfer Reaction:

$$H^+(fluorobenzene) + B_2 = fluorobenzene + B_2H$$
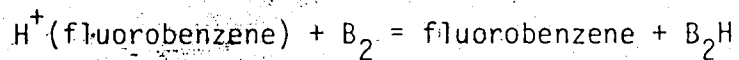
B_1	B_2	P_{B_1}/P_{B_2}	P_{CH_4} (torr)	P_{B_1} (mtorr)	P_{B_2} (mtorr)	K	$-\Delta G^o_{600}$ (kcal/mole)
fluorobenzene	benzene	0.945	2.40	5.94	6.29	2.00	
			3.40	8.42	8.91	2.05	
			4.05	10.0	10.6	1.96	
		9.58	1.60	31.8	3.32	1.82	
			3.55	70.6	7.36	1.92	
			4.10	81.5	8.51	1.87	
			4.25	84.5	8.82	1.79	
					Ave.	1.94	0.79

Table 3.13 Equilibrium Constants for the Proton Transfer Reaction:

$$H^+(\text{benzene}) + B_2 = \text{benzene} + B_2H^+$$

B_1	B_2	P_{B_1}/P_{B_2}	P_{CH_4} (torr)	P_{B_1} (mtorr)	P_{B_2} (mtorr)	K	$-\Delta G^o_{600}$ (kcal/mole)
benzene	acetaldehyde	2.10	1.50	4.32	2.06	7.06	
			2.50	6.75	3.21	7.54	
			3.70	9.99	4.76	7.25	
		2.18	2.60	14.3	6.57	7.47	
			3.60	19.8	9.10	7.10	
			4.50	24.8	11.4	6.91	
		2.33	2.40	33.1	14.2	6.99	
			2.50	34.5	14.8	6.59	
			3.80	52.4	22.5	6.99	
		5.52	1.40	19.3	3.50	7.57	
			2.00	27.6	5.00	7.10	
			3.00	41.4	7.50	7.10	
			3.70	51.1	9.25	7.10	
		11.4	1.80	24.8	2.18	7.40	
			2.50	34.5	3.03	7.30	
			3.80	52.4	4.60	7.40	
		19.3	2.00	34.5	1.78	7.61	
			2.70	46.4	2.41	7.96	
			3.70	63.5	3.30	7.78	
					Ave.	7.27	2.35
benzene	acetonitrile	10.5	1.70	10.7	1.02	34.9	
			2.20	13.9	1.32	35.8	
			2.70	17.0	1.62	34.9	
			3.60	22.7	2.16	31.5	
		23.1	2.30	15.0	0.647	36.4	
			2.80	18.2	0.788	36.4	

(continued..........)

Table 3.13 (continued)

B_1	B_2	P_{B_1}/P_{B_2}	P_{CH_4} (torr)	P_{B_1} (mtorr)	P_{B_2} (mtorr)	K	$-\Delta G^o_{600}$ (kcal/mole)
			3.60	23.4	1.01	34.4	
		58.9	1.40	18.9	0.321	38.4	
			2.30	31.1	0.527	36.0	
			3.30	44.6	0.755	33.5	
			3.50	47.3	0.802	32.6	
			3.80	51.3	0.871	34.5	
						Ave. 34.8	4.25
benzene	ethanol	4.39	1.60	9.44	2.15	20.5	
			2.50	14.8	3.36	22.0	
			4.00	23.6	5.38	20.1	
		13.1	2.00	13.8	1.05	21.0	
			2.70	18.6	1.42	21.5	
			2.80	19.3	1.47	21.0	
			4.00	27.6	2.11	21.0	
		26.0	1.80	11.7	0.450	18.9	
			2.80	18.2	0.700	20.6	
			3.50	22.8	0.875	18.9	
		26.0	1.60	10.4	0.400	19.4	
			2.60	16.9	0.650	20.8	
			3.80	24.7	0.950	20.1	
						Ave. 20.4	3.60

Table 3.14   Equilibrium Constants for the Proton Transfer Reaction:

$$H^+(acetaldehyde) + B_2 = acetaldehyde + B_2H^+$$
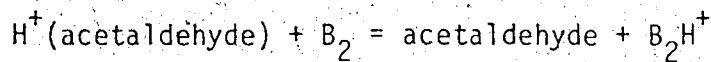
B_1	B_2	P_{B_1}/P_{B_2}	P_{CH_4}	P_{B_1} (mtorr)	P_{B_2} (mtorr)	K	$-G^0_{600}$ (kcal/mole)
acetalde-hyde	aceto-nitrile	0.930	1.75	19.1	20.5	5.12	
			2.80	30.5	32.8	5.65	
			3.00	32.7	35.2	4.77	
			3.80	41.4	44.5	4.94	
		1.07	1.70	4.25	3.97	5.18	
			2.80	7.00	6.54	5.18	
			3.60	9.00	8.41	5.18	
		2.78	1.80	11.7	4.21	5.77	
			2.60	16.9	6.08	5.90	
			3.80	24.7	8.88	6.57	
			4.50	29.3	10.5	5.71	
		7.23	2.50	63.5	8.78	5.49	
			3.90	99.1	13.7	5.90	
					Ave.	5.10	1.94

Table 3.15 Equilibrium Constants for the Proton Transfer Reaction:

$$H^+(ethanol) + B_2 = ethanol + B_2H^+$$

B_1	B_2	P_{B_1}/P_{B_2}	P_{CH_4} (torr)	P_{B_1} (mtorr)	P_{B_2} (mtorr)	K	$-\Delta G^0_{600}$ (kcal/mole)
ethanol	methyl formate	0.211	1.60	6.72	31.9	2.85	
			3.00	12.6	59.7	3.13	
			3.60	15.2	71.7	2.94	
		1.06	1.50	23.6	22.2	3.33	
			2.50	39.3	37.0	3.33	
			3.00	47.1	44.4	3.05	
			4.00	62.8	59.3	3.10	
						Ave. 3.06	1.35
ethanol	acetonitrile	0.300	1.80	9.45	31.5	1.37	
			2.00	10.5	35.0	1.37	
		0.911	1.80	18.9	20.8	1.42	
			2.50	26.3	28.8	1.33	
			3.10	32.6	35.7	1.33	
						Ave. 1.37	0.40

Table 3.16 Equilibrium Constants for the Proton Transfer Reaction:

$$H^+(\text{acetonitrile}) + B_2 = \text{acetonitrile} + B_2H^+$$

B_1	B_2	P_{B_1}/P_{B_2}	P_{CH_4} (torr)	P_{B_1} (mtorr)	P_{B_2} (mtorr)	K	$-\Delta G^o_{600}$ (kcal/mole)
acetonitrile	methyl formate	0.295	2.80	12.9	43.7	1.91	
			2.90	13.3	45.2	1.96	
			4.10	18.9	63.9	1.98	
		0.591	1.60	24.5	41.4	1.99	
			2.50	38.3	64.7	1.99	
			3.80	58.1	98.4	2.09	
		1.19	2.20	38.7	32.5	2.00	
			3.00	77.7	44.4	2.06	
			3.70	95.8	54.7	2.13	
					Ave.	2.02	0.84
acetonitrile	toluene	1.01	2.00	23.2	23.0	6.71	
			2.90	33.6	33.3	6.53	
			4.00	46.4	45.9	6.23	
		4.05	1.80	55.6	13.7	6.19	
			2.40	74.2	18.3	6.19	
			3.00	92.7	22.9	5.95	
			4.20	130	32.0	5.35	
		4.08	2.70	62.1	15.2	5.99	
			3.10	71.3	17.5	5.66	
			3.70	85.1	20.9	5.27	
		10.0	1.90	27.6	2.76	5.99	
			2.70	39.2	3.92	5.76	
			4.20	60.9	6.09	5.64	
					Ave.	5.94	2.14

Table 3.17 Equilibrium Constants for the Proton Transfer Reaction:

$$H^+(\text{methyl formate}) + B_2 = \text{methyl formate} + B_2H^+$$

B_1	B_2	P_{B_1}/P_{B_2}	P_{CH_4} (torr)	P_{B_1} (mtorr)	P_{B_2} (mtorr)	K	$-\Delta G^0_{600}$ (kcal/mole)
methyl formate	ethyl formate	0.518	1.90	16.0	30.8	24.3	
			3.50	29.4	56.8	23.8	
		5.14	2.40	56.4	11.0	24.5	
			4.00	94.0	18.3	25.2	
		10.4	1.60	27.7	2.66	20.7	
			2.30	39.8	3.83	22.3	
			3.70	64.0	6.15	23.3	
			3.80	65.7	6.32	24.1	
		11.7	1.70	45.1	3.85	25.1	
			2.90	78.9	6.57	26.2	
			3.60	95.4	8.15	28.6	
						Ave. 24.4	3.81
methyl formate	toluene	1.01	1.80	26.5	26.2	3.77	
			2.30	33.8	33.5	3.72	
			4.00	58.8	58.2	3.66	
		3.45	1.80	47.3	13.7	3.45	
			3.00	78.9	22.9	3.45	
			4.00	105	30.5	3.54	
		3.45	1.40	55.6	16.1	3.46	
			2.40	95.3	27.6	3.21	
			3.70	147	42.6	3.35	
		8.71	2.20	71.5	8.21	3.98	
			3.00	97.5	11.2	4.16	
			4.20	137	15.7	4.16	
						Ave. 3.66	1.55

Table 3.18 Equilibrium Constants for the Proton Transfer Reaction:

$$H^+(\text{toluene}) + B_2 = \text{toluene} + B_2H^+$$
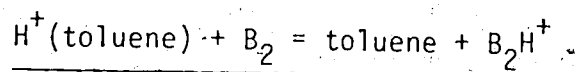
B_1	B_2	P_{B_1}/P_{B_2}	P_{CH_4} (torr)	P_{B_1} (mtorr)	P_{B_2} (mtorr)	K	$-\Delta G^o_{600}$ (kcal/mole)
toluene	ethylbenzene	0.5713	2.50	14.3	24.9	2.19	
			3.50	20.0	34.9	2.25	
		1.15	1.80	14.5	13.5	2.09	
			3.60	30.9	26.9	1.74	
		5.77	2.50	36.0	6.24	2.16	
			3.00	43.2	7.49	2.20	
			3.80	54.7	9.48	2.33	
					Ave.	2.22	0.96
toluene	ethyl formate	1.53	2.00	15.4	10.1	6.68	
			2.80	21.6	14.1	6.98	
			3.90	30.0	19.6	7.64	
		7.59	2.50	51.8	6.82	5.58	
			2.80	58.0	7.64	5.26	
			3.00	62.1	8.18	5.66	
			3.60	74.5	9.82	5.66	
			3.70	76.6	10.1	5.89	
			3.80	78.7	10.4	6.14	
		18.4	1.60	35.2	1.91	5.45	
			2.80	61.6	3.35	6.21	
			3.80	83.6	4.54	6.21	
			4.00	88.0	4.78	6.56	
					Ave.	6.37	2.23

Table 3.19   Equilibrium Constants for the Proton Transfer Reaction:

$$H^+(\text{isopropanol}) + B_2 = \text{isopropanol} + B_2H^+$$

B_1	B_2	P_{B_1}/P_{B_2}	P_{CH_4} (torr)	P_{B_1} (mtorr)	P_{B_2} (mtorr)	K	$-\Delta G^o_T$ (kcal/mole)
isopro-panol	nitro-benzene	1.34	1.90	30.4	22.7	8.58	
			2.10	33.6	25.1	8.42	
			2.90	46.4	34.6	8.47	
		2.03	1.75	25.0	12.3	9.39	
			2.40	34.3	16.9	8.80	
			3.40	48.6	24.0	8.67	
		13.6	1.65	47.7	3.51	12.4	
			2.10	60.7	4.46	11.1	
			3.20	92.5	6.80	11.5	
					Ave:	9.64	2.30[a]
isopro-panol	toluene	0.278	1.65	2.38	8.55	0.599	
			2.70	3.89	14.0	0.641	
			3.90	5.62	20.2	0.658	
		0.346	2.00	6.40	18.5	0.532	
			2.90	9.28	26.8	0.535	
			3.45	11.0	31.9	0.575	
		1.39	2.10	6.57	4.73	0.678	
			2.75	8.61	6.19	0.721	
			3.70	11.6	8.33	0.699	
					Ave:	0.633	-0.43[b]

[a] at 511°K

[b] at 475°K

Table 3.20   Equilibrium Constants for the Proton Transfer Reaction:

$$H^+(ethylbenzene) + B_2 = ethylbenzene + B_2H^+$$
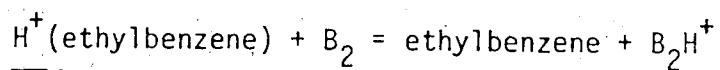
B_1	B_2	P_{B_1}/P_{B_2}	P_{CH_4} (torr)	P_{B_1} (mtorr)	P_{B_2} (mtorr)	K	$-\Delta G^o_{600}$ (kcal/mole)
ethylbenzene	ethyl formate	0.652	1.80	9.04	13.9	2.44	
			3.40	17.1	26.2	2.47	
			3.80	19.1	29.3	2.29	
		6.05	1.70	23.0	3.79	2.28	
			3.10	41.9	6.92	2.28	
			3.60	48.6	8.03	2.23	
					Ave.	2.32	1.01

Table 3.21   Equilibrium Constants for the Proton Transfer Reaction:

$$H^+(\text{ethyl formate}) + B_2 = \text{ethyl formate} + B_2H^+$$
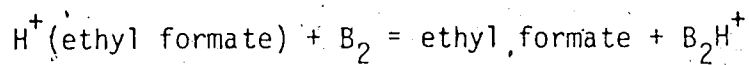
B_1	B_2	P_{B_1}/P_{B_2}	P_{CH_4} (torr)	P_{B_1} (mtorr)	P_{B_2} (mtorr)	K	$-\Delta G^o_{600}$ (kcal/mole)
ethyl formate	nitrobenzene	0.503	2.75	11.8	23.5	1.58	
			3.60	15.5	30.8	1.61	
			4.20	18.1	35.9	1.67	
		5.18	3.60	21.6	4.17	1.65	
			4.00	24.0	4.63	1.51	
					Ave.	1.59	0.56
ethyl formate	phenol	3.50	2.00	4.56	1.30	12.6	
			2.40	5.47	1.56	13.4	
			3.00	6.84	1.95	13.9	
			4.15	9.46	2.70	11.9	
			4.30	9.80	2.80	12.5	
		4.31	2.20	49.9	11.6	11.6	
			3.60	81.7	19.0	13.5	
			3.95	89.7	20.8	11.5	
		29.4	3.70	196.1	6.67	11.1	
			4.00	212.0	7.21	11.0	
					Ave.	11.8	2.95

Table 3.22 Equilibrium Constants for the Proton Transfer Reaction:

$$H^+(\text{nitrobenzene}) + B_2 = \text{nitrobenzene} + B_2H^+$$
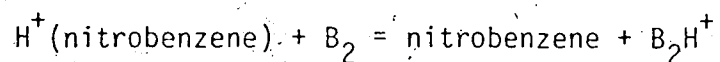
B_1	B_2	P_{B_1}/P_{B_2}	P_{CH_4} (torr)	P_{B_1} (mtorr)	P_{B_2} (mtorr)	K	$-\Delta G^0_{600}$ (kcal/mole)
nitrobenzene	acetone	3.59	2.70	53.7	15.0	13.0	
			4.10	81.6	22.7	13.9	
		24.8	2.10	36.5	1.47	11.9	
			3.55	61.6	2.49	13.9	
			4.50	78.1	3.15	13.3	
					Ave.	13.2	3.08
nitrobenzene	benzo-nitrile	1.50	2.30	32.9	21.9	9.54	
			3.30	47.2	31.5	8.26	
			4.05	57.9	38.6	8.87	
		10.1	1.85	30.0	2.97	7.68	
			3.35	54.3	5.37	8.33	
			3.60	58.3	5.77	7.86	
					Ave.	8.22	2.51

Table 3.23   Equilibrium Constants for the Proton Transfer Reaction:

$$H^+(\text{n-propyl formate}) + B_2 = \text{n-propyl formate} + B_2H^+$$
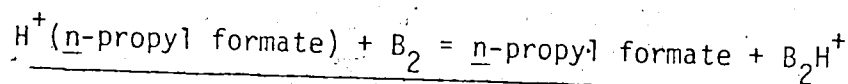
B_1	B_2	P_{B_1}/P_{B_2}	P_{CH_4} (torr)	P_{B_1} (mtorr)	P_{B_2} (mtorr)	K	$-\Delta G^0_{600}$ (kcal/mole)
n-propyl formate	isobutene	8.03	2.5	83.3	10.4	3.85	
			3.4	113	14.1	3.75	
			4.0	133	16.6	3.68	
		0.896	2.8	37.3	41.6	4.14	
			3.2	42.6	47.5	4.18	
			3.8	50.6	56.5	4.11	
					Ave.	3.96	1.64
n-propyl formate	acetone	30.25	2.0	54.8	1.81	13.1	
			3.6	98.6	3.26	13.9	
		7.42	3.4	45.9	6.19	11.7	
			4.7	63.5	8.55	11.3	
		5.05	2.4	32.9	6.51	13.3	
			3.9	53.4	10.6	13.2	
			4.3	58.9	11.7	13.8	
		3.03	3.5	48.0	15.8	12.9	
			4.2	57.5	19.0	12.9	
					Ave.	12.9	3.05
n-propyl formate	methyl acetate	8.13	2.50	34.0	4.18	28.3	
			3.20	43.5	5.35	30.6	
			4.10	55.8	6.86	29.0	
		13.34	2.80	154	11.5	29.5	
			3.40	187	14.0	28.9	
			3.60	198	14.8	29.8	
			4.00	220	16.5	29.1	
			4.10	226	16.9	27.3	

Table 3.23 (continued)

B_1	B_2	P_{B_1}/P_{B_2}	P_{CH_4} (torr)	P_{B_1} (mtorr)	P_{B_2} (mtorr)	K	$-\Delta G^{0}_{600}$ (kcal/mole)
		8.29	2.10	142	1.72	24.6	
			2.10	142	1.72	23.7	
			3.00	203	2.45	23.9	
			3.90	264	3.18	22.6	
		84.2	2.70	184	2.18	24.1	
			3.20	218	2.58	26.3	
			3.90	265	3.15	23.7	
					Ave.	26.8	3.92

Table 3.24 Equilibrium Constants for the Proton Transfer Reaction:

$$H^+(\text{isobutene}) + B_2 = \text{isobutene} + B_2H^+$$
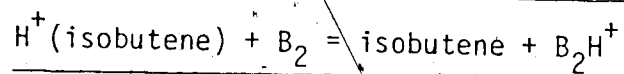
B_1	B_2	P_{B_1}/P_{B_2}	P_{CH_4} (torr)	P_{B_1} (mtorr)	P_{B_2} (mtorr)	K	$-\Delta G^o_{600}$ (kcal/mole)
isobutene	acetone	1.07	1.40	40.0	37.4	4.30	
			1.50	42.9	40.1	4.18	
			1.90	54.3	50.7	3.97	
		1.10	1.70	48.6	44.0	3.58	
			2.20	62.9	56.9	4.09	
		2.07	1.60	45.8	22.1	4.12	
		0.552	1.90	27.2	49.2	4.00	
			0.74	10.6	19.2	4.05	
			0.45	6.44	11.7	3.83	
		0.548	1.50	42.8	78.2	3.54	
					Ave.	3.97	1.64
isobutene	methyl acetate	1.87	3.20	64.0	34.2	7.80	
			3.50	70.0	37.4	7.44	
			4.40	88.0	47.1	7.40	
		2.80	2.60	52.0	18.6	7.94	
			3.50	70.0	25.0	7.10	
			3.80	76.0	27.1	7.94	
			4.20	84.0	30.0	7.19	
		12.0	2.50	63.0	5.25	7.32	
			4.30	108	9.03	7.19	
					Ave.	7.46	2.40

Table 3.25 Equilibrium Constants for the Proton Transfer Reaction:

$$H^+(\text{naphthalene}) + B_2 = \text{naphthalene} + B_2H^+$$

Temperature: 600°K

B_1	B_2	P_{B_1}/P_{B_2}	P_{IS}^* (torr)	P_{B_1} (mtorr)	P_{B_2} (mtorr)	K	$-\Delta G^0_{600}$ k(cal/mole)
naphthalene	acetone	0.549	1.75	20.8	37.9	1.76	
			2.80	33.3	60.7	1.80	
			3.50	41.7	75.9	1.82	
			4.20	50.0	91.0	1.93	
		4.00	1.70	22.1	5.53	1.64	
			2.70	35.1	8.78	1.78	
			3.00	39.0	9.75	1.78	
		5.66	2.40	40.8	7.21	1.64	
			3.10	52.7	9.31	1.64	
					Ave.	1.75	0.67
naphthalene	isobutene	0.228	1.06	6.57	28.8	0.508	
			1.60	9.92	43.5	0.524	
			2.20	13.6	59.8	0.488	
			2.50	15.5	68.0	0.488	
			3.20	19.8	87.0	0.472	
			4.00	24.8	109	0.452	
		1.29	1.60	27.2	21.1	0.490	
			2.40	40.8	31.6	0.503	
			3.10	52.7	40.8	0.503	
			4.60	78.2	60.6	0.478	
					Ave:	0.491	-0.85

* Ion source pressure

Table 3.26   Equilibrium Co-stants for the Proton Transfer Reaction:

$$H^+(phenol) + B_2 = phenol + B_2H^+$$
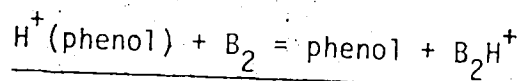
B_1	B_2	P_{B_1}/P_{B_2}	P_{CH_4} (torr)	P_{B_1} (mtorr)	P_{B_2} (mtorr)	K	$-\Delta G^0_{600}$ (kcal/mole)
phenol	benzonitrile	0.132	2.50	4.00	30.3	1.06	
			3.70	5.92	44.9	1.09	
		2.03	3.50	21.4	10.5	1.17	
			3.90	23.8	11.7	1.14	
			4.05	24.7	12.2	1.17	
					Ave.	1.13	0.14
phenol	methyl acetate	0.741	2.65	15.1	20.4	3.23	
			3.25	18.5	25.0	3.44	
			3.95	22.5	30.4	3.17	
		1.52	3.20	18.9	12.4	3.32	
			3.45	20.4	13.4	3.39	
			3.80	22.4	14.8	3.61	
			4.25	25.1	16.5	3.38	
					Ave.	3.35	1.45
phenol	acetone	0.300	3.00	15.0	50.0	1.40	
			3.15	15.8	52.5	1.35	
			4.25	21.3	70.8	1.45	
		0.640	1.80	19.3	30.1	1.77	
			1.90	20.3	31.8	1.92	
			3.20	34.2	53.5	1.63	
		0.752	2.65	16.7	22.2	1.44	
			2.70	17.0	22.6	1.44	
			3.75	23.6	31.4	1.44	
			4.00	25.2	33.5	1.30	
					Ave.	1.53	0.51

Table 3.27   Equilibrium Constants for the Proton Transfer Reaction:

$$H^+(\text{benzonitrile}) + B_2 = \text{benzonitrile} + B_2H^+$$

B_1	B_2	P_{B_1}/P_{B_2}	P_{CH_4}	P_{B_1}	P_{B_2}	K	$-\Delta G^o_{600}$
			(torr)	(mtorr)	(mtorr)		(kcal/mole)
benzo-nitrile	acetone	0.720	2.00	34.0	47.2	1.59	
			3.10	52.7	73.2	1.69	
			4.10	69.7	96.8	1.52	
		3.64	1.95	38.4	10.6	1.51	
			2.00	39.4	10.8	1.37	
			2.75	54.2	14.9	1.51	
			3.15	62.1	17.1	1.54	
			3.45	68.0	18.7	1.51	
			4.00	78.8	21.7	1.44	
		7.21	2.60	47.8	6.49	1.70	
			2.95	53.1	7.36	1.49	
			3.60	64.8	8.99	1.56	
			3.95	71.1	9.86	1.36	
					Ave.	1.52	0.50
benzo-nitrile	methyl acetate	0.780	2.20	26.4	33.9	3.44	
			3.00	36.0	46.2	3.22	
			3.10	37.2	47.7	3.71	
			4.15	49.8	63.9	3.18	
			4.30	51.6	66.2	3.59	
		1.17	1.70	23.8	20.3	2.98	
			3.20	44.8	38.3	2.98	
			3.50	49.0	41.9	2.86	
			4.20	58.8	50.3	3.03	
		4.67	2.50	45.0	9.64	3.32	
			3.20	57.6	12.3	3.14	
			3.50	63.0	13.5	3.45	
			4.25	76.5	16.4	3.14	

Table 3.27 (continued)

B_1	B_2	P_{B_1}/P_{B_2}	P_{CH_4} (torr)	P_{B_1} (mtorr)	P_{B_2} (mtorr)	K	$-\Delta G^o_{600}$ (kcal/mole)
		12.2	2.30	50.6	4.15	3.34	
			3.75	82.5	6.76	3.39	
			4.20	92.4	7.57	3.21	
					Ave.	3.25	1.41

Table 3.28   Equilibrium Constants for the Proton Transfer Reaction:

$$H^+(acetone) + B_2 = acetone + B_2H^+$$
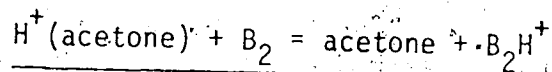
B_1	B_2	P_{B_1}/P_{B_2}	P_{CH_4} (torr)	P_{B_1} (mtorr)	P_{B_2} (mtorr)	K	$-\Delta G^o_{600}$ (kcal/mole)
acetone	methyl acetate	1.08	3.40	29.6	27.4	2.35	
		1.09	2.40	28.8	26.4	2.33	
			3.00	36.0	33.0	2.18	
			3.20	38.4	35.2	2.16	
		1.71	1.40	25.5	14.9	2.50	
			2.80	51.0	29.8	2.44	
		10.8	2.90	78.6	7.28	2.40	
			3.70	100	9.28	2.42	
			4.20	114	10.5	2.33	
		10.8	2.80	67.2	6.22	2.18	
			3.50	84.0	7.78	2.37	
			3.60	86.4	8.00	2.37	
					Ave.	2.34	1.01
acetone	benzoic acid	4.41	0.70	3.29	0.75	2.42	
			1.60	7.52	1.71	2.26	
			2.50	11.8	2.66	2.50	
		10.7	2.90	27.8	2.60	2.30	
			4.00	38.4	3.59	2.42	
			5.00	48.0	4.49	2.42	
					Ave.	2.39	1.04

Table 3.29 Equilibrium Constants of the Proton Transfer Reactions:

$$B_1H^+ + \text{ketene} = B_1 + (\text{ketene})H^+$$

B_1	B_2	P_{B_1}/P_{B_2}	P_{CH_4} (torr)	P_{B_1} (mtorr)	P_{B_2} (mtorr)	K	$-\Delta G^o_{600}$ (kcal/mole)
acetone	ketene	0.251	2.50	8.35	33.3	1.26	
			3.50	11.7	46.6	1.28	
			3.80	12.7	50.5	1.25	
			4.60	15.4	61.2	1.20	
		0.356	2.80	16.7	47.0	1.26	
			3.20	19.1	53.8	1.22	
			4.05	24.2	68.0	1.17	
			4.20	25.1	70.6	1.31	
		0.54	2.20	14.5	26.9	1.24	
			3.50	23.1	42.8	1.16	
			4.30	28.4	52.6	1.18	
		3.25	2.40	31.2	9.60	1.14	
			3.60	46.8	14.4	1.16	
			4.65	60.5	18.6	1.08	
		3.70	2.80	55.9	15.1	1.14	
			3.20	63.9	17.3	1.22	
			3.50	69.9	18.9	1.27	
			4.60	91.9	24.8	1.14	
					Ave:	1.19	0.207
isobutene	ketene	0.790	2.20	6.16	7.80	3.93	
			3.40	9.52	12.1	3.84	
			4.20	11.8	14.9	3.99	
		1.29	2.00	7.72	5.98	3.95	
			2.50	9.65	7.48	4.10	
			3.25	12.5	9.72	4.37	
			3.90	15.1	11.7	3.98	
		8.22	2.15	19.3	2.34	4.00	

Table.3.29(continued)

B_1	B_2	P_{B_1}/P_{B_2}	P_{CH_4} (torr)	P_{B_1} (mtorr)	P_{B_2} (mtorr)	K	$-\Delta G^o_{600}$ (kcal/mole)
			3.20	28.7	3.49	4.23	
			4.35	39.0	4.74	4.39	
					Ave:	4.08	1.68
ethyl formate	ketene	4.60	2.30	41.4	9.00	22.3	
			3.60	64.8	14.1	21.4	
			4.30	77.4	16.8	18.1	
		5.64	2.70	81.0	14.4	20.7	
			3.60	108.0	19.2	18.9	
			4.30	129.0	22.9	18.9	
		9.05	2.50	90.0	9.94	22.7	
			3.40	122.4	13.5	19.5	
			4.20	151.2	16.7	18.6	
		32.2	2.90	123.0	3.82	21.8	
			3.40	144.2	4.48	21.2	
			4.55	192.9	5.99	21.2	
		54.1	2.70	97.2	1.80	19.4	
			3.70	133.2	2.46	17.6	
			4.20	151.2	2.79	20.2	
			4.45	160.2	2.96	19.0	
					Ave:	20.2	3.58
diethyl ether	ketene	0.0182	2.55	1.21	66.3	0.0493	
			3.25	1.54	84.5	0.0512	
			4.55	2.15	118.3	0.0510	
		0.0578	2.55	3.63	62.7	0.0493	
			3.10	4.41	76.3	0.0458	
			4.40	6.26	108.2	0.0513	
		0.183	3.00	7.08	38.7	0.0537	
			3.80	8.97	49.0	0.0512	
			4.10	9.68	52.9	0.0520	
					Ave:	0.0505	-3.56

Table 3.30 Equilibrium Constants for the Proton Transfer Reaction:

$$H^+(\text{methyl acetate}) + B_2 = \text{methyl acetate} + B_2H^+$$
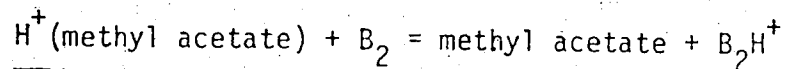
B_1	B_2	P_{B_1}/P_{B_2}	P_{CH_4} (torr)	P_{B_1} (mtorr)	P_{B_2} (mtorr)	K	$-\Delta G^o_{600}$ (kcal/mole)
methyl acetate	benzalde-hyde	3.84	1.80	31.3	8.16	9.20	
			2.80	48.7	12.7	9.20	
			4.10	71.3	18.6	9.40	
		26.6	2.10	46.0	1.73	9.08	
			2.70	59.1	2.22	9.24	
			3.85	84.3	3.17	9.39	
					Ave.	9.26	2.68
methyl acetate	anisole	1.37	2.70	40.5	29.6	14.4	
			3.15	47.3	34.5	15.1	
			3.95	59.3	43.3	15.5	
		4.11	1.80	31.1	7.58	13.4	
			2.80	48.4	11.8	13.6	
			3.90	64.5	16.4	14.1	
		27.1	1.95	56.6	2.09	15.1	
			2.60	75.4	2.78	14.6	
			3.40	98.6	3.64	16.5	
			3.80	110.2	4.07	15.1	
					Ave.	14.7	3.21
methyl acetate	n-propyl acetate	5.81	2.55	39.3	6.76	20.6	
			3.40	52.4	9.01	20.0	
			3.90	60.1	10.3	20.0	
		13.2	2.40	50.2	3.80	20.6	
			2.85	59.6	4.51	21.7	
			3.80	79.4	6.02	20.9	

163

Table 3.30 (continued)

B_1	B_2	P_{B_1}/P_{B_2}	P_{CH_4} (torr)	P_{B_1} (mtorr)	P_{B_2} (mtorr)	K	$-\Delta G^o_{600}$ (kcal/mole)
		11.40	2.35	70.5	0.618	20.5	
			3.00	90.0	0.789	22.2	
			3.90	117.0	1.03	22.9	
					Ave.	21.0	3.63
methyl acetate	benzoic acid	1.42	1.80	2.70	1.90	1.25	
			2.60	3.90	2.75	1.29	
			3.00	4.50	3.17	1.33	
			3.85	5.78	4.07	1.25	
		7.54	1.15	10.2	1.36	1.20	
			2.25	20.0	2.66	1.21	
			3.10	27.6	3.66	1.25	
			3.35	29.8	3.95	1.24	
			4.00	35.6	4.72	1.25	
			4.10	36.5	4.84	1.25	
			4.20	37.4	4.96	1.33	
					Ave.	1.25	0.266

Table 3.31 Equilibrium Constants for the Proton Transfer Reaction:

$$H^+(benzoic\ acid) + B_2 = benzoic\ acid + B_2H^+$$
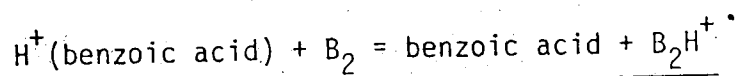
B_1	B_2	P_{B_1}/P_{B_2}	P_{CH_4} (torr)	P_{B_1} (mtorr)	P_{B_2} (mtorr)	K	$-\Delta G^{0}_{600}$ (kcal/mole)
benzoic acid	diethyl ether	3.47	2.60	20.0	5.77	12.2	
			3.30	25.4	7.32	11.6	
			4.10	31.6	9.10	11.4	
		6.21	2.00	2.40	0.39	13.3	
			3.10	3.72	0.60	14.1	
			3.50	4.20	0.68	14.5	
			3.90	4.68	0.75	14.5	
		7.21	2.50	25.3	3.50	11.0	
			3.30	33.3	4.62	11.0	
			3.50	35.4	4.90	11.5	
						Ave. 12.5	3.01

Table 3.32 Equilibrium Constants for the Proton Transfer Reaction:

$$H^+(\text{benzaldehyde}) + B_2 = \text{benzaldehyde} + B_2H^+$$
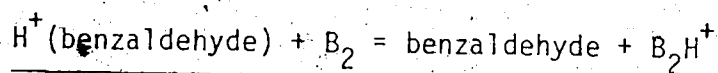
B_1	B_2	P_{B_1}/P_{B_2}	P_{CH_4}	P_{B_1}	P_{B_2}	K	$-\Delta G^o_{600}$
			(torr)	(mtorr)	(mtorr)		(kcal/mole)
benzalde-hyde	anisole	0.267	1.80	6.48	24.3	1.16	
			1.90	6.84	25.6	1.16	
			3.00	10.8	40.5	1.15	
			3.80	13.7	51.2	1.25	
		5.27	1.80	27.0	5.12	1.43	
			1.80	27.0	5.12	1.38	
			3.30	49.5	9.39	1.38	
			3.90	58.5	11.1	1.33	
		1.07	1.90	22.8	21.3	1.34	
			2.80	33.6	31.4	1.28	
			3.80	45.6	42.6	1.27	
			4.00	48.0	44.9	1.21	
					Ave.	1.28	0.29
benzalde-hyde	diethyl ether	2.06	1.50	18.0	8.74	1.32	
			2.60	31.2	15.2	1.32	
			3.50	42.0	20.4	1.28	
		6.31	2.40	37.2	5.90	1.19	
			3.90	60.5	9.58	1.15	
					Ave.	1.23	0.25

Table 3.33   Equilibrium Constants for the Proton Transfer Reaction:

$$H^+(\text{diethyl ether}) + B_2 = \text{diethyl ether} + B_2H^+$$
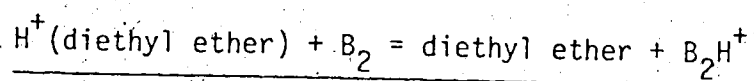
B_1	B_2	P_{B_1}/P_{B_2}	P_{CH_4} (torr)	P_{B_1} (mtorr)	P_{B_2} (mtorr)	K	$-\Delta G^o_{600}$ (kcal/mole)
diethyl ether	anisole	0.347	2.00	8.80	25.4	1.17	
			3.00	13.2	38.0	1.20	
			3.80	16.7	48.2	1.20	
		3.12	2.00	26.4	8.46	1.13	
			3.00	39.6	12.7	1.13	
			4.45	58.7	18.8	1.13	
					Ave.	1.16	0.18

Table 3.34   Equilibrium Constants for the Proton Transfer Reaction:

$$H^+(anisole) + B_2 = anisole + B_2H^+$$

B_1	B_2	P_{B_1}/P_{B_2}	P_{CH_4} (torr)	P_{B_1} (mtorr)	P_{B_2} (mtorr)	K	$-\Delta G^o_{600}$ (kcal/mole)
anisole	n-propyl acetate	0.263	2.65	11.9	45.3	1.41	
			3.30	14.9	56.5	1.41	
			4.20	18.9	71.9	1.43	
		1.05	2.60	27.8	26.5	1.35	
			3.40	36.4	34.7	1.41	
			3.50	37.5	35.7	1.41	
		2.11	2.65	39.7	18.8	1.31	
			3.45	51.7	24.5	1.35	
			4.10	61.4	29.1	1.25	
					Ave.	1.37	0.375

Table 3.35   Equilibrium Constants for the Proton Transfer Reaction

$$H^+(\underline{n}\text{-propyl acetate}) + B_2 = \underline{n}\text{-propyl acetate} + B_2H^+$$
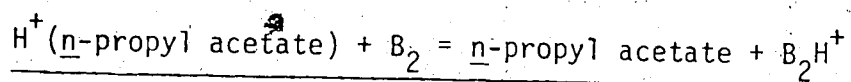
B_1	B_2	P_{B_1}/P_{B_2}	P_{CH_4}	P_{B_1}	P'_{B_2}	K	$-\Delta G^o_{600}$
			(torr)	(mtorr)	(mtorr)		(kcal/mole)
$\underline{n}$-propyl acetate	ammonia	3.24	2.10	44.7	13.8	7.15	
			2.10	44.7	13.8	7.75	
			3.85	82.0	25.3	7.00	
		4.05	1.60	17.1	4.23	7.22	
			2.30	24.6	6.08	6.85	
			2.40	25.7	6.34	6.85	
			3.90	41.7	10.3	6.67	
					Ave.	7.07	2.33

Table 3.36   Equilibrium Constant for the Proton Transfer Reaction:

$$H^+(ammonia) + B_2 = ammonia + B_2H^+$$
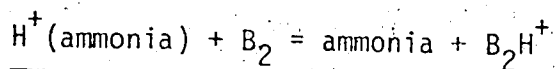
B_1	B_2	P_{B_1}/P_{B_2}	P_{CH_4} (torr)	P_{B_2} (mtorr)	P_{B_2} (mtorr)	K	$-\Delta G^o_{600}$ (kcal/mole)
ammonia	aceto-phenone	3.11	2.15	19.1	6.13	5.91	?
			2.60	23.0	7.41	6.15	
			3.25	28.8	9.26	6.62	
			3.60	31.9	10.3	6.38	
		4.82	1.70	4.61	0.965	5.32	
			2.30	6.23	1.29	4.72	
			2.55	6.91	1.43	5.01	
			3.55	9.62	2.00	4.72	
			4.10	11.1	2.31	4.87	
			4.20	11.4	2.36	5.09	
		21.8	1.95	23.8	1.09	5.15	
			2.25	27.5	1.26	6.59	
			2.40	29.3	1.34	5.15	
			3.00	36.6	1.68	5.68	
			3.70	45.2	2.07	5.00	
						Ave. 5.49	2.03
ammonia	m-chloro-aniline	2.26	1.40	10.0	4.42	22.8	
			2.20	15.7	6.95	21.2	
			2.35	16.8	7.42	22.2	
			3.00	21.4	9.48	22.2	
			3.90	27.9	12.3	22.8	
			4.30	30.7	13.6	25.8	
		10.98	2.10	14.6	1.33	18.8	
			2.60	18.1	1.65	19.5	
			2.90	20.2	1.84	18.8	
			3.40	23.7	2.16	18.8	
			3.60	25.1	2.28	17.6	
			4.70	32.7	2.98	19.5	
						Ave. 20.8	3.62

Table 3.37 \ Equilibrium Constants for the Proton Transfer Reaction:

$$H^+(\text{acetophenone}) + B_2 = \text{acetophenone} + B_2H^+$$
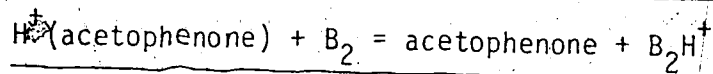
B_1	B_2	P_{B_1}/P_{B_2}	P_{CH_4} (torr)	P_{B_1} (mtorr)	P_{B_2} (mtorr)	K	$-\Delta G^o_{600}$ (kcal/mole)
aceto-phenone	m-chloro-aniline	0.899	2.20	13.2	14.7	3.85	
			2.80	16.8	18.7	3.92	
			3.10	18.6	20.7	3.58	
		0.900	1.35	3.86	4.13	4.05	
			2.70	7.72	8.58	4.19	
			3.50	10.0	11.1	4.19	
			4.30	12.3	39.1	4.27	
		.902	1.05	6.35	7.04	4.42	
			3.00	18.1	20.1	3.93	
			4.10	24.8	27.5	4.35	
		8.11	1.35	20.0	2.47	3.59	
			1.35	20.0	2.47	3.43	
			2.20	32.6	4.02	3.48	
			2.40	35.6	4.39	3.46	
			3.15	46.7	5.76	3.71	
			3.45	51.2	6.31	3.63	
					Ave.	3.87	1.61
aceto-phone	pyrrole	2.26	1.40	10.0	4.42	22.8	
			2.20	15.7	6.95	21.2	
			2.35	16.8	7.42	22.2	
			3.00	21.4	9.48	22.2	
			3.90	27.9	12.3	22.8	
		11.0	2.10	14.6	1.33	18.8	
			2.60	18.1	1.65	19.5	
			2.90	20.2	1.83	18.8	
			3.40	23.7	2.15	18.8	
			4.70	32.7	2.97	19.5	
					Ave.	20.7	3.61

Table 3.37 (continued)

B_1	B_2	P_{B_1}/P_{B_2}	P_{CH_4}	P_{B_1} (mtorr)	P_{B_2} (mtorr)	K	$-\Delta G^O_{600}$ (kcal/mole
aceto-phenone	aniline	15.3	1.70	18.2	1.19	70.1	
			2.50	26.8	1.75	69.0	
			2.75	29.4	1.92	73.4	
			3.60	38.5	2.52	78.8	
		21.5	1.80	38.7	1.80	81.6	
			2.35	50.5	2.35	87.7	
			3.70	79.6	3.70	82.5	
					Ave.	77.6	5.19

Table 3.38 Equilibrium Constants for the Proton Transfer Reaction:

H^+(m-chloroaniline) + B_2 = m-chloroaniline + B_2H^+

B_1	B_2	P_{B_1}/P_{B_2}	P_{CH_4} (torr)	P_{B_1} (mtorr)	P_{B_2} (mtorr)	K	$-\Delta G^o_{600}$ (kcal/mole)
m-chloro-aniline	pyrrole	0.658	1.99	6.02	9.15	4.61	
			3.10	9.57	14.6	4.66	
			3.25	10.0	15.3	5.04	
		3.33	1.80	9.54	2.86	5.13	
			2.10	11.1	3.34	4.85	
			3.00	15.9	4.77	5.65	
			3.60	19.1	5.73	5.69	
			4.65	24.7	7.40	5.13	
					Ave.	5.10	1.95
m-chloro-aniline	aniline	8.64	1.40	8.12	0.94	15.3	
			2.00	11.6	1.34	15.7	
			2.25	13.1	1.51	16.2	
			2.50	14.5	1.68	15.7	
			3.25	18.9	2.18	15.5	
			4.10	23.8	2.75	16.0	
		8.87	2.50	28.8	3.24	15.9	
			3.90	44.9	5.06	15.9	
			4.10	47.2	5.32	17.7	
		35.2	1.30	16.0	0.454	17.5	
			1.80	22.1	0.629	18.3	
			2.00	24.6	0.699	15.5	
			2.60	32.0	0.909	18.7	
			3.40	41.8	1.19	16.7	
			4.25	52.3	1.49	16.0	
					Ave.	16.4	3.34

Table 3.39 Equilibrium Constants for the Proton Transfer Reaction:

$$H^+(pyrrole) + B_2 = pyrrole + B_2H^+$$

B_1	B_2	P_{B_1}/P_{B_2}	P_{CH_4}	P_{B_1}	P_{B_2}	K	$-\Delta G^0_{600}$
			(torr)	(mtorr)	(mtorr)		(kcal/mole)
pyrrole	aniline	0.262	1.60	1.27	4.84	2.85	
			2.30	1.82	6.96	3.19	
			2.50	1.98	7.57	2.85	
			3.40	2.70	10.3	2.79	
			3.40	2.70	10.3	2.85	
			4.10	3.25	12.4	2.96	
		1.83	2.30	1.11	0.832	3.33	
			2.90	1.39	1.05	3.01	
			3.60	1.73	1.30	3.18	
			4.10	1.97	1.48	3.18	
		1.33	1.30	6.25	4.70	3.18	
			2.70	13.0	9.76	3.33	
			3.80	18.3	13.7	3.11	
						Ave.3.06	1.33
pyrrole	DMSO	3.11	1.70	12.3	3.95	11.3	
			2.80	20.2	6.50	11.3	
			4.20	30.3	9.75	11.5	
		9.14	1.55	13.2	1.44	9.72	
			2.00	17.0	1.86	11.0	
			2.70	22.9	2.51	10.6	
			3.20	27.2	2.97	11.5	
			3.50	29.7	3.25	12.0	
		12.1	1.50	20.0	1.65	10.9	
			2.30	30.6	2.53	11.1	
			3.30	43.9	3.63	10.9	
			4.10	54.5	4.51	11.1	
						Ave.11.1	2.87

Table 3.39 (continued)

B_1	B_2	P_{B_1}/P_{B_2}	P_{CH_4} (torr)	P_{B_1} (mtorr)	P_{B_2} (mtorr)	K	$-\Delta G^o_{600}$ (kcal/mole)
pyrrole	methyl amine	10.5	2.00	38.4	3.66	34.7	
			2.80	53.8	5.12	34.7	
			3.20	61.4	5.85	36.8	
			4.00	76.8	7.31	36.8	
		19.6	1.70	49.0	2.50	38.2	
			2.20	63.4	3.23	37.2	
			2.80	80.6	4.11	35.3	
			3.30	95.0	4.85	35.3	
			4.30	123.8	6.32	33.3	
					Ave.	35.8	4.27

Table 3.40   Equilibrium Constants for the Proton Transfer Reaction:

$$H^+(aniline) + B_2 = aniline + B_2H^+$$
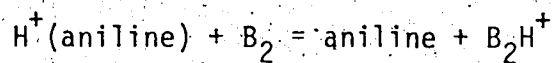
B_1	B_2	P_{B_1}/P_{B_2}	P_{CH_4} (torr)	P_{B_1} (mtorr)	P_{B_2} (mtorr)	K	$-\Delta G^0_{600}$ (kcal/mole)
aniline	DMSO	0.787	2.70	9.84	12.5	3.95	
			2.80	10.2	13.0	4.17	
			3.90	14.2	18.1	3.80	
			3.90	14.2	18.1	3.89	
		3.94	2.05	12.5	3.17	3.86	
			2.80	17.0	4.33	3.86	
			4.00	24.4	6.18	3.86	
					Ave.	3.93	1.63
aniline	methyl-amine	7.44	1.60	17.6	2.37	13.7	
			2.10	23.1	3.10	13.7	
			2.75	30.3	4.07	13.0	
			3.20	35.2	4.73	13.4	
			3.30	36.3	4.88	13.4	
			3.90	42.9	5.77	13.7	
		20.5	1.55	22.6	1.10	11.4	
			2.30	33.6	1.64	11.4	
			2.50	36.5	1.78	11.1	
			2.60	38.0	1.85	11.1	
			3.30	48.2	2.35	11.1	
			4.00	58.4	2.85	11.1	
		22.1	1.55	55.0	2.49	11.6	
			1.90	67.4	3.05	11.3	
			2.30	81.6	3.69	9.22	
					Ave.	12.0	2.96

Table 3.41 Equilibrium Constants for the Proton Transfer Reaction:

$$H^+(DMSO) + B_2 = DMSO + B_2H^+$$
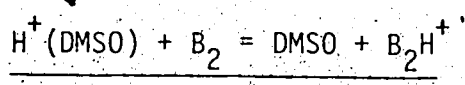
B_1	B_2	P_{B_1}/P_{B_2}	P_{CH_4} (torr)	P_{B_1} (mtorr)	P_{B_2} (mtorr)	K	$-\Delta G^0_{600}$ (kcal/mole)
DMSO	Methylamine	0.804	0.85	2.38	2.96	3.78	
			1.40	3.92	4.88	3.46	
			2.20	6.16	7.66	3.66	
			2.40	6.72	8.38	3.98	
			2.60	7.28	9.05	3.34	
			3.10	8.68	10.8	3.26	
			3.40	9.52	11.8	3.42	
			3.90	10.9	13.6	3.18	
		1.73	1.30	6.10	3.52	3.60	
			2.10	9.85	5.69	3.85	
			2.70	12.7	7.32	3.68	
			3.80	17.8	10.3	3.60	
			4.30	20.2	11.7	3.51	
		3.25	2.10	9.85	3.03	4.00	
			3.00	14.1	4.33	4.02	
			4.35	20.4	6.28	3.99	
					Ave.	3.65	1.54

Table 3.42   Equilibrium Constants for the Proton Transfer Reaction:

$$H^+(\text{methylamine}) + B_2 = \text{methylamine} + B_2H^+$$

Temperature: 600°K
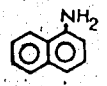
B_1	B_2	P_{B_1}/P_{B_2}	P_{IS}^* (torr)	P_{B_1} (mtorr)	P_{B_2} (mtorr)	K	$-\Delta G^o_{600}$ (kcal/mole)
methyl-amine	o-anisi-dine	5.68	1.80	12.8	2.25	4.07	
			2.70	19.2	3.38	3.83	
			3.90	27.7	4.88	4.07	
		45.4	1.16	33.6	0.74	4.34	
			2.60	75.4	1.66	4.11	
			3.60	104	2.30	4.11	
			3.90	113	2.49	4.11	
					Ave:	4.09	1.68
methyl-amine	NH₂ (naphthylamine)	10.5	2.50	17.8	1.70	29.2	
			2.60	18.5	1.77	26.2	
			3.50	25.0	2.38	30.3	
			3.70	26.4	2.51	30.3	
			5.00	35.7	3.40	30.3	
		11.9	1.50	19.5	1.64	26.1	
			2.80	36.4	3.06	23.5	
			3.20	41.6	3.50	23.1	
			4.70	61.1	5.13	26.1	
		25.2	1.30	37.2	1.48	27.7	
			1.60	45.8	1.82	27.7	
			2.60	74.4	2.95	31.6	
			2.90	82.9	3.29	32.5	
			3.40	97.2	3.86	33.5	
			4.00	114	4.54	34.4	
		140	1.35	215	1.53	25.3	
			2.00	318	2.27	26.0	
			2.40	382	2.73	26.3	
			3.40	540.6	3.86	28.8	
			3.70	588	4.20	26.0	
					Ave.	29.6	4.04

Table 3.42 (continued)

B_1	B_2	P_{B_1}/P_{B_2}	P_{IS}^* (torr)	P_{B_1} (mtorr)	P_{B_2} (mtorr)	K	$-\Delta G_{600}^o$ (kcal/mole)
methyl-amine	pyridine	181	1.45	232	1.28	665	
			2.60	416	2.30	665	
			3.30	528	2.92	729	
			4.70	752	4.15	683	
		1132	1.10	1100	0.97	608	
			2.00	2000	1.77	563	
			2.60	2600	2.30	609	
			3.50	3500	3.09	609	
					Ave:	641	7.71

*Ion source pressure

Table 3.43 Equilibrium Constants for the Proton Transfer Reaction:

$$H^+(\underline{o}\text{-anisidine}) + B_2 = \underline{o}\text{-anisidine} + B_2H^+$$
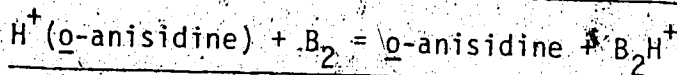
Temperature: 600°K
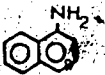
B_1	B_2	P_{B_1}/P_{B_2}	P_{IS}* (torr)	P_{B_1} (mtorr)	P_{B_2} (mtorr)	K	$-\Delta G^o_{600}$ (kcal/mole)
o-anisi- dine	pyridine	7.15	1.30	8.19	1.15	103	
			2.60	16.4	2.29	122	
			3.90	24.6	3.44	120	
		28.6	1.40	17.6	0.62	106	
			2.60	32.8	1.15	117	
			3.30	41.6	1.45	119	
			4.40	55.4	1.94	119	
		40.8	2.10	52.5	1.29	114	
			2.60	65.0	1.59	111	
			2.90	72.5	1.78	119	
			4.00	100	2.45	110	
					Ave:	115	5.65

*Ion source pressure

Table 3.44 Equilibrium Constants for the Proton Transfer Reaction

$$H^+(\text{naphthyl-}NH_2) + B_2 = (\text{naphthyl-}NH_2) + B_2H^+$$

Temperature: 600°K

B_1	B_2	P_{B_1}/P_{B_2}	$P_{IS}*$ (torr)	P_{B_1} (mtorr)	P_{B_2} (mtorr)	K	$-\Delta G^o_{600}$ (kcal/mole)
(naphthyl-NH_2)	pyridine	2.49	1.65	1.98	0.80	17.6	
			2.35	2.82	1.13	19.5	
			3.55	4.26	1.71	19.3	
		7.64	1.90	13.5	1.77	17.0	
			2.20	15.6	2.04	18.9	
			2.60	18.5	2.42	19.4	
			3.70	26.3	3.44	16.6	
		11.5	2.35	2.59	0.22	18.9	
			3.10	3.41	0.30	18.7	
			4.10	4.51	0.39	18.7	
						Ave: 18.5	3.48

*Ion source pressure

Table 3.45   Equilibrium Constants for the Proton Transfer Reaction:

$$H^+(\text{pyridine}) + B_2 = \text{pyridine} + B_2H^+$$

Temperature: 600°K
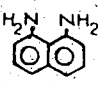
B_1	B_2	P_{B_1}/P_{B_2}	P_{IS}* (torr)	P_{B_1} (mtorr)	P_{B_2} (mtorr)	K	$-\Delta G^0_{600}$ (kcal/mole)
pyridine		8.29	2.75	12.2	1.47	5.33	
			3.50	15.5	1.87	5.46	
			4.25	18.9	2.28	5.55	
		14.6	1.85	24.8	1.70	5.49	
			2.10	28.1	1.93	5.49	
			2.95	39.5	2.71	6.13	
			3.55	47.6	3.26	5.81	
			3.85	51.6	3.53	6.37	
			3.90	52.3	3.58	6.24	
		30.2	1.75	31.2	1.03	5.75	
			2.70	48.1	1.59	5.75	
			3.40	60.5	2.00	6.55	
			4.00	71.2	2.36	6.55	
					Ave:	5.88	2.11

*Ion source pressure

Table 3.46   Equilibrium Constants for the Proton Transfer Reaction:

$$H^+(\text{(aniline-NH}_2\text{)}) + B_2 = \text{(NH}_2\text{)} + B_2H^+$$
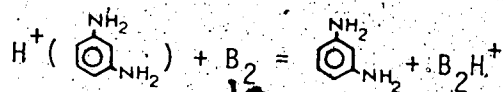
Temperature: 460°K and 600°K

B_1	B_2	P_{B_1}/P_{B_2}	P_{IS}* (torr)	P_{B_1} (mtorr)	P_{B_2} (mtorr)	K	$-\Delta G^o_T$ (kcal/mole)
(diaminobenzene)	(diaminonaphthalene)	0.257	2.50	1.29	5.00	4.53	
			3.30	1.70	6.60	4.50	
		1.87	1.80	5.04	2.70	4.38	
			3.00	8.40	4.49	4.82	
			4.30	12.0	6.44	4.97	
		2.80	2.45	9.68	3.46	4.36	
			3.00	11.9	4.23	4.85	
			4.00	15.8	5.64	4.85	
					Ave:	4.66	1.41[a]
(diaminobenzene)	piperi-dine	2.13	3.40	2.10	0.99	14.9	
			3.75	2.32	1.09	13.7	
			4.30	2.66	1.25	14.9	
		4.93	2.30	1.96	0.40	18.8	
			3.40	2.89	0.59	20.2	
			3.55	3.02	0.61	19.5	
			4.00	3.40	0.69	19.5	
			4.50	3.83	0.78	18.7	
		9.45	2.10	7.62	0.81	20.2	
			2.85	10.4	1.09	20.2	
			3.50	12.7	1.34	21.6	
					Ave:	18.4	3.47[b]

*Ion source pressure

[a]at 460°K

[b]at 600°K

Table 3.47 Equilibrium Constants for the Proton Transfer Reaction:

$$H^+ \left(\underset{H_2N \;\; NH_2}{\bigcirc\!\bigcirc} \right) + B_2 = \underset{H_2N \;\; NH_2}{\bigcirc\!\bigcirc} + B_2H^+$$
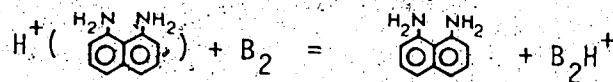
Temperature: 460°K
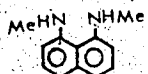
B_1	B_2	P_{B_1}/P_{B_2}	P_{IS}*	P_{B_1} (mtorr)	P_{B_2} (mtorr)	K	$-\Delta G^o_{460}$ (kcal/mole)
$\underset{H_2N\;\;NH_2}{\bigcirc\!\bigcirc}$	piperi-dine	2.18	95	4.64	2.13	10.5	
		2.85		6.78	3.11	10.1	
		3.75		8.97	4.09	10.1	
		5.20	1.25	3.38	0.54	8.69	
			2.15	5.81	0.94	7.90	
			3.00	8.10	1.31	8.51	
			4.00	10.8	1.74	8.20	
		10.9	1.75	5.25	0.48	11.7	
			2.60	7.80	0.72	12.3	
			3.40	10.2	0.94	12.0	
			4.45	13.4	1.22	12.3	
		18.3	1.20	3.16	0.17	11.9	
			2.60	6.84	0.37	11.9	
			3.45	9.07	0.50	12.2	
					Ave:	10.3	2.13
$\underset{H_2N\;\;NH_2}{\bigcirc\!\bigcirc}$	$NH_2(CH_2)_5NH_2$						
		14.1	1.40	4.62	0.33	228	
			2.00	6.60	0.47	221	
			3.20	10.6	0.75	228	
			3.80	12.5	0.89	250	
		18.5	1.60	3.30	0.18	261	
			2.30	4.74	0.26	207	
			3.30	6.80	0.37	261	
			5.00	10.3	0.56	261	
		33.2	2.30	5.75	0.17	202	

Table 3.47 (continued)
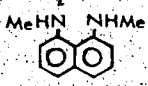
B_1	B_2	P_{B_1}/P_{B_2}	P_{IS}* (torr)	P_{B_1} (mtorr)	P_{B_2} (mtorr)	K	$-\Delta G^{0}_{460}$ (kcal/mole)
			3.00	7.50	0.23	225	
		57.0	2.85	7.64	0.13	234	
			3.50	9.38	0.16	219	
			4.60	12.3	0.22	219	
					Ave:	232	4.98
		61.2	2.10	6.09	0.10	1878	
			2.60	7.54	0.12	1959	
			4.50	13.1	0.21	2132	
			4.60	13.3	0.22	2047	
		177.6	2.20	6.64	0.04	1899	
			2.30	6.95	0.04	1532	
			3.40	10.3	0.06	1813	
			3.50	10.6	0.06	2100	
					Ave:	1920	6.91

*Ion source pressure

Table 3.48 Equilibrium Constants for the Proton Transfer Reaction:

$$H^+(\text{piperidine}) + B_2 = \text{piperidine} + B_2H^+$$

Temperature: 460°K
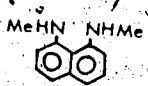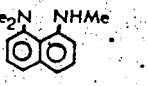
B_1	B_2	P_{B_1}/P_{B_2}	P_{IS}^* (torr)	P_{B_1} (mtorr)	P_{B_2} (mtorr)	K	$-\Delta G^o_{460}$ (kcal/mole)
piperidine	$NH_2(CH_2)_5NH_2$	2.98	1.25	0.55	0.18	30.6	
			2.15	0.95	0.32	28.1	
			3.00	1.32	0.44	28.7	
			4.00	1.76	0.59	28.7	
		16.4	1.35	0.85	0.05	30.7	
			2.15	1.35	0.08	30.7	
			3.05	1.91	0.12	35.5	
			4.50	2.82	0.17	38.6	
		16.4	1.30	13.0	0.79	29.8	
			1.75	17.5	1.07	29.8	
			3.50	35.0	2.13	33.3	
					Ave:	31.3	3.14
piperidine	MeHN NHMe (ring structure)	12.2	1.80	40.5	3.32	187	
			2.50	56.3	4.61	187	
			3.20	72.0	5.90	195	
			4.20	94.5	7.75	187	
		26.9	1.95	109	4.04	163	
			2.50	139	5.18	158	
			4.20	234	8.70	173	
					Ave:	179	4.74

*Ion source pressure

Table 3.49 Equilibrium Constants for the Proton Transfer Reaction:

$$H^+(NH_2(CH_2)_5NH_2) + B_2 = NH_2(CH_2)_5NH_2 + B_2H^+$$

Temperature: 460°K

B_1	B_2	P_{B_1}/P_{B_2}	P_{IS}* (torr)	P_{B_1} (mtorr)	P_{B_2} (mtorr)	K	$-\Delta G^o_{460}$ (kcal/mole)
$NH_2(CH_2)_5NH_2$	MeHN NHMe	0.450	1.80	2.14	4.76	7.62	
			2.95	3.51	7.80	7.85	
			3.90	4.64	10.3	7.62	
			4.90	5.83	13.0	7.38	
		1.61	1.40	3.30	2.05	6.48	
			2.80	6.61	4.10	6.61	
			3.70	8.73	5.42	5.99	
			4.70	11.1	6.89	5.99	
		2.06	1.50	4.80	2.33	5.97	
			2.05	6.56	3.18	6.60	
			3.00	9.60	4.66	6.07	
			3.10	9.92	4.82	5.70	
			4.00	12.8	6.21	6.23	
					Ave:	6.65	1.73
$NH_2(CH_2)_5NH_2$	Me₂N NHMe	18.9	1.20	5.60	0.30	703	
			2.70	12.5	0.67	574	
			3.00	14.0	0.74	645	
			4.25	19.9	1.05	533	
		47.2	1.20	4.50	0.10	893	
			1.80	6.75	0.14	834	
			2.70	10.1	0.21	805	
			3.30	12.4	0.26	863	
		115	1.30	12.1	0.11	749	
			2.30	21.4	0.19	766	
			3.50	32.6	0.28	642	
			4.60	42.8	0.37	642	
					Ave:	721	6.01

*Ion source pressure

Table 3.50   Equilibrium Constants for the Proton Transfer Reaction:

$$H^+(\text{MeHN-naphthalene-NHMe}) + B_2 = \text{MeHN-naphthalene-NHMe} + B_2H^+$$

Temperature: 460°K

B_1	B_2	P_{B_1}/P_{B_2}	$P_{IS}*$ (torr)	P_{B_1} (mtorr)	P_{B_2} (mtorr)	K	$-\Delta G^0_{460}$ (kcal/mole)
MeHN NHMe (naphthalene)	NMe$_2$ NMe$_2$ (benzene)	14.3	1.80	4.28	0.30	76.7	
			3.00	7.14	0.50	63.5	
			3.10	7.38	0.52	70.4	
			4.60	11.0	0.77	74.0	
		36.3	2.25	6.55	0.18	78.2	
			3.15	9.14	0.25	75.5	
			4.15	12.1	0.33	59.4	
			4.15	12.1	0.33	66.1	
			5.00	14.6	0.40	62.1	
			7.00	20.4	0.56	58.0	
					Ave:	68.4	3.87
MeHN NHMe	Me$_2$N NHMe	12.8	2.00	4.40	0.34	107	
		38.0	1.80	5.49	0.14	120	
			1.80	5.49	0.14	128	
			3.50	10.7	0.28	138	
			3.50	10.7	0.28	131	
			4.90	15.0	0.39	124	
			6.40	19.5	0.51	121	
			6.40	19.5	0.51	114	
		70.0	1.42	3.44	0.05	137	
			1.72	4.16	0.06	132	
			2.35	5.69	0.08	127	
			3.00	7.26	0.10	137	
			4.00	9.68	0.14	127	
			5.70	13.8	0.20	123	
		73.2	1.60	4.71	0.06	119	
			2.80	8.24	0.11	114	
			3.50	10.3	0.14	109	
					Ave:	120	4.38

* Ion source pressure

Table 3.51   Equilibrium Constants for the Proton Transfer Reaction:

$$H^+(\text{C}_6\text{H}_4(NMe_2)(NMe_2)) + B_2 = \text{C}_6\text{H}_4(NMe_2)(NMe_2) + B_2H^+$$

<div align="center">Temperature: 460°K</div>

B_1	B_2	P_{B_1}/P_{B_2}	P_{IS}^* (torr)	P_{B_1} (mtorr)	P_{B_2} (mtorr)	K	$-\Delta G_{460}^0$ (kcal/mole)
(C₆H₄(NMe₂)₂)	(Me₂N, NHMe naphthalene)	0.116	1.80	0.51	4.36	1.42	
			2.55	0.72	6.18	1.72	
			2.70	0.76	6.54	1.31	
			4.35	1.22	10.5	1.76	
			4.50	1.26	10.9	1.36	
		0.345	2.10	1.05	3.04	1.17	
			2.20	1.10	3.19	1.55	
			3.40	1.70	4.93	1.62	
			3.50	1.75	5.07	1.25	
			4.00	2.00	5.80	1.44	
			4.30	2.15	6.23	1.69	
		1.33	1.30	4.10	3.08	1.31	
			1.30	4.10	3.08	1.77	
			2.30	7.25	5.47	1.34	
			2.35	7.40	5.57	1.83	
			3.55	11.2	8.41	1.90	
			3.65	11.5	8.64	1.40	
					Ave:	1.47	0.35

*Ion source pressure

Table 3.52 Equilibrium Constants for the Proton Transfer Reaction

$$H^+(\text{Me}_2N\ \text{NHMe}) + B_2 = \text{Me}_2N\ \text{NHMe} + B_2H^+$$

Temperature: 460°K

B_1	B_2	P_{B_1}/P_{B_2}	P_{IS}* (torr)	P_{B_1} (mtorr)	P_{B_2} (mtorr)	K	$-\Delta G^0_{460}$ (kcal/mole)
Me₂N NHMe	Me₂N NMe₂	21.4	7.20	38.5	1.80	1951	
			8.00	42.7	2.00	2341	
		41.8	4.00	42.2	1.01	2065	
			5.00	52.8	1.26	1902	
			6.00	63.3	1.51	2445	
		42.7	4.60	25.5	0.60	2109	
			6.00	33.2	0.78	2276	
			7.60	42.1	0.99	2387	
		42.8	6.00	16.9	0.39	2114	
			8.00	22.5	0.53	2782	
		103	2.50	23.03	0.22	1936	
					Ave:	2210	7.04

*Ion source pressure
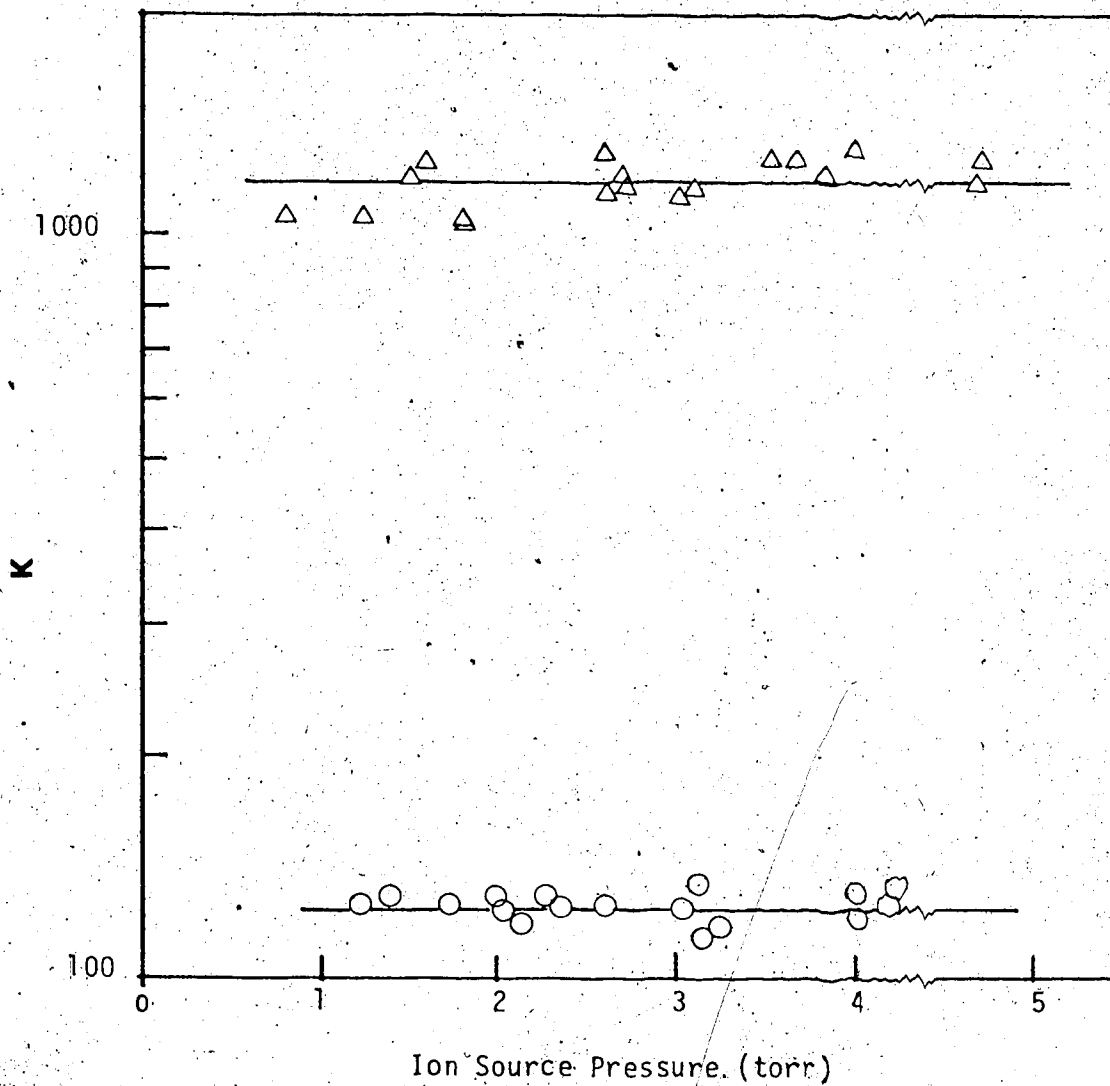
Figure 3.1 Equilibrium Constants versus Ion Source Pressures for the reaction:

$$H^+(\text{Hydrogen Sulfide}) + B = \text{Hydrogen Sulfide} + BH^+$$
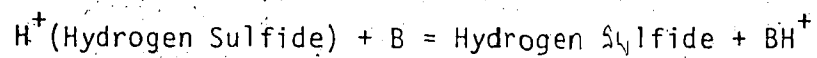
(O) B = malonitrile; ($\triangle$) B = Formic Acid;
Temperature 600°K
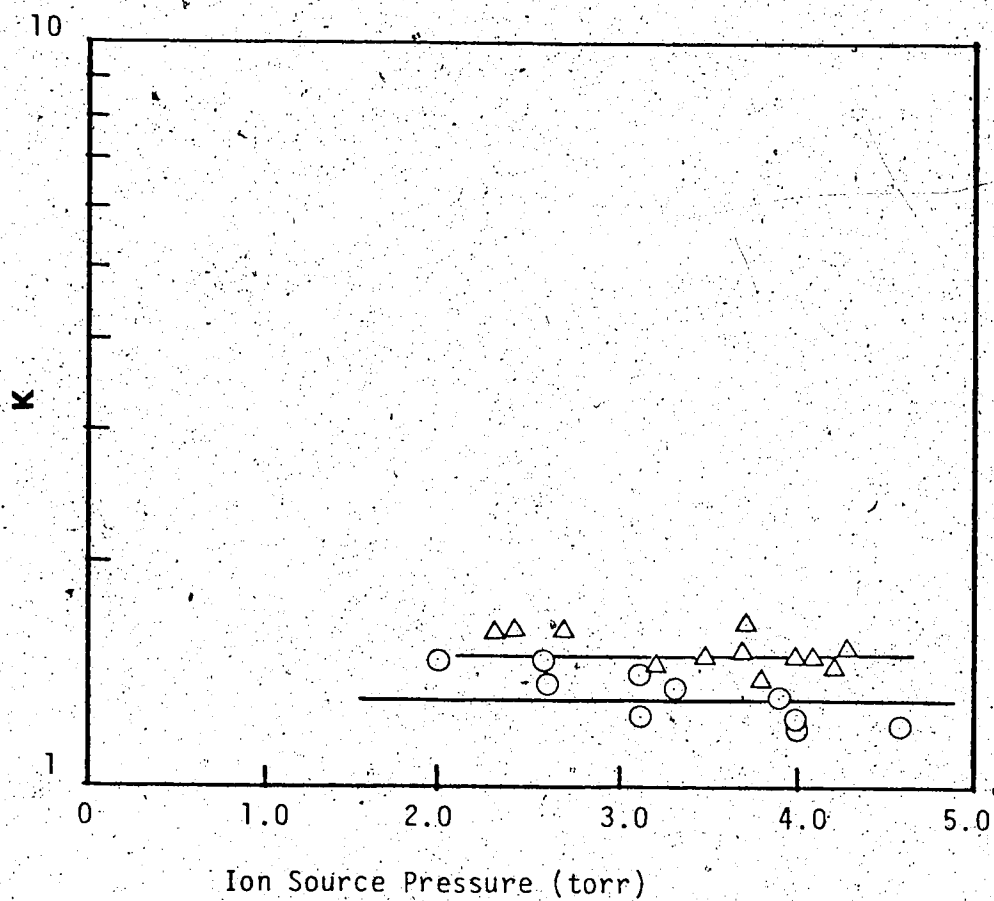
Figure 3.2 Equilibrium Constants versus Ion Source

Pressures for the Reaction

H^+(methanol) + B = methanol + BH^+
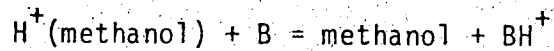
($\triangle$) B = fluorobenzene, ($\bigcirc$) B = chloro-

benzene; temperature: 600°K.
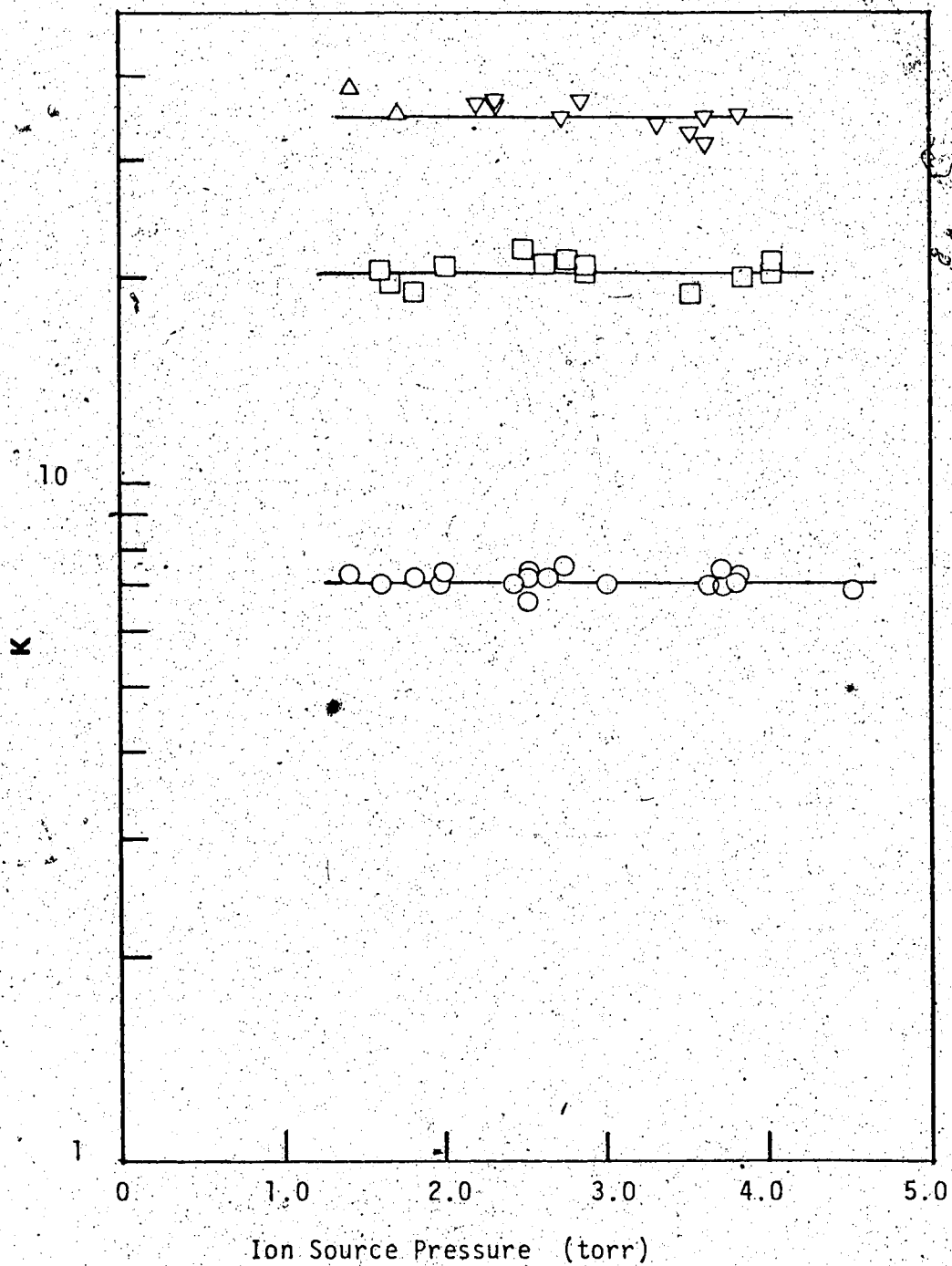
Figure 3.3 Equilibrium Constants versus Ion Source Pressures for the reaction: H^+(benzene) + B = benzene + BH^+

($\triangle$) B = acetonitrile, ($\square$) B = ethanol, ($\bigcirc$) B = acetaldehyde; temperature: 600°K.
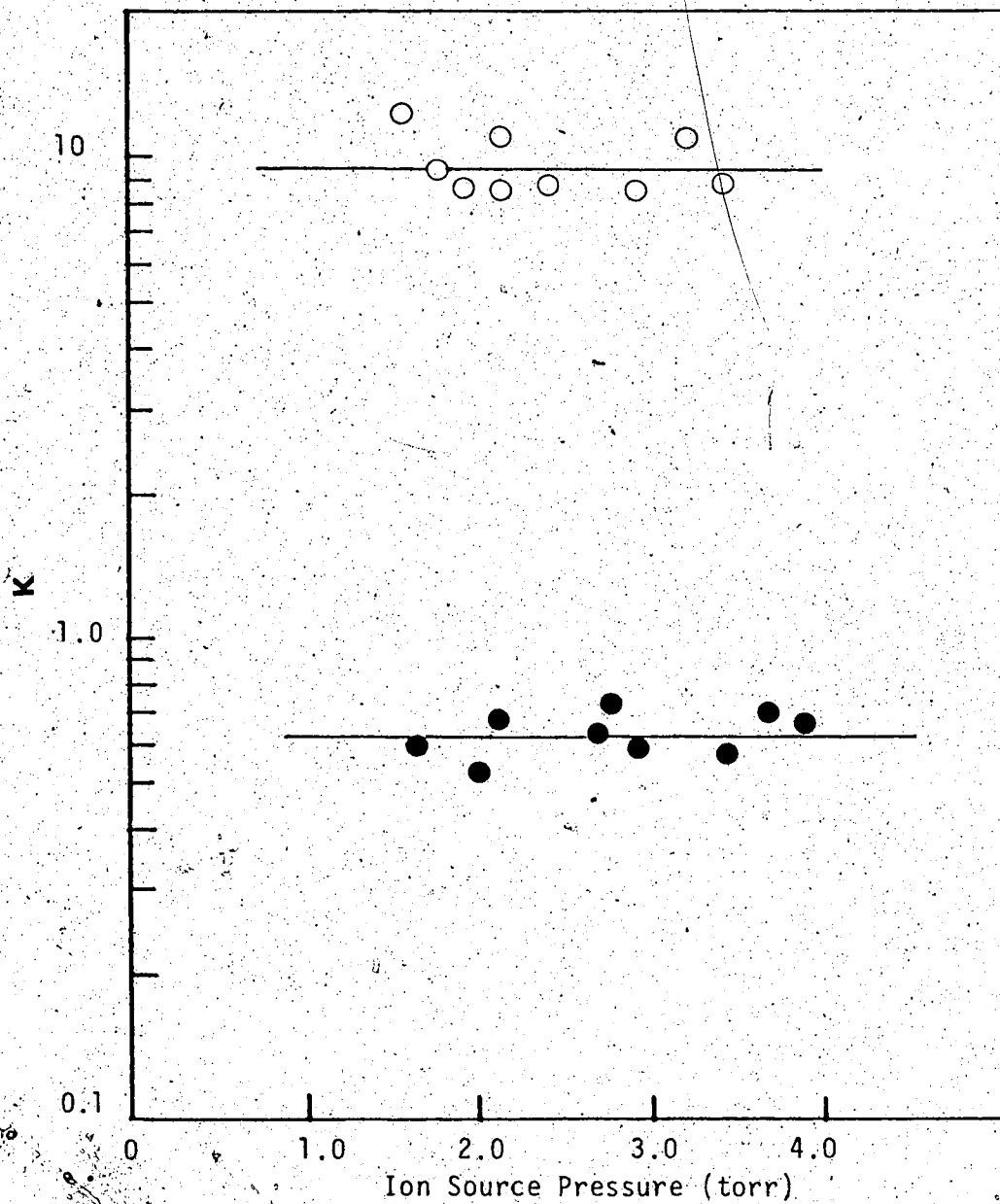
FIGURE 3.4 Equilibrium Constants _versus_ Ion Source Pressures for

the Reaction: H^+(isopropanol) + B = isopropanol + BH^+

(○) B = nitrobenzene, Temperature: 511°K

(●) B = toluene, Temperature: 475°K
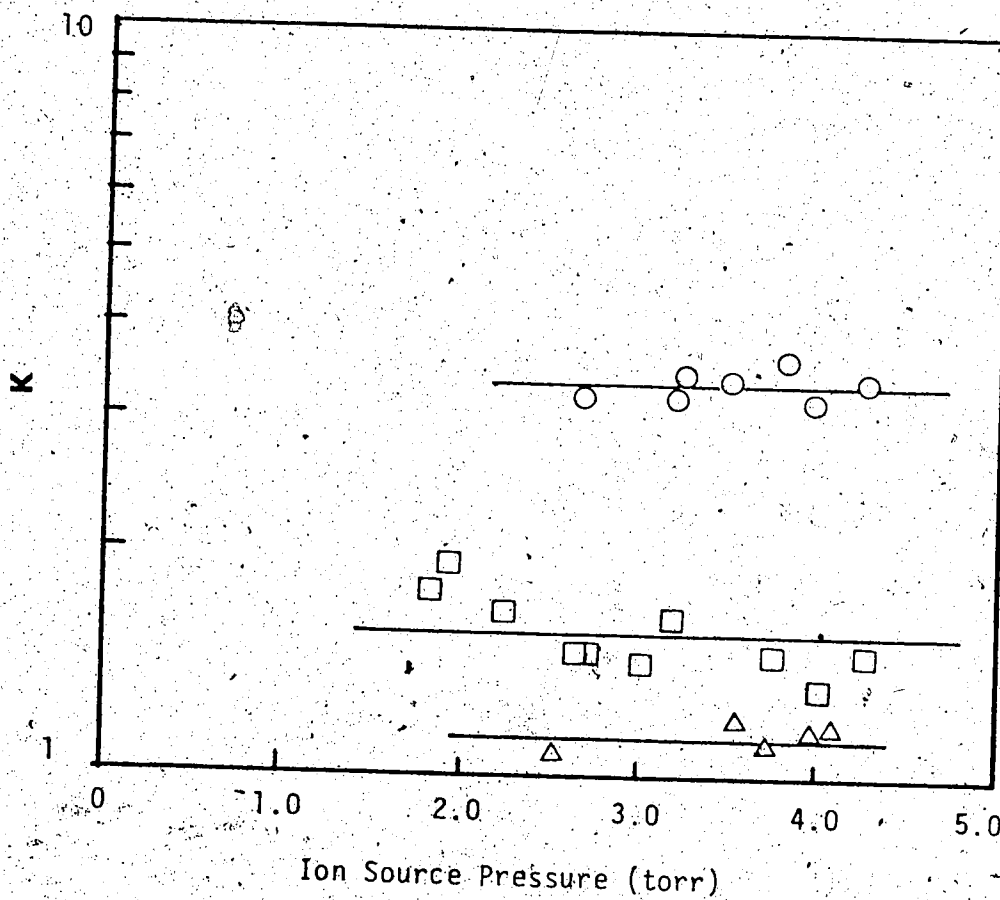
FIGURE 3.5   Equilibrium Constants versus Ion Source
Pressures for the Reaction:
H^+(phenol) + B^+ = phenol + BH^+
(○) B = methyl acetate, (△) B = benzo-
nitrile. (□)= acetone. Temperature: 600°K.
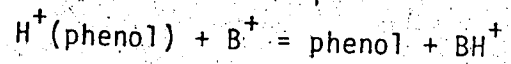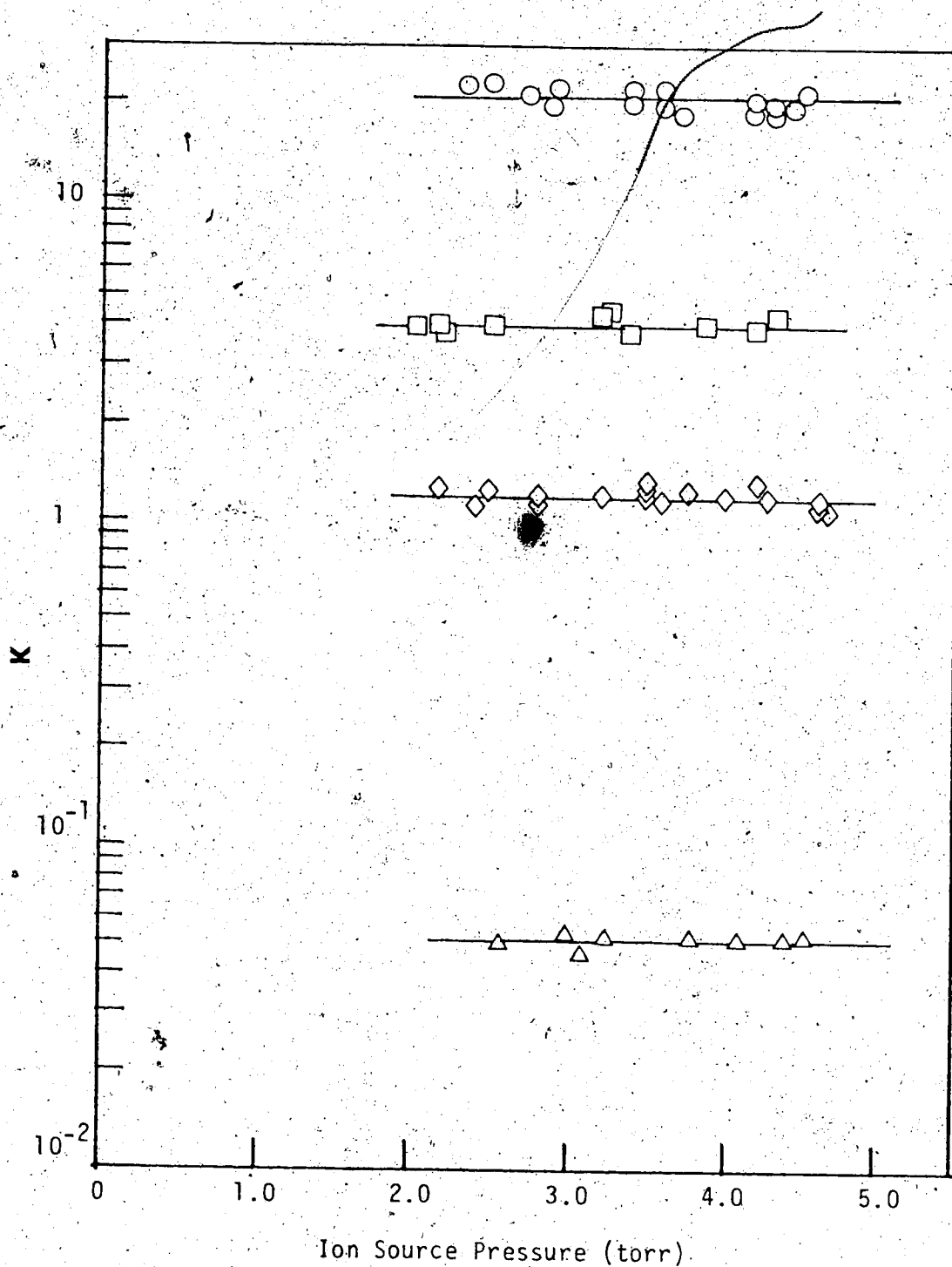
FIGURE 3.6 Equilibrium Constants versus Ion Source Pressures
for the Reaction:

$$BH^+ + ketene = B + (ketene)H^+$$
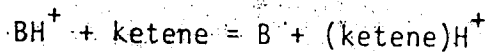
(○) B = ethyl formate; (□) B = isobutene

(◇) B = acetone; (△) B = diethyl ether.

Temperature: 600°K
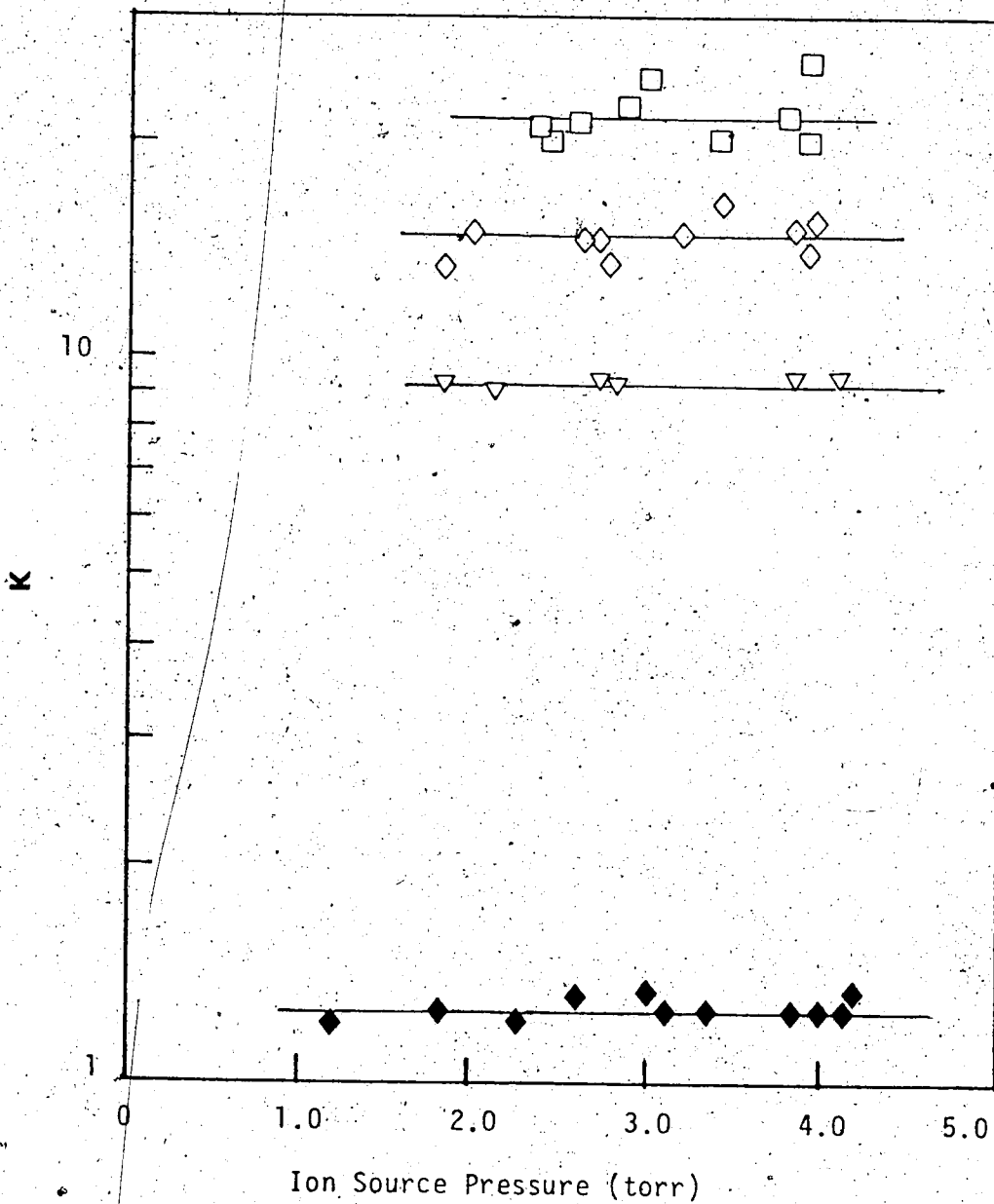
FIGURE 3.7 Equilibrium Constants versus Ion Source Pressures for
the Reaction:

H^+(methyl acetate) + B = methyl acetate + BH^+
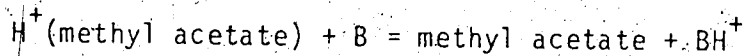
($\square$) B = $\underline{n}$-propyl acetate,   ($\diamond$) B = anisole

($\triangledown$) B = benzaldehyde, ($\blacklozenge$) B = benzoic acid
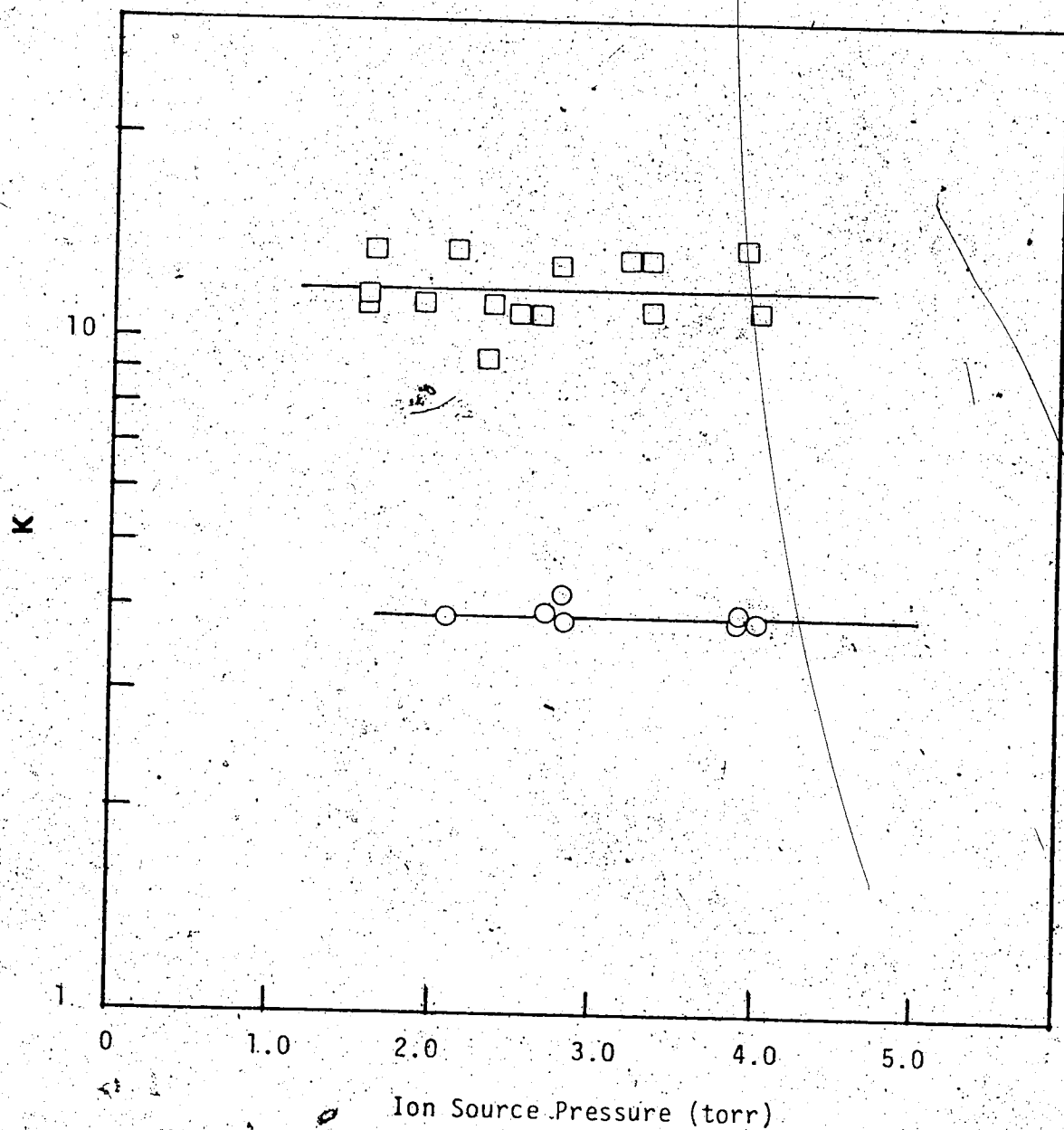
Temperature: 600°K.

FIGURE 3.8 Equilibrium Constants versus Ion Source Pressures for the Reaction:

H^+(aniline) + B = aniline + BH^+
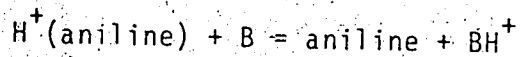
(□) B = methylamine, (○) B = DMSO

Temperature: 600°K.
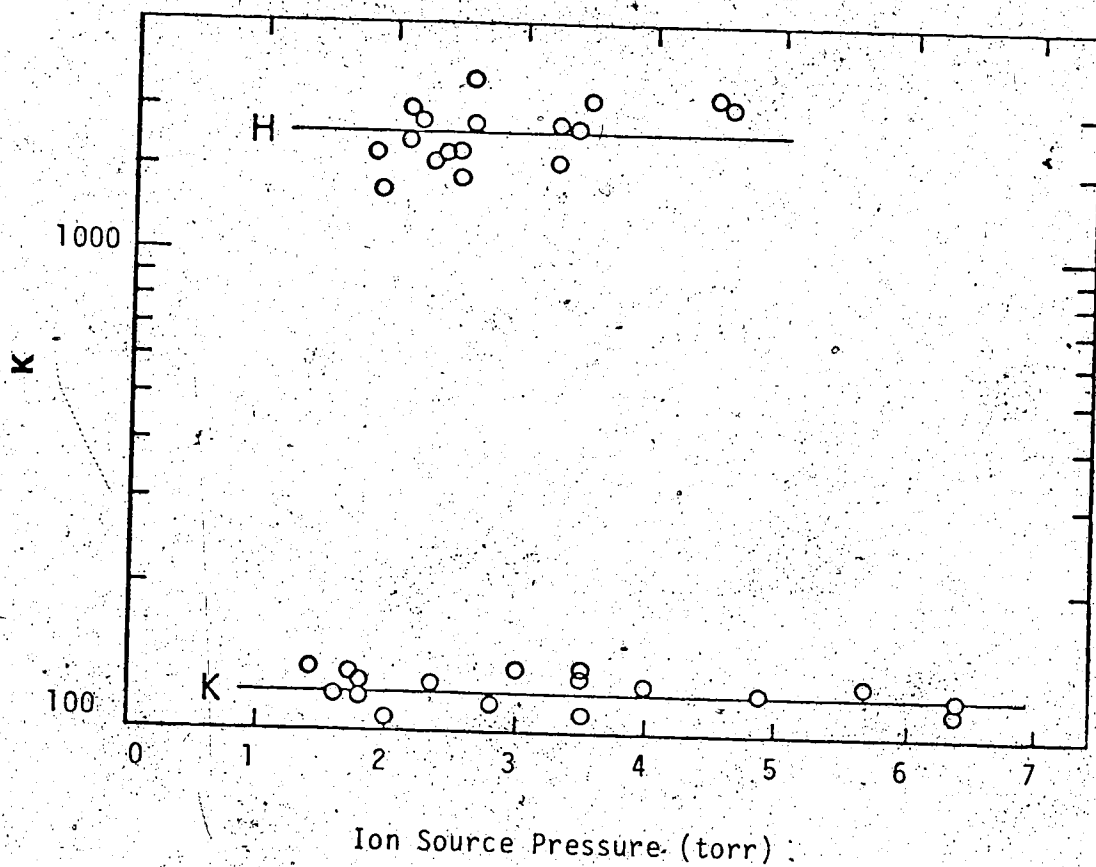
FIGURE 3.9 Results showing the invariance of equilibrium constant, K, with ion source pressure for the reaction:

$$B_1H^+ + B_2 \rightleftharpoons B_1 + B_2H^+$$
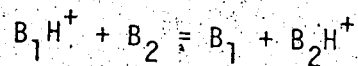
(B_1, B_2) for

H, (1,8-diaminonaphthalene, 1,8-bis(methylamino)naphthalene)

K, (1,8-bis(methylamino)naphthalene, 1-dimethylamino-8-methylaminonaphthalene)
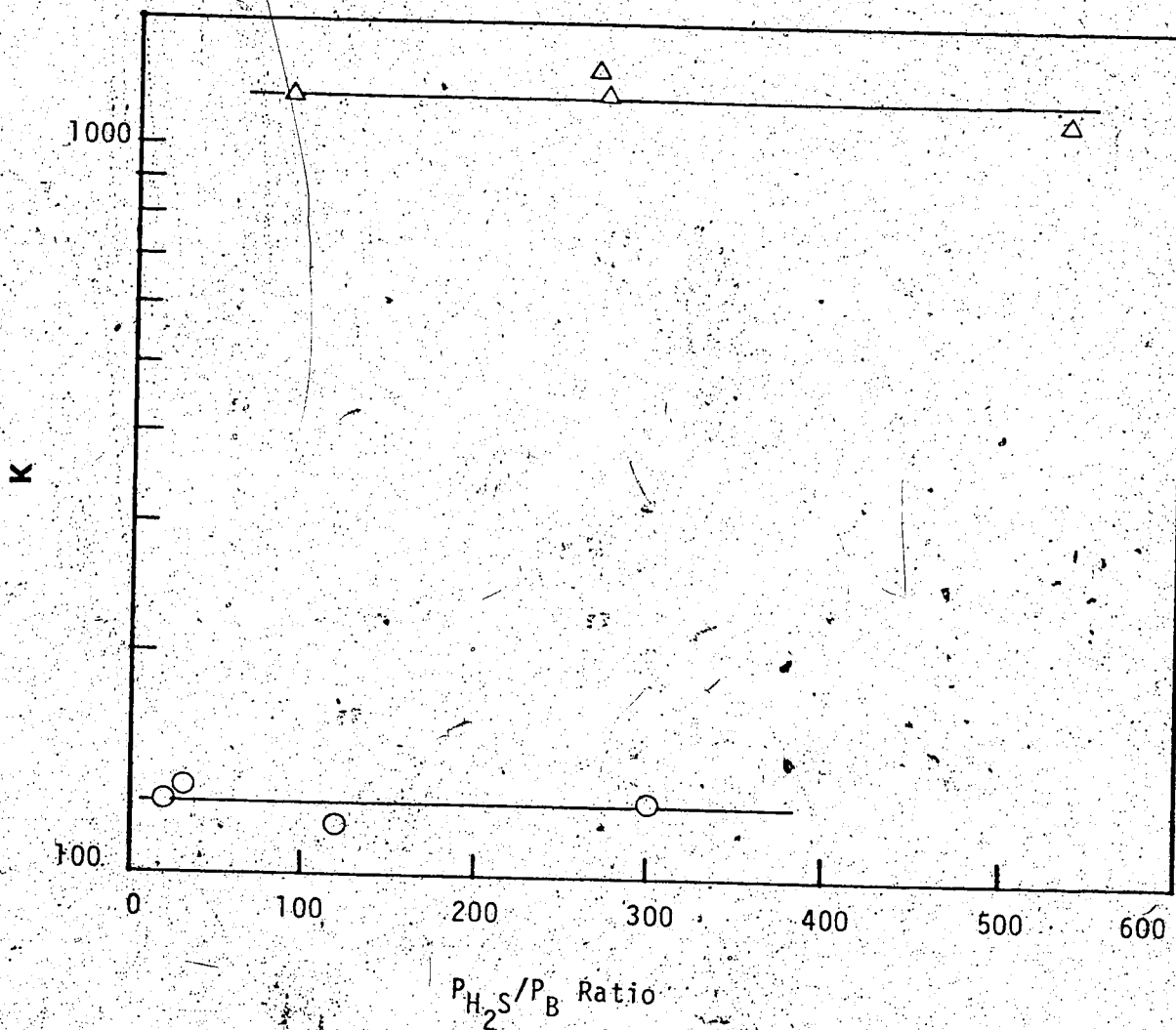
Temperature: 460°K.

FIGURE 3.10 Equilibrium Constants _versus_ P_{H_2S}/P_B Ratios for the

Reaction:

H^+ (hydrogen sulfide) + B = hydrogen sulfide + BH^+
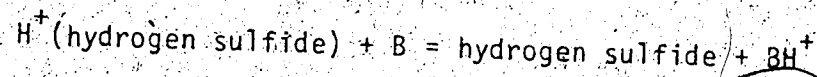
(◯) B = malononitrile: (△) formic acid

Temperature: 600°K.
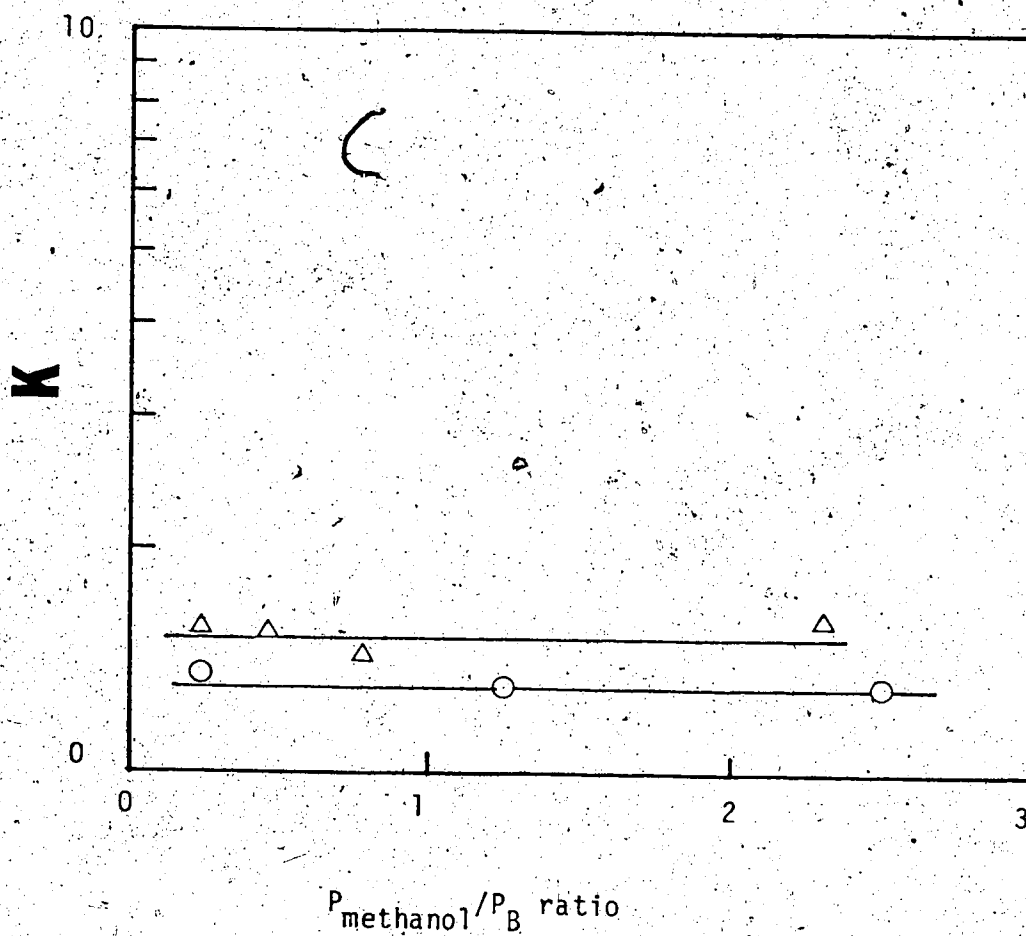
Figure 3.11 Equilibrium Constants <u>versus</u> Concentration
Ratios of Neutrals for the Reaction:

H^+(methanol) + B = methanol + BH^+
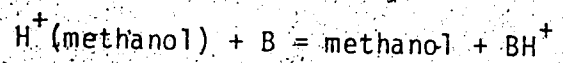
($\triangle$) B = fluorobenzene, ($\bigcirc$) = chlorobenzene
Temperature: 600°K.
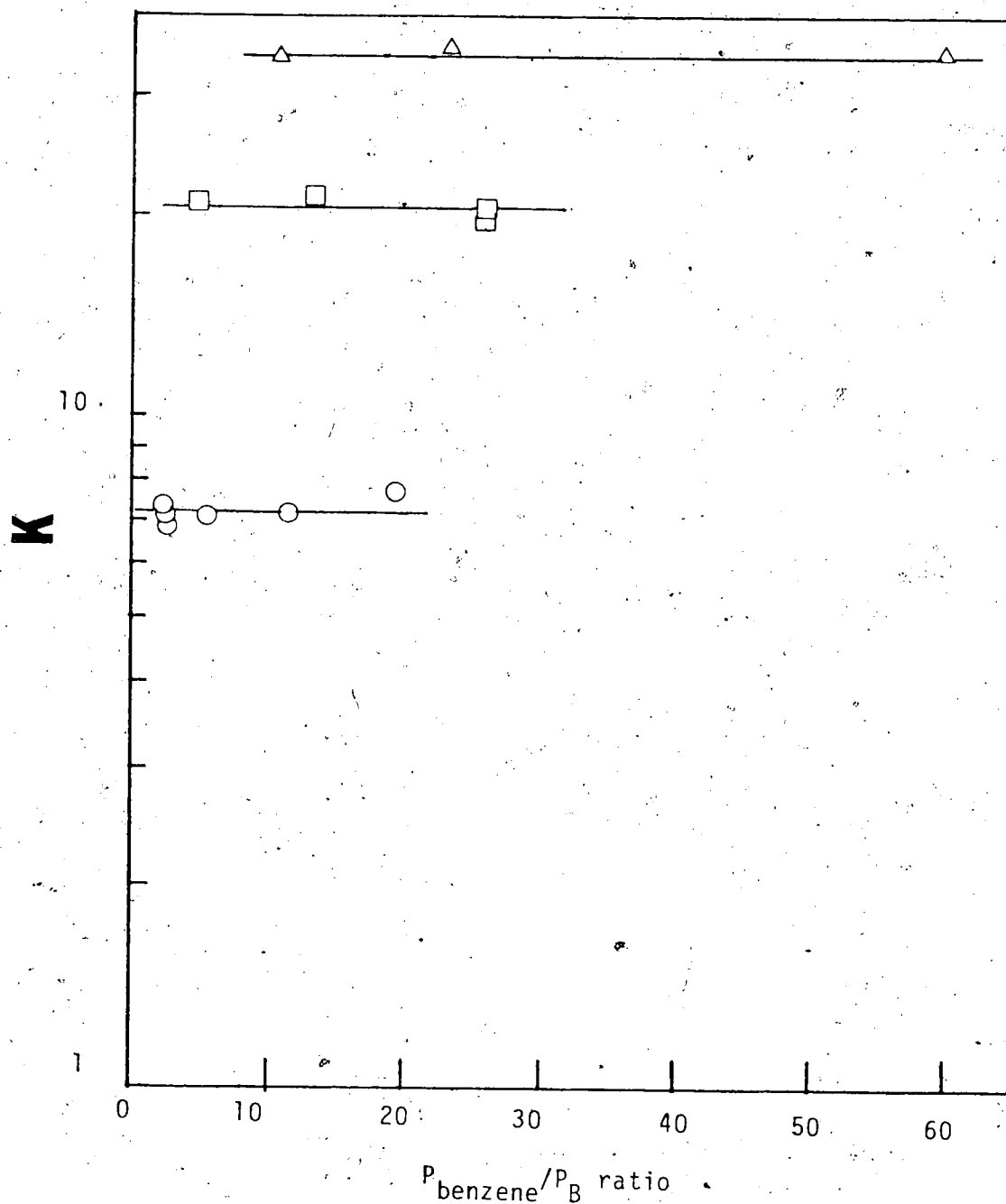
FIGURE 3.12 Equilibrium Constants versus Concentration Ratios of

Neutrals for the Reaction:

H^+(benzene) + B = benzene + BH^+
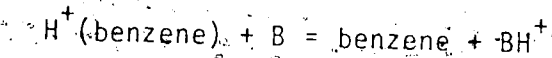
($\triangle$) B = acetonitrile, ($\square$) B = ethanol, ($\bigcirc$) B = Acetal-

dehyde. Temperature: 600°K.
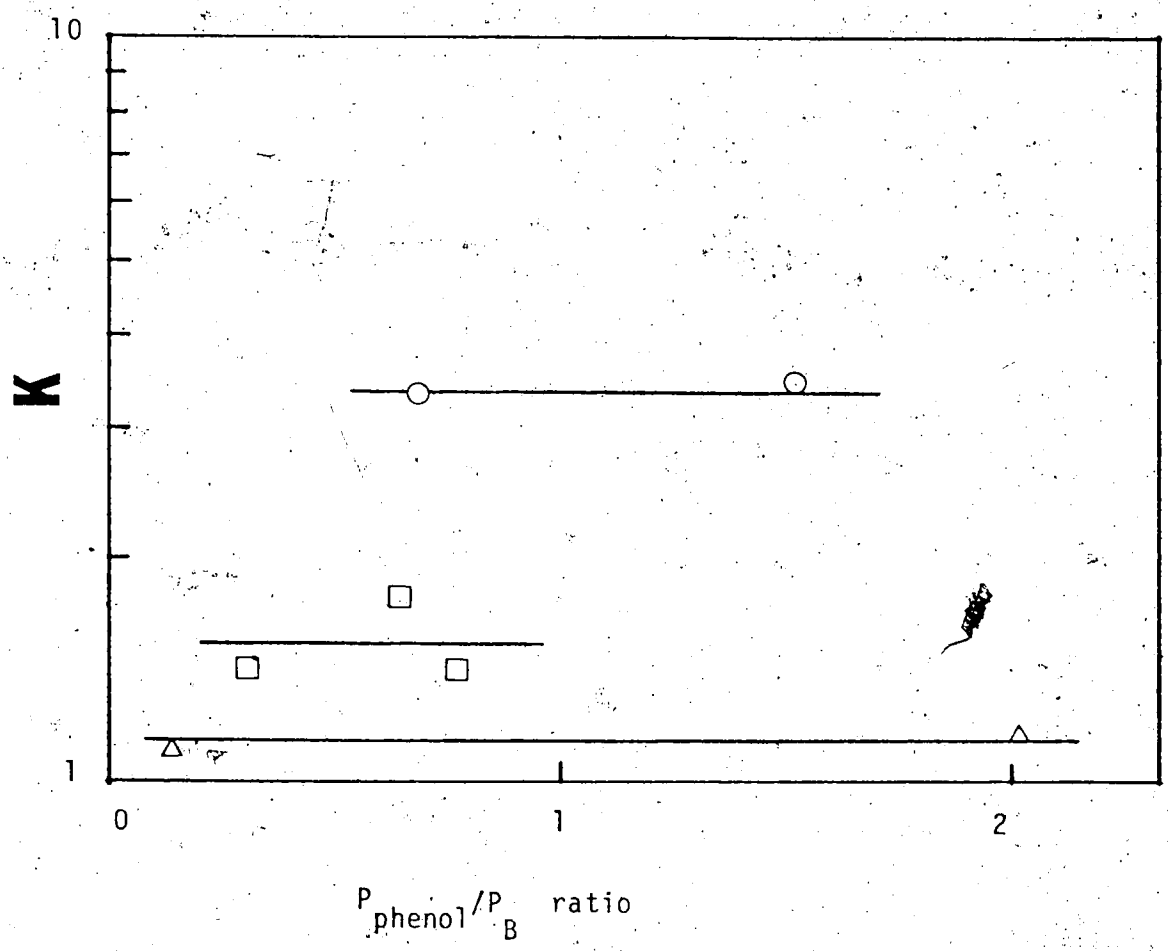
FIGURE 3.13 Equilibrium Constants _versus_ Concentration Ratios of

Neutrals for the Reaction:

H^+(phenol) + B = phenol + BH^+
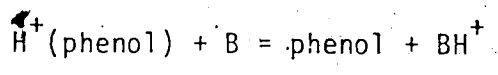
(○) B = methyl acetate (□) B = acetone, (△) B =

benzonitrile. Temperature: 600°K.
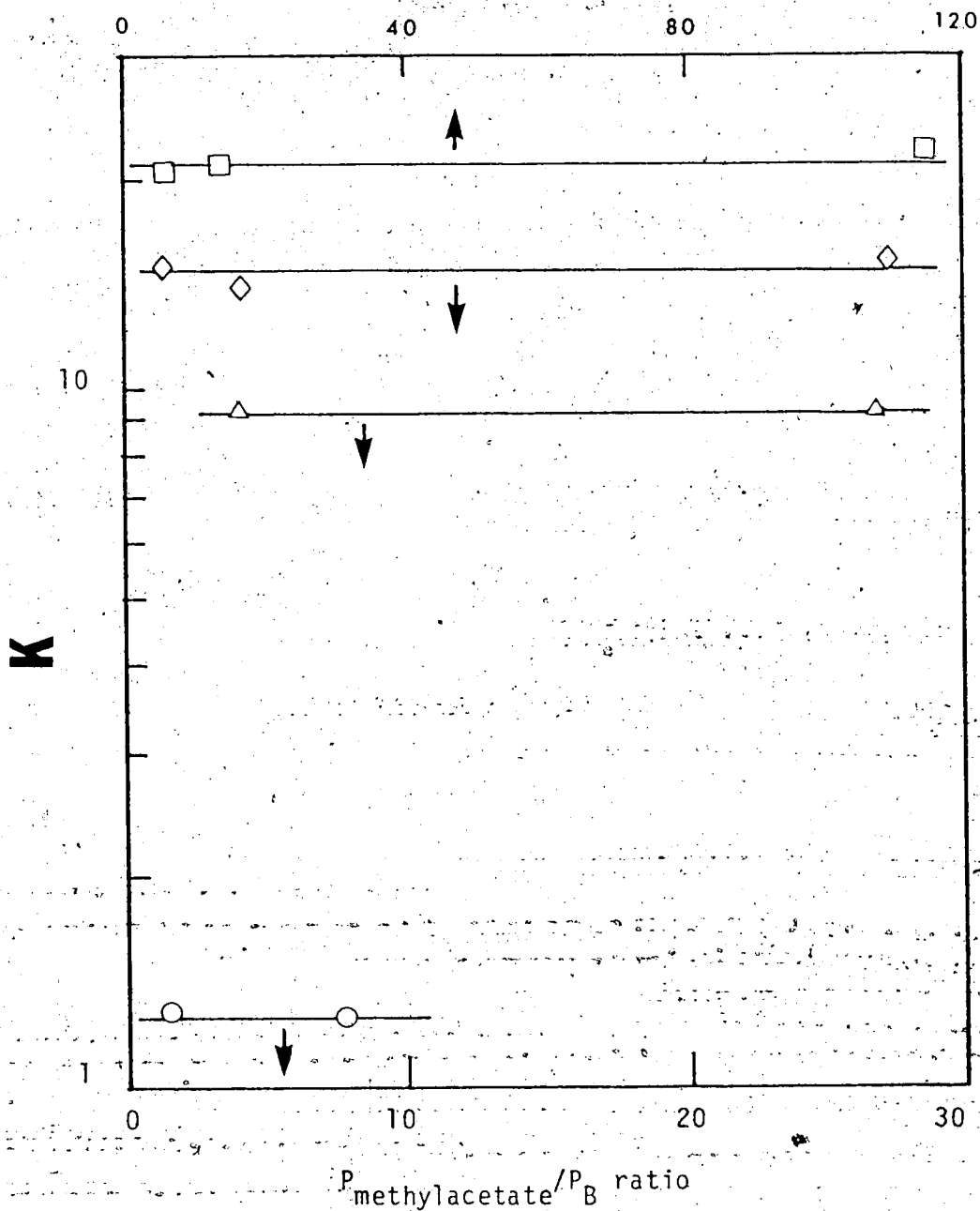
FIGURE 3.14. Equilibrium Constants versus Concentration Ratios

of Neutrals for the Reaction:

H^+(methyl acetate) + B = methyl acetate + BH^+
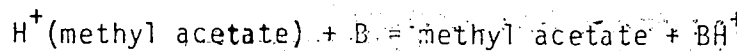
($\square$) B = n-propyl acetate, ($\diamond$) B = anisole

($\triangle$) B = benzaldehyde, ($\bigcirc$) B = benzoic acid
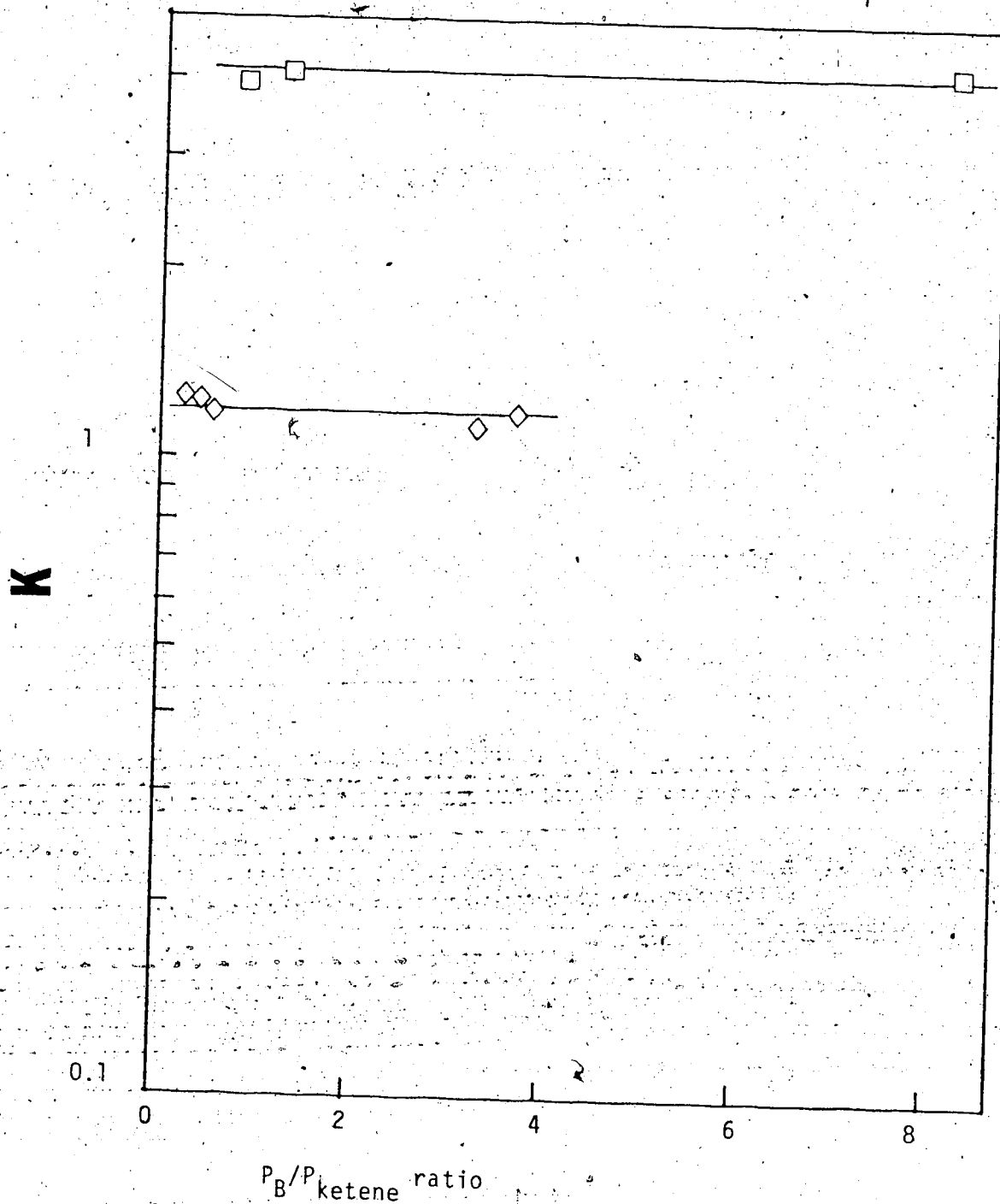
Temperature: 600°K.

FIGURE 3.15A Equilibrium Constants versus Concentration Ratios of Neutrals for the Reaction:

$$BH^+ + ketene = B + (ketene)H^+$$
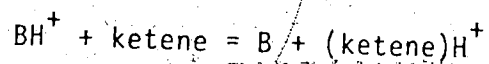
(◇) B = acetone, (□) B = (isobutene)

Temperature: 600°K.
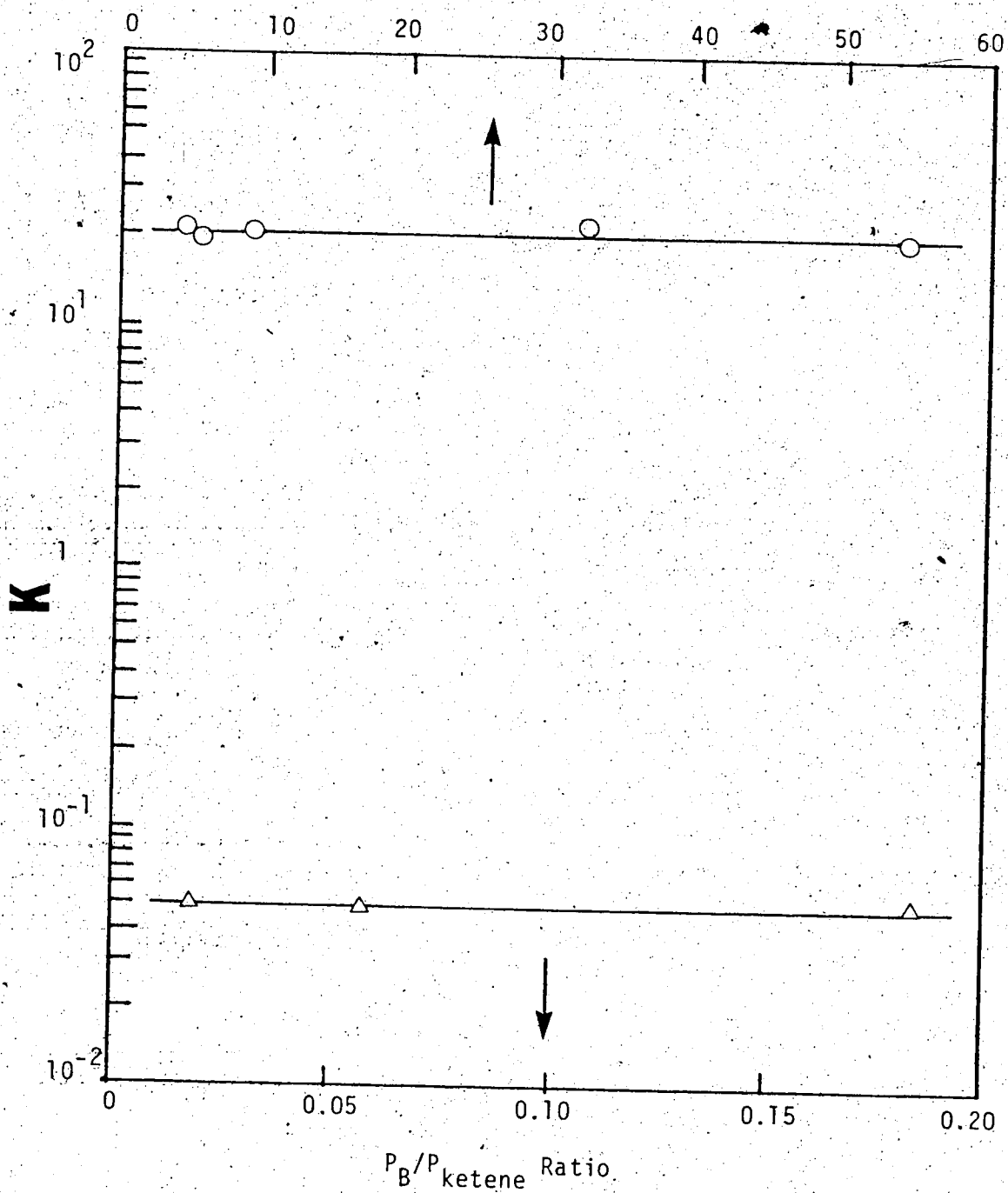
FIGURE 3.15B Equilibrium Constants *versus* Concentration Ratios of Neutrals for the Reaction:

$$BH^+ + ketene = B + (ketene)H^+$$
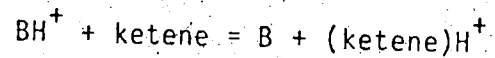
(◯) B = ethyl formate, (△) B = diethyl ether

Temperature: 600°K.
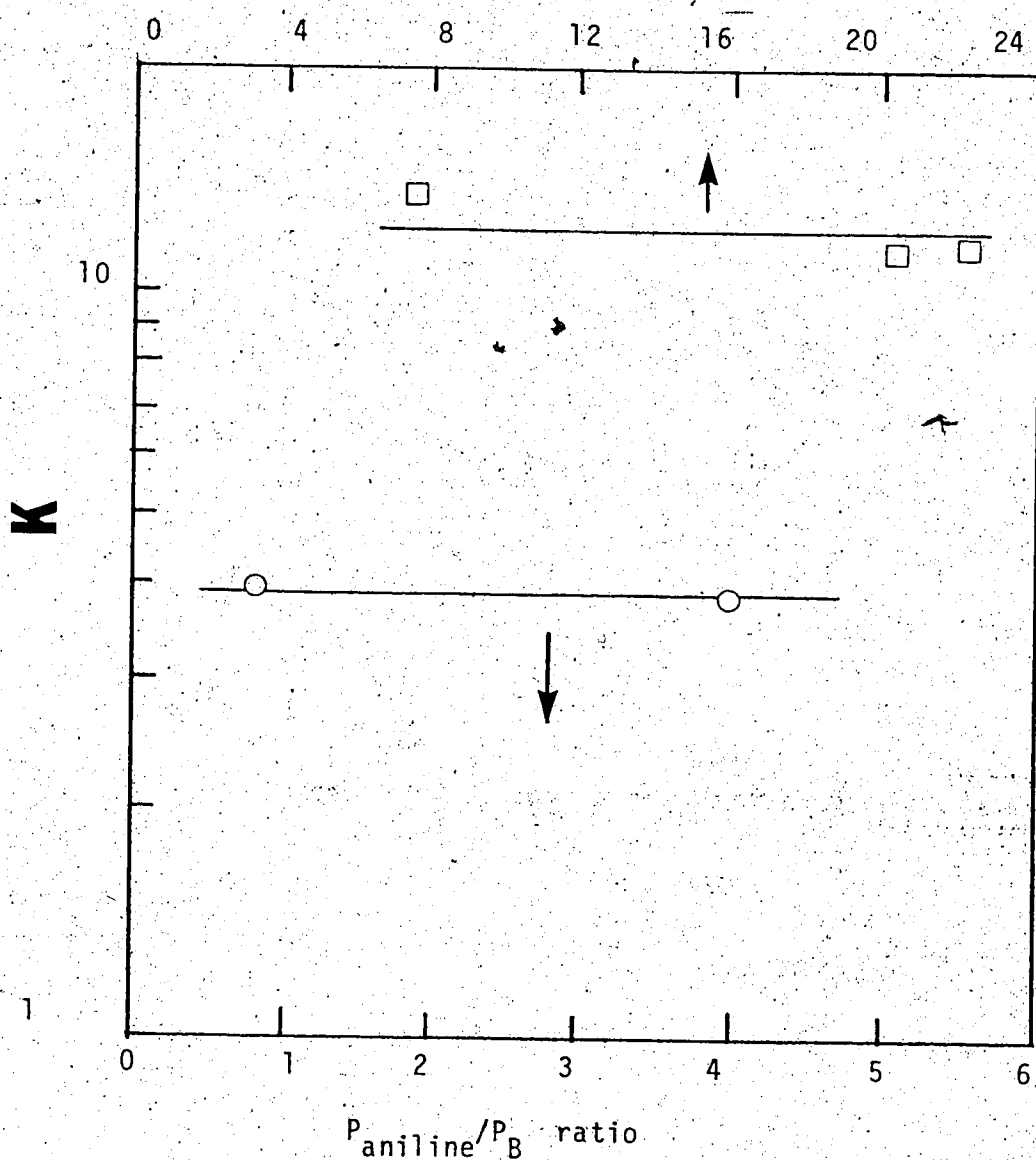
FIGURE 3.16 Equilibrium Constants _versus_ Concentration Ratios of

Neutrals for the Reaction:

$H^+(aniline) + B = aniline + BH^+$
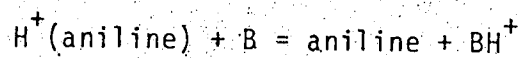
(□) B = methylamine, (○) B = DMSO

Temperature: 600°K.

FIGURE 3.17 Results showing the invariance of equilibrium

constant, K, with neutral ratio for the reaction:
$$B_1H^+ + B_2 = B_1 + B_2H^+$$
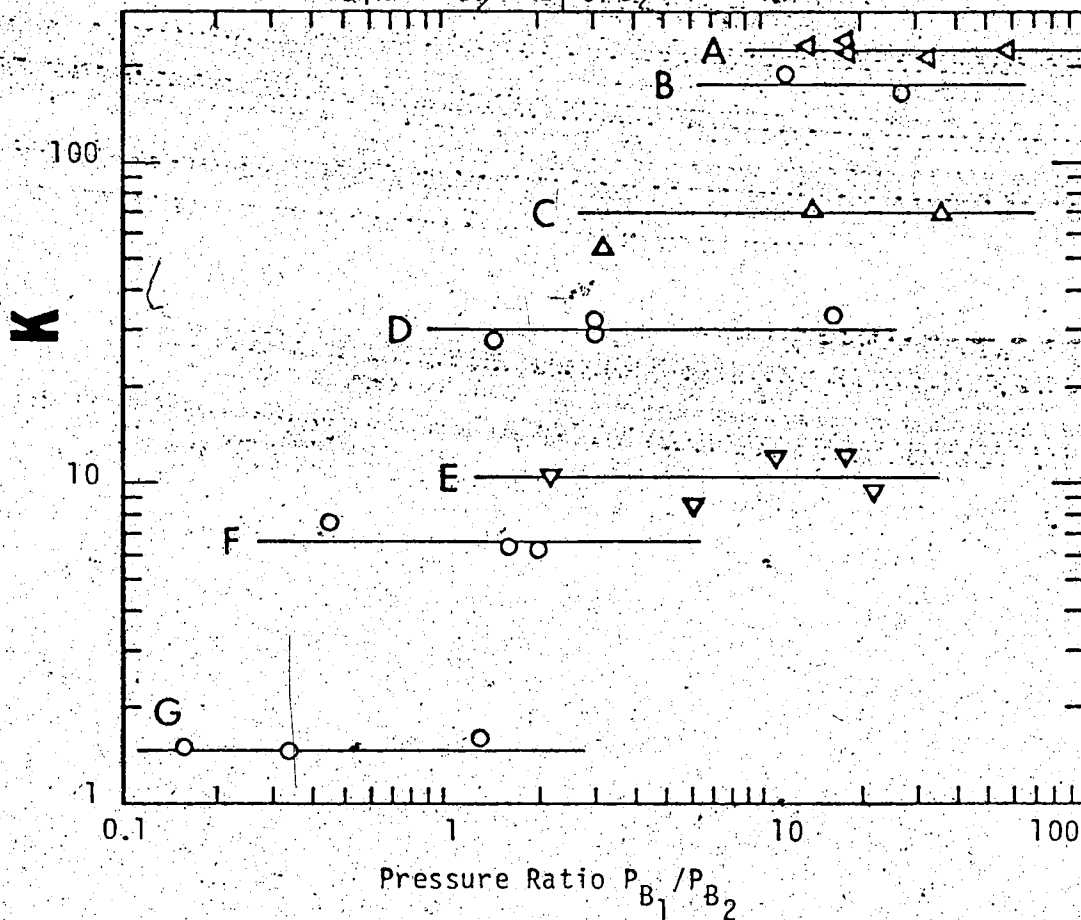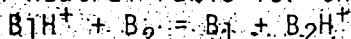
(B_1, B_2) for

A, (1,8-diaminonaphthalene, 1,5-diaminopentane)

B, (piperidine, 1,8-bis(methylamino)naphthalene)

C, (1,8-bis(methylamino)naphthalene, 1,2-bis(dimethylamino)benzene)

D, (piperidine, 1,5-diaminopentane)

E, (1,8-diaminonaphthalene, piperidine)

F, (1,5-diaminopentane, 1,8-bis(methylamino)naphthalene)

G, (1,2-bis(dimethylamino)benzene, 1-dimethylamino-8-methyl-
    aminonaphthalene)

Temperature: 460°K

two monosubstituted benzenes, fluorobenzene and chloro-
benzene, over a wide range of temperature (30°C-330°C).
The results showing the invariance of equilibrium con-
stants with the variation of ion source pressures and
concentration ratios of neutrals at a given temperature
are shown in Figures 3.18-3.21. The van't Hoff plots
for the two reactions are used to obtain the ΔH^o and the
ΔS^o of the reactions. They are shown in Figure 3.22. The
results of the van't Hoff plots are summarized in Table
3.53. The expected entropy changes due to changes of
rotational symmetry numbers, $\Delta S^o_{rot.s.}$, in these two
reactions are also shown in Table 3.53.

3.2 Proton Affinity Scale

The absolute proton affinities of various compounds
may be obtained from the relative basicity ladder (Table
3.1) if the proton affinity of one compound on the ladder
is known. In previous work from this laboratory, iso-
butene was chosen as the external standard for two rea-
sons. First, isobutene has a proton affinity which is
close to that of ammonia, and ammonia is commonly used
as a reference in comparing gas-phase basicities. Second,
it was believed that a reliable proton affinity value for
isobutene could be obtained from the enthalpies of forma-
tion of reactants and products in the reaction.

$$(CH_3)_3C^+ = (CH_3)_2C=CH_2 + H^+ \qquad (3.2)$$
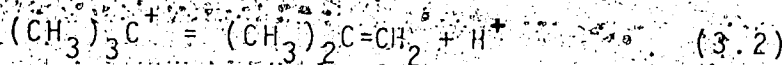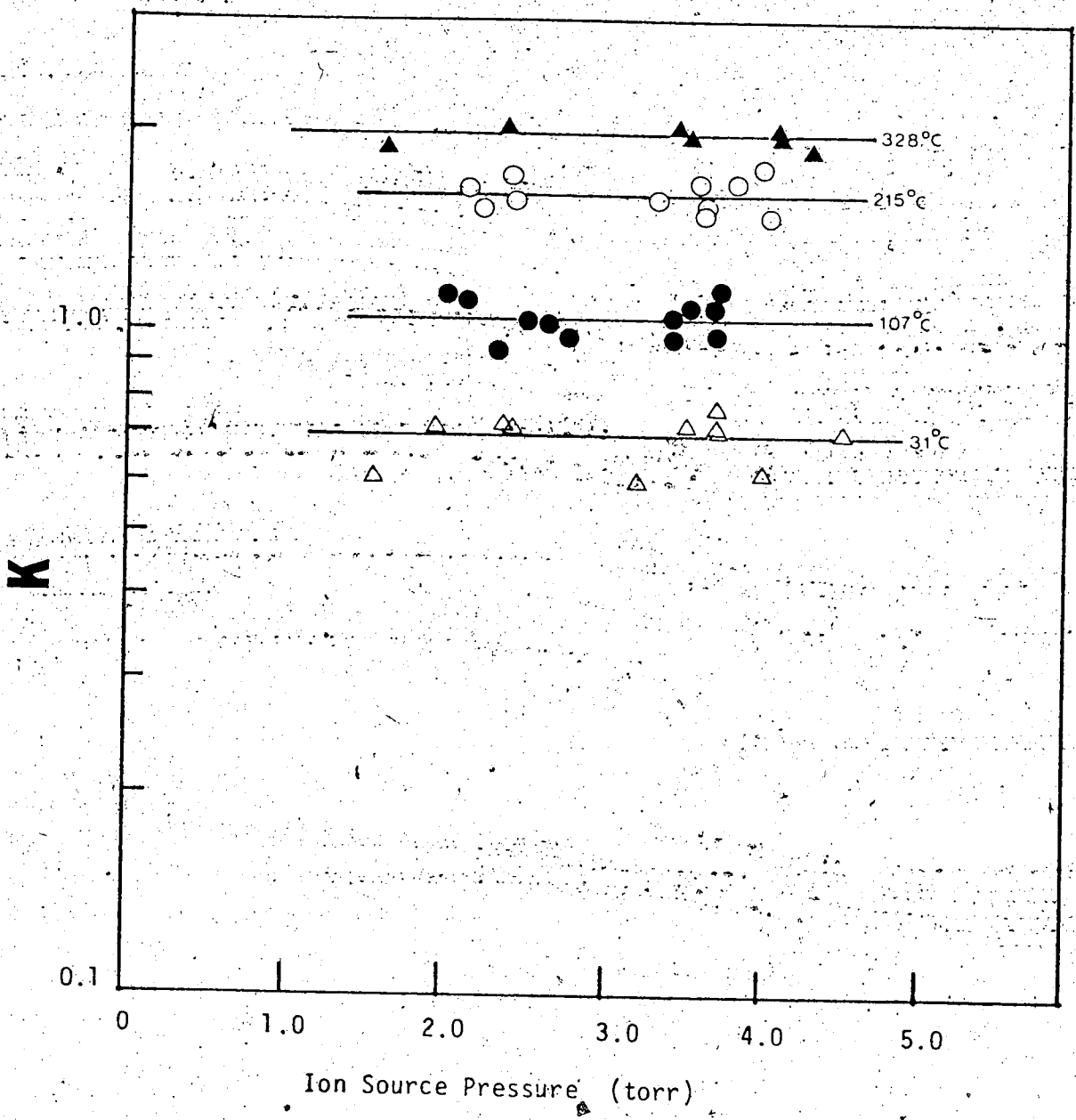
FIGURE 3.18 Equilibrium Constants versus Ion Source Pressures at Different Temperatures for the Reaction:

H^+(fluorobenzene) + benzene = fluorobenzene + H^+(benzene)
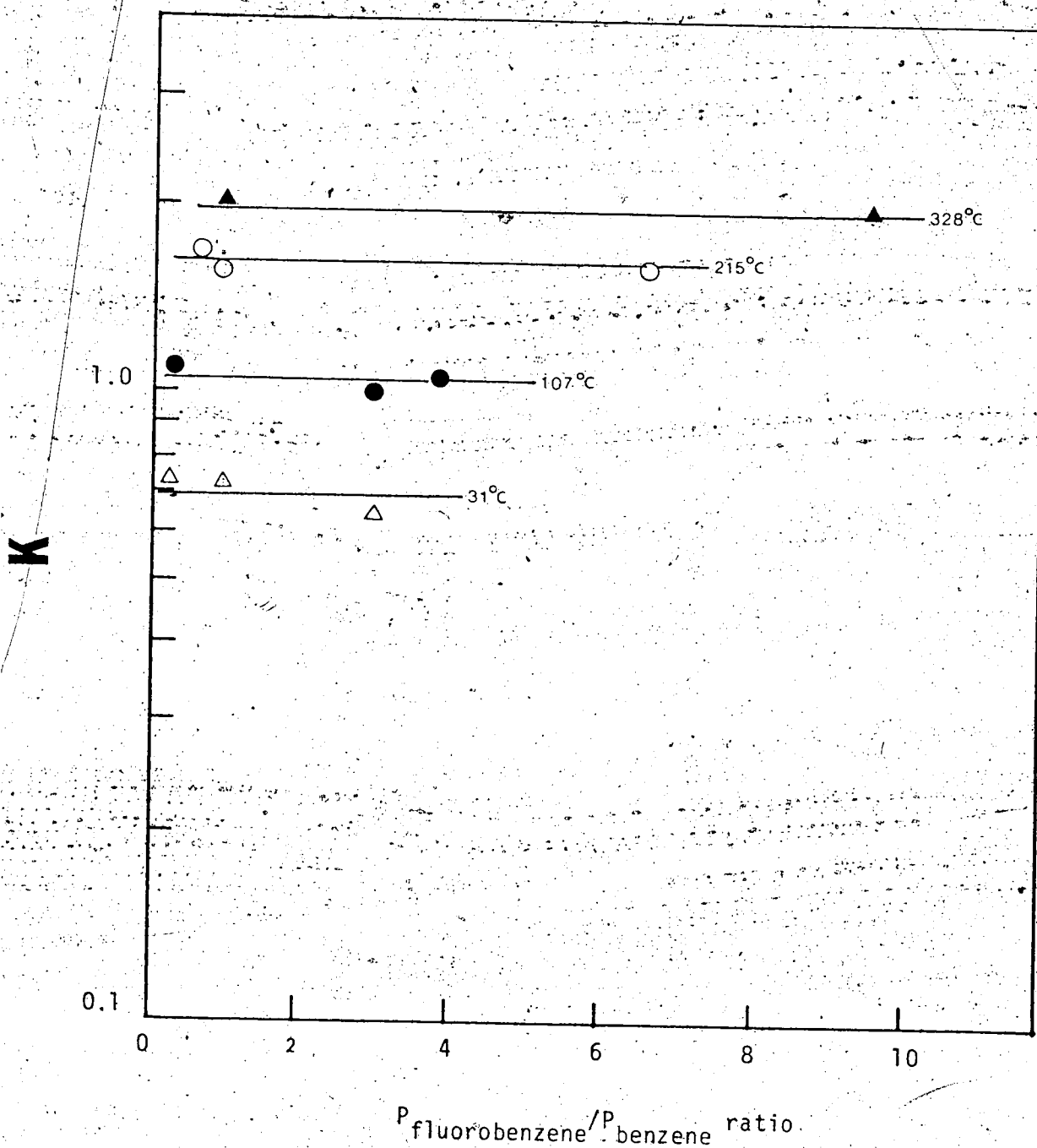
FIGURE 3.19   Equilibrium Constants _versus_ Concentration Ratios of Neutrals at Different Temperatures for the Reaction:

$$H^+(\text{fluorobenzene}) + \text{benzene} = \text{fluorobenzene} + H^+(\text{benzene})$$

FIGURE 3.20 Equilibrium Constants _versus_ Ion Source Pressures at Different Temperatures for the Reaction:

H^+(chlorobenzene) + benzene = chlorobenzene + H^+(benzene)
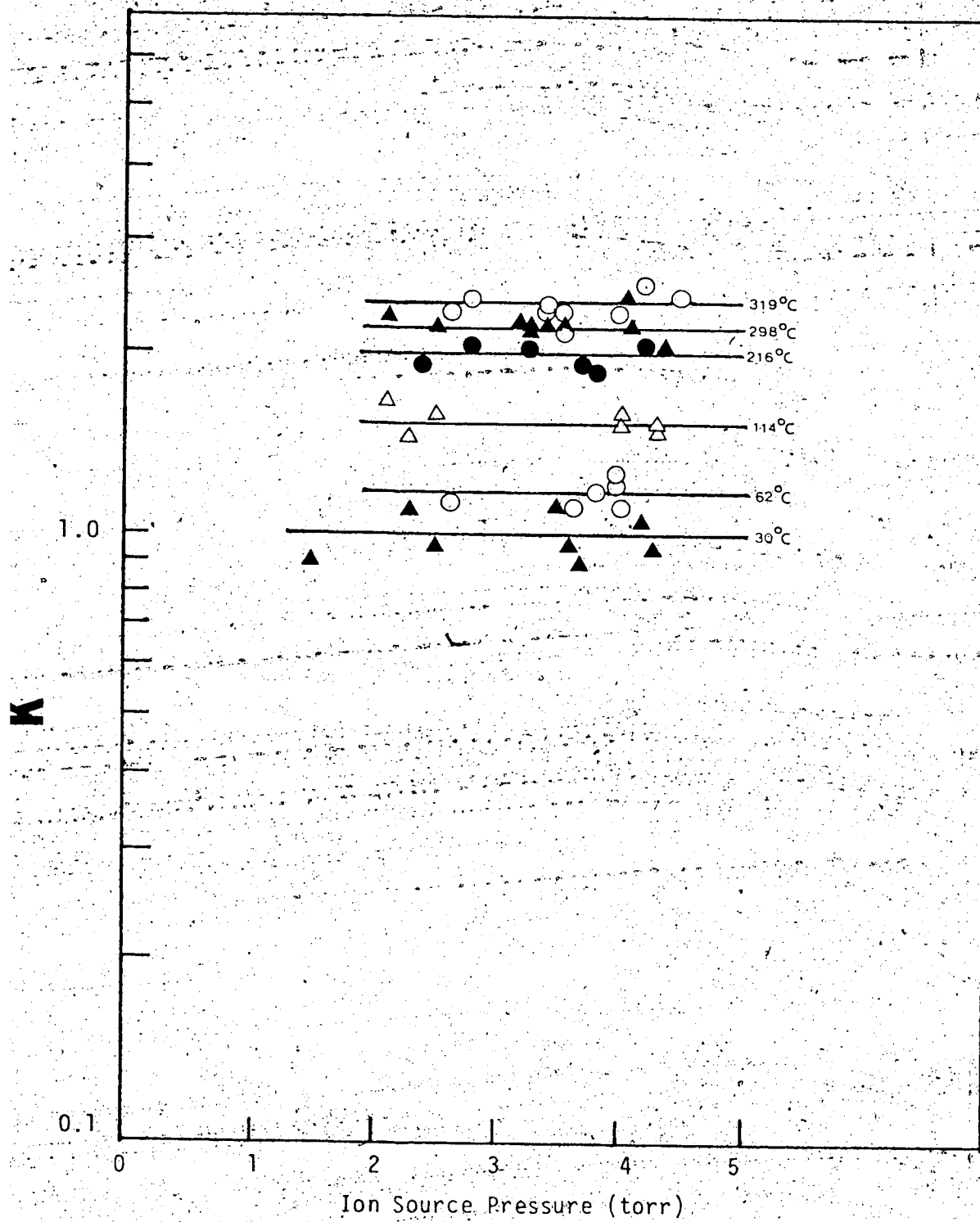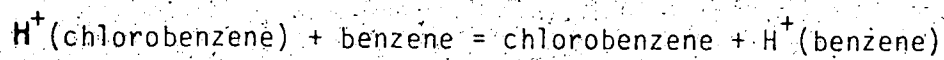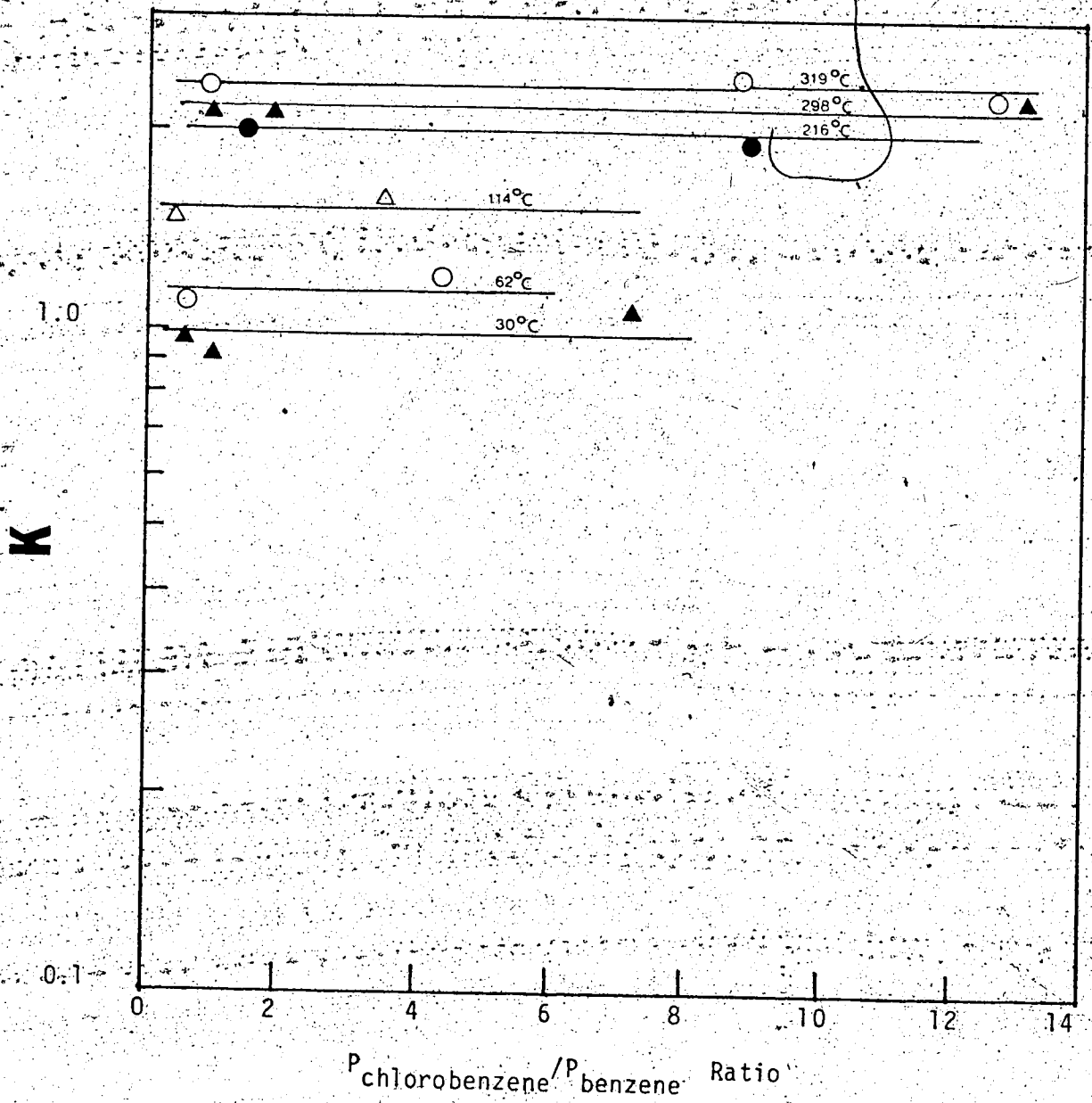
FIGURE 3.21 Equilibrium Constants versus Concentration Ratios of Neutrals at Different Temperatures for the Reaction:

$$H^+(chlorobenzene) + benzene = chlorobenzene + H^+(benzene)$$
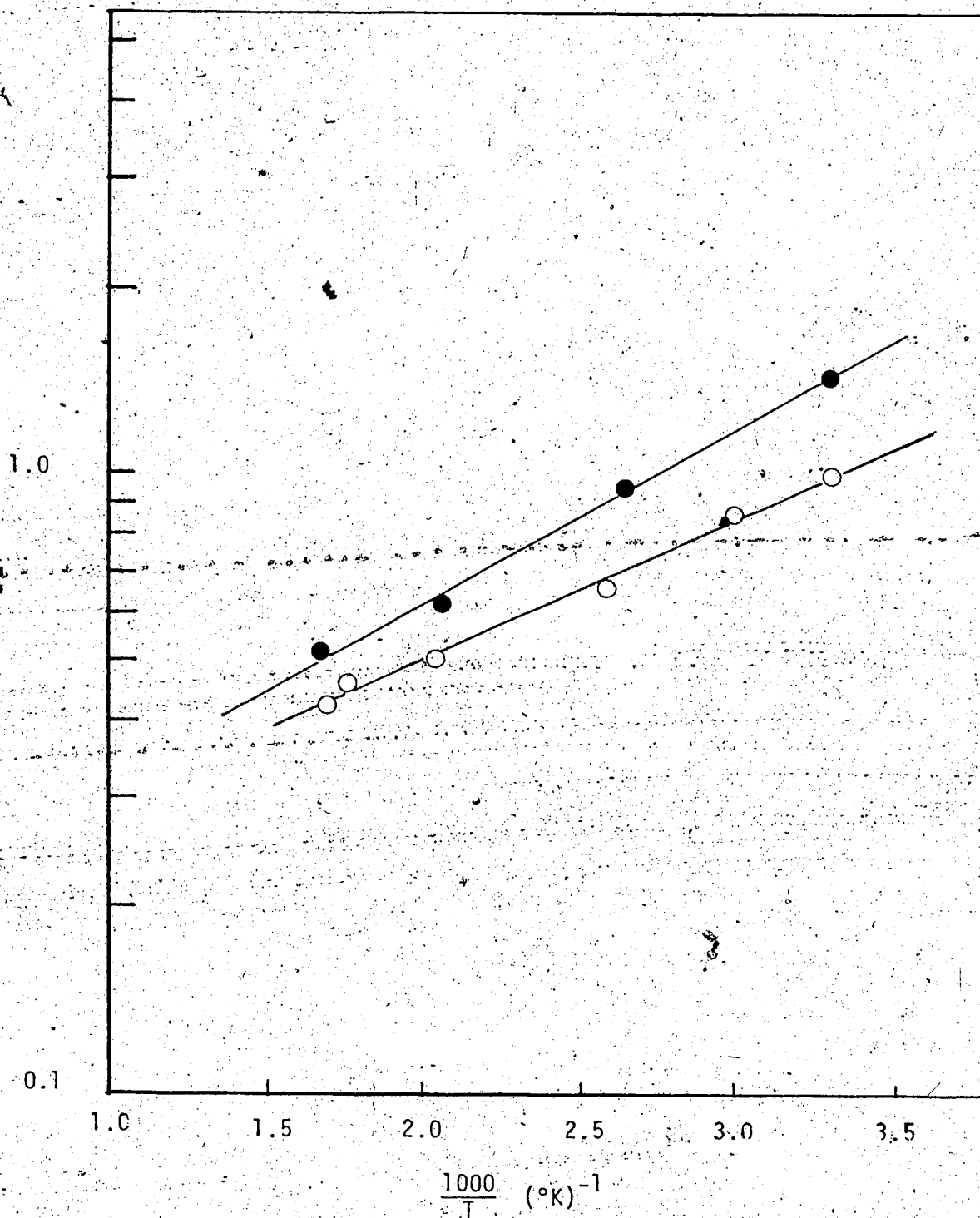
FIGURE 3.22 van't Hoff type plots of the equilibrium constants for the reaction:

$$H^+(\text{benzene}) + B = \text{benzene} + BH^+$$
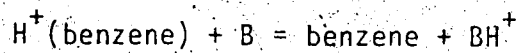
(●) B = fluorobenzene,   (○) B = chlorobenzene

Table 3.53. Summary of experimental thermodynamic functions from the van't Hoff plots for the reaction:

$$H^+(benzene) + B = benzene + BH^+$$

Reaction with B as	$-\Delta H^o$ (kcal/mole)	$-\Delta G^o_{298}$ [a] (kcal/mole)	$-\Delta S^{oa}$ (eu)	$-\Delta S^o_{rot.s.}$ [a,b] (eu)
Fluorobenzene	1.29 ± 0.06	0.24 ± 0.07	3.52 ± 0.15	3.56
Chlorobenzene	1.09 ± 0.05	0.01 ± 0.06	3.41 ± 0.12	3.56

[a] Standard state 1 atm.

[b] $\Delta S^o_{rot.s.} = R\ln\left(\dfrac{\sigma_{H^+(benzene)}}{\sigma_{benzene}}\right)\left(\dfrac{\sigma_B}{\sigma_{BH^+}}\right) = R\ln\left(\dfrac{2}{1\,2}\right)(1).$

where

$$PA(\text{isobutene})° = \Delta H_f^0(\text{isobutene}) + \Delta H_f^0(H^+) - \Delta H_f^0(\text{tert-butyl}^+) \quad (3.3)$$

The accuracy of the proton affinity values obtained in this way are ultimately based on the accuracy of the thermo-chemical data used in calculating the proton affinity of isobutene. As it is shown in equation 3.3, these include $\Delta H_f^0(\text{isobutene})$, $\Delta H_f^0(H^+)$ and $\Delta H_f^0(\text{t-butyl}^+)$. The literature values of $\Delta H_f^0(\text{isobutene}) = -4.04$ kcal/mole (76) and $\Delta H_f^0(H^+) = 367.2$ kcal/mole (77) are believed to be reliable. The heat of formation of tert-butyl cation may be derived from the heat of formation of tert-butyl radical and the ionization potential of the tert-butyl radical. A summary of the available ΔH_f^0 and IP values for tert-butyl radical in the literature together with the corresponding references are tabulated in Table 3.54. The values of the heat of formation of tert-butyl radical are mostly due to Tsang (78) from the studies of thermal decomposition of alkanes by the shock-tube method at 1000-1200°K. Two assumptions were used. First, radical recombination has zero activation energy. Second, the heat capacities of the alkyl radicals are intermediate between those of the corresponding alkanes and alkenes. As it is shown in Table 3.54, the $\Delta H_f^0(\text{t-butyl})$ values reported are consistently around 9.0 kcal/mole. A recent analysis by Tsang (79) suggested strong temperature dependence

Table 3.54 Thermochemical data for the evaluation of
$$\Delta H_f^0(\text{t-butyl}^+)$$
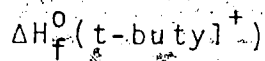
$\Delta H_{f,300}^0$ (t-butyl) (kcal/mole)	References
6.8	J.A. Kerr, Chem. Review, <u>69</u>, 125 (1969)
7.5	W. Tsang, J. Chem. Phys., <u>44</u>, 4283 (1966)
9.1	W. Tsang, Int. J. Chem. Kinet., <u>1</u>, 245 (1969)
9.3	W. Tsang, Int. J. Chem. Kinet., <u>2</u>, 311 (1970)
12 ± 1	W. Tsang, Int. J. Chem. Kinet., <u>10</u>, 821 (1978)

preferred value $\Delta H_{f,300}^0$ (t-butyl) = 9.0 kcal/mole

IP(t-butyl) (kcal/mole at 298°K)	References
159.8	F. P. Lossing and G. P. Semeluk, Can. J. Chem., <u>48</u>, 143 (1972)
154.5	F. A. Houle and J. L. Beauchamp, J. Am. Chem. Soc., to be published

preferred value IP(t-butyl) = 154.5 kcal/mole

of the A factor in the Arrhenius rate constant expression,
$k = Ae^{-E_a/RT}$, for the decomposition reaction 3.4.

$$\text{hexamethylethane} \xrightarrow[k_r]{k_d} 2 \text{ t-butyl} \qquad (3.4)$$
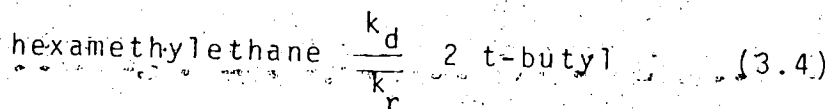
The analysis was based on the theoretical calculations of
the entropy change for reaction 3.4, and the experimental
rate constant expressions for decomposition (k_d) obtained
at 1000-1200°K and for recombination (k_r) obtained by
Parkes and Quinn (80) at 300-600°K. Results of these
considerations would lead to a slightly higher value of
ΔH_f^0(t-butyl) = ~12 kcal/mole. Until further evidence is
obtained, the more consistent recommended value of
ΔH_f^0(t-butyl) = 9.0 kcal/mole should be preferred. The
ionization potential of tert-butyl radical was reported
earlier by Lossing and Semeluk (81) to be 159.8 kcal/mole.
A recent determination by Beauchamp (82) suggested that
the previous value is slightly higher and an IP(t-butyl)
value of 154.5 kcal/mole was reported. It is believed
that the latter value is more reliable. The preferred
value for the heat of formation of tert-butyl cation is
therefore chosen to be 165.0±3 kcal/mole as shown in table
3.55. The PA(isobutene) may then be calculated from equa-
tion 3.3 to be 198.2 kcal/mole. It should be noted that the
proton affinity results reported previously from this
laboratory (3,83) were calibrated by the external.

TABLE 3.55 ΔH_f^o of tert-butyl cation and proton affinity of isobutene

1. $\underline{\Delta H_f^o(\text{t-butyl}^+)^{a,b}}$

$$t\text{-}C_4H_9 \longrightarrow t\text{-}C_4H_9^+ + e^- \quad \text{(at 298°K)}$$

$$-\int_0^{298} C_p(t\text{-}C_4H_9)dT \qquad\qquad \int_0^{298}[C_p(t\text{-}C_4H_9^+) + C_p(e^-)]dT$$

$$t\text{-}C_4H_9 \xrightarrow{\;IP(t\text{-}C_4H_9)\;} t\text{-}C_4H_9^+ + e^- \quad \text{(at 0°K)}$$
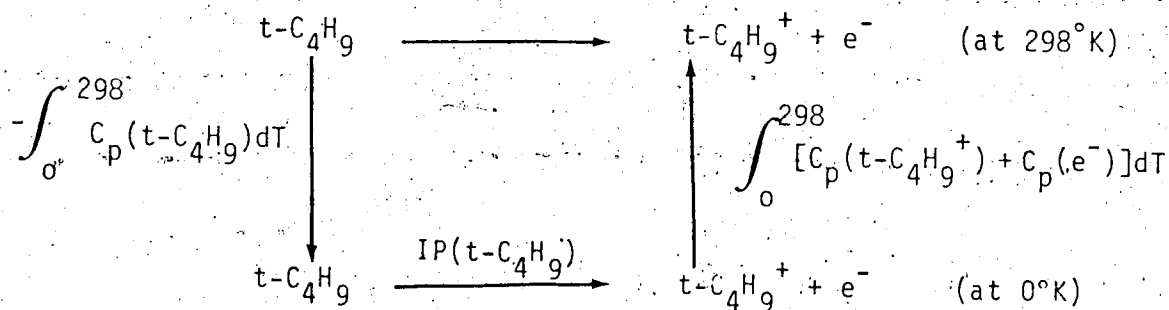
$$\Delta H_{f,298}^o(t\text{-}C_4H_9^+) = \Delta H_{f,298}^o(t\text{-}C_4H_9) + IP(t\text{-}C_4H_9) + \int_0^{298}[C_p(t\text{-}C_4H_9^+)$$
$$+ C_p(e^-) - C_p(t\text{-}C_4H_9)]dT$$

$$\approx \Delta H_{f,298}^o(t\text{-}C_4H_9) + IP(t\text{-}C_4H_9) + \int_0^{298} C_p(e^-)dT$$

$$= [9.0 + 154.5 + \frac{5}{2}R(298)] \quad \text{kcal/mole}$$

$$= 165.0 \text{ kcal/mole}$$

2. $\underline{\Delta H_f^o(H^+)^{a,c}}$

$$H \longrightarrow H^+ + e^- \quad \text{(at 298°K)}$$

$$-\int_0^{298} C_p(H)dT \qquad\qquad \int_0^{298}[C_p(H^+) + C_p(e^-)]dT$$
$$\text{(at 0°K)}$$

$$H \xrightarrow{\;IP(H)\;} H^+ + e^-$$
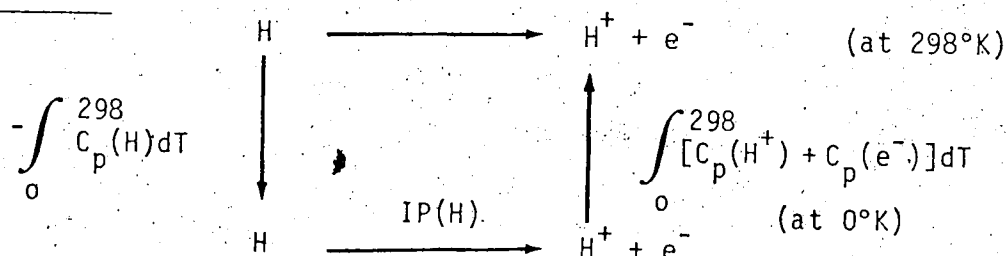
$$\Delta H_{f,298}^o(H^+) = \Delta H_{f,298}^o(H) + IP(H) + \int_0^{298}[C_p(H^+) + C_p(e^-) - C_p(H)]dT$$

$$\approx \Delta H_{f,298}^o(H) + IP(H) + \int_0^{298} C_p(e^-)dT$$

TABLE 3.55 (continued)

$$= [52.1 + 313.6 + \frac{5}{2} R (298)] \ \text{kcal/mole}$$

$$= 367.2 \ \text{kcal/mole}$$

3. Proton Affinity of Isobutene

$$PA(\text{isobutene}) = \Delta H^o_f(\text{isobutene}) + \Delta H^o_f(H^+) - \Delta H^o_f(\text{t-butyl}^+)$$

$$= (-4.04 + 367.2 - 165.0) \ \text{kcal/mole}$$

$$= 198.2 \ \text{kcal/mole}$$

[a] Calculations based on two assumptions: (1) the electron is an ideal gas with heat capacity $C_p = \frac{5}{2} R$; (2) heat capacities of the neutral M and the ionized species M^+ are the same, i.e. $C_p(M) = C_p(M^+)$.

[b] $\Delta H^o_f(\text{t-}C_4H_9)$ and $IP(\text{t-}C_4H_9)$ values from Table 3.54.

[c] $\Delta H^o_f(H)$ and $IP(H)$ values from JANAF thermochemical tables, Nat. Stand. Ref. Data Ser., Nat. Bur. Stand. (U.S.) 37 (1971).

standard PA(isobutene = 194 kcal/mole) based on the work
of Lossing (81). The present adjustment of the external
standard PA(isobutene) will result in higher values for
proton affinities previously reported, but it will not
affect the relative basicities among different compounds.

The proton affinities of other compounds may be cal-
culated from $\Delta H^O = \Delta G^O + T\Delta S^O$ for the proton transfer
reaction 1.13 and linking the relative proton affinities,
ΔH^O, to the standard PA(isobutene). The relative gas-
phase basicity, ΔG^O, between two bases, B, is determined
experimentally in the equilibrium measurements. The
entropy change for the proton transfer reaction 1.13

$$B_1H^+ + B_2 = B_1 + B_2H^+ \tag{1.13}$$
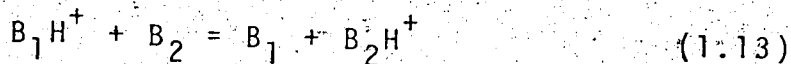
is given by the sum of the contributions from translation-
al, rotational and vibrational entropy changes:

$$\Delta S^O = \Delta S^O_{trans} + \Delta S^O_{rot} + \Delta S^O_{vib} \tag{3.5}$$

Each term on the right hand side of equation 3.5 can be
evaluated separately. To a first approximation, the
contributions of ΔS^O_{trans} and ΔS^O_{vib} may be assumed to be
zero because in both cases, the contributions from the
products and reactants tend to cancel each other. The
entropy change for a proton transfer reaction may then
be ascribed exclusively to changes in rotational
entropy in going from reactants to products. The

rotational entropy contribution may be evaluated by splitting the rotational motion into external and internal rotations. The external rotational entropy of a molecule is related to its moments of inertia and its external rotational symmetry number which is the number of non-identical but indistinguishable positions into which a molecule can be turned by simple complete rotations of the molecule. The internal rotational entropy is a result of the rotation of a group around a bond within the molecule. Its magnitude depends not only on the reduced moments of inertia and the internal rotational symmetry number, but also on the energy barrier of the internal rotation. Since in most proton transfer reactions, there is no addition or removal of internal rotation, the latter contribution can often be ignored. Under these circumstances, the total entropy change can be determined just by considering the contribution from external rotation entropies. As the changes of moments of inertia going from reactants to products are usually insignificant, the external rotational entropy change can be estimated just by considering the change in external rotational symmetry number. This leads to the relationship:

$$\Delta S^o \approx \Delta S^o_{ext.rot} \approx \Delta S^o_{rot.s.} \qquad (3.6)$$

which holds fairly well for most proton transfer reactions. The change in the symmetry number is easy to predict if

the geometries of the ions and neutrals are known. Unfortunately, this is not always the case particularly for the ions whose exact geometries are often uncertain. A large entropy change is expected when molecules of high symmetry are involved which lose their symmetry in the reaction. In the case of benzene and its derivatives, the experimental results from the study of temperature dependence of the proton transfer equilibria (see Table 3.53) showed that rotational symmetry change is the only major contribution to the entropy change. However, there are exceptions where internal rotation may play a significant role in determining the rotational entropy change. A prime example is the conversion of the methylene group to a methyl group in the protonation of isobutene. The removal of the double bond generates an additional mode of relatively "free" internal rotation of the methyl group with respect to the rest of the molecule upon protonation of isobutene to tert-butyl ion. Since isobutene was chosen as the external standard for determining the proton affinity of the reference compound, ammonia, and for calibrating the proton affinity scale, it is justified to consider in more detail the rotational entropy change of the proton transfer reaction involving isobutene and ammonia.

The evaluation of the entropy change for the reaction 3.7 can be split into the evaluation of entropy

$$(CH_3)_3C^+ + NH_3 = (CH_3)_2C=CH_2 + NH_4^+ \qquad (3.7)$$
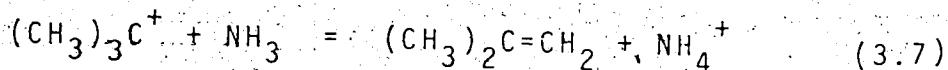
changes of two half-reactions:

$$(CH_3)_3C^+ = (CH_3)_2C=CH_2 \qquad (3.8)$$

$$NH_3 = NH_4^+ \qquad (3.9)$$
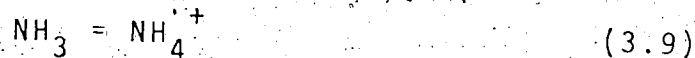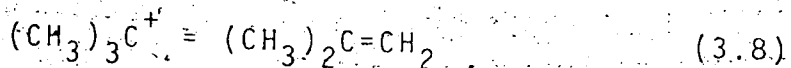
In both cases, only the rotational entropy changes are considered. The entropy of a molecule may be expressed by equation 3.10 from statistical thermodynamics (84),

$$S^o = R\ln Q + RT\frac{d\ln Q}{dT} \qquad (3.10)$$

where Q is the corresponding partition function of the molecule. The external rotational partition function for a non-linear polyatomic molecule is given by equation 3.11 (84),

$$Q_{ext.rot.} = \frac{(8)^{5/2}(kT)^{3/2}(I_x I_y I_z)^{1/2}}{\sigma h^3} \qquad (3.11)$$

where I_x, I_y, I_z are the three moments of inertia about the three principal axes and σ is the external rotational symmetry number. The external rotational entropy is then given by:

$$S^o_{ext.rot.} = R\ln Q_{ext.rot} + 3/2R \qquad (3.12)$$

Within the framework of this model, the external rotational

entropy change for the proton transfer reaction 3.8 may be simplified into:

$$\Delta S^0_{ext.rot.} = R\ln\left\{\left[\frac{(I_x I_y I_z)_{isobutene}}{(I_x I_y I_z)_{t-Bu^+}} \times \frac{(I_x I_y I_z)_{NH_4^+}}{(I_x I_y I_z)_{NH_3}}\right]^{\frac{1}{2}}\right.$$

$$\left.\times \left[\frac{\sigma_{t-Bu^+}}{\sigma_{isobutene}} \times \frac{\sigma_{NH_3}}{\sigma_{NH_4^+}}\right]\right\} \tag{3.13}$$

The principal axes chosen for the calculations of moments of inertia for all species involved are shown in Figure 3.23. The bond lengths and bond angles used in the calculations are shown in Table 3.56 together with the moments of inertia calculated. Tert-butyl ion was taken to be planar and the ammonium ion tetrahedral. The external symmetry number for tert-butyl ion, isobutene, ammonia and ammonium ion is 6, 2, 3 and 12, respectively. This leads to the external rotational entropy change:

$$\Delta S^0_{ext.rot.} = R\ln\left\{[0.738 \times 1.84] \times \left[\frac{6}{2} \times \frac{3}{12}\right]\right\}$$

$$= R\ln\left(1.36 \times \frac{6}{2} \times \frac{3}{12}\right)$$

$$= 0.04 \text{ eu.} \tag{3.14}$$

The $\Delta S^0_{ext.rot.}$ value can be divided between the two half-reactions (3.8 and 3.9): +1.58 eu. for the deprotonation of tert-butyl ion and -1.54 eu. for the proton-
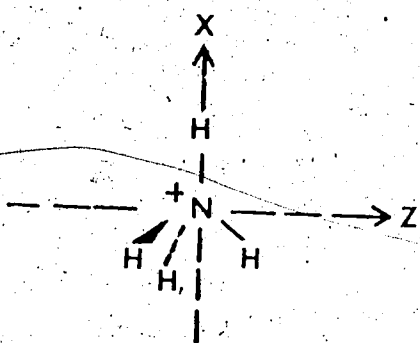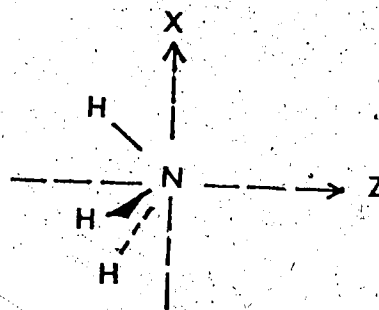
FIGURE 3.23 Principal Axes Chosen for the Calculations of
Moments of Inertia.
(Y axis is mutually perpendicular to the X and Z axes)

Table 3.56 <u>Moments of inertia, bond distances and bond angles for species involved in the calculation</u>

Species	I_x ($\times 10^{40}$ g cm^{-2})	I_y ($\times 10^{40}$ g cm^{-2})	I_z ($\times 10^{40}$ g cm^{-2})
tert-Butyl ion	103.5	7.87	101.9
Isobutene	102.3	5.25	84.2
Ammonion ion (tetrahedral)	2.26	2.26	2.26
Ammonia	2.19	2.17	0.712

Bond angles (degree)	Tetrahedral	Planar	Ammonia
	109.5	120	107

Bond length (Å)	C——H	C——C	C==C	N——H
	1.09	1.54	1.34	1.01

ation of ammonia.

Only internal rotations which would change in the proton transfer process were considered. Since no internal rotation exists in NH_3 and NH_4^+, the only internal rotational entropy change for reaction 3.7 is contributed from the other half-reaction 3.8.

$$(CH_3)_3C^+ = (CH_3)_2C=CH_2 \qquad (3.8)$$
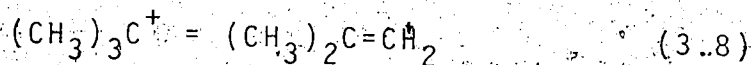
The relatively "free" internal rotation of a methyl group around the C-C bond in the tert-butyl ion would disappear upon deprotonation. It is only compensated by the generation of a highly restricted rotation of the methylene group around the C=C bond in isobutene. The entropy for free internal rotation for individual species can be calculated from their corresponding partition functions. The partition function for the free internal rotation, Q_f, is given by equation 3.15 (85),

$$Q_f = \frac{1}{n}\left(\frac{8\pi^3 I_r kT}{h^2}\right)^{\frac{1}{2}} \qquad (3.15)$$

where n is the internal symmetry number which is the number of indistinguishable positions per complete rotation around the bond, and I_r is the reduced moment of inertia. The reduced moment of inertia is expressed as:

$$I_r = \frac{I_1 I_2}{I_1 + I_2} \qquad (3.16)$$

where I_1 and I_2 are the moments of inertia of the rotating

group and the rest of the rigid molecule. From equation 3.10, the free internal rotational entropy S_f^o is then derived as shown in equation 3.17.

$$S_f^o = R \ln Q_f + \frac{R}{2}$$ (3.17)

Since the internal rotations considered are not exactly "free" rotations, there is a decrease in entropy from free rotation, $(S_f^o - S^o)$, due to the presence of the energy barrier in the rotation. The internal rotational entropy is thus given by:

$$S_{int.rot.}^o = S_f^o - (S_f^o - S^o)$$ (3.18)

The decrease in entropy, $(S_f^o - S^o)$, was evaluated using the table of Pitzer (86). In the table, the value of $(S_f^o - S^o)$ is tabulated as a function of $1/Q_f$ and V/RT where V is the potential barrier in the rotation. It should be pointed out that the table of Pitzer used in the calculation of entropy for hindered internal rotation is valid for rotation of a symmetric top about a rigid framework. In the tert-butyl ion as well as iso-butene, the rest of the molecule is not rigid with respect to the rotating group. However, it was shown by Pitzer (87) that the table also has approximate validity for molecules with non-rigid frameworks and unsymmetric tops.

The potential barrier for the rotation of a methyl

group about the C-C bond in the tert-butyl ion was taken
to be 3 kcal/mole (88), same as that in ethane, whereas
in isobutene, the π bond barrier was assumed to be the
same as that in ethylene, i.e. 26 kcal/mole (89). Other
parameters used in the evaluation of the internal rotation-
al entropy for tert-butyl ion and isobutene are tabulated
in Table 3.57. The internal rotational entropy for tert-
butyl ion and isobutene was calculated to be 3.65 eu.
and 1.4 eu., respectively. The internal rotational
entropy change for reaction 3.8 as well as reaction 3.7
is therefore given by:

$$\Delta S^0_{int.rot.} = S^0_{int.rot.}(isobutene) - S^0_{int.rot.}(t\text{-}Bu^+)$$

$$= -2.2 \text{ eu.} \qquad\qquad (3.19)$$

The overall entropy change for the proton transfer reaction
3.7 is the sum of the rotational entropy changes:

$$\Delta S^0 \approx \Delta S^0_{rot.} = \Delta S^0_{ext.rot.} + \Delta S^0_{int.rot}$$

$$\qquad\qquad\qquad (3.20)$$

$$= (0.04 - 2.2) \text{ eu.} = -2.2 \text{ eu.}$$

The foregoing estimate of the entropy change for
the proton transfer reaction involving isobutene and
ammonia indicates that the entropy change of the re-
action is entirely due to changes in internal rotations
from the deprotonation of tert-butyl ion to isobutene.
If the changes in internal rotation and moments of

Table 3.57   Parameters used for the evaluation of internal rotation entropies of tert-butyl ion and iso-butene.

(1)   (2)

tert-Butyl ion

(1)   (2)
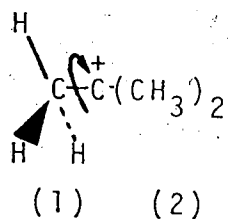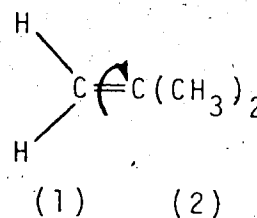
Isobutene

	$I \times 10^{40}$ g cm^{-2}						
	I_1	I_2	I_r	n	V	S_f^o	$S_{int.rot.}^o$
					(kcal/mole)	(eu)	
tert-Butyl ion	5.26	104.6	5.00	3	3	4.23	3.65
Isobutene	2.96	104.6	2.88	2	60	4.49	1.4

($S_{int.rot.}^o$ calculated for temperature 600°K)

inertia are ignored and only the change in symmetry num-
bers is considered, the entropy change for the same re-
action would be close to zero, $\Delta S^o_{rot.s.} = R\ell n\left(\dfrac{3 \times 6}{12 \times 2}\right) =$
-0.6 eu. The calculated results suggested that if
entropy corrections are to be made for obtaining proton
affinity values, changes in modes of internal rotation,
if any, cannot be ignored.

A ΔG^o_{600} value of -8.1 kcal/mole (see Table 3.1) was
determined in the present work for the proton transfer
reaction 3.7, from tert-butyl ion to ammonia. The
ΔG^o_{300} for the same reaction measured by ion cyclotron
resonance method was reported to be -8.6 kcal/mole (31).
With the calculated $\Delta S^o = -2.2$ eu., these give $\Delta H^o_{600} =$
-9.4 kcal/mole and $\Delta H^o_{300} = -9.3$ kcal/mole. The good
agreement between the two enthalpy change values suggests
that the internal rotations do make a contribution to the
entropy change of the reaction. With the external
standard of PA(isobutene) = 198.2 kcal/mole, the ammonia
would have a proton affinity of 207.6 kcal/mole. This is
in agreement with the value, PA(NH_3) = 207 kcal/mole,
reported by Haney and Franklin (53,90), although their
value was obtained by non-equilibrium appearance potential
measurements.

Finally, it should be pointed out that in the
absence of changes in internal rotation, the approxima-
tion $\Delta S^o = \Delta S^o_{rot.s.}$ does hold fairly well for proton

transfer reactions. This viewpoint is supported by the fair agreement between the ΔH^O values for proton transfer reactions calculated from ΔG^O_{600} from the present work and from the corresponding ΔG^O_{300} determined by ICR spectroscopy as reported by Taft et al. (31), using the relationship $\Delta H^O = \Delta G^O_T + T\Delta S^O_{rot.s.}$ The estimations of $\Delta S^O_{rot.s.}$ values are valuable as the experimental determinations of entropy changes in proton transfer reactions by high pressure mass spectrometry are often hindered by the formation of protonated dimers at lower temperatures. Previous attempts have been made in this laboratory to measure the entropy changes from a temperature range of 560-650°K for a few proton transfer reactions such as between H_2O and H_2S (3). The results showed that all the experimentally measured ΔS^O are within ± 1 eu. but their values do not reflect their corresponding symmetry changes which are thought to be the only contribution. The conclusion reached was that either the measurements were not accurate enough to reflect such small ΔS^O values or there are some other real effects. The only convincing agreement between ΔS^O_{expt} and $\Delta S^O_{rot.s.}$ was obtained in systems with benzene and fluoro- or chloro-benzene (see Table 3.53) where measurements can be carried out over a larger temperature range (300 - 600°K) and $\Delta S^O_{rot.s.}$ is large (~ 3.5 eu.). In view of the small magnitude of the ΔS^O value usually associated with proton-

transfer reaction (ΔS^o < 2 eu. which will have a contribution of < 1.2 kcal/mole in converting ΔG^o_{600} to ΔH^o it is often assumed that ΔS^o = 0 and ΔH^o = ΔG^o for proton-transfer reactions. Previous proton affinity data reported from this laboratory (2,3) were based on this assumption. The assumption is justified by the fact that the uncertainties imposed on the PA values would be small compared with that in the present standard proton affinity of isobutene (~3 kcal/mole) It is believed that the $\Delta S^o_{rot.s.}$ corrections do provide valuable information as long as the corrections are consistent. No confusion would arise if the symmetry numbers for ions and molecules used are given and the corrections made are pointed out. Such corrections were made in the calculations of the proton affinities of the monosubstituted benzenes and some selected compounds. They are calculated from the equation 3.21,

$$PA(B) = 207.6 - \Delta H^o(NH_3 \text{ to } B) \quad \text{kcal/mole} \quad (3.21)$$

where $\Delta H^o(NH_3$ to B) is the ΔH^o for the reaction 3.1

$$NH_4^+ + B = NH_3 + BH^+ \qquad (3.1)$$
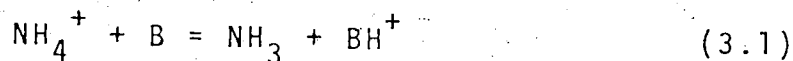
calculated from $\Delta H^o = \Delta G^o + T\Delta S^o_{rot.s.}$. The ΔG^o values are from Table 3.1. These results are presented in Table 3.58. Similar calculations may be performed on all compounds on the ΔG^o ladder in Table 3.1.

Table 3.58 Proton affinities of monosubstituted benzenes and some selected compounds
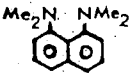
Compound (B)	σ_B/σ_{BH^+}	$\Delta S^o_{rot.s.}$[a] (eu)	ΔH^o(from NH_3)[a] (kcal/mole)	Proton Affinity (kcal/mole)
Aniline	1	2.8	-5.2	212.8
Acetophenone	1	2.8	-0.3	207.9
Anisole	1	2.8	+4.4	203.2
Benzaldehyde	1	2.8	+4.7	202.9
Benzoic acid	1	2.8	+7.4	200.2
Benzonitrile	1	2.8	+8.7	198.9
Phenol	1	2.8	+8.8	198.8
Nitrobenzene	1	2.8	+11.2	196.4
Ethylbenzene	1	2.8	+12.8	194.8
Toluene	1	2.8	+13.8	193.8
Fluorobenzene	1	2.8	+20.9	186.7
Chlorobenzene	1	2.8	+21.1	186.5
Benzene	6	6.3	+22.2	185.4
Me_2N NMe_2 (naphthalene structure)	1	2.8	-37.5	245.1
Methylamine	1/3	0.57	-9.7	217.3
DMSO	1	2.8	-6.8	214.4
Ammonia	3/12	0	0	207.6[c]
Acetone	2	4.1	+9.0	198.6
Isobutene			+9.4	198.2[b]
Ethanol	1	2.8	+16.4	191.2

Table 3.58 (continued)

Acetaldehyde	1	2.8	+17.8	189.8
Methanol	1	2.8	+21.4	186.2
Water	2/3	2.0	+35.9	171.7

[a] $\Delta S^0_{rot.s.}$ and ΔH^0 are for the reaction $NH_4^+ + B = NH_3 + BH^+$

$\Delta S^0_{rot.s.} = R\ln(\frac{12}{3})(\frac{\sigma_B}{\sigma_{BH^+}}); \quad \Delta H^0 = \Delta G^0 + T\Delta S^0_{rot.s.}$

[b] External standard PA(isobutene) = 198.2 kcal/mole.

[c] Reference PA(NH_3) = 207.6 kcal/mole, see text; all other PA values are based on this value.

GAS-PHASE BASICITIES OF COMPOUNDS BETWEEN WATER AND METHYL-
AMINE. PROTON AFFINITIES OF ISO-PROPANOL, TERT-BUTANOL AND
DMSO

CHAPTER IV

4.1 Gas-Phase Basicities of Compounds Between Water and Methylamine

The gas-phase basicities of various compounds between
water and methylamine have been determined previously by
equilibrium measurements using the high pressure mass
spectrometer (1,3) and the ICR technique (30,31). Where
overlapping, a comparison of the present results with those
reported in the literature can be made. (See Table 3.1)
In this section, discussion will be limited to cases where
there are disagreements between the present results and
those from the literature. The gas-phase basicities of
the substituted benzenes as a class will be discussed in
a subsequent chapter.

A. Formic Acid and Methanol

The relative gas-phase basicities of compounds bet-
ween ammonia and water have been reported from equilibrium
measurements made with a high-pressure pulsed electron
beam mass spectrometer by Yamdagni et al. in this labora-
tory (3) and with low-pressure pulsed ion cyclotron res-
onance by Taft et al. (31). On the whole, the agreement
between the results from the two completely different

236

techniques is good where there is overlapping (see Table 3.1). The major disagreement occurs in the interval between formic acid and methanol. Taft et al. (31) from ICR measurements reported a ΔG^o_{300} value of 2.5 kcal/mole for reaction 4.1, while the high pressure mass spectrometric deter-

$$(CH_3OH)H^+ + HCO_2H = CH_3OH + (HCO_2H)H^+ \qquad (4.1)$$
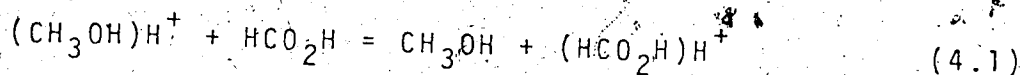
minations of equilibrium constants resulted in a ΔG^o_{600} value of 4.0 kcal/mole for the same reaction. The present independent determinations yielded a ΔG^o_{600} value of 3.9 kcal/mole for reaction 4.1, in complete agreement with the previous value reported earlier from this laboratory (3). Appropriate entropy corrections can be made for comparing ΔG^o_{600} with ΔG^o_{300} to account for the difference in the temperature of measurements. Assuming that changes in rotational symmetry numbers, σ, are the only contributions to the entropy change in reaction 4.1, and $CH_3OH_2^+$ ion has a non-planar trigonal pyramid structure (91), the entropy change for reaction 4.1 can be calculated to be:

$$\Delta S^o \approx \Delta S_{rot.s} = R\ln \frac{\sigma_{CH_3OH_2^+}}{\sigma_{CH_3OH}} \times \frac{\sigma_{HCO_2H}}{\sigma_{HCO_2H_2^+}}$$

$$= R\ln \frac{1 \times 1}{1 \times 2} = -1.38 \text{ eu} \qquad (4.2)$$

This leads to a ΔH^o_{600} value of 3.1 kcal/mole and a ΔH^o_{300} value of 2.1 kcal/mole for reaction 4.1. As the difference in heat capacities between products and reactants, ΔC_p,

in a proton transfer reaction is negligible, from equation
4.3, the enthalpy change may be taken as constant over the

$$\Delta H^o_{T_2} - \Delta H^o_{T_1} = \int_{T_1}^{T_2} \Delta C_p dT \qquad (4.3)$$

temperature range between 300 - 600°K. The difference of 1
kcal/mole in the ΔH^o value is higher than the experimental
uncertainties of the two techniques which are around 0.2 -
0.5 kcal/mole. The discrepancies between the results
from the two types of measurements may be caused by un-
certainties associated with the measurements of neutral
concentrations and detection of ion signals. Since the
present determination is consistent with the results of
other measurements in the ladder (Table 3.1) and Taft's
value is consistent with theirs, it is uncertain as to
what are the sources of the difference. Assuming ΔH^o is
constant over the temperature range of 300 - 600°K, the
experimental ΔS^o may be calculated to be -4.7 eu from
equation 4.4. The $-\Delta S^o_{(expt)}$ is much larger than is

$$\Delta S^o_{(expt)} = \frac{\Delta G^o_{300} - \Delta G^o_{600}}{300} \qquad (4.4)$$

expected from changes in rotational symmetry numbers of
species involved. Although the difference may just be a
reflection of larger errors in the ICR measurements
with compounds having basicities between those of methanol
and formic acid, it may also be due to some real effects.

A larger $-\Delta S^o$ value for reaction 4.1 may result from the restricted rotation in protonated formic acid due to the presence of internal hydrogen bonding in structure I:

$$
\begin{array}{c}
O \\
H-C \overset{+}{\diamond} H \\
O \\
H
\end{array}
\quad (I)
$$
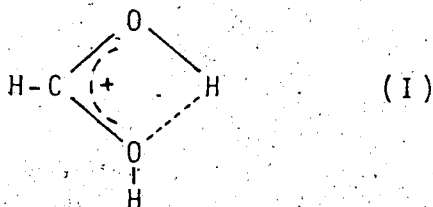
The above structure of formic acid has been suggested from the results of NMR experiments in which the two O-H protons were identified as non-equivalent at low temperature (92,93). Similar structure for protonated acetic acid has also been suggested by Davidson et al. in this laboratory (94). In their study of the hydration reaction of acetyl cation, structure II was proposed for the pro-

$$
\begin{array}{c}
O \\
CH_3-C \overset{+}{\diamond} H \\
O \\
H
\end{array}
\quad (II)
$$
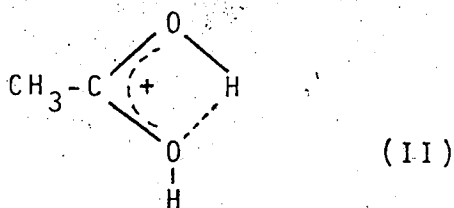
tonated acetic acid as an explanation for the observation that the measured $-\Delta S^o$ value for reaction 4.5 is a few

$$CH_3CO^+ + H_2O = CH_3CO_2H_2^+ \qquad (4.5)$$
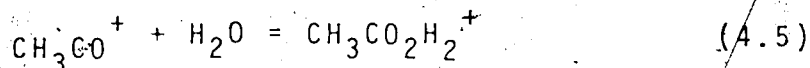
eu larger than the average $-\Delta S^o$ values for similar association reactions Since the present experimental entropy

change for the proton transfer reaction 4.1 is based on measurements at only two temperatures with different methods, more refined entropy measurements have to be made before any concrete conclusion can be drawn.

B. Hydrogen Sulfide and Formic Acid

On examining the results presented in table 3.1, the relative gas-phase basicities of compounds between water and ammonia determined in the present study, where overlapping, are in agreement (within ~0.5 kcal/mole) with those reported earlier from this laboratory (3), except for the interval between formic acid and hydrogen sulfide. In the previous study by Yamdagni (3), the gas-phase basicity difference between formic acid and hydrogen sulfide was determined by direct measurements of the equilibrium constant for reaction 4.6. The measured ΔG^{o}_{600}

$$H_3S^+ + HCO_2H = H_2S + HCO_2H_2^+ \qquad (4.6)$$
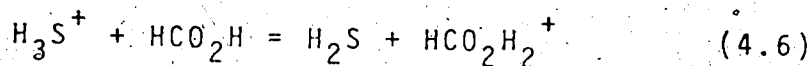
value for the reaction was reported to be -6.1 kcal/mole. This was the only step linking compounds having lower basicities than that of hydrogen sulfide to the overall basicity ladder. The present remeasurements of equilibrium constant for reactions 4.6 gave a ΔG^{o}_{600} value of -8.4 kcal/mole. The equilibrium constant in the present determinations was found to be independent of the neutral concentration ratio (varied by a factor of 6) and the

ion source pressure (varied from 1-4 torr) within the experimental error (~10-20%) as shown in Figures. 3.1 and 3.10. A $-\Delta G_{600}^0$ value of 8.4 corresponds to an equilibrium constant of 1174 at 600°K. In order to bring the ion ratios to within an order of magnitude so as to minimize errors in the detection of ion signals, large neutral ratios, $[H_2S]/[HCO_2H]$, have to be used. As shown in Table 3.5, only runs with the lowest neutral ratio were done in the presence of CH_4 as a third gas, other runs with higher neutral ratios were made with only H_2S and HCO_2H in the ion source. In the absence of CH_4, the H_3S^+ ions were produced by self-protonation of H_2S which was present in large excess as shown in reactions 4.7 and 4.8. Proton transfer reaction 4.6 then proceeded

$$H_2S + e \longrightarrow H_2S^+, HS^+, S^+ \text{ etc.} \qquad (4.7)$$
$$H_2S^+ + H_2S \longrightarrow H_3S^+ + HS \qquad (4.8)$$
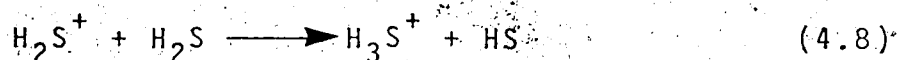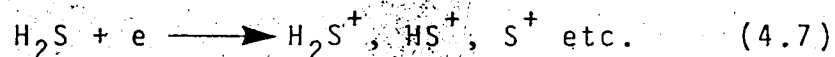
towards equilibrium. Proton transfer reactions with large magnitude of $-\Delta G^0$ values such as reactions 4.6 are not very desirable for direct equilibrium measurements. The strong exothermicity of the reaction always leads to products with large excess energy initially. The thermalization of products before entering the reverse reaction depends on the quenching of the excess energy by collisions with molecules in the ion source. With a carrier gas such as CH_4 in large excess, thermalization of ions by collisions with the carrier gas molecules will likely be

achieved. In the absence of a carrier gas, collisions of the non-thermalized ions with reacting molecules may result in non-equilibrium conditions. The invariance of the equilibrium constant measured for reaction 4.6 with and without the addition of a third carrier gas indicates that thermal equilibria were achieved in both cases in the present measurements.

To check on the reliability of the present results, the basicity of malononitrile which is in between those of formic acid and hydrogen sulfide was determined. All measurements were carried out in the presence of CH_4 in large excess. As shown in table 3.1, good agreement is obtained in different multiple thermodynamic cycles, giving an average $-\Delta G^o_{600}$ value of 8.2 kcal/mole for reaction 4.6. It is concluded that the previously reported

$$H_3S^+ + HCO_2H = H_2S + HCO_2H^+ \qquad (4.6)$$
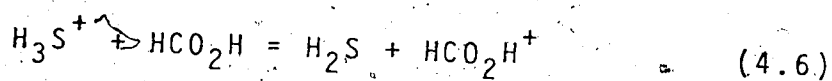
$-\Delta G^o_{600}$ value of 6.1 kcal/mole is too low. It is interesting to note that Taft et al. (31) using ICR method, determined a $-\Delta G^o_{300}$ value of 6.0 kcal/mole for the same reaction. It is difficult to explain the difference on basis of entropy terms. By substituting $\Delta G^o_{600} = -8.2$ kcal/mole and $\Delta G^o_{300} = -6.1$ kcal/mole into equation 4.4, it leads to an experimental ΔS^o value of 7.3 eu for reaction 4.6. The entropy change of the reaction due to changes in rotational symmetry number σ, can be calculated to be:

$$\Delta S^o_{rot.s.} = R\ln \frac{(\sigma_{H_3S^+})(\sigma_{HCO_2H})}{(\sigma_{H_2S})(\sigma_{HCO_2H_2^+})} = R\ln \frac{3 \times 1}{2 \times 2} \quad (4.9)$$

$$= -0.57 \text{ eu}$$

As suggested earlier in this section, the protonated formic acid probably has a "tight" structure I resulted from the internal hydrogen bonding. The restricted rotations

(I)
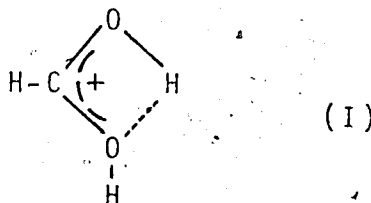
associated with the protonated formic acid would result in a ΔS^o value which is a few eu more negative than -0.57 eu for reaction 4.6, in disagreement with the experimental ΔS^o value of 7.3 eu as obtained by equilibrium measurements at the two different temperatures. It is uncertain as to why the discrepancy occurs in the results obtained from the two different methods.

C. Water and Ammonia

From table 3.1, a value of $\Delta G^o_{600} = 34.7$ kcal/mole is obtained for the reaction 4.10. The enthalpy change of
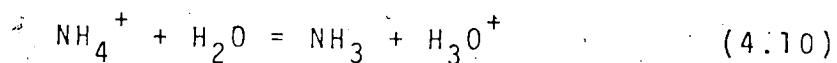
$$NH_4^+ + H_2O = NH_3 + H_3O^+ \quad (4.10)$$

the reaction may be calculated by correcting for ΔS^o due to rotational symmetry numbers:

$$\Delta S^0 \approx \Delta S^0_{rot.s.} = R\ln \frac{(\sigma_{NH_4^+})(\sigma_{H_2O})}{(\sigma_{NH_3})(\sigma_{H_3O^+})}$$

(4.11)

$$= R\ln \frac{12 \times 2}{3 \times 3} = 1.95 \text{ eu}$$

From the relationship $\Delta H^0 = \Delta G^0 + T\Delta S^0$, the ΔH^0 for re-action 4.10, or the proton affinity difference between ammonia and water, is determined to be 35.9 kcal/mole. This can be compared with the ΔH^0 value of 33.0 kcal/mole reported earlier from independent measurements in this laboratory (3). The difference of 2.9 kcal/mole is mainly due to the disagreement in the proton affinity difference between formic acid and hydrogen sulfide. The present determination indicates that the proton affinity differ-ence in that interval is 2.1 kcal/mole larger than was reported earlier. Taft et al. (31) in a similar study at 300°K using the ICR method obtained a ΔH^0 value of 32.0 kcal/mole for reaction 4.10. The major discrep-ancy with the present results is also in the interval between formic acid and hydrogen sulfide.

Using PA(isobutene) = 198.2 ± 3 kcal/mole as the external standard (79,80), leads to PA(ammonia) = 207.6 kcal/mole as shown in section 3.2. This combined with the present results gives PA(water) = 171.7 kcal/mole.

Based on the proton affinity values and the following

ΔH_f^o values: $\Delta H_f^o(H^+)$ = 367.2 kcal/mole (77), $\Delta H_f^o(NH_3)$ = -11.02 kcal/mole and $\Delta H_f^o(H_2O)$ = -57.8 kcal/mole (79), it may be calculated that $\Delta H_f^o(NH_4^+)$ = 148.6 kcal/mole and $\Delta H_f^o(H_3O^+)$ = 137.7 kcal/mole. Although the accuracy of the present determination on the absolute proton affinities of bases and the heats of formation of the protonated bases ultimately depends on the accuracy of the heat of formation of tert-butyl ion as mentioned in section 3.2, the uncertainties in results are minimized by the internal consistency in equilibrium measurements. Literature values on the estimated proton affinities of ammonia and water by non-equilibrium measurements are not always consistent with one another. A summary of the values of the proton affinities of ammonia and water derived from the literature values of $\Delta H_f^o(NH_4^+)$ and $\Delta H_f^o(H_3O^+)$ are tabulated in table 4.1. The present PA(NH_3) = 207.6 kcal/mole is in good agreement with the best estimated PA(NH_3) = 207 kcal/mole by Haney and Franklin (53) while the present PA(H_2O) = 171.7 kcal/mole is higher than most of the reported PA(H_2O) obtained by non-equilibrium measurements. The proton affinity difference between ammonia and water as reported by Haney and Franklin (53) was 42 ± 4 kcal/mole which is about 6 kcal/mole higher than the present value of 35.9 kcal/mole. Their values were obtained by using the appearance potential technique in which the excess translational energy of fragment ions

Table 4.1 A comparison of $\Delta H_f^o(NH_4^+)$, $\Delta H_f^o(H_3O^+)$, PA(NH$_3$), and PA(H$_2$O) obtained from equilibrium measurements and other methods.

I. $\underline{NH_3}$

$\Delta H_f^o(NH_4^+)$ (kcal/mole)	PA(NH$_3$) (kcal/mole)	Method	Reference
148.6	207.6	Present equilibrium measurements	
148	207	Appearance potential, corrected for kinetic energy of fragments	a
≤158	≥198	Ion-molecule reaction	b
138	218	Crystal-lattice energy	c
148	208	Crystal-lattice energy (not considering H-bonding)	d
148	208	Crystal-lattice energy (not considering H-bonding)	e

II. $\underline{H_2O}$

$\Delta H_f^o(H_3O^+)$ (kcal/mole)	PA(H$_2$O) (kcal/mole)	Method	Reference
137.7	171.7	Present equilibrium measurements	
143	165	Appearance potential corrected for kinetic energy of fragments	a
143 ± 4	166 ± 4	Ion-molecule reaction	f
≤148	≥161	Photon-impact on ethanol	b
157 ± 3	152 ± 3	Electron-impact on several compounds	g
136-145	173-164	Ion-molecule reaction	h
140 ± 7	169 ± 7	Crystal-lattice energy	e

Table 4.1 (continued)

126   183   crystal-lattice energy (not
                                      considering H-bonding)   d

a. M. A. Haney and J. L. Franklin, J. Chem. Phys. 50, 2028 (1969).

b. W. A. Chupka and M. E. Russell, J. Chem. Phys. 48, 1527 (1968).

c. W. E. Bleick, J. Chem. Phys. 2, 160 (1934).

d. J. Sherman, Chem. Rev. 11, 164 (1932).

e. S. I. Vetchinkin, E. I. Pshenichnov and N. D. Sokolov, J. Phys.
    Chem. Moscow 33, 1269 (1959).

f. J. L. Beauchamp and S. E. Buttrill, Jr., J. Chem. Phys. 48, 1783
    (1968).

g. D. VanRaalt and A. G. Harrison, Can. J. Chem. 41, 3118 (1963).

h. V. I. Tal'rose and E. L. Frankevich, Dokl. Akad. Nauk. USSR
    111, 376 (1956).

was determined experimentally and used for correcting the total energy of excitation in a semi-empirical way. The present results indicate that their measurements probably had a larger uncertainty than was quoted.

Bohme et al. (95) have measured the relative proton affinities of H_2O, H_2S, HCN and H_2CO by the flowing after-glow method. The proton affinity of H_2O was assigned to be 166.4 ± 2.4 kcal/mole using the external standard of PA(formaldehyde) = 172.1 ± 0.7 kcal/mole. The proton affinity of formaldehyde was derived from the photoion-ization appearance potential of 11.67 ± 0.03 eV for H_2COH^+ from CH_3OH as measured by Refaey and Chupka (51). The proton affinity difference of 4.5 kcal/mole between H_2CO and H_2O was obtained from the measurement ΔG^0_{298} = -5.2 ± 1.1 kcal/mole for reaction 4.12 after symmetry number correction.

$$H_3O^+ + H_2CO = H_2COH^+ + H_2O \qquad (4.12)$$
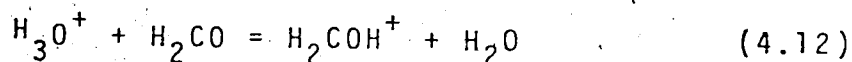
The PA(H_2O) = 166.4 kcal/mole is 5.3 kcal/mole lower than the value of 171.7 kcal/mole determined in this work. Direct comparison of proton affinity values is not appro-priate in this case since different external standards are used to calibrate the proton affinity scale. It is believed that the difference is mainly due to uncertain-ties associated with the ΔH^0_f (t-butyl$^+$) and ΔH^0_f(CH_2OH^+) values used in the calculations of standard proton affinities of isobutene and formaldehyde. It should

be noted that the appearance potential technique used in determining the $\Delta H_f^0(CH_2OH^+)$ does not always give the true thermodynamic value for the heat of formation of the corresponding ion. Very often, the presence of excess internal energy in the molecule or the presence of excess energy in the ion fragment may lower or increase respectively the energy threshold for the appearance of the ion in the mass spectrum. It is believed that the $\Delta H_f^0(t\text{-}butyl^+)$ value which is obtained from $\Delta H_f^0(t\text{-}butyl)$ and IP(t-butyl) is more reliable and the difference in the $PA(H_2O)$ values is mostly associated with the uncertainty in the $\Delta H_f^0(CH_2OH^+)$ value.

D. Ammonia and Methylamine

The gas-phase basicity of methylamine was previously reported to be 10.8 kcal/mole higher than that of ammonia from equilibrium measurements in this laboratory (1). The result was obtained by direct measurements of the proton transfer reaction 4.13. As mentioned earlier

$$NH_4^+ + CH_3NH_2 = NH_3 + CH_3NH_3^+ \qquad (4.13)$$
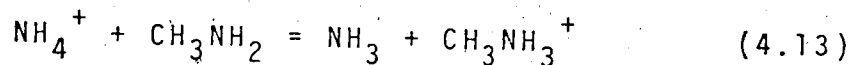
in this section, direct equilibrium measurement of such strong exothermic reaction is not desirable because the thermalization of the system may not be achieved. The present results gave $\Delta G_{600}^0 = -10.0$ kcal/mole for reaction 4.13 (see table 3.1). The value was obtained

from the average of many multicycles involving several proton transfer reactions of smaller exothermicity. The present value is believed to be more reliable than the one previously reported. Taft et al. (30) reported ΔG^o_{300} = -9.1 kcal/mole. By considering only the rotational symmetry corrections, these values lead to ΔH^o_{600} = -9.6 kcal/mole and ΔH^o_{300} = -9.0 kcal/mole. The difference is slightly larger than the expected precision (~0.5 kcal/mole) of the two techniques.

4.2 Proton Affinities of iso-Propanol and tert-Butanol

The gas-phase basicities of iso-propanol and tert-butanol were determined relative to other bases on the ΔG^o ladder in table 3.1. Due to the lack of stability of protonated iso-propanol and protonated tert-butanol, no condition was found where direct equilibrium measurements of the proton transfer reaction were not accompanied by other competitive reactions. At 600°K, measurements of proton equilibria involving iso-propanol were not successful. The protonated iso-propanol was found to rapidly decompose to an ion of molecular weight less by two mass units. Probably the protonated iso-propanol ion is pyrolysed according to reaction 4.14 in the presence

$$s\text{-}C_3H_7OH_2^+ + M \longrightarrow C_3H_7O^+ + H_2 + M \quad (4.14)$$
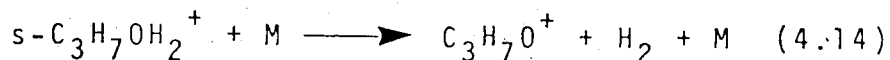
of a buffer molecule M, and the product $C_3H_7O^+$ is protonated acetone. The enthalpy change of reaction 4.14 can be calculated from the heats of formations of the species involved. By considering the heats of formation and the proton affinities of acetone and iso-propanol, it was estimated that reaction 4.14 is endothermic by some 9 kcal/mole. Reactions with such small endothermicity can occur at higher temperature. Since the concentration of the buffer molecule is in large excess in the ion source, the rate of reaction 4.14 may be appreciable compared to the rates of forward and reverse proton transfer reaction concerned. Under these conditions, direct equilibrium measurements would not be possible. It was observed that at the lower temperature 500°K, the $C_3H_7O^+$ ion was not formed in a significant amount and direct equilibrium measurements of the proton transfer reaction 4.15 were

$$s-C_3H_7OH_2^+ + B = s-C_3H_7OH + BH^+ \qquad (4.15)$$
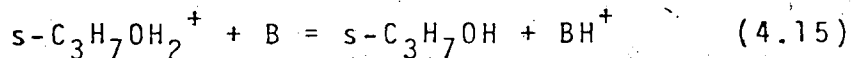
possible. The bases, B, used in the above reaction were nitrobenzene and toluene. During measurements at 500°K, the clustering reaction 4.16 was observed to compete

$$s-C_3H_7OH_2^+ + s-C_3H_7OH = (s-C_3H_7OH)_2H^+ \quad (4.16)$$
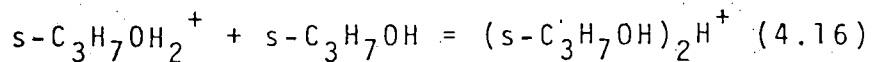
with the proton transfer reaction 4.15 at all times. A normalized temporal profile of ion intensities for a system involving iso-propanol and nitrobenzene is shown in Figure 4.1. The invariance of all ion intensities
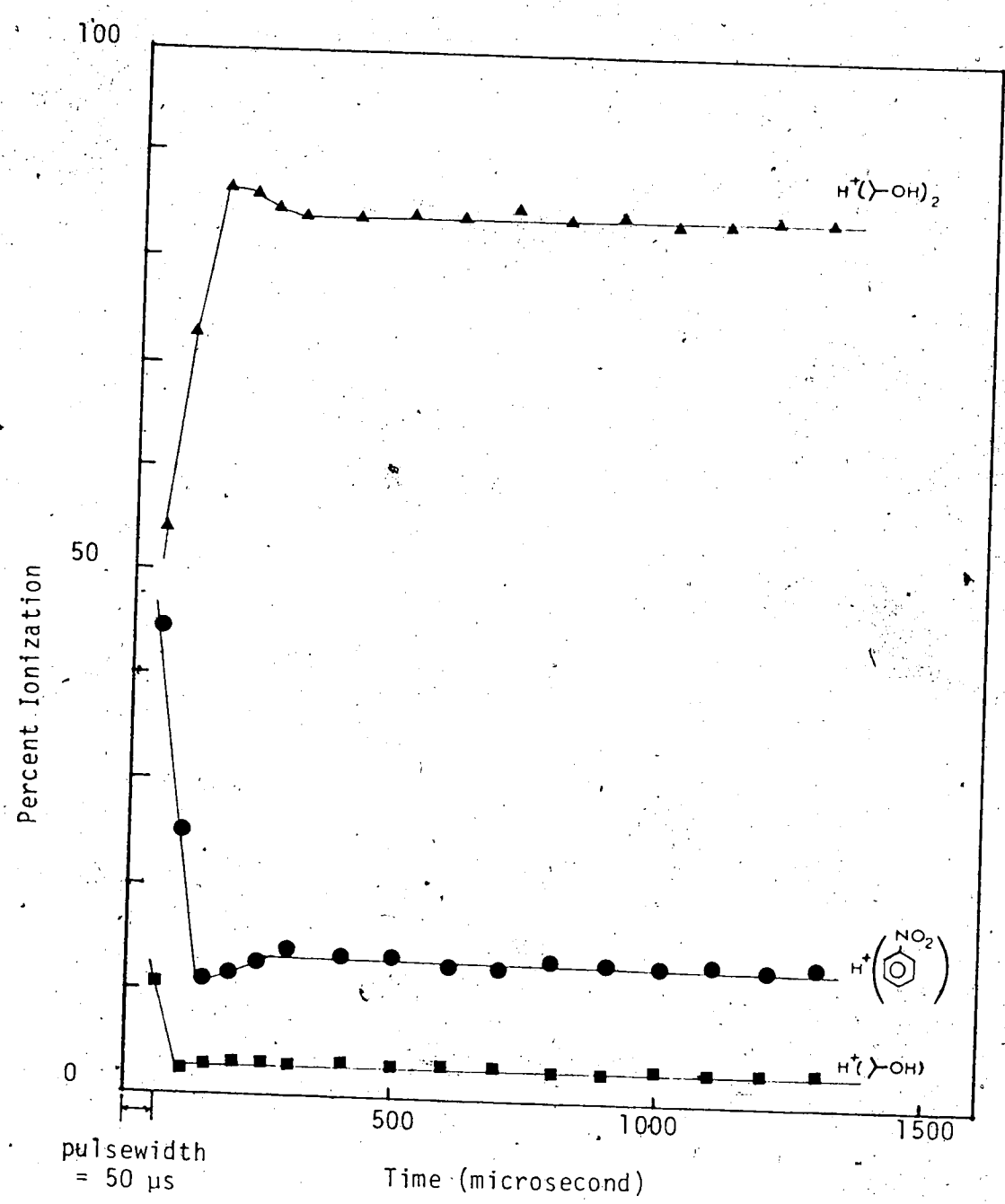
FIGURE 4.1. The Time Dependence of Normalized Ion Intensities:
Methane at 2.4 torr, isopropanol at 34.3 mtorr,
nitrobenzene at 16.9 mtorr. Temperature: 511°K.

after some 400 microseconds suggests that both reactions 4.15 and 4.16 are at equilibrium. Results of equilibrium measurements involving iso-propanol are presented in table 3.19 and Figure 3.4. The present results when incorporated with other results in table 3.1 leads to a $\Delta G^o_{600}(NH_3$ to iso-propanol) value of 11.7 kcal/mole (see table 3.1). With the reference $PA(NH_3) = 207.6$ kcal/mole, the proton affinity of iso-propanol was determined to be 194.2 kcal/mole after making rotational entropy corrections.

Direct proton-transfer equilibrium measurements involving tert-butanol were made with the reference bases, nitrobenzene and isobutene. The tert-butyl ion was observed to be the major ion present in the system even at 450°K. An example of the temporal profile of normalized ion intensities with tert-butanol, nitrobenzene and methane in the ion source is shown in figure 4.2. The invariance of intensities of the tert-butyl ion, the protonated nitrobenzene and the protonated tert-butanol with time from some 300 µsec after the electron pulse suggested that they were interrelated by some equilibrium reactions. One may wonder whether the tert-butyl ion may be formed by the protonation of isobutene which may be formed by acid-catalyzed dehydration of tert-butanol (96) as in reaction 4.17. However, a simple calculation

$$t-C_4H_9OH \xrightarrow[85-90°C]{H^+} (CH_3)_2C=CH_2 + H_2O \quad (4.17)$$
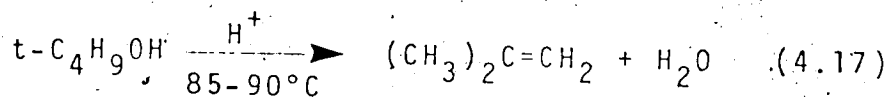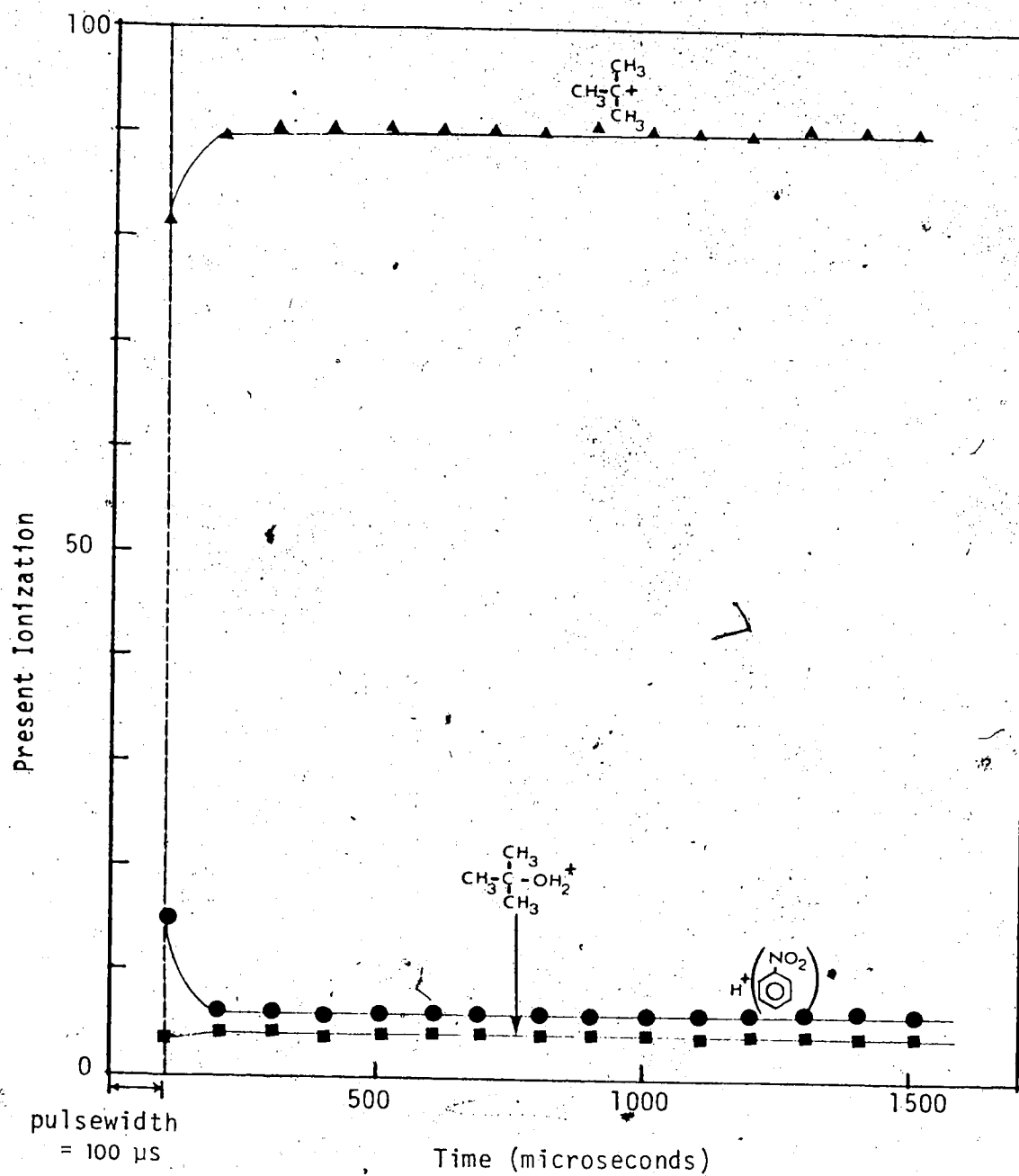
FIGURE 4.2 The Time Dependence of Normalized Ion Intensities.
Methane at 3.5 torr, nitrobenzene at 55.7 mtorr,
t-butanol at 29.6 mtorr. Temperature: 482°K

shows that this is not the case. Isobutene is more basic than nitrobenzene by 1.4 kcal/mole (table 3.1). In order to have an equilibrium ratio of 15 for $[t\text{-}butyl^+]/[H^+(nitrobenzene)]$ with 55.7 mtorr nitrobenzene in the ion source as in the run shown in figure 4.2, it would require 194 mtorr of isobutene which is about seven times the tert-butanol pressure in the ion source. The formation of tert-butyl ion may be explained by the dehydration of the protonated tert-butanol, reaction 4.18, occurring side by side with

$$t\text{-}C_4H_9OH_2^+ = t\text{-}C_4H_9^+ + H_2O \qquad (4.18)$$
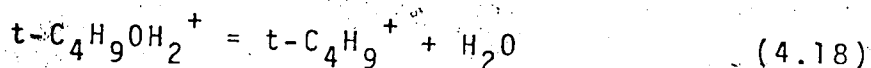
the proton transfer reaction 4.19. Reaction 4.18 has been

$$t\text{-}C_4H_9OH_2^+ + nitrobenzene = t\text{-}C_4H_9OH + H^+(nitrobenzene)$$
$$(4.19)$$
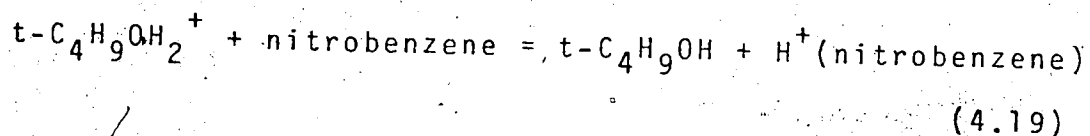
studied by Hiraoka and Kebarle (97). A $\Delta H^o = 11.2$ kcal/mole and a $\Delta S^o = 22$ eu were determined for reaction 4.18. In the absence of a substantial amount of water, the formation of tert-butyl ion from protonated tert-butanol is very much favored at about 500°K. It should be noted that the observed stationary ion ratio of $[t\text{-}C_4H_9^+]/[t\text{-}C_4H_9OH_2^+]$ in figure 4.2 cannot be explained by the equilibrium reaction 4.18. In the present study, no additional water was present in the ion source except traces of background water concentration which is always

present in the mass spectrometer. It may be calculated from ΔH^o and ΔS^o values for reaction 4.18 that under the conditions as shown in figure 4.2, a water concentration of 18 torr is required to produce the observed $[t\text{-}C_4H_9^+]/[T\text{-}C_4H_9OH^+]$ ion ratio! There must be other reactions to channel back the $t\text{-}C_4H_9^+$ ion to $t\text{-}C_4H_9OH^+$ ion, otherwise their ion intensity ratio will not be constant. One possible path is by the proton-transfer reaction 4.20.

$$t\text{-}C_4H_9^+ + \begin{array}{c} \text{nitrobenzene} \\ \text{or} \\ t\text{-}C_4H_9OH \end{array} = \text{isobutene} + \begin{array}{c} H^+(\text{nitrobenzene}) \\ \text{or} \\ t\text{-}C_4H_9OH_2^+ \end{array} \qquad (4.20)$$
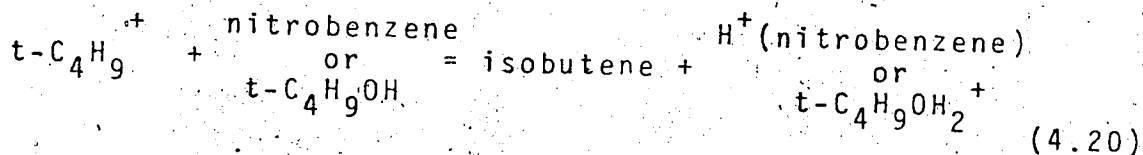
The PA(isobutene) is higher than the PA(nitrobenzene) by 1.8 kcal/mole (see table 3.57). The tert-butanol is estimated to have similar proton affinity as that of nitrobenzene from the observed equilibrium quotients in runs such as shown in figure 4.2. Reaction 4.20 would be endothermic and is expected to be slower than the proton transfer reaction 4.19. If the rate of dehydration of the $t\text{-}C_4H_9OH^+$ ion (reaction 4.18) is slow relative to the rate of its proton transfer (reaction 4.19), equilibrium 4.19 can still occur and direct measurements of the equilibrium constant is possible. The results of the measurements on the proton transfer equilibrium 4.19 are shown in figure 4.3. It was seen from figure 4.3 that the measured equilibrium constants vary by a factor of about 2 on varying the neutral concentrations. It is
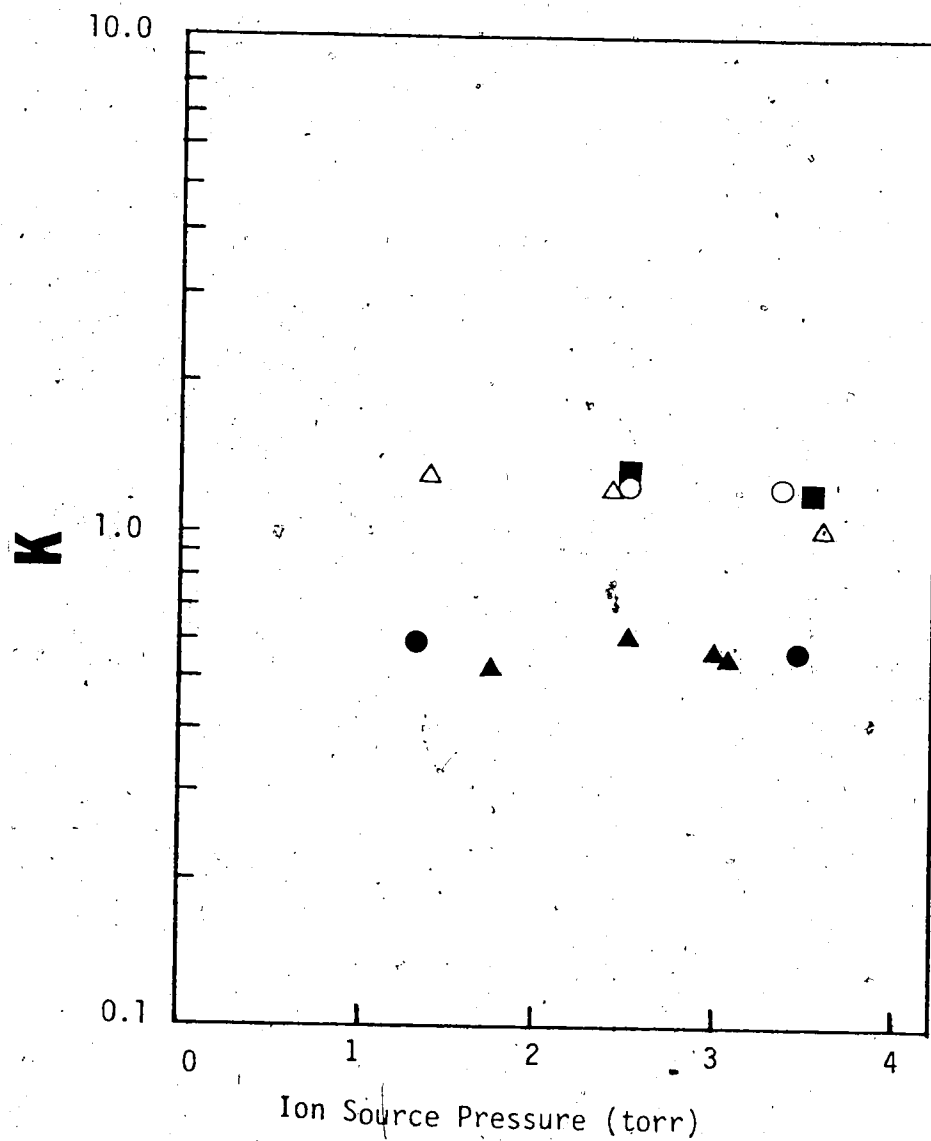
FIGURE 4.3 Equilibrium Constants _versus_ Ion Source Pressures for the Proton Transfer Reaction:

$$H^+(nitrobenzene) + t\text{-butanol} = nitrobenzene + H^+(t\text{-butanol})$$

	Concentration in mtorr/torr ion		Temperature °K
	[Nitrobenzene]	[t-butanol]	
(◯)	12.0	13.1	516
(△)	8.93	9.66	516
(■)	15.9	8.47	482
(●)	13.7	4.39	516
(▲)	19.2	5.11	516

concluded that the decomposition of $t-C_4H_9OH_2^+$ (reaction 4.18) must be affecting the observed proton transfer equilibrium 4.19. The proton affinity of tert-butanol may only be estimated to be similar to that of nitrobenzene (within ~1 kcal/mole) from the above results.

A similar proton transfer reaction using isobutene as the reference base was also investigated. The reactions that occurred in the system include the proton transfer reaction 4.21 and the dehydration reaction 4.18.

$$i-C_4H_8 + t-C_4H_9OH_2^+ \underset{k-1}{\overset{k_1}{\rightleftharpoons}} t-C_4H_9^+ + t-C_4H_9OH \qquad (4.21)$$

$$t-C_4H_9OH_2^+ + CH_4 \xrightarrow{k_2} t-C_4H_9^+ + H_2O + CH_4 \qquad (4.18)$$
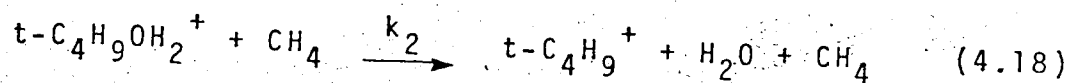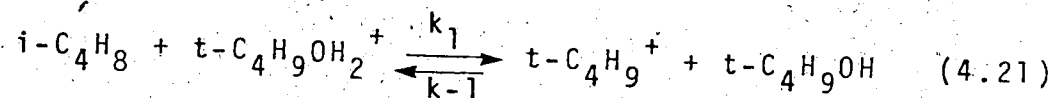
Reaction 4.18 is assumed to be second-order because its reverse reaction, a clustering reaction, is usually a termolecular reaction (97). Methane is taken as the third body since it is present in large excess. A constant ion ratio of $[t-C_4H_9^+]/[t-C_4H_9OH^+]$ was observed for every individual run. The results of measurements are shown as plots of equilibrium constants versus ion source pressure in figure 4.4. It was observed that the equilibrium constant is invariant with ion source pressures for a fixed neutral ratio but varies when the neutral ratio is changed. For runs at the same temperature and a constant tert-butanol/methane concentration ratio, the observed equilibrium constant tends to increase
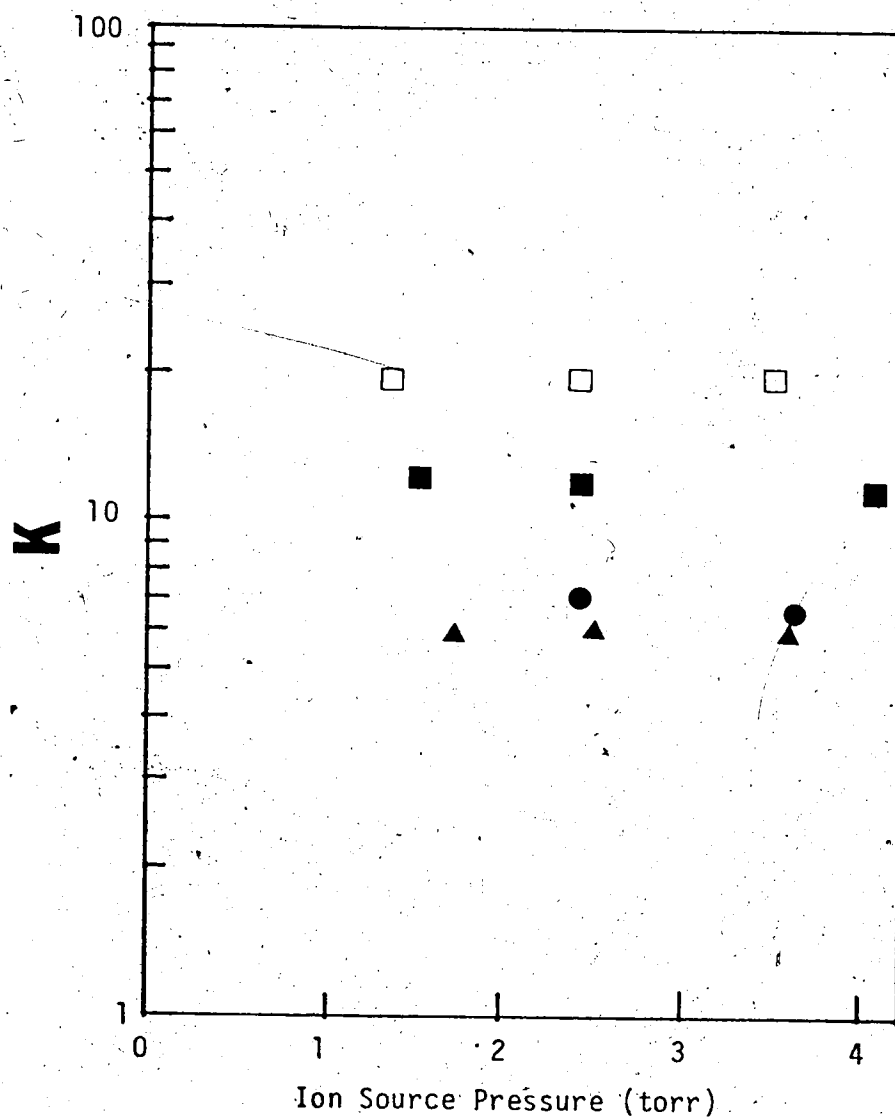
FIGURE 4.4 Equilibrium Constants _versus_ Ion Source Pressures for the Proton Transfer Reaction:

$$H^+(\underline{t}\text{-butanol}) + \text{isobutene} = \underline{t}\text{-butanol} + \underline{t}\text{-butyl}^+$$
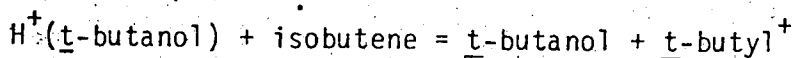
Concentration in mtorr/torr ion source pressure		Temperature
[t-butanol]	[isobutene]	(°K)
(●) 13.0	13.5	452
(▲) 13.0	8.52	452
(■) 13.0	3.96	452
(□) 26.1	6.50	516

with a decrease in isobutene/methane concentration ratio. Since reactions 4.21 and 4.18 combined form a chain reaction, a kinetic analysis may be done to obtain some interesting information. The rate of formation of the $t-C_4H_9OH_2^+$ and $t-C_4H_9^+$ may be written for reactions 4.21 and 4.18. The backward reaction of 4.18 is assumed to be negligible since there was no significant concentration of water in the system. As the concentrations of the neutrals were much larger than the concentrations of ions at all times, all second-order reactions may be taken as pseudo first-order reactions. By letting $k_1' = k_1[i-C_4H_8]$, $k_{-1}' = k_{-1}[t-C_4H_9OH]$ and $k_2' = k_2[CH_4]$, the following rate expressions may be written:

$$\frac{d[t-C_4H_9OH_2^+]}{dt} = -k_1'[t-C_4H_9OH_2^+] + k_{-1}'[t-C_4H_9^+] - k_2'[t-C_4H_9OH_2^+]$$
(4.22)

$$\frac{d[t-C_4H_9^+]}{dt} = k_1'[t-C_4H_9OH_2^+] - k_{-1}'[t-C_4H_9^+] + k_2'[t-C_4H_9OH_2^+]$$
(4.23)

The appearance of constant ion ratio of $[t-C_4H_9^+]/[t-C_4H_9OH_2^+]$ during equilibrium measurements implies that:

$$\frac{d[t-C_4H_9OH_2^+]}{dt} = \frac{d[t-C_4H_9^+]}{dt}$$
(4.24)

It follows then:

$$2\{-(k'_1 + k'_2)[t\text{-}C_4H_9OH_2^+] + k'_{-1}[t\text{-}C_4H_9^+]\} = 0$$

$$\frac{[t\text{-}C_4H_9^+]}{[t\text{-}C_4H_9OH_2^+]} = \frac{k'_1}{k'_{-1}} + \frac{k'_2}{k'_{-1}}$$

or,

$$\frac{[t\text{-}C_4H_9^+]}{[t\text{-}C_4H_9OH_2^+]} = \frac{k_1[i\text{-}C_4H_8]}{k_{-1}[t\text{-}C_4H_9OH]} + \frac{k_2[CH_4]}{k_{-1}[t\text{-}C_4H_9OH]} \qquad (4.25)$$

Multiplying both sides of the equation 4.25 by $[t\text{-}C_4H_9OH]/$ $[i\text{-}C_4H_8]$:

$$\frac{[t\text{-}C_4H_9OH]}{[i\text{-}C_4H_8]} \times \frac{[t\text{-}C_4H_9^+]}{[t\text{-}C_4H_9OH_2^+]} = \frac{k_1}{k_{-1}} + \frac{k_2}{k_{-1}} \frac{[CH_4]}{[i\text{-}C_4H_8]} \qquad (4.26)$$

Equation 4.26 may be simply written as:

$$K_{obs.} = K_{true} + \frac{k_2}{k_{-1}} \frac{[CH_4]}{[i\text{-}C_4H_8]} \qquad (4.27)$$

where $K_{obs.}$ and K_{true} are the observed and the true thermodynamic equilibrium constants for reaction 4.21. Equation 4.27 shows that $K_{true} \leq K_{obs}$ and the observed equilibrium constant would increase with increasing neutral ratio of $[CH_4]/[i\text{-}C_4H_8]$. This explains the observations that the observed equilibrium constant does not change with the ion source pressure if the ratio $[CH_4]/[i\text{-}C_4H_8]$ is kept constant but increases when $[CH_4]/[i\text{-}C_4H_8]$ is increased. According to equation

4.27 a plot of K_{obs} versus $[CH_4]/[i-C_4H_8]$ would yield a straight line with an intercept of K_{true} and a slope of k_2/k_{-1}. The average K_{obs} values measured with three different $[CH_4]/[i-C_4H_8]$ ratios at 452°K are plotted in figure 4.5. An intercept of 3.5 ± 1.9 and a slope of 0.031 ± 0.012 were given by the least square analysis. This leads to $-\Delta G^0_{452}$ = 1.1 ± 0.6 kcal/mole for reaction 4.21. If we assume the forward rate constant for the exothermic proton transfer reaction 4.21 to be 10^{-9} cm^3 $molecule^{-1}$ sec^{-1} (proceeds with ion-molecule collision frequency with no activation energy), one may obtain $k_{-1} = k_1/K = 3 \times 10^{-10}$ cm^3 $molecule^{-1}$ sec^{-1}. The value of k_2 may be calculated from the slope of figure 4.5: $k_2 = (slope) \times k_{-1} = 9 \times 10^{-12}$ cm^3 $molecule^{-1}$ sec^{-1} at 452°K. The rates of the proton transfer and the dehydration at 452°K may be compared by comparing their corresponding reaction frequencies, ν. For the proton transfer reaction, $\nu_1 = k_1[i-C_4H_8]$. With a pressure of 10 mtorr of isobutene, its number density is about 2×10^{14} molecules cm^{-3} at 452°K. This leads to a $\nu_1 \approx 2 \times 10^5$ sec^{-1}. For the dehydration of the $t-C_4H_9OH_2^+$ ion, $\nu_2 = k_2[CH_4]$. With an ion source pressure of 3 torr $\nu_2 \approx 5 \times 10^5$ sec^{-1}. The results show that the rate of dehydration reaction 4.18 is actually slightly faster than the rate of proton transfer reaction 4.21 at 452°K and its interference with direct equilibrium measurements
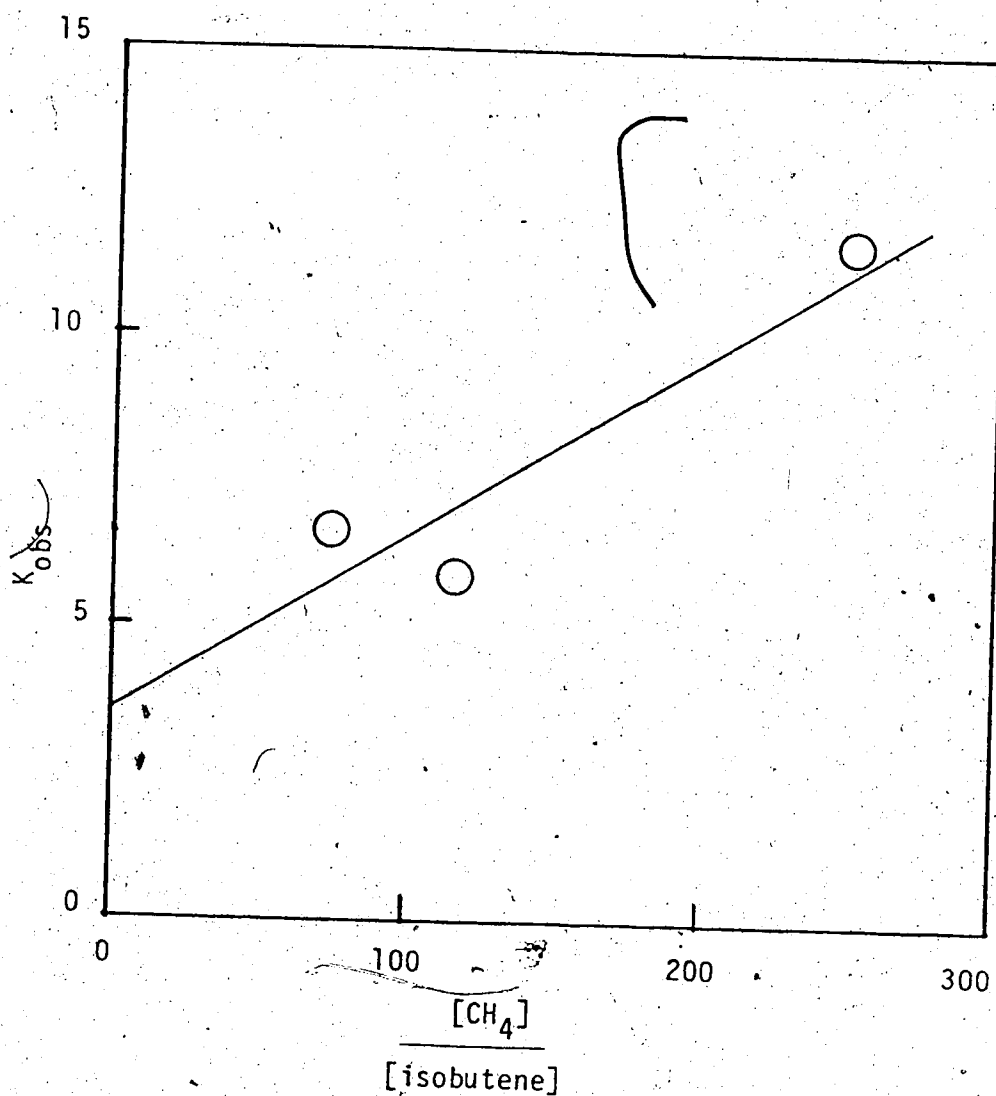
FIGURE 4.5 Observed Equilibrium Constants versus $[CH_4]/[isobutene]$
Ratios at 452°K for the Reaction :
Isobutene + H^+(t-butanol) = t-butyl$^+$ + t-butanol

of the proton transfer reaction cannot be neglected.

The rate constant for the reverse reaction 4.18 may

$$t-C_4H_9OH_2^+ + CH_4 \underset{k_{-2}}{\overset{k_2}{\rightleftarrows}} t-C_4H_9 + H_2O + CH_4 \quad (4.18)$$
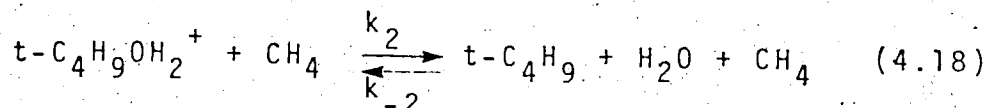
be calculated if the equilibrium constant at 452°K is known. Using the values of ΔH^O = 11.2 kcal/mole and ΔS^O = 22 eu for reaction 4.18 reported by Hiraoka and Kebarle (97), a value of ΔG_{452}^O = 1.25 kcal/mole is obtained. This leads to K = 187.7 torr or 3.8 x 10^{18} molecule cm^{-3} at 452°K. By equating K = k_2/k_{-2}, one may calculate that k_{-2} = 2 x 10^{-30} cm^6 molecule^{-2} sec^{-1} at 452°K. The rate constant for the hydration of tert-butyl ion, k_{-2}, can be compared with that for the hydration of sec-propyl ion, reaction 4.28.

$$s-C_3H_7^+ + H_2O = s-C_3H_7OH_2^+ \quad (4.28)$$
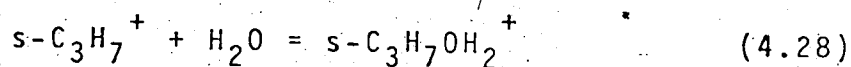
Hiraoka and Kebarle (97) reported a value of k ≈ 5 x 10^{-28} cm^6 molecule^{-2} sec^{-1} at 303°K, assuming it is third-order. The present result indicates that the rate constant for the hydration of tert-butyl ion is much smaller although it is expected that the third-order rate constants for termolecular reactions such as k_{-2} would increase with decreasing temperature. It is interesting to note that the assumption of a third-body dependence on the rate of hydration of the $t-C_4H_9^+$ ion is justified by the present experimental observation.

According to equation 4.27 the K_{obs} increases with the ratio $[CH_4]/[i-C_4H_8]$ only if the hydration reaction is third-order. If it is second order, K_{obs}' would decrease with increase of $[i-C_4H_8]$, and K_{obs} would be expected to decrease with an increase in the ion source pressure under the present conditions. This was not observed in the experiments.

The measured ΔG^o value for the proton transfer reaction 4.21 is fitted into the thermodynamic ladder as shown in table 3.1. After making the rotational symmetry corrections for the entropy term, the proton affinity of tert-butanol is determined to be 196.7 kcal/mole based on $PA(NH_3)$ = 207.6 kcal/mole.

A comparison may be made with the ΔH^o values for the following reactions:

$$t-C_4H_9^+ + t-C_4H_9OH = i-C_3H_8 + t-C_4H_9OH_2^+ \quad \Delta H^o = 1.5 \text{ kcal/mole}$$
$$(4.21)$$

$$t-C_4H_9OH_2^+ = t-C_4H_9^+ + H_2O \quad \Delta H^o = 11.2 \text{ kcal/mole}$$
$$(4.18)$$

___

$$t-C_4H_9OH = i-C_4H_8 + H_2O \quad \Delta H^o = 12.7 \text{ kcal/mole}$$
$$(4.29)$$
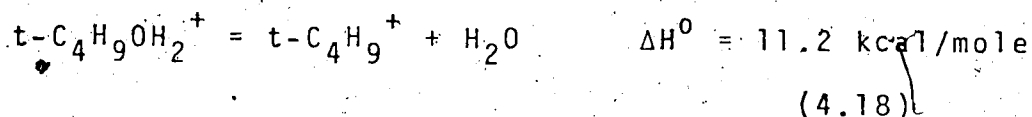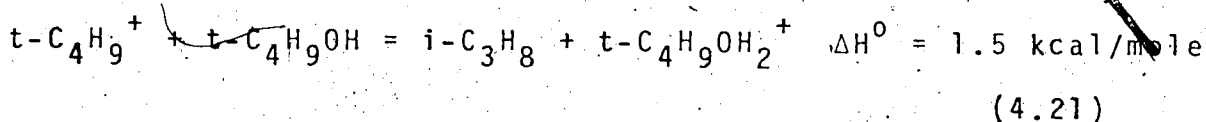
The ΔH^o for reaction 4.21 is obtained from PA(isobutene) - PA(t-butanol). The ΔH^o for reaction 4.18 is from Hiraoka (97). The $\Delta H^c = 12.7$ kcal/mole for reaction 4.29 is in good agreement with the value 13.1 kcal/mole calculated

from the following heat of formation values: $\Delta H_f^O(H_2O) =$ -57.8 kcal/mole (76), ΔH_f^O(isobutene) = 4.04 kcal/mole (76), $\Delta H_f^O(t-C_4H_9OH)$ = -74.9 kcal/mole (98). The chain reactions shown above may be regarded as an interesting case of "ion-catalyzed" dehydration of tert-butanol. It can be shown to be occurring spontaneously in the present system at 452°K. The ΔG_{452}^O value for reaction 4.29 is calculated to be 2.4 kcal/mole. This corresponds to K = 5.3 x 10^4 mtorr. If one expresses:

$$K = \frac{[i-C_4H_8]_{eq}[H_2O]_{eq}}{[t-C_4H_9OH]_{eq}} = 5.3 \times 10^4 \text{ mtorr} \qquad (4.30)$$

and assumes $[i-C_4H_8]_{eq} = [H_2O]_{eq}$, where the subscript eq refers to equilibrium concentration, a value of $[t-C_4H_9OH]_{eq}$ = 10 mtorr would yield $[i-C_4H_8]_{eq} = [H_2O]_{eq}$ = 740 mtorr. Since the residence time of the gases in the ion source is short (~milliseconds), reaction 4.29 probably will not affect the neutral concentrations in the present measurements.

The present results, coupled with those in table 3.57, show that in the alcohol series ROH, with R = CH_3, C_2H_5, $i-C_3H_7$ and $t-C_4H_9$, the proton affinities are: 186.2, 191.2, 194.2 and 196.7 kcal/mole. The successive differences on additional methyl substitutions are 5, 3 and 2.5 kcal/mole. Taft and co-workers (99) have reported successive differences of 3.9, 3.8 and 3.5 for this series

by ab initio calculations at the 4-31G level. The present experimental results are more in line with the expectation that the charge stabilizing power of the methyl group attenuates with successive methyl substititions.

The heats of formation of $s-C_3H_7OH_2^+$ and $t-C_4H_9OH_2^+$ may be calculated from the corresponding proton affinities by the following expressions:

$$\Delta H_f^o(s-C_3H_7OH_2^+) = \Delta H_f^o(s-C_3H_7OH) + \Delta H_f^o(H^+) - PA(s-C_3H_7OH) \qquad (4.31)$$

$$\Delta H_f^o(t-C_4H_9OH_2^+) = \Delta H_f^o(t-C_4H_9OH) + \Delta H_f^o(H^+) - PA(t-C_4H_9OH) \qquad (4.32)$$

The present experimental results yield $PA(s-C_3H_7OH) = 194.2$ kcal/mole and $PA(t-C_4H_9OH) = 196.7$ kcal/mole. Combining these values with $\Delta H_f^o(H^+) = 367.2$ kcal/mole (77), $\Delta H_f^o(s-C_3H_7OH) = -65.4$ kcal/mole and $\Delta H_f^o(t-C_4H_9OH) = -74.9$ kcal/mole (98), one obtains $\Delta H_f^o(s-C_3H_7OH_2^+) = 107.6$ kcal/mole and $\Delta H_f^o(t-C_4H_9OH_2^+) = 95.6$ kcal/mole. A comparison can be made with the ΔH^o values for the hydration of the corresponding carbonium ions. For the tert-butyl ion, Hiraoka and Kebarle (97) reported a $\Delta H^o = -11.2$ kcal/mole for the hydration reaction 4.33. Using the values of

$$t-C_4H_9^+ + H_2O = t-C_4H_9OH_2^+ \qquad \Delta H^o = -11.2 \text{ kcal/mole} \qquad (4.33)$$
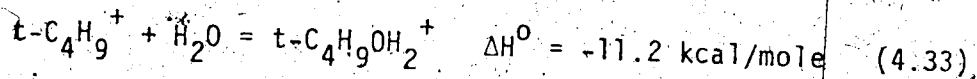
$\Delta H_f^o(t-C_4H_9^+) = 165.0$ kcal/mole by Beauchamp, and Tsang (see table 3.55), and $\Delta H_f^o(H_2O) = -57.8$ kcal/mole (76), the $\Delta H_f^o(t-C_4H_9OH_2^+)$ is calculated to be 96.0 kcal/mole. The excellent agreement in $\Delta H_f^o(t-C_4H_9OH_2^+)$ values indicates

that the monohydrate of tert-butyl ion has the same

structure of the protonated tert-butanol. It should be

noted that the good internal consistency of both

$\Delta H_f^o(t\text{-}C_4H_9OH_2^+)$ values is not affected by the uncertainties

of the $\Delta H_f^o(t\text{-}C_4H_9^+)$ value since they both depend on the
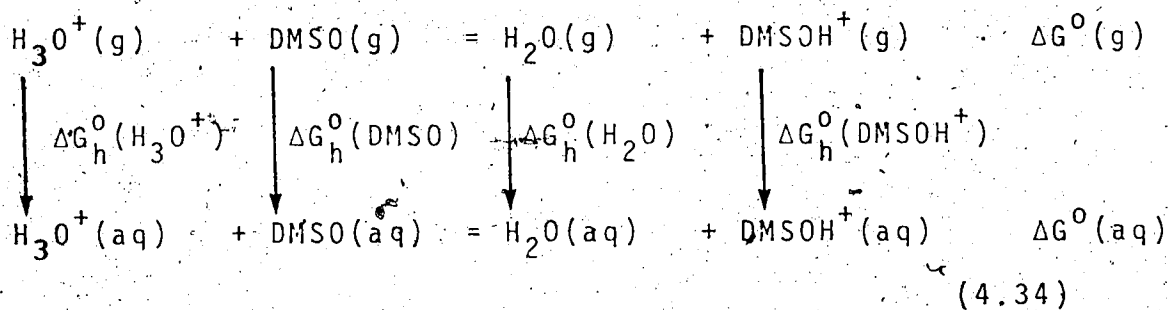
$\Delta H_f^o(t\text{-}C_4H_9^+)$ value to the same extent.

The hydration of $s\text{-}C_3H_7^+$ ion was studied by Beggs and

Field (100). A $\Delta H^o = -17.6$ kcal/mole was reported for

reaction 4.28. With literature values of $\Delta H_f^o(s\text{-}C_3H_7^+) =$

$$s\text{-}C_3H_7^+ + H_2O = s\text{-}C_3H_7OH_2^+ \quad \Delta H^o = -17.6 \text{ kcal/mole}$$

$$(4.28)$$
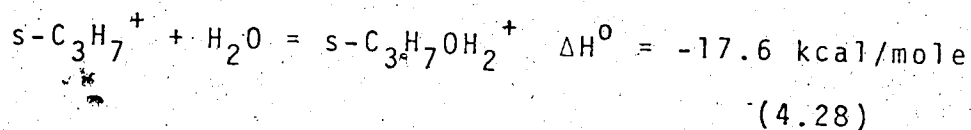
188.8 kcal/mole from Beauchamp (82) and $\Delta H_f^o(H_2O) = -57.8$

kcal/mole (76), one obtains $\Delta H_f^o(s\text{-}C_3H_7OH_2^+) = 113.4$ kcal/

mole. This value is 5.8 kcal/mole higher than that

obtained from the present proton affinity determination.

As there is no reasonable alternate $C_3H_8O^+$ isomer with a

heat of formation so close to that of protonated iso-

propanol, we may assume that the condensation product of

reaction 4.28 is the protonated iso-propanol. Although

some uncertainties may be present in the $\Delta H_f^o(t\text{-}C_4H_9^+)$

and $\Delta H_f^o(s\text{-}C_4H_9^+)$ values, they are not expected to cause

such a big difference in the two $H_f^o(s\text{-}C_4H_9OH_2^+)$ values.

It is believed that the 5.8 kcal/mole difference is due

mainly to the experimental errors in Field's equilibrium

measurements on reaction 4.28.

4.3   Proton Affinity of Dimethyl Sulfoxide (DMSO)

DMSO is a common dipolar aprotic molecule which has a large permanent dipole but no acidic hydrogen capable of forming hydrogen bonding. Its proton affinity was determined in the present work to be 214.4 kcal/mole (tables 3.1 and 3.57). Comparing with the proton affinity of water, $PA(H_2O) = 171.7$ kcal/mole (tables 3.1 and 3.57), the proton affinity of DMSO is higher than that of water by 42.7 kcal/mole. In aqueous solution, the pK_a values for H_3O^+ and $DMSOH^+$ are -1.7 (101) and -1.54 (102) respectively. This corresponds to a slightly higher aqueous basicity (0.2 kcal/mole) for H_2O than DMSO. The difference is mainly due to the differential cationic solvation which heavily favors the hydration of the H_3O^+ ion because of the larger number of possible H-bonding sites in the cation. The following thermodynamic cycle may be used to evaluate the difference in standard free energy change of hydration ΔG^o_h, between H_3O^+ and $DMSOH^+$.

$$H_3O^+(g) \quad + DMSO(g) \quad = H_2O(g) \quad + DMSOH^+(g) \quad \Delta G^o(g)$$

$$\downarrow \Delta G^o_h(H_3O^+) \quad \downarrow \Delta G^o_h(DMSO) \quad \downarrow \Delta G^o_h(H_2O) \quad \downarrow \Delta G^o_h(DMSOH^+)$$

$$H_3O^+(aq) \quad + DMSO(aq) \quad = H_2O(aq) \quad + DMSOH^+(aq) \quad \Delta G^o(aq)$$

$$(4.34)$$

It is evident from the thermodynamic cycle that equation 4.35 holds. The relative aqueous basicity of the reaction,

$$\Delta G^o(g) - \Delta G^o(aq) = [\Delta G_h^o(H_3O^+) - \Delta G_h^o(DMSOH^+)] - [\Delta G_h^o(H_2O) - \Delta G_h^o(DMSO)]$$

$$(4.35)$$

$\Delta G^o(aq)$, given by $\Delta G^o(aq) = -2.303\,RT[pK_a(DMSOH^+) - pK_a(H_3O^+)]$, has a value of 0.2 kcal/mole at 298°K. The corresponding $\Delta G^o(g)$ value of -42.9 kcal/mole was obtained from the present results after correcting for temperature difference by using $\Delta S_{rot.s.}^o$. Using the values in Arnett's tabulation (103), $\Delta G_h^o(H_2O) - \Delta G_h^o(DMSO) = 3.7$ kcal/mole at 298°K. From equation 4.35, it is calcaulted that the difference in standard free energy of hydration between H_3O^+ and $DMSOH^+$, $\Delta G_h^o(H_3O^+) - \Delta G_h^o(DMSOH^+)$, is equal to -39.0 kcal/mole at 298°K. Similar thermodynamic cycles may be used to calculate the difference in enthalpy change of hydration ΔH_h^o, between H_3O^+ and $DMSOH^+$. With the literature values: $\Delta H_h^o(H_2O) = -10.5$ kcal/mole (104); $\Delta H_h^o(DMSO) = 17.1$ kcal/mole (105); $\Delta H^o(aq) = 2.2$ kcal/mole (103), and the present experimental value of $\Delta H^o(g) = -42.7$ kcal/mole, it follows that:

$$\Delta H_h^o(H_3O^+) - \Delta H_h^o(DMSOH^+) = [\Delta H^o(g) - \Delta H^o(aq)] + [\Delta H_h^o(H_2O) - \Delta H_h^o(DMSO)]$$

$$= -38.3 \text{ kcal/mole} \qquad (4.35)$$

Results from the above calculations verify the previous statement that the difference in the gas-phase and aqueous basicities of DMSO and H_2O (43 kcal/mole) is accounted for

predominantly by the difference in ion solvation energies (39 kcal/mole). With the availability of gas-phase data, the ion solvation energies in different solvents may be assessed. This will provide valuable information in the understanding of solvation effects in solution chemistry.

THE PROTON AFFINITY OF KETENE AND THE HEAT OF FORMATION OF CH_3CO^+
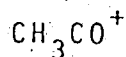
CHAPTER V

5.1 Introduction

Ketene is an interesting molecule which is commonly used as a source of methylene in organic reactions. Its conjugated acid, CH_3CO^+, is a very important ion as evident by the presence of m/e = 43 peak in the mass spectra of many organic compounds. It has been suggested (106) that ketene be used as a reference for proton affinity determinations. However, an examination on the thermochemical data from the literature shows that there are internal inconsistencies in the heat of formation of the CH_3CO^+ ion as well as the proton affinity of ketene.

Previous determinations of $\Delta H_f^o(CH_3CO^+)$ were based on appearance potentials determined by photoionization measurements (107,108). The recommended value $\Delta H_f^o(CH_3CO^+) = 152$ kcal/mole (76) was based on the appearance potential $A_p(CH_3CO^+, CH_3COCH_3)$ from the ionization efficiency curve for acetone (107,108). It was noted that the appearance potential of CH_3CO^+ from acetaldehyde (108) leads to a higher value of $\Delta H_f^o(CH_3CO^+) = 158$ kcal/mole. Recent redeterminations of the above photoionization potentials by Beauchamp (109) reproduced similar results which lead to $\Delta H_f^o(CH_3CO^+)$ values of 153.1 kcal/mole and 157.8 kcal/mole derived from acetone and acetaldehyde,

272

respectively. The disagreement in the appearance potential could result from thermal shift (the presence of excess internal energy in the molecule giving rise to a lower dissociation and ionization threshold) in the case of acetone or from kinetic shift (the excess energy required to cause dissociation within the time of observation in the mass spectrometer) in the case of acetaldehyde. From the study of relative stabilites of different carbonium ions by ion-molecule reactions, Beauchamp and coworkers (109) selected the higher value for the heat of formation of CH_3CO^+, $\Delta H_f^o(CH_3CO^+) = 157.8$ kcal/mole. Their argument was based on the observation that the bromide transfer reaction 5.1

$$(CH_3)_3CBr + CH_3CO^+ = (CH_3)_3C^+ + CH_3COBr \quad (5.1)$$
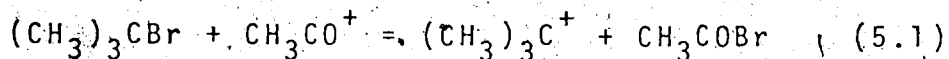
proceeds to the right towards completion, indicating that reaction 5.1 is exothermic. Therefore, the following inequality should hold:

$$\Delta H_f^o(CH_3CO^+) + \Delta H_f^o(t\text{-butyl Br}) > \Delta H_f^o(t\text{-butyl}^+) + \Delta H_f^o(\text{acetyl Br}) \quad (5.2)$$

With the literature values (110) of $\Delta H_f^o(t\text{-butyl Br}) = -31.9$ kcal/mole and $\Delta H_f^o(\text{acetyl Br}) = -45.6$ kcal/mole, it implies that:

$$\Delta H_f^o(t\text{-butyl}^+) - \Delta H_f^o(CH_3CO^+) < 13.7 \text{ kcal/mole} \quad (5.3)$$

Adopting the earlier value of $\Delta H_f^o(t\text{-butyl}) = 169$ kcal/mole from the work of Lossing (81) and Tsang (78), equation

5.3 requires that $\Delta H_f^o(CH_3CO^+) > 155.3$ kcal/mole. It is
interesting to note that with the revised value of
$\Delta H_f^o(t\text{-butyl}^+) = 165.0$ kcal/mole by Beauchamp (82), the
observation of reaction 5.1 leads to $\Delta H_f^o(CH_3CO^+) \not> 151.3$
kcal/mole. Consequently, the argument used by Beauchamp
in rejecting the lower value of $\Delta H_f^o(CH_3CO^+)$ is no longer
valid. Other comparisons have to be made as to determine
which appearance potential, if any, does refer to the
true thermodynamic value of CH_3CO^+.

The proton affinity of ketene can be calculated
from the heats of formation of the neutral and the cor-
responding ions as shown in equation 5.4.

$$PA(ketene) = \Delta H_f^o(H^+) + \Delta H_f^o(CH_2CO) - \Delta H_f^o(CH_3CO^+) \tag{5.4}$$

Using $\Delta H_f^o(H^+) = 367.2$ kcal/mole (77), $\Delta H_f^o(CH_2CO) = -11.4$
kcal/mole (111) and the higher value $\Delta H_f^o(CH_3CO^+) = 158$
kcal/mole, the proton affinity of ketene would be calcu-
lated to be 198 kcal/mole. On the other hand, the lower
value $\Delta H_f^o(CH_3CO^+) = 152$ kcal/mole leads to PA(ketene) =
204 kcal/mole.

An early investigation by Long and Munson (106)
with "occurrence-nonoccurrence" method reported the
observation of the proton transfer reaction 5.5.

$$CH_3CO^+ + (CH_3)_2CO = CH_2CO + (CH_3)_2COH^+ \tag{5.5}$$
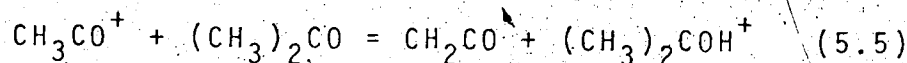
From this, it was concluded that reaction 5.5 is exo-
thermic and the proton affinity of ketene is lower than

that of acetone (PA(acetone) =198.6 kcal/mole from present results, see Table 3.57). However, recent equilibrium determinations by Ausloos and Lias (112), and by Beauchamp et al. (113) indicated that reaction 5.5 has a negative ΔG^0_{300} value indicating that ketene is more basic than acetone.

The gas-phase basicity of ketene relative to the compounds previously studied was determined with a high pressure mass spectrometer in the present work. This leads to a proton affinity of ketene. The heat of formation of the acyl ion CH_3CO^+ derived from the PA(ketene) value is compared with the two $\Delta H^0_f(CH_3CO^+)$ values available in the literature as well as to the $\Delta H^0_f(CH_3CO^+)$ value obtained from the dehydration enthalpy of the protonated acetic acid determined by Davidson in this laboratory (94).

5.2 Preparation of Ketene

Ketene was prepared by pyrolysis of acetone as outlined by Williams and Hurd (114):

$$CH_3COCH_3 \xrightarrow[\Delta]{Ni/Cr} CH_2CO + CH_4 \qquad (5.6)$$
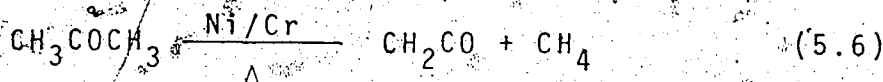
A schematic diagram of the apparatus used for the pyrolysis of acetone vapor is shown in Figure 5.1. The apparatus was made of Pyrex glass. Acetone in flask A was refluxed gently throughout the preparation. The filament was made
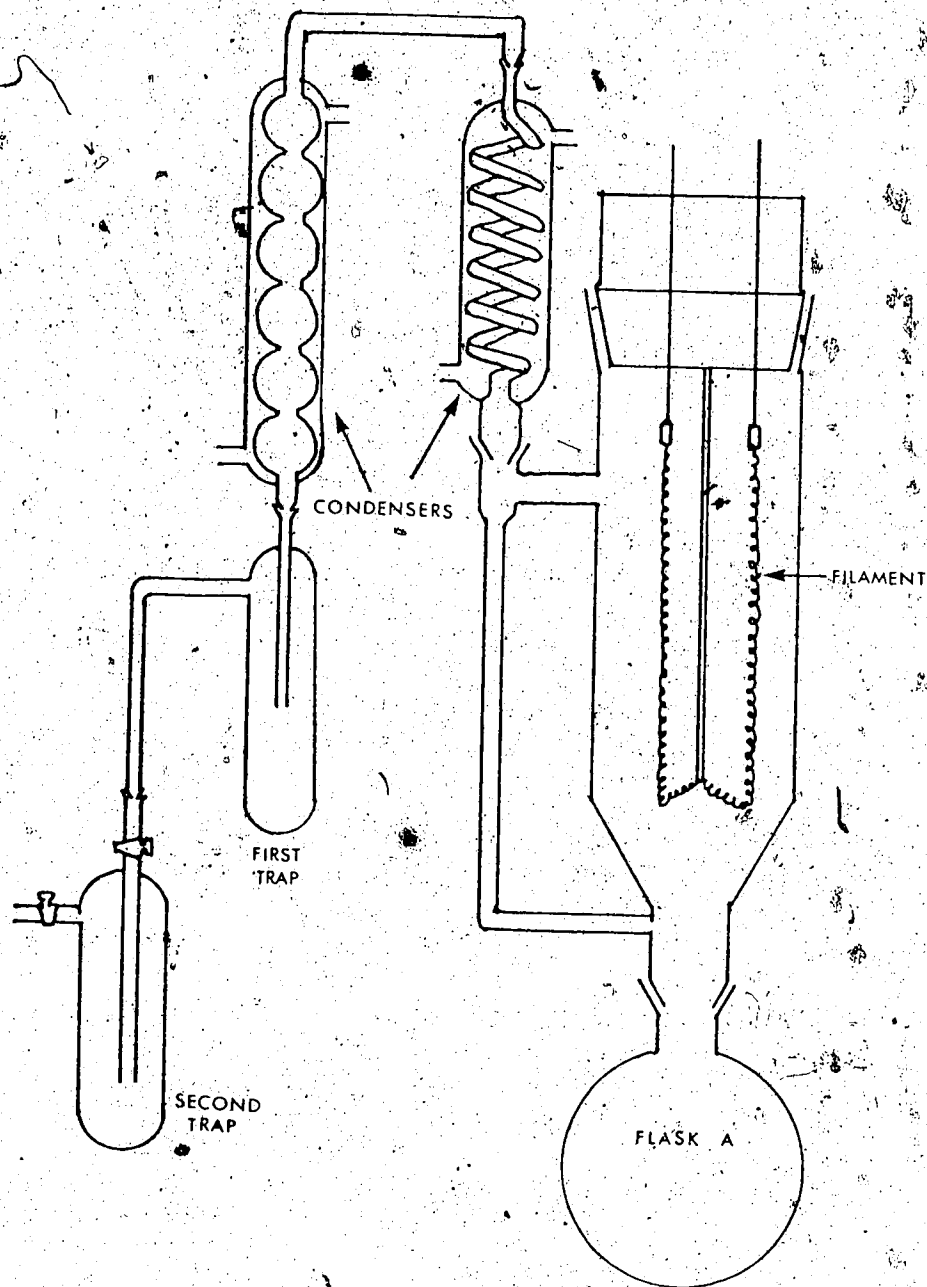
FIGURE 5.1   Apparatus for the Preparation of Ketene

of gauge 24 Chromel A wire (an alloy of 80% nickel and 20% chromium). The two ends of the filament were connected to an a.c. power source through a Variac transformer. During pyrolysis, the filament was heated to a dull red glow (temperature about 700-750°C). Unreacted acetone passing through the condensers was removed by the first trap immersed in a dry ice-50:50 CCl_4/$CHCl_3$ bath (-80°C). Ketene and methane were collected in the second trap cooled with liquid nitrogen (-196°C). At the end of the run, the source of the heat was removed from flask A and the filament current was turned off. The second trap was removed from the apparatus and transferred to a vacuum rack equipped with four cold traps. Methane was removed and ketene was further purified by several trap-to-trap distillations. Analysis of the ketene sample by mass spectrometric methods using the electron-impact low pressure ion source revealed no discernible impurities. A small amount of ketene dimer was detected on the mass spectrum of ketene sample after it was stored for several days. Because of this reason, the purity of ketene was checked every day by mass spectrometric methods before it was used and fresh ketene was prepared every three or four days.

5.3   Discussion

The proton affinity of ketene is best evaluated by comparing the basicity of ketene with that of isobutene as shown in reaction 5.7.

$$(CH_3)_3C^+ + CH_2CO = (CH_3)_2CCH_2 + CH_3CO^+ \qquad (5.7)$$
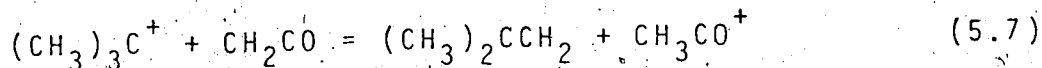
The increase in internal rotations for the protonation of ketene is cancelled by the similar decrease in internal rotation for the deprotonation of the tert-butyl cation. Therefore, it is reasonable to assume that the entropy change for reaction 5.7 is due entirely to changes in external rotational symmetry number, σ, of species involved in the reaction (i.e. $\Delta S^o = \Delta S^o_{rot.s}$):

$$\Delta S^o \approx \Delta S^o_{rot.s.} = R\ell n\left(\frac{\sigma_{t-butyl^+}}{\sigma_{isobutene}}\right)\left(\frac{\sigma_{ketene}}{\sigma_{CH_3CO^+}}\right)$$

$$\qquad (5.8)$$

$$= R\ell n \left(\frac{6}{2}\right)\left(\frac{2}{3}\right) = 1.4 \, eu$$

A value of $\Delta S^o_{rot.s} = 1.4$ eu leads to an estimated $T\Delta S^o = 0.8$ kcal/mole at 600°K for reaction 5.7. As shown in Table 3.1 the free energy change for the proton transfer reaction 5.7 was measured to be -1.8 kcal/mole. From the relationship $\Delta H^o = \Delta G^o + T\Delta S^o$, the ΔH^o for reaction 5.7 is calculated to be -1.0 kcal/mole. Since isobutene which was chosen as the external standard has a proton affinity of 198.2 kcal/mole (see section 3.2), the proton affinity of ketene may then be calculated to be

199.2 kcal/mole.

Beauchamp et al. (113) in a recent investigation by the ICR method reported a proton affinity for ketene, PA(ketene) = 195.9 ± 2 kcal/mole, relative to PA(isobutene) = 194.0 ± 2 kcal/mole. A similar study by Ausloos and Lias (112) resulted in PA(ketene) = 189.5 kcal/mole, relative to PA(isobutene) = 189 ± 2 kcal/mole. If corrected to the presently preferred value of PA(isobutene) = 198.2 kcal/mole, the former gives PA(ketene) = 200.1 ± 2 kcal/mole and the latter yields PA(ketene) = 198.7 ± 2 kcal/mole. Both are in agreement with the present results. The present results also imply that the PA(ketene) is slightly higher than the PA(acetone) = 198.6 kcal/mole, indicating that the proton transfer from CH_3CO^+ to acetone is endothermic, in disagreement with the conclusion drawn by Long and Munson (106).

The heat of formation of acetyl cation, CH_3CO^+, may be evaluated from PA(ketene), $\Delta H_f^0(H^+)$ and $H_f^0(ketene)$. From the deprotonation reaction 5.9, $\Delta H_f^0(CH_3CO^+)$ is given

$$CH_3CO^+ = CH_2CO + H^+ \qquad \Delta H^0 = PA(ketene) \qquad (5.9)$$
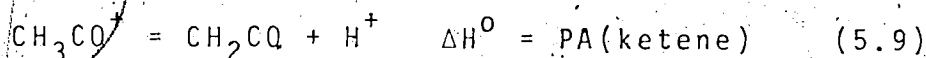
by equation 5.10

$$\Delta H_f^0(CH_3CO^+) = \Delta H_f^0(CH_2CO) + \Delta H_f^0(H^+) - PA(ketene) \quad (5.10)$$

The present value of PA(ketene) = 199.2 kcal/mole when combined with $\Delta H_f^0(CH_2CO)$ = -11.4 kcal/mole (111) and $\Delta H_f^0(H^+)$ = 367.2 kcal/mole (77) leads to $\Delta H_f^0(CH_3CO^+)$ = 156.6 kcal/

mole. As mentioned in the introduction, from appearance potential measurements, $\Delta H_f^0(CH_3CO^+)$ values of 150 kcal/mole (from acetone) and 158 kcal/mole (from acetaldehyde) were obtained (107-109). It is noted that these ΔH_f^0 values are obtained using the usual mass spectrometrist's assumption th▓▓e integrated heat capacity of the electron is zero. ▓▓e results in this work are calculated assuming that the electron is an ideal gas with a heat capacity of $\frac{5}{2}R$ (see page 218). In order to compare these numbers with the present value, one needs to add 1.5 kcal/mole ($\frac{5}{2}R(298)$; see page 218) to the values of ΔH_f^0 from the literature. The corrected literature values of $\Delta H_f^0(CH_3CO^+)$ are then 153.5 kcal/mole (from acetone) and 159.5 kcal/mole (from acetaldehyde). The present value of 156.6 kcal/mole is 3.1 kcal/mole higher than the former value and 2.9 kcal/mole lower than the latter value. It is very possible that both $\Delta H_f^0(CH_3CO^+)$ values obtained from appearance potential measurements do not represent the true thermodynamic value.

The $\Delta H_f^0(CH_3CO^+)$ has also been evaluated from a study of the association reaction 5.11 involving acetyl cation and water by Davidson in this laboratory (94) using a high pressure mass spectrometer.

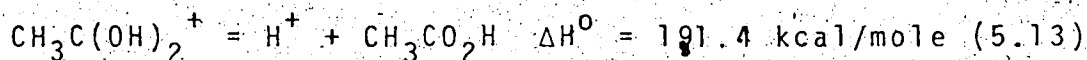$$CH_3CO^+ + H_2O = CH_3C(OH)_2^+ \qquad (5.11)$$
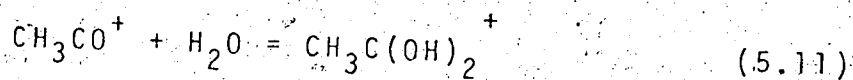
The enthalpy change of the reaction was determined to be -24.6 kcal/mole. Since the product of reaction 5.11

is the protonated acetic acid whose heat of formation can be evaluated from its proton affinity, the $\Delta H_f^o(CH_3CO^+)$ may be calculated from the ΔH^o of the reaction 5.11, PA(acetic acid), $\Delta H_f^o(H^+)$ and the heats of formation of neutrals in- volved. The ΔG_{600}^o for the reaction 5.12 was determined

$$NH_4^+ + CH_3CO_2H = NH_3 + CH_3C(OH)_2^+ \qquad (5.12)$$
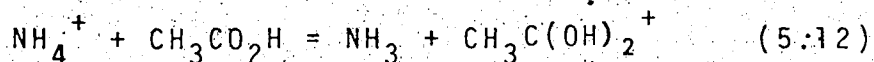
previously to be 14.5 kcal/mole in this laboratory (115). Correcting for $\Delta S_{rot.s.}^o$ leads to the value of $\Delta H^o = 16.2$ kcal/mole. With PA(NH_3) = 207.6 kcal/mole as reference, PA(acetic acid) = 191.4 kcal/mole. By combining the appropriate reactions 5.13 and 5.11, reaction 5.14 results

$$CH_3C(OH)_2^+ = H^+ + CH_3CO_2H \quad \Delta H^o = 191.4 \text{ kcal/mole} \quad (5.13)$$

$$CH_3CO^+ + H_2O = CH_3C(OH)_2^+ \quad \Delta H^o = -24.6 \text{ kcal/mole} \quad (5.11$$

$$\overline{CH_3CO^+ + H_2O = H^+ + CH_3CO_2H \quad \Delta H^o = 166.8 \text{ kcal/mole} \quad (5.14)}$$
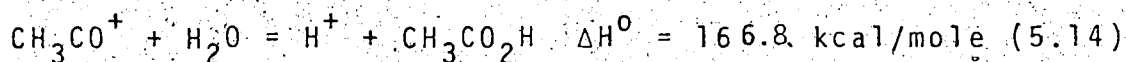
which leads to an expression for $\Delta H_f^o(CH_3CO^+)$ as shown in equation 5.15.

$$\Delta H_f^o(CH_3CO^+) = \Delta H_f^o(H^+) + \Delta H_f^o(CH_3CO_2H) - \Delta H_f^o(H_2O) - 166.8 \text{ kcal/mole}$$

$$(5.15)$$

With the following literature values: $\Delta H_f^o(H^+)$ = 367.2 kcal/mole (77), $\Delta H_f^o(CH_3CO_2H)$ = -103.3 kcal/mole (76) and $\Delta H_f^o(H_2O)$ = -57.8 kcal/mole (76), the heat of formation of CH_3CO^+ was cal-

culated to be 154.9 kcal/mole. This is in reasonably good agreement with the present value of $\Delta H_f^o(CH_3CO^+) = 156.6$ kcal/mole, considering the number of thermodynamic data used in the derivation. It should be pointed out that the above agreement in $\Delta H_f^o(CH_3CO^+)$ obtained is independent of the uncertainty in $\Delta H_f^o(t\text{-butyl}^+)$ on which both values depend to the same extent, therefore, it cannot be used to judge the accuracy of the $\Delta H_f^o(CH_3CO^+)$ value. However, the agreement does show the internal consistency between the results from proton-transfer measurements and those from association reactions measured in our laboratory.

Finally, it is noted that there are three possible isomers for the CH_3CO^+ ion (structures I - III).

$$\underset{\text{I}}{\overset{\displaystyle H}{\underset{\displaystyle H}{H}}C - \overset{+}{C} = O} \qquad \underset{\text{II}}{\overset{\displaystyle H}{\underset{\displaystyle H}{H}}C = \overset{+}{C} = O - H} \qquad \underset{\text{III}}{\overset{\displaystyle H}{\underset{\displaystyle H}{H}}\overset{+}{C} - \overset{\displaystyle O}{\underset{\displaystyle H}{C}}}$$
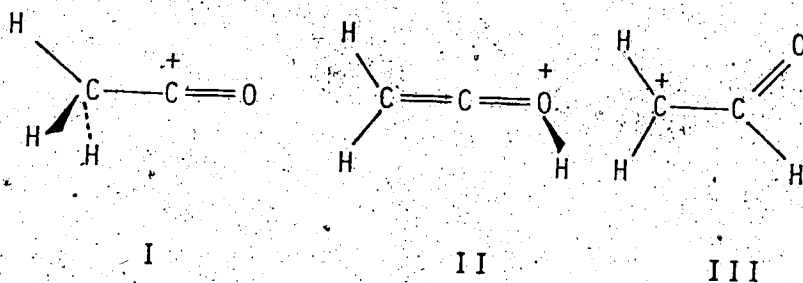
Theoretical calculations on the energies of the three isomers by Hopkinson [116], and by Yarkany and Schaefer [117] show that isomer I (acetyl cation) is the most stable structure. Isomers II and III are respectively ~35 kcal/mole and 65 kcal/mole less stable than the acetyl cation. The large energy difference excluded the possibility of any other isomeric contribution to the acetyl cation in the gas phase equilibrium measurements.

The results from NMR studies by Olah et al. (118) showed
that ketene in solution is also protonated cleanly on the
methylene carbon to form the acetyl cation. From the
results of the LCAO-MO-SCF calculations on the energies
of the acetyl cation and ketene, Hopkinson (116) estimated
that PA(ketene) = 217 kcal/mole. This is somewhat higher
than the present experimental value.

SUBSTITUENT EFFECTS ON THE INTRINSIC BASICITY OF BENZENE

CHAPTER VI

6.1   Introduction

The substituent effects on equilibria and reaction rates have long been an important subject in physical organic chemistry. Their correlations in aromatic systems have been studied in great detail in solution (119). Recently, there has been considerable interest in examining the intrinsic substituent effects on the gas-phase basicity of benzene. The interest is justified by the fact that ring protonation of benzene represents a prototype of electrophilic attack on the benzene ring and is closely related to the Hammett type linear free energy relationships (120). The intrinsic basicity studied in the gas phase is independent of solvent and is indispensable in separating the structural effects from the solvent effects of the substituents.

The protonation of a monosubstituted benzene may occur at the ring or at the substituent:

$$\text{(6.1)}$$
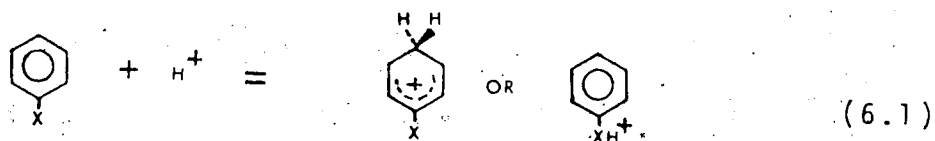
The question of the preferred site of protonation in the dilute gas phase has aroused considerable interest among different workers (83, 121-123). In solution, whether protonation occurs preferentially at the ring or at the

substituent often depends on environmental conditions, namely, the type of solvent and temperature. For example, the NMR spectrum of a solution of anisole in HF saturated with BF_3 shows the presence of ring-protonated and oxygen-protonated isomers in a 3:2 ratio at -83°C. With increasing temperature, the equilibrium shifts in favor of ring-protonation. At a temperature of -8°C, the fraction of oxygen-protonated isomer drops to about 2% in the same solution (124). In $HFSO_3$, only the ring-protonated ion is detected for anisole over the similar temperature range (125). These observations may be explained on the basis of specific solvent effects on the oxygen substituents. Another interesting observation is on the protonation of aminobenzenes. Although aniline is a well-known nitrogen base in solution, the protonation of 1,3,5-tri-aminobenzene and its derivatives in aqueous solutions occurs at the ring in preference to the amino groups (126). This indicates that the combined strong electron-releasing effects of the three amino groups at the 1-, 3- and 5- positions in benzene are so enormous that the basicity of the benzene ring is higher than that of the amino group. Since the interpretation of solution-phase basicities is always complicated by the presence of solvent, it is hoped that the gas-phase basicities of substituted benzenes which reflect the pure electronic effects of the substituents would provide the answer for the preferred

site of protonation in substituted benzenes in the absence
of solvent. In this Chapter, linear free energy relation-
ships are used to correlate the substituent effects on the
equilibrium constants of the proton transfer reaction 6.2.

$$\text{(6.2)}$$
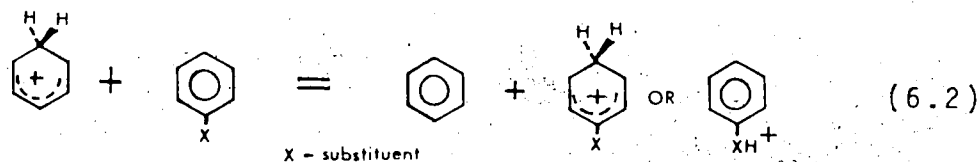
The correlations of the measured proton affinities with the
STO-3G calculated results and with the core electron bind-
ing energies will also be presented.

6.2   The Hammett Type Linear Free Energy Relationships
        The effects of substituents on equilibrium constants
or rate constants of a reaction depend on the electron-
donating or electron-withdrawing nature of substituents.
With hydrogen as the reference substituent, substituents
which encourage the development of positive charges and
discourage the development of negative charges at the
reaction center are known as electron-donating substitu-
ents. Substituents which have the opposite effects are
known as the electron withdrawing substituents. The
stabilization of positive or negative charges at the re-
action center is due to a combination of inductive and
resonance effects. It was observed that the electron-
donating or electron-withdrawing nature is character-
istic of the particular substituents and is independent

of the type of reactions. The regularities in substitu-
ent effects are observed most commonly with aromatic
compounds. With the ionization of benzoic acid as the
reference reaction, Hammett (127) expressed the sub-
stituent effects on the equilibrium constants of aromatic
reactions as follows:

$$\log\left(\frac{K_X}{K_H}\right)_{reaction} = \rho \, \log\left(\frac{K_X}{K_H}\right)_{reference} \qquad (6.3)$$

$(K_X/K_H)_{reaction}$ is the ratio of equilibrium constants for
an aromatic reaction with and without the substituent X
in the aromatic ring. $(K_X/K_H)_{reference}$ is the ratio of
equilibrium constant for the ionization of the substituted
and unsubstituted benzoic acid in water at 25°C, the
substituent, X, being identical and at the same position
in the ring relative to the reaction centers in both
cases. ρ is a proportionality constant. By defining
a fixed constant for a given substituent as in equation
6.4, the ordinary form of the Hammett equation (equation

$$\sigma_X = \log\left(\frac{K_X}{K_H}\right)_{reference} \qquad (6.4)$$

$$\log\left(\frac{K_X}{K_H}\right)_{reaction} = \rho\sigma_X \qquad (6.5)$$

6.5) is obtained. According to equation 6.4, σ_X has a
negative value for electron-donating substituents and

it is positive for electron-withdrawing substituents. The
more negative (positive) the σ_x value is, the larger is
the electron-donating (electron-withdrawing) effect of
the substituent relative to hydrogen. ρ is a constant and
depends on the nature of the reaction (including the re-
action temperature and solvent in the system). For a
reaction which is facilitated by the presence of an
electron-donating group, ρ has a negative value and vice
versa. The ionization of benzoic acid which is the ref-
erence reaction has a ρ value of 1. Since electrophilic
reactions involve the attack of an "electron-rich"
reaction site, they are facilitated by the presence of
electron-donating groups. Consequently, they will have
negative values of ρ.

Considering the ring-protonation reaction of ben-
zenes: (K being the equilibrium constant)

$$K_H \qquad (6.6)$$

$$K_X \qquad (6.7)$$
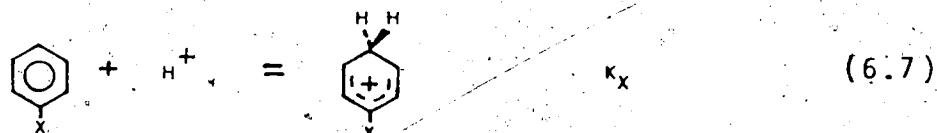
The ratio of (K_X/K_H) can be obtained by studying the
proton transfer reaction 6.8.

$$K = K_X/K_H \qquad (6.8)$$
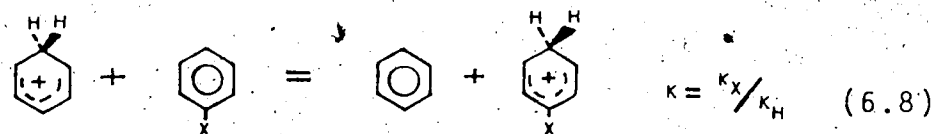
Since there is a linear relationship between the logar-
ithms of equilibrium constant and the standard free

energy change, ΔG^O, equation 6.5 may be rewritten for the proton transfer reaction 6.8 as follows:

$$-\Delta G^O = 2.303RT\log K = (2.303RT\rho)\sigma_x \qquad (6.9)$$

A careful examination of reaction 6.8 indicates that there are six equivalent sites for the protonation of benzene whereas there is only one reaction site for the protonation of monosubstituted benzene with the substituent para to the site of protonation. For pure statistical reasons, K_H will be six times larger than it should be if protonation was to occur at one particular site in benzene. Since the structural effects on equilibrium constants have nothing to do with the symmetry of the molecules, symmetry corrections have to be made on the equilibrium constants. The following treatment may be used. For the reaction:

$$A + B = C + D \qquad (6.10)$$

the equilibrium constant may be expressed in terms of the partition functions, Q, of the species involved in the equilibrium (119, p.1) as in equation 6.11.

$$K = \frac{Q_C Q_D}{Q_A Q_B} e^{-\Delta E_0^O/RT} \qquad (6.11)$$

The partition function, Q, for a given species is taken as the product of its translational, rotational, vibrational,

electronic and nuclear spin components. ΔE_o^o is the change in energy for the reaction at absolute zero. Since only the rotational partition function contains in its denominator the term of symmetry number σ, the contribution from the symmetry of the molecule can be separated from the rest of the partition function. The equilibrium constant

$$Q = \frac{1}{\sigma} Q'$$

(6.12)

can then be rewritten as in equations 6.13 and 6.14,

$$K = \frac{\sigma_A \sigma_B}{\sigma_C \sigma_D} \times \left(\frac{Q'_C Q'_D}{Q'_A Q'_B} \times e^{-\Delta E_o^o / RT} \right)$$

(6.13)

$$= K_{rot.s.} \cdot K_{chem.}$$

(6.14)

where $K_{rot.s.}$ is the symmetry contributions to the equilibrium constant, and K_{chem} is the "chemical" equilibrium constant of the reaction. In comparing the structural effects on equilibrium constants, K_{chem} should be used instead of K. The symmetry correction on the standard free energy change is a correction in the entropy change, ΔS^o, of the reaction. An expression analogous to equation 6.14 may be written for the entropy change of a reaction (equation 6.15), where ΔS^o_{chem} is the

$$\Delta S^o = \Delta S^o_{rot.s.} + \Delta S^o_{chem}$$

(6.15)

"chemical" entropy change of reaction. $\Delta S^o_{rot.s.}$ is the entropy change due to the change in rotational symmetry

numbers going from reactants to products, and it is given by:

$$\Delta S^{o}_{rot.s.} = -R\ln\frac{\sigma_C\sigma_D}{\sigma_A\sigma_B} \qquad (6.16)$$

In reactions such as proton transfer reactions in which there is no change in the number of molecules between products and reactants, $\Delta S^{o}_{chem} \approx 0$. The symmetry correction is the only major contribution to the standard entropy change. Using the well-known thermodynamic equation, $\Delta G^{o} = \Delta H^{o} - T\Delta S^{o}$, it may be written:

$$-\Delta H^{o} = -\Delta G^{o} - T\Delta S^{o}_{rot.s.}$$
$$= RT\ln K + RT\ln\frac{1}{K_{rot.s.}} \qquad (6.17)$$

or in a simpler form:

$$-\Delta H^{o} = (2.303RT)\log K_{chem} \qquad (6.18)$$

where ΔH^{o} is the standard enthalpy change of the reaction assuming the changes in rotational symmetry number is the only contribution to the standard entropy change of the reaction. The above derivations when applied to the proton transfer reaction 6.8 imply that the substituent effects on protonation of benzenes should follow the relationship:

$$-\Delta H^{o} = (2.303RT\rho)\sigma_x \qquad (6.19)$$

if protonation is to occur at the ring. The linear relationship would not be followed if protonation is to occur at the substituent.
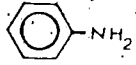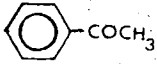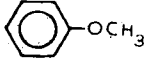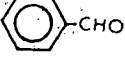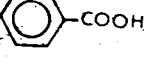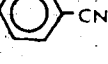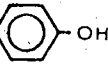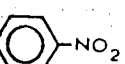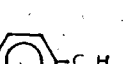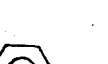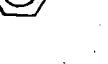
6.3   General Discussion

The monosubstituted benzenes examined in the present study include aniline, acetophenone, anisole, benzaldehyde, benzoic acid, benzonitrile, phenol, nitrobenzene, ethyl-, benzene, toluene, fluorobenzene and chlorobenzene. Their basicities relative to that of benzene expressed as $-\Delta G^{o}_{600}$ for the reaction 6.2 are shown in table 6.1. These $-\Delta G^{o}_{600}$

$$(6.2)$$
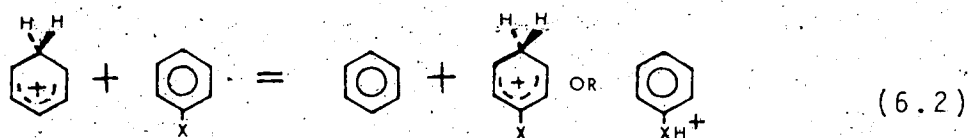
values are extracted from table 3.1. Results from NMR studies of benzenium ion and monoalkylbenzenium ions in superacid media (HF-SbF_5-SO_2ClF-SO_2F_2) by Olah and co-workers (128) indicated that the monoalkylbenzenes are protonated preferentially para to the substituent. Hehre and co-workers (75) also reported that the experimentally obtained proton affinity differences between various monoalkylbenzenes and methylbenzene are in good agreement with the results from the theoretical STO-3G calculations by assuming para-protonation in all monoalkylbenzenes. It is assumed that if a monosubstituted benzene is ring-protonated, para-protonation will result in the most stable ion. In order to compare the substituent effects on the intrinsic basicity of benzene, symmetry correc-tions have to be made on the equilibrium constants and the ΔG^{o} for reaction 6.2. The symmetry correction in

Table 6.1   Relative Basicities of Monosubstituted Benzenes

Compound (B)	$-\Delta G^o_{600}$ (kcal/mole)[a] Benzene to B	σ_B/σ_{BH^+} [b]	$-T\Delta S^o_{rot.s.}$ [c] (kcal/mole)	$-\Delta H^o$ (kcal/mole)[d] Benzene to B
C6H5–NH2	25.3	1	2.1	27.4
C6H5–COCH3	20.4	1	2.1	22.5
C6H5–OCH3	15.7	1	2.1	17.8
C6H5–CHO	15.4	1	2.1	17.5
C6H5–COOH	14.7	1	2.1	16.8
C6H5–CN	11.4	1	2.1	13.5
C6H5–OH	11.3	1	2.1	13.4
C6H5–NO2	8.9	1	2.1	11.0
C6H5–C2H5	7.3	1	2.1	9.4
C6H5–CH3	6.3	1	2.1	8.4
C6H6	0	6	0	0
C6H5–F	-0.8	1	2.1	1.3
C6H5–Cl	-1.0	1	2.1	1.1

Footnotes to Table 6.1

a. Free energy change at 600°K for the reaction:

H^+(benzene) + B = benzene + BH^+.

b. Ratio of rotational symmetry numbers of B to BH^+.

c. $\Delta S^o_{rot.s}$ represents entropy change due to changes of the rotational symmetry σ number. $\Delta S^o_{rot.s.}$ = $-R\ln(\sigma_B/\sigma_{BH^+})(1/6)$. This is believed to be the major contribution to the total entropy change of reaction.

d. $\Delta H^o = \Delta G^o + T\Delta S^o_{rot.s.}$

ΔG^O is a correction in the entropy change of reaction as discussed in section 6.2. Experimental results on proton transfer reaction 6.2 with F and Cl as the substituent gave ΔS^O of -3.5 ± 0.2 eu and -3.4 ± 0.2 eu respectively (see table 3.53). This is in good agreement with the calculated (rotational symmetry) entropy change assuming para-protonation in both reactions, $\Delta S^O_{rot.s.} = -3.56$ eu. The closeness of the experimental ΔS^O and $\Delta S^O_{rot.s.}$ values suggests that the assumption $\Delta S^O_{chem} \approx 0$ leading to $\Delta S^O \approx \Delta S^O_{rot.s.}$ is valid for these two and probably most other substituents. The ΔH^O for the proton transfer reactions shown in table 6.1 were obtained from the measured ΔG^O values and equation $\Delta G^O = \Delta H^O - T\Delta S^O$. It was assumed that the calculated ΔS^O due to rotational symmetry changes is equal to the total ΔS^O for the reaction. The results in table 6.1 show that the intrinsic basicity of benzene is enhanced to a greater or lesser extent by the introduction of any one of the substituents studied. It does not matter whether the substituent is electron-donating or electron-withdrawing. An electron-donating substituent may release electrons via its inductive effect or resonance to the benzene ring, thus stabilizing the resulting substituted benzenium ion relative to the unsubstituted benzenium ion. The effect is strongest if the proton attack is para to the substituent. Consequently, benzenes carrying electron donating substituents would be expected to have enhanced basicities

relative to that of benzene. The protonated toluene
(monomethylbenzenium ion) provides an illustration to
the stabilization of benzenium ion by inductive effect
of an electron-donating substituent. Para-protonation
of toluene results in an ion which is a hybrid of the
following structures:

$$I \qquad II \qquad III \qquad\qquad (6.20)$$
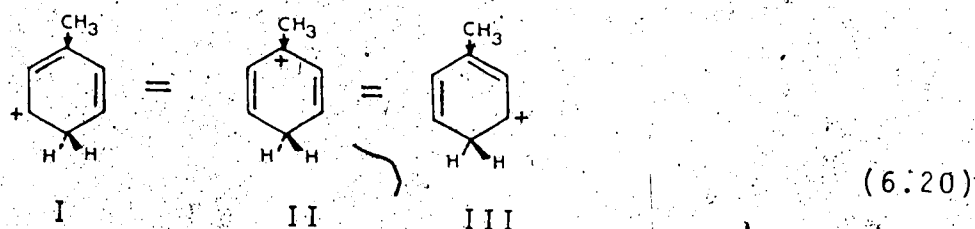
Although -CH_3 releases electrons to all positions in the
ring, it does so most strongly to the carbon nearest to
it. The most stable structure, II, is primarily respon-
sible for the increased stability of p-methylbenzenium
ion over the benzenium ion. The assumption that the
position para to the substituent is the preferred site
of protonation may be justified by examining the hybrid
structures of its meta- and ortho-isomers. Meta-pro-
tonation of toluene results in an ion which has hybrid
structures of:

$$I \qquad II \qquad III \qquad\qquad (6.21)$$
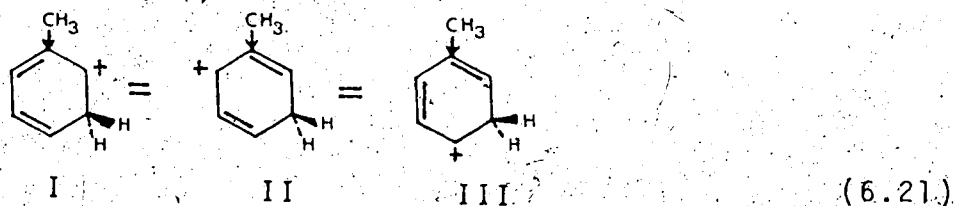
Since no hybrid structure with charge on the carbon
carrying the substituent exists, the stabilizing effect
by an electron donating group meta to the site of pro-
tonation is less than that of para-protonation. For

protonation at the ortho position of toluene, the follow-
ing hybrid structures are possible:

$$\text{I} \qquad \text{II} \qquad \text{III} \qquad\qquad (6.22)$$
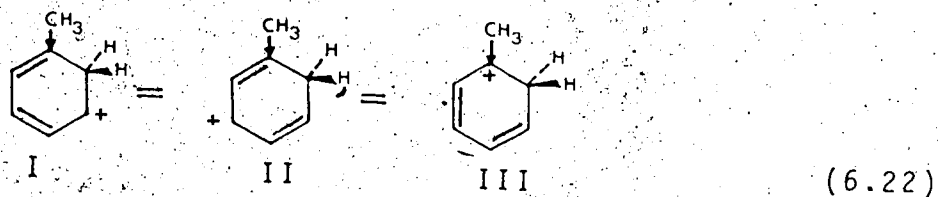
The presence of structure III indicates that o-methylben-
zenium ion would be more stable than its meta-isomer. If
everything being equal, the ortho- and para-isomers would
have the same stability. Because of the close vicinity
between the substituent and the ortho position, ortho-
protonated ions are very liable to steric hindrance. It
is therefore not surprising that results in the gas
phase (75) as well as in superacid solution (128) indi-
cate that toluene protonates preferentially para to the
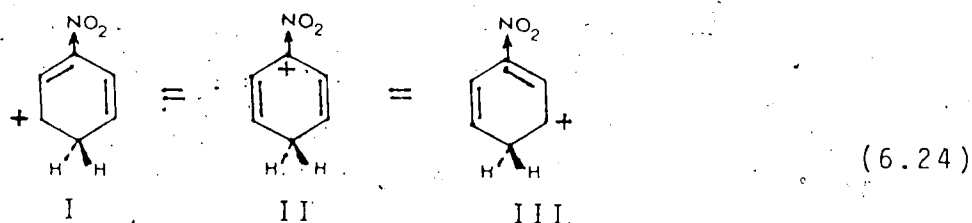substituent.

The stabilization of the benzenium ion by electron
release via resonance may be demonstrated by the addition
of a methoxy group in the benzenium ion. The p-methoxy-
benzenium ion is a hybrid of the following structures:

$$\text{I} \qquad \text{II} \qquad \text{III} \qquad \text{IV} \qquad (6.23)$$
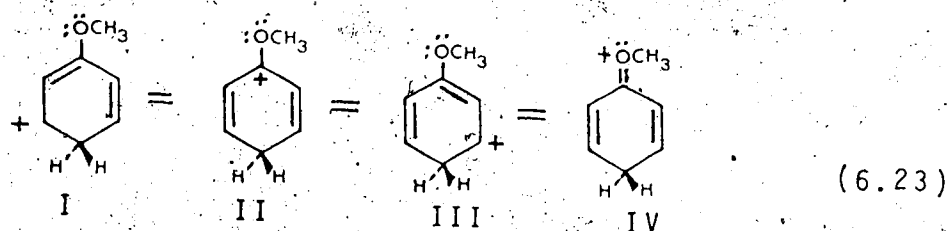
Because of the presence of lone pair electrons in oxygen,
the resulting ion is not just a hybrid of structures I-
III, but also structure IV in which the positive charge
is carried by oxygen. The structure IV is especially

stable since every carbon and oxygen atom has a complete octet of electrons and each hydrogen atom has a fully filled outer valent shell as well. The presence of structure IV enhances the stability of the benzenium ion to a great extent. Previous arguments that the meta- and probably also the ortho-isomers are not as stable as para-protonated isomer may be applied here.

The introduction of an electron — withdrawing group in benzene should lower the basicity of benzene for ring protonation. This is because the presence of the electron-withdrawing group always destabilizes the positive charge in the benzenium ion and the destabilizing effect is stronger when the protonation occurs para and ortho to the substituent. The addition of a nitro group in the benzenium ion is a good example:


$$(6.24)$$

Structure II is especially unstable because the electron-withdrawing substituent withdraws electrons most efficiently from the carbon atom nearest to it, thus making the carbon atom positive. Consequently, it has little tendency to accommodate the positive charge. The ortho isomer has a hybrid structure similar to structure II. Therefore, the destabilizing effect of the ortho nitro group is similar to that of the para isomers. Although the

presence of an electron-withdrawing group in the meta

position relative to the site of protonation would have

a less destabilizing effect than that in ortho or para

position, nevertheless, it would be expected that the

resulting substituted benzenium ion would be less stable.

than the unsubstituted benzenium ion. This is expected

because the electron-withdrawing group withdraws elect-

ron from all positions in the ring and thus destabilizes

the positive charge. The present experimental results

which show that strong electron-withdrawing substituents

(e.g. $-COCH_3$, $-CHO$, $-CO_2H$, $-CN$ and $-NO_2$) enhance the

basicity of benzene by 11-22.5 kcal/mole can be explained

if one assumes these substituents themselves have higher

basic sites than the carbons in the ring. Substituent-

protonation is therefore preferred for acetophenone,

benzaldehyde, benzoic acid, benzonitrile and nitroben-

zene.

6.4 The Preferred Site of Protonation for Monosubsti-

tuted Benzenes. Correlation of Their Intrinsic

Basicities with the STO-3G Calculated Results and

Aromatic Substituent Constants.

Hehre and co-workers (129) have calculated the

internal energy changes, ΔE, of the isodesmic proton

transfer reaction 6.8 for various substituents using the
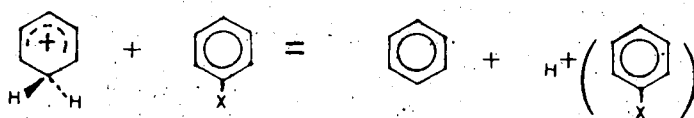

$$(6.8)$$
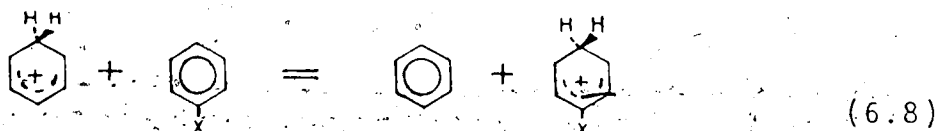
minimal basis set STO-3G method. Reaction 6.8 is called an isodesmic process because the number of a given type of bonds is preserved in the process and there is only a change in their relationship to one another (130). Their calculated ΔE values together with the present corresponding experimental enthalpy change, ΔH^O, (obtained by assuming $\Delta S^O \simeq \Delta S^O_{rot.s.}$) for reaction 6.8 are tabulated in table 6.2. Figure 6.1 gives a plot showing the correlation between ΔE and ΔH^O with the straight line corresponding to the perfect correlation. Strong electron-withdrawing substituents such as NO_2 and CN are not shown in the figure. Their correlations are way off indicating these substituted benzenes are not protonated at the ring. The good agreement between ΔH^O and ΔE value in figure 6.1 suggests that for benzene with the substituent NH_2, OCH_3, OH, C_2H_5, CH_3 or F, protonations do occur at the ring para to the substituent. It is not clear as to why deviations occur between ΔH^O and ΔE results for OH and OCH_3 substituents. No comparison could be made for Cl substituent as no corresponding ΔE value is available.

It was mentioned in section 6.2 that for the isodesmic proton transfer process 6.8, the effects of substituents are expected to follow the Hammett type linear free energy relationship 6.19, where ΔH^O is the

$$-\Delta H^O = (2.303RT\rho)\,\sigma_{p(x)} \qquad (6.19)$$

Table 6.2. <u>Experimental Enthalpy Changes and Calculated Energy Differences for the Reaction</u>

Substituent X(B= ◎-X)	$-\Delta H^0$ (kcal/mole)[a] Benzene to B	$-\Delta E$(kcal/mole)[b] Benzene to B	σ_p^+ [c]
$-NH_2$	27.4	27.2	-1.3[d]
$-COCH_3$	22.5		0.489
$-OCH_3$	17.8	15.7	-0.778
$-CHO$	17.5		0.44[e]
$-CO_2H$	16.8		0.421
$-CN$	13.5	-13.8	0.66
$-OH$	13.4	16.0	-0.91
$-NO_2$	11.0	-22.1	0.79
$-C_2H_5$	9.4	9.7	-0.295
$-CH_3$	8.4	8.5	-0.311
$-H$	0	0	0
$-F$	1.3	3.7	-0.073
$-Cl$	1.1		0.114

a. Experimental enthalpy change calculated from $\Delta H^0 = \Delta G^0 + T\Delta S^0_{rot.s.}$ for the reaction H^+(benzene) + B = benzene + HB^+.

b. Theoretical results LCAO-MO, STO-3G obtained by Hehre for same reactions as in (a) but assuming ring protonation para to the substituent. J. M. McKelvey, S. Alexandratos, A. Streitwieser, Jr., J.-L.M. Abboud and W. J. Hehre, J. Am. Chem. Soc. <u>98</u>, 244 (1976).

Footnotes to Table 6.2 continued

c. Unless otherwise stated, values are from H. C. Brown and Y.
Okamoto, J. Am. Chem. Soc., $\underline{80}$, 4979 (1958).

d. J. E. Leffler and E. Grunwald, "Rates and Equilibria in Organic
Chemistry", Wiley, New York, N.Y. 1963, p.204.

e. σ_p^- values from D. H. McDaniel and H. C. Brown, J. Org. Chem.,
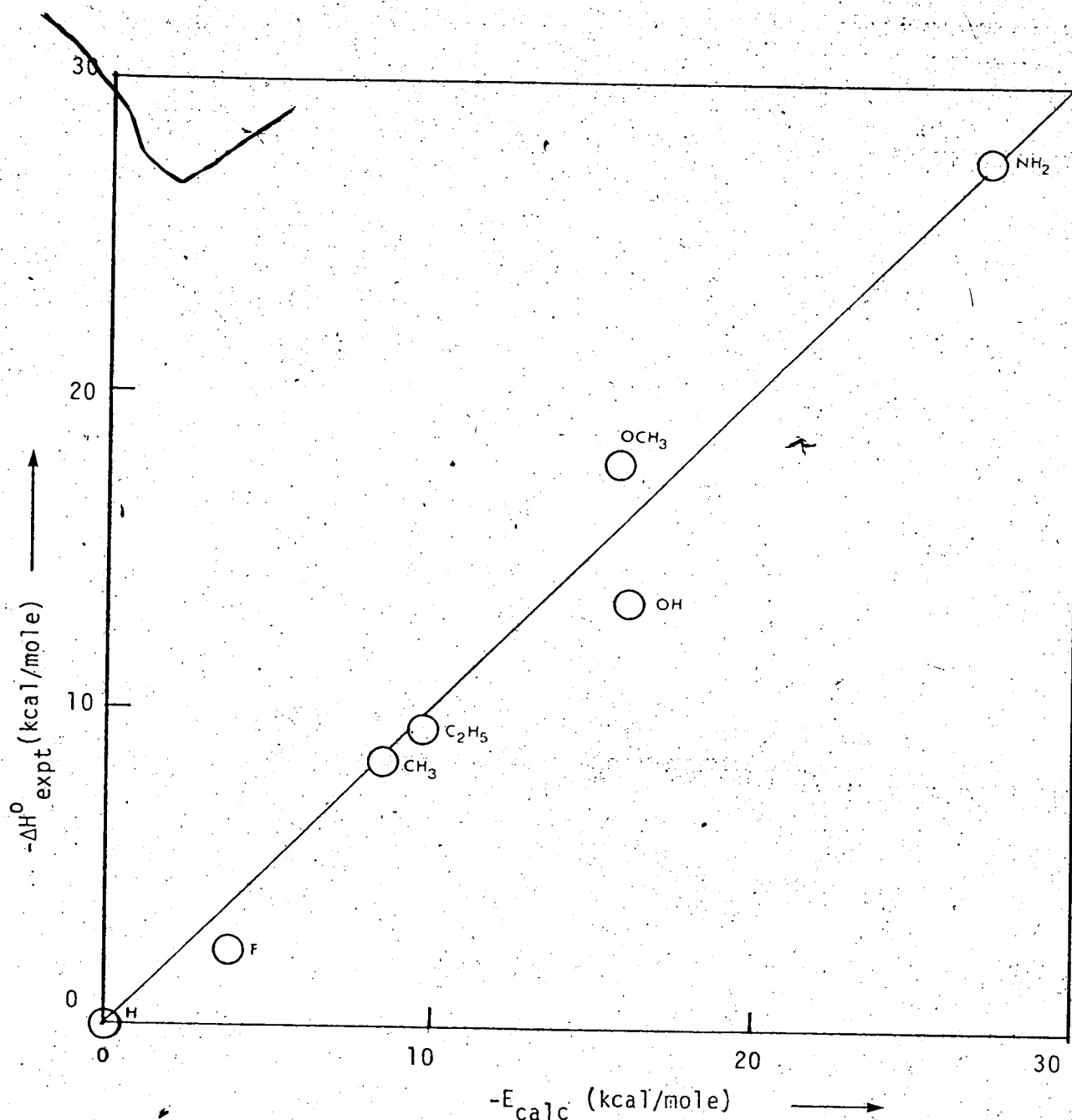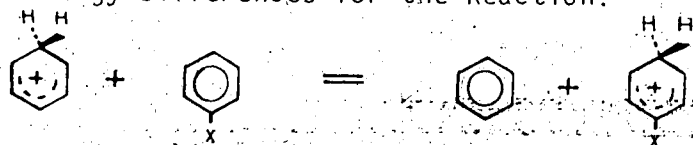$\underline{23}$, 420 (1958).

FIGURE 6.1   Correlation between Experimental Enthalpy Changes and Calculated Energy Differences for the Reaction:

(straight line corresponds to 1:1 or perfect correlation)

enthalpy change for reaction 6.8. $\sigma_{p(x)}$ is the Hammett's
para substituent constant for substituent x. ρ is the
reaction constant depending on the nature of the reaction
and the conditions under which it is studied. Although
the Hammett substituent constants have provided satis-
factory description of the substituent effects on a
variety of reactions involving benzene derivatives, it
was observed that in electrophilic reactions, when strong
resonance interactions occur between electron-supplying
substituents and the electron deficient centers of the
reacting system, the Hammett substituent constants, σ,
do not provide a satisfactory linear free energy rela-
tionship (131,132). This is the case for reactions in-
volving the formation of a fully or partially formed
carbonium ion when strongly electron-releasing sub-
stituents such as NH_2 and OCH_3 are in a position allow-
ing conjugation with the resulting carbonium ion. Because
of the above reason, another set of substituent constants,
σ^+, was derived by Brown and Okamoto (131,133) from the
study of solvolysis of substituted phenyldimethylcar-
binyl chloride (t-cumyl chloride), a reaction which pro-
ceeds by the formation of such an electron-deficient
center. The Brown σ^+ values are expected to provide
a more satisfactory description of the substituent
effects on the intrinsic basicity of benzene because
protonolysis reactions 6.6 and 6.7 are electrophilic

reactions involving the formation of carbonium ions.

The σ_p^+ values (p = para) for different substituents are tabulated in table 6.2. Although σ_m^+ values (m = meta) should properly be used for electron-withdrawers for ring protonation, their σ_p^+ values should have some validity. This is because the σ_m^+ value for an electron-withdrawer is in general only smaller than its σ_p^+ value by less than 0.2 unit. The correlation between ΔH^o and σ_p^+ is shown in figure 6.2. Also shown in figure 6.2 are the theoretical ΔE values. A good correlation is obtained between ΔH^o and the Brown para substituent constants, σ_p^+, except for acetophenone, benzaldehyde, benzoic acid, benzonitrile and nitrobenzene, which are way out. Evidently, protonation for these five compounds occurs not on the ring but on the substituent. All these strongly electron-withdrawing substiuents which destabilize the ring-protonated ion have lone pairs to accommodate the proton. Therefore, it is not surprising that substituent protonation is preferred. By comparing the experimental ΔH^o and calculated ΔE values, it may be estimated that for benzonitrile and nitrobenzene, substituent-protonation is energetically more favorable than ring-protonation by 27.3 and 33.1 kcal/mole respectively.

The good agreement of the results in figure 6.2 suggests that ring protonation para to the substituent can be occurring for chloro- and fluorobenzene, methyl- and ethylbenzene, phenol, anisole and aniline. Ring protonation for fluoro- and chlorobenzene is not
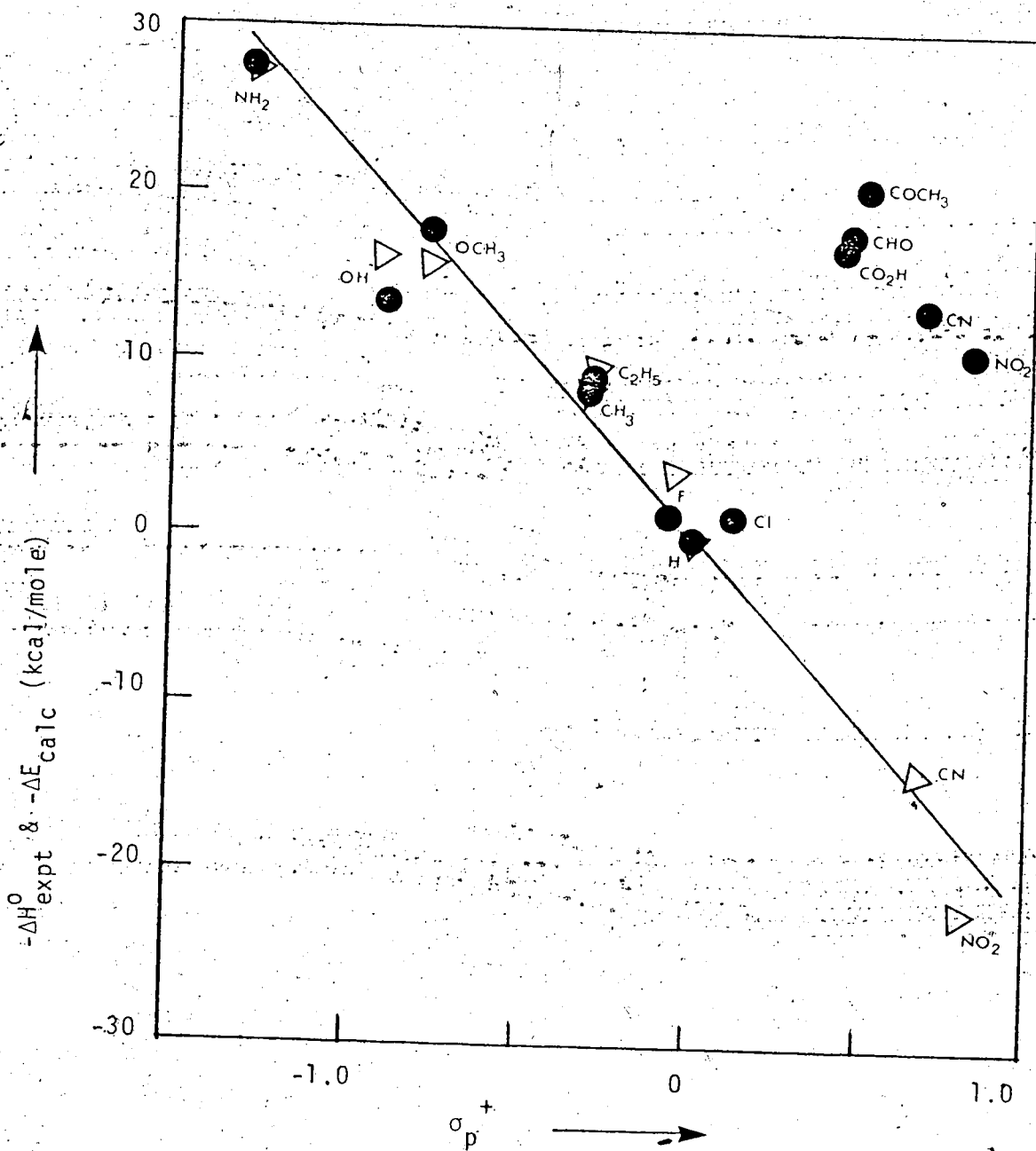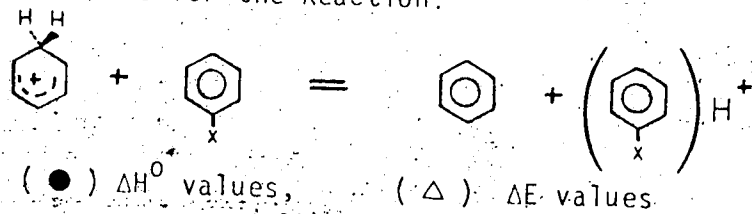
FIGURE 6.2 Correlations of ΔH^0 and ΔE with σ_p^+ Substituent Constants for the Reaction:

(●) ΔH^0 values,   (△) ΔE values

surprising. Although the halo-group destabilizes the protonated base by σ withdrawal (inductive effect), it also has an opposing tendency to stabilize the resulting benzenium ion by π donation (resonance effect) when it is para to the reaction center. The present experimental results show that the presence of a p-halo-group slightly enhances the basicity of benzene indicating the π donating effect is slightly greater than the σ withdrawal effect. Previous results (3) from our laboratory showed that the introduction of a second and the third fluorine to fluorobenzene lowers its basicity successively. Therefore, m-difluorobenzene and benzene have similar basicity and 1,3,5-trifluorobenzene is less basic than benzene. This is in agreement with the fact that the π donation effect attenuates faster than the σ withdrawal effect in multiple substitution.

Ring protonation in toluene and ethylbenzene is in agreement with the ICR results (75) and STO-3G calculations reported by Hehre et al. (129). The present result that ethylbenzene is more basic than toluene is consistent with their findings that the stabilizing effects of alkyl substituents increase in the order of Me < Et < i-Pr < t-Bu. By contrast, the reverse order (Baker-Nathan order: Me > Et, > i-Pr > t-Bu) is observed in solution. For example, the heat of protonation of toluene is 2.74 kcal/mole greater than that of ethyl-

benzene in superacid solution (134), but in the gas phase,
the ordering is reversed and the proton affinity of
ethylbenzene is higher than that of toluene by 1.2 kcal/
mole. The comparison is a manifestation that the Baker-
Nathan ordering of alkyl substituent effects in solution
is a result of differential solvation effects, with the
smaller ions having more exothermic solvation energies.
This seems to support the notion that steric effects
cause increased shielding to solvation for the bulky sub-
stituent and thus result in a reduction in solvation
energies (135). The sequence of intrinsic stabilization
of protonated benzene by para positioned alkyl group is
mainly due to the polarization effect, with the bulkier
group having a higher polarizability and thus can
accommodate a charge more comfortably. The energy of
interaction E, between a point charge, q, and a polar-
izable group separating at a distance, r, may be
expressed as in equation 6.25 (136), where α is the

$$E = -\frac{\alpha q^2}{2 \varepsilon r^4} \qquad (6.25)$$

polarizability of the group and ε is the effective di-
electric constant of the medium. It is evident from
equation 6.25 that the energy of interaction does not
depend on the sign of the charge. It is expected that
similar stabilization effects of alkyl groups would
operate on positive ions as well as on negative ions.

Thus both the intrinsic basicities and intrinsic acidities (137) of alcohols increase in the same order of H_2O < MeOH < EtOH, but it is not so in solution. The above reasoning also explains the observation that ethylbenzene is slightly deviated from the correlation between ΔH^o or ΔE with σ_p^+ in figure 6.2. It has been shown by Hehre et al. (129) that there is a progressive deviation of alkyl groups other than methyl in such a correlation, with the bulkier alkyl groups having larger deviations. These observations indicate that σ^+ values do not give a complete description of the substituent effects for isolated molecules, and care must be exercised in comparing solution data with dilute gas phase data.

Ring protonation for hydroxy and methoxy groups may be explained by the strong resonance interactions between the electron lone pairs on oxygen and the benzenium ion. The electron-releasing effects by resonance strongly stabilize the benzenium ion. On the other hand, the inductive electron-withdrawing effects of the phenyl group destabilize substituent protonation. Thus, the protonation occurs at the ring to take advantage of the stabilizing effect of the substituent. Figure 6.2 shows considerable deviation for hydroxy group in the σ^+ correlation, suggesting that hydroxy group is not as effective in stabilizing a positively charged center as indicated by its σ^+ value. It has been pointed out that

the "apparent" higher stabilizing effect in solution is due to the hydrogen bonding of the hydroxy substituent to the solvent s as in structure I (138,175). In the
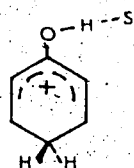

(I)

absence of a solvent as in the dilute gas phase, the stabilizing power of the hydroxy group is smaller. No such hydrogen bonding is possible for the methoxy group. Consequently, its effect on the intrinsic basicity of benzene follows the σ^+ correlation.

The correlation which indicates that aniline is also ring protonated is rather unexpected. Amines and aniline are well-known nitrogen bases in solutions because of the strongly basic lone pair in nitrogen which can readily accommodate the proton (139). The present results show that the presence of an amino group in the benzene ring stabilizes the benzenium ion through resonance to such a great extent that the intrinsic basicity of the ring is comparable with that of the amino group. In solutions, the protonation of the amino group in aniline is preferred exclusively because the localized positive charge on the hydrogens in the $-NH_3^+$ group favors hydrogen bonding formation with solvent molecules and thus further stabilizes the resulting anilinium ion. Ring protonation of aniline results in

an ion with the positive charge delocalized in the ring, a condition that is not favorable for hydrogen bonding with solvent molecules. In the absence of solvation effects, it is shown that ring protonation of aniline is as compatible as substituent protonation, if it is not energetically more favorable, since its gas phase basicity follows the σ^+ correlation.

Recent theoretical STO-3G calculations on the two isodesmic processes 6.26 and 6.27 by Hehre et al. (140) show that nitrogen protonation is energetically more

$$\Delta E = -2.5 \text{ kcal/mole} \quad (6.26)$$

$$\Delta E = 19.9 \text{ kcal/mole} \quad (6.27)$$
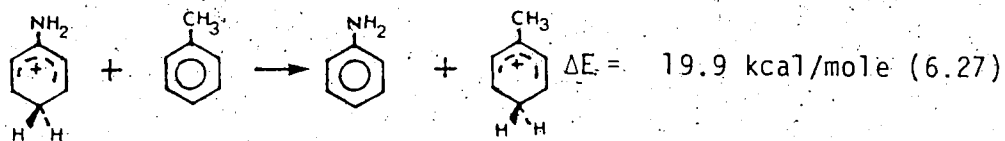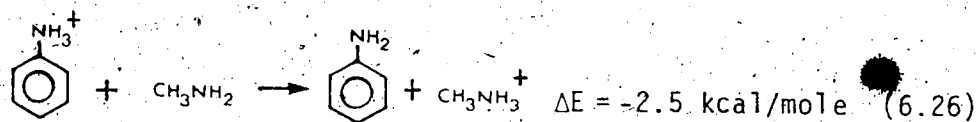
favorable than ring protonation in aniline. They concluded that protonation on the aromatic ring is some 1-3 kcal/mole less favorable than on the N substituent. The fact that the two isomers are so close in basicities is in agreement with our observations and the observed protonated aniline ion probably consists of an equilibrium distribution of the two isomers according to their energy difference. The energy difference is too small to show up in the σ^+ correlation. It should also be noted that the possibility of hydrogen bonding of the

amino group to the solvent may have influenced its
empirical solution σ^+ value.

From the least square analysis of the correlation
in figure 6.2, the relationship: $-\Delta H^O = (-20.21 \pm$
$1.26)\sigma_p^+ + (1.43 \pm 0.80)$, is obtained. The analysis
does not include the OH and C_2H_5 groups whose σ_p^+ values
are probably influenced by hydrogen bonding and steric
shielding of ion solvation, respectively. Since the
slope of the correlation is equal to $(2.303RT\rho)$ from
equation 6.19, it corresponds to a value of the reaction
constant, ρ, of -15 at 25°C for the ring-protonation of
benzene, reaction 6.6. Comparing with the ρ values for
normal electrophilic aromatic substitutions in solution
which range from -6 to -12 (131), the present ρ value
is slightly higher. The difference may be partly due to
solvation effects and partly due to the fact that in
protonation reactions, the positively charged species are
the final products whereas in electrophilic substitution
reactions, the positively charged species only occur in
the transition state, and the substituent effects on the
transient ions may not be fully developed.

In summary, it is noted that direct comparison
between σ_p^+ values and gas phase data should only be
made if the solvation effects for different species in-
volved are similar. This is because the σ_p^+ values are
for solution, and they do not separate the solvation

effects from the electronic effects of the substituents.

6.5   The Confirmation of Protonation Site from Correlation
       of Proton Affinities with Core Electron Binding
   Energies.

A linear correlation (equation 6.28) between proton
affinities, PA, and core electron binding energies, $E_B(X_{1s})$,
was proposed by Martin and Shirley (141) for alcohol (X =
O) and amines (X = N):

$$PA = -E_B(X_{1s}) + constant \qquad (6.28)$$

The correlation is based on the fact that both the protona-
tion reaction 6.29:

$$A + H^+ = AH^+ \qquad \Delta H° = -PA(A) \quad (6.29)$$

and the core-level ionization process 6.30:

$$A \longrightarrow A^+(core\text{-}level\ hole) + e^- \quad \Delta H° = B_E(X_{1s})$$

$$(6.30)$$
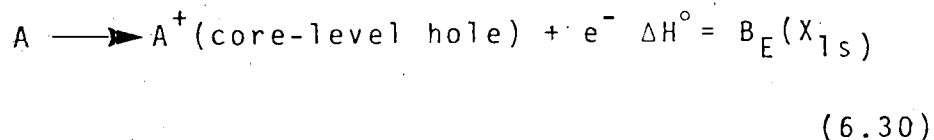
result in the formation of a positive ion, and the energy
involved in both processes is composed of two terms: one
related to the electron density in the orbital where ion-
ization occurs (inductive effects in the initial state);
and the other related to the stabilization of the charge
following ionization (polarization effects in the final
state). The change of substituents in a given class
of compounds may alter the energy involved in both

processes by affecting the first term (inductive effect) and/or the second term (polarization effect). Since the overall polarization effect, namely, the relaxation of electronic charge to shield the excessive positive charge on or near the site of ionization is similar in the two modes of ionization, a linear relationship between PA and $-E_B(X_{1s})$ within a given class of compounds implies that the polarization effects dominate the energy change due to variations of substituents in both modes of ionization. Under such conditions, it may be expected that the relationship $\Delta PA \cong -\Delta E_B(X_{1s})$ would hold for a given class of compounds with the protonation occurs at the atom X.

The above correlation is very useful in predicting values of proton affinity as well as confirming sites of protonation. Benoit and Harrison (142) recently studied the correlation of oxygen 1s core electron energies with proton affinities of oxygenated molecules. From their correlations involving various alcohols, esters, acids, ketones and aldehydes, they reported predicted values of PA(benzaldehyde) = 205.6 kcal/mole and PA(anisole) = 189.5 kcal/mole (based on present PA(NH_3) = 207.6 kcal/mole) assuming both are protonated at the oxygen. The present experimental results of PA(benzaldehyde) = 202.9 kcal/mole is in agreement with the predicted value indicating benzaldehyde is indeed oxygen protonated. The measured PA(anisole) = 203.2 kcal/mole is about 14 kcal/mole higher than the predicted value, indicating that the

ring protonated form is more stable for anisole, in agreement with our previous conclusion. Similar correlation with nitrogen 1s core electron energies involving amines and amides was reported by Cavell and Allison (123). Their correlation suggested that aniline is nitrogen-protonated. This is not in direct conflict with our conclusion that ring protonation occurs in aniline as the calculated proton affinities for ring and nitrogen sites are within 1-3 kcal/mole (140), therefore aniline may offer two equally probable protonation sites.

6.6   Chemical Ionization Mass Spectrometric Studies for
   Predicting Protonation Site in Substituted Benzenes

Two types of reactions which occur under chemical ionization conditions have been utilized in determining the site of protonation in substituted benzenes.

A.   Deuterium Exchange Reactions

Deuterium exchange has been used in mass spectrometric studies to determine the number of acidic hydrogens (e.g. O-H, N-H, S-H and COO-H) present in the molecule. Hunt and co-workers (143) have developed a procedure utilizing chemical ionization mass spectrometry with D_2O as reactant gas for the particular analysis. It was observed that hydrogen bonded to heteroatoms in alcohols, phenols, carboxylic acids, amines, amides and mercaptans undergo essentially complete deuterium exchange prior to

the protonation by the reactant ion, D_3O^+. In addition, they reported that the extent of exchange is relatively small (<15%) in ketones, aldehydes and esters. No deuterium exchange was observed between D_2O and unsaturated compounds such as benzene, stilbene and 3,3-dimethyl-1-butene.

A recent ion cyclotron resonance spectroscopic study of reactions of protonated benzenes with D_2O by Beauchamp et al. (121) showed that a number of protonated aromatic compounds formed by chemical ionization using D_2O as the reactant gas do undergo sequential deuterium exchange with D_2O, leading to various degrees of ring deuteration. For example, with a mixture of benzene and D_2O, the formation of $C_6H_6D^+$ by the following reactions was observed:
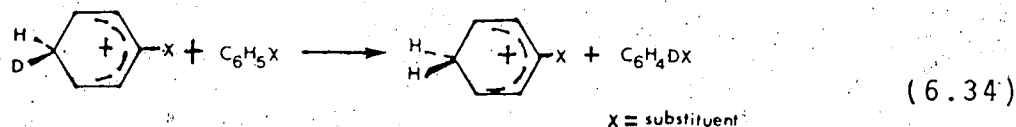
$$D_2O^+ + C_6H_6 \longrightarrow C_6H_6D^+ + OD \qquad (6.31)$$

$$D_3O^+ + C_6H_6 \longrightarrow C_6H_6D^+ + D_2O \qquad (6.32)$$
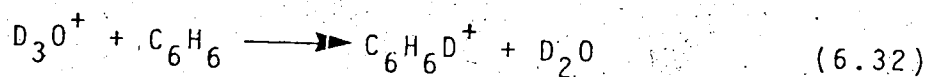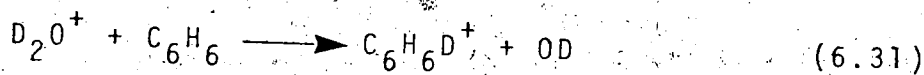
It was followed by stepwise exchange of H for D as in reaction 6.33. Reaction 6.33 is probably slightly endo-

$$C_6H_{7-n}D_n^+ + D_2O \longrightarrow C_6H_{6-n}D_{n+1}^+ + HDO \qquad (6.33)$$
$$(n = 1-6)$$
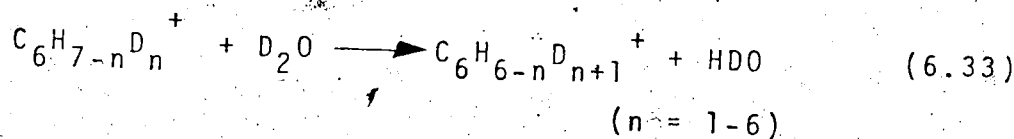
thermic as the heavy isotope in general would favor the stronger bond at equilibrium. In the presence of excess D_2O, reaction 6.33 is still possible even if it is slightly endothermic. Using the double resonance technique, it was observed that the product ion of reaction

6.33 disappeared totally upon ejection of the ion having one less mass unit (121). This showed that only one deuterium was exchanged per reaction. The mechanism of exchange reaction 6.33 probably involves the formation of an activated complex of the protonated benzene with D_2O, which dissociates to form the isotopically exchanged species. It is not very clear as to why the exchange reaction 6.33 was not observed under Hunt's chemical ionization conditions. It probably lies on the fact that reaction 6.33 is endothermic and therefore slow. If a strong ion repeller voltage is used in the ion source, the ion-residence time in the ion source will be short compared with the half-life of reaction 6.33. Under such conditions, the exchange reaction 6.33 will not be observed. From the results of Hunt and Beauchamp, it may be concluded that the benzene molecule will not undergo deuterium exchange with D_2O whereas the benzenium ion will.

It was shown by Beauchamp et al. (121) that all substituted benzenes which undergo various degree of deuterium exchange reaction 6.33 also undergo the symmetrical thermoneutral proton transfer reaction 6.34.

$$H \atop D \diagdown \bigcirc \!\!\!\!\! + \!\!\!\!\! - X + C_6H_5X \longrightarrow {H \atop H} \diagdown \bigcirc \!\!\!\!\! + \!\!\!\!\! - X + C_6H_4DX$$

X = substituent

(6.34)

The appearance of non-deuterated benzenium ion from the reaction can only be explained by ring-protonation of the substituted benzene. If substituent-protonation occurs,

products identical to reactants would result in the symmetrical proton transfer reaction 6.35. In the absence

$$\bigcirc\!\!\!\!\!\!\!-XD^+ + C_6H_5X \rightleftharpoons \bigcirc\!\!\!\!\!\!\!-XD^+ + C_6H_5X \qquad (6.35)$$

$$X \equiv substituent$$
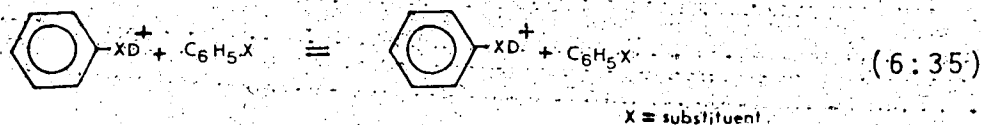
of deuterated substituted benzene molecule C_6H_4DX in the ion source, the occurrence of reaction 6.34 toward comple-tion indicates ring-protonation. Similar argument was also used in the observation of the proton transfer re-action 6.36 to a stronger base, B. The formation of BH^+

$$(C_6H_5X)D^+ + B \longrightarrow \begin{cases} BH^+ + C_6H_4DX \\ \\ BD^+ + C_6H_5X \end{cases} \qquad (6.36)$$
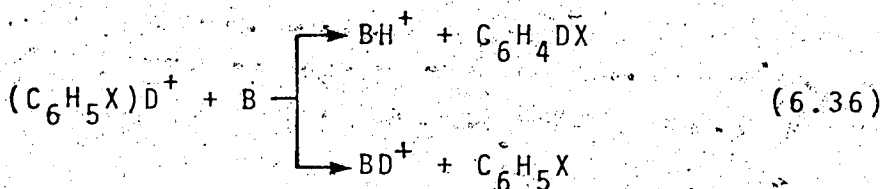
beside BD^+ ascertains ring-protonation of the substituted benzene. Based on these observations, Beauchamp and co-workers (121) concluded that ring protonation which re-sults in delocalization of the positive charge in the ring is a necessary condition for deuterium exchange to occur under chemical ionization conditions. These authors were quick to point out that it is not always a sufficient condition as the protonated anisole failed to undergo deuterium exchange but did undergo reaction 6.34 indicat-ing it is ring-protonated. Their findings that benzene, fluorobenzene, toluene and anisole are ring-protonated while benzonitrile, benzaldehyde and acetophenone are

substituent-protonated, are in agreement with the present results.

Similar observations on deuterium exchange of the protonated substituted benzenes under D_2O chemical ionization were reported by Martinson and Buttrill (122). They suggested oxygen-protonation for phenol and anisole based on the absence of deuterium exchange. This is in disagreement with our present results. Their conclusion is probably in error as it was pointed out by Beauchamp (121) that ring-protonation does not necessarily guarantee the occurrence of the deuterium exchange although ring-protonation is guaranteed if deuterium exchange is observed.

B. Formation of Water Clusters with Substituent-Protonated Benzenes

Under normal chemical ionization conditions where the ion source is at relatively high pressure (~0.1 to 0.4 torr) and at room temperature, clustering reactions between ions and neutrals are possible if strong hydrogen bonds can be formed between them. Using H_2O as the reactant gas and substituted benzenes as M, it may be expected that the protonated molecule, MH^+, formed by chemical ionization, will form hydrogen-bonded clusters with one or more water molecules if the proton in MH^+ resides on a heteroatom, like nitrogen or oxygen, of the substituent. The formation of these clusters will

$$MH^+ + H_2O = MH^+(H_2O) \tag{6.37}$$

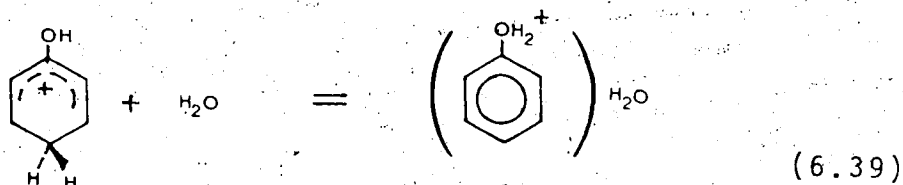$$MH^+(H_2O)_n + H_2O = MH^+(H_2O)_{n+1} \tag{6.38}$$
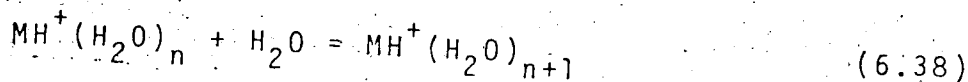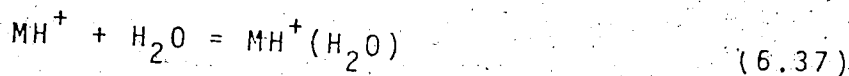
be unlikely if the benzene ring is protonated. The charge in the benzenium ion being strongly delocalized, no stable H-bonds with H_2O are to be expected. Buttrill and co-worker (122) studied the H_2O chemical ionization spectra of different substituted benzenes. They reported that for compounds which they found to undergo ring hydrogen-deuterium exchange (reaction 6.33), no water-clustered ion, $MH^+(H_2O)_n$, was observed, whereas aromatic compounds in which ring hydrogen-deuterium exchange was absent always formed water-clustered ions, $MH^+(H_2O)$, $MH^+(H_2O)_2$, etc. in "normal" amounts. The conclusion reached was, that the observation of the protonated molecular ion clustered with H_2O under H_2O chemical ionization conditions indicates that the proton is located on the substituent and not on the ring.
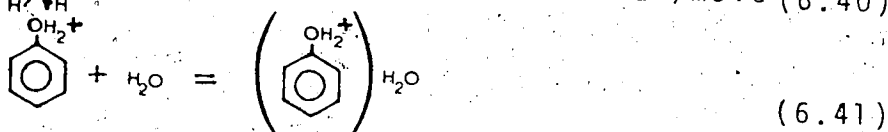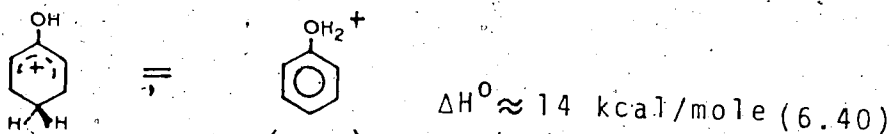
Based on the observation that hydrates were formed with protonated phenol, anisole, benzaldehyde, nitrobenzene and aniline while no hydrates were formed for protonated benzene and alkylbenzenes, Buttrill et al. (122) concluded that the first group is protonated on the substituent whereas the second group is ring-protonated. This is in agreement with our findings except for aniline, anisole and phenol. As it was discussed previously, the basicities of

ring carbon and nitrogen in aniline are similar, aniline is probably protonated both on the ring as well as on the substituent. However, our results together with results from the deuterium exchange study by Beauchamp (121) and the oxygen 1s core electron energy study by Harrison (142) all indicate that anisole and phenol are ring-protonated. Nevertheless, our conclusion does not necessarily invalidate Buttrill's observation that protonation occurred at the oxygen of phenol and anisole in his system. Our result indicated that ring-protonated anisole and phenol are energetically more stable than their corresponding substituent-protonated isomers. According to the correlation of core electron energies with proton affinities, the estimated proton affinity for oxygen protonation of anisole is about 14 kcal/mole lower than for ring protonation of anisole (142). But with sufficiently acidic donors such as H_3O^+ reacting with anisole, protonation will occur on both the ring and the oxygen of anisole. This is because the oxygen proton affinity of anisole (~189 kcal/mole) is also considerably higher than that of water, $PA(H_2O)$ = 171.7 kcal/mole (see table 3.57). Therefore, under the non-equilibrium chemical ionization conditions where the system is probably under kinetic control rather than thermodynamic control, it is not necessarily that the most stable ion prevails in the system. Consequently, protonation may well occur pre-

ferentially at any of the two possible sites. It is also
possible that the energy difference of ~14 kcal/mole bet-
ween the two protonated isomers may be offset by the exo-
thermicity of the clustering reactions resulting from the
formation of strong hydrogen bonds between oxygen-protonated
anisole and water molecules. But the following calculation
shows that there is not enough driving force for this to
occur under the normal chemical ionization conditions. The
reaction 6.39 which is of interest can be split into two

$$\text{(structure with OH, ring)} + H_2O = \left(\text{(structure with } OH_2^+\text{)}\right)H_2O \qquad (6.39)$$

reactions, reactions 6.40 and 6.41.

$$\text{(structure with OH)} \rightleftharpoons \text{(structure with } OH_2^+\text{)} \qquad \Delta H^o \approx 14 \text{ kcal/mole} \quad (6.40)$$

$$\text{(structure with } OH_2^+\text{)} + H_2O = \left(\text{(structure with } OH_2^+\text{)}\right)H_2O \qquad (6.41)$$

The ΔH^o of reaction 6.41 may be roughly estimated to be
-24 kcal/mole, similar to that of protonated ethanol-water
system as measured by Sensharma and Kebarle in this lab-
orabory (41). This leads to $\Delta H^o = -10$ kcal/mole for re-
action 6.39. The ΔS^o for reaction 6.39 may be taken to
be -25 eu, an average value for similar clustering reaction
(41). From the relationships, $\Delta G^o = \Delta H^o - T\Delta S^o = -RT\ln K$,
it may be estimated that reaction 6.39 has values of

ΔG^o_{298} = -2.6 kcal/mole and K = 0.1 torr^{-1} at 298°K. With a H_2O pressure of 0.5 torr in the ion source, the equilibrium ion ratio of $[H^+(phenol)(H_2O)]/[H^+(phenol)]$ is only of the order of 5 x 10^{-2}. Therefore, the shifting of the protonation site due to solvation effect is not very favorable with such a small water concentration. However, it would become more and more favorable as the water concentration increases. It may be expected that the above mentioned shifting of the protonation site would be completely favored in liquid water.

6.7   Comparison of Cationic Stability by Polarization

       Effect of Phenyl Group and Methyl Group

The gas-phase basicities of the substituent-protonated benzenes PhX, are found to be higher than those of the corresponding methyl compounds MeX. This is illustrated by the negative ΔG^o values for the reaction 6.42, with
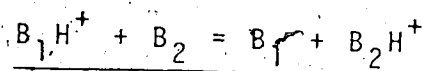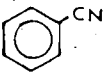
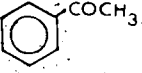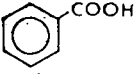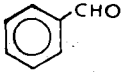$$MeXH^+ + PhX = MeX + PhXH^+ \qquad\qquad (6.42)$$
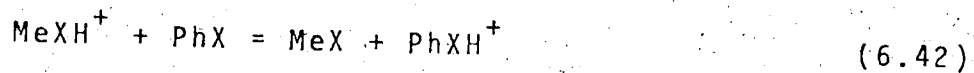
X = CN, COCH$_3$, CO$_2$H and CHO (see table 3.1). The observation may be explained by the fact that the phenyl group, being bulkier than the methyl group, has a higher polarizability and thus can disperse and stabilize the charge on PhXH$^+$ more efficiently than the methyl group can on MeXH$^+$. The polarization effect is larger than the opposing inductive and resonance effects by which the stabiliza-

ion of $MeXH^+$ and the free aromatic base PhX are favored, respectively. The overriding polarization effect results in higher gas-phase basicity for the phenyl substituted bases than their corresponding methyl substituted counterparts.

The relative gas-phase basicities and aqueous basicities of four pairs of compounds: benzonitrile and acetonitrile, acetophenone and acetone, benzoic acid and acetic acid, benzaldehyde and acetaldehyde are given in table 6.3. It is evident from the table that the aqueous basicity for a given pair changes little in replacing the methyl group by the phenyl group, whereas the gas-phase basicity increases by roughly 9 kcal/mole going from methyl to phenyl substitution. The difference is mainly due to the difference in hydration energies of the protonated cations $PhXH^+$ and $MeXH^+$, and it may be used to evaluate approximately the difference in polarization stabilizing effect between the phenyl group and the methyl group. As mentioned earlier, the relative gas-phase basicity between PhX and MeX given as $\Delta G^o(g)$ for reaction 6.42 depends on the sum of the contributions from the difference in stabilization by inductive effects, resonance effects and polarization effects. It may be expected that for oxygen and nitrogen bases, stabilization by polarization effects of the phenyl or methyl group on the protonated bases would not be important in

Table 6.3   <u>Relative Basicities in the Gas Phase and the</u>
<u>Aqueous Phase from the Reaction:</u>

$$B_1H^+ + B_2 = B_1 + B_2H^+$$

B_1	$pK_a{}^a$	B_2	$pK_a{}^a$	$\Delta G^o(aq)^b$ (kcal/mole)	$\Delta G^o(g)^b$ (kcal/mole)	$[\Delta G^o(g) - \Delta G^o(aq)]$ (kcal/mole)
⬡CN	-10.45	CH_3CN	-10.13	-0.4	7.5	7.9
⬡COCH₃	6.3	CH_3COCH_3	-7.2	1.2	8.5	7.3
⬡COOH	-7.2	CH_3COOH	-6.1	-1.5	9.0^c	10.5
⬡CHO	7.1	CH_3CHO	~-8	~1	11.5	~10.5

a. pK_a values for the conjugated acids, BH^+ of bases, B;

   pK_a values from E. M. Arnett in "Progress in Physical Organic

   Chemistry," S. G. Cohen <u>et al.</u> ed., vol. 1. Interscience Publisher,

   1963.

b. $\Delta G^o(aq) = -2.303(R)(298)[pK_a(B_2H^+) - pK_a(B_1H^+)]$ for the reaction at

   298°K, $\Delta G^o(g)$ at 600°K.

c.   Acetic acid is 14.5 kcal/mole less basic than ammonium by ΔG^o_{600}

   measurements in this laboratory (combination of present results

   in table 3.1 and that in reference 3).

aqueous solution, because more efficient charge dispersal to bulk solvent results from the attachment of water molecules to the protonated bases by hydrogen bonding. The bulk solvent would therefore take over in large part the role played by the polarizable substituent in stabilizing the ion. Assuming similar external stabilization by bulk solvent for $PhXH^+$ and $MeXH^+$ (since both have the same number of possible H-bonding sites), the relative aqueous basicity between PhX and MeX given as $\Delta G^o(aq)$ for reaction 6.42 would only depend on the inductive effects and resonance effects. The difference of $[\Delta G^o(g) - \Delta G^o(aq)]$ is then an approximate, but quantitative measure of the difference in stabilization energy by polarization effect between a phenyl group and a methyl group.

As shown in table 6.3, the comparisons of basicities in the two phases for the four pairs of compounds place the cationic stability by polarization of the phenyl group as about 9 ± 2 kcal/mole greater than that of a methyl group. Similar examinations on amines by Taft (30) showed that the stabilizing effect by polarization of a phenyl group is greater than that of a methyl group by about 7 kcal/mole.

6.8   Summary

(a)   The intrinsic basicities of all monosubstituted benzenes are higher than that of benzene. Their proton

affinities decrease in the order of aniline > acetophenone > anisole > benzaldehyde > benzoic acid > benzonitrile > phenol > nitrobenzene > ethylbenzene > toluene > fluoro-benzene > chlorobenzene > benzene.

(b)   From the correlation of relative basicities with σ_p^+ substituent constants and STO-3G calculated results, it is suggested that ring-protonation occurs in aniline, anisole, phenol, ethylbenzene, toluene, fluorobenzene, chloroben-zene and benzene. Acetophenone, benzaldehyde, benzoic acid, benzonitrile, nitrobenzene are substituent-protonated.

(c)   The above conclusion agrees with the results from studies of 1s core electron binding energies and deuterium exchange with the exception of aniline. STO-3G calcula-tions indicates that nitrogen protonation is about 1-3 kcal/mole energetically more favorable than ring protona-tion in aniline. The small energy difference may result in two probable sites of protonation for aniline.

(d)   For the monosubstituted benzenes which protonate at the substituent, the replacement of the phenyl group by a methyl group reduces their intrinsic basicities by about 9 kcal/mole. By comparing the basicities of these com-pounds in the gas phase and in the aqueous phase, it is suggested that the cationic stabilizing effect by polariza-tion of a phenyl group is about 9 kcal/mole over that of a methyl group.

GAS-PHASE BASICITIES OF N-METHYL SUBSTITUTED 1,8-DIAMINO-NAPHTHALENES AND RELATED COMPOUNDS

CHAPTER VII

7.1 Introduction

The aqueous basicities of a series of N-methyl substituted 1,8-diaminonaphthalenes have been determined by Alder and co-workers (144). The remarkably high basicity of 1,8-bis(dimethylamino)naphthalene in aqueous solution reported was attributed to the steric strain present in the neutral molecule whose strain is effectively removed on protonation (141). Since steric effects are intrinsic molecular properties which should not be much affected by solvation, it may be expected that the tetramethyl compound should show a similarly high basicity in the gas phase. A comparison of the gas-phase and aqueous phase basicities enables one to test this expectation and to assess the effect of the solvent. It is also desired that these compounds be connected to the gas-phase basicity ladder established in the present work so that a continuous gas-phase basicity scale from water (lowest basicity) to 1,8-bis(dimethylamino)naphthalene (highest basicity) could be obtained.

The possible sites of protonation for the amino-substituted aromatic compounds in the gas phase are not a priori known. In aqueous solutions, N-protonation occurs exclusively since the resulting ammonium ions are

stabilized by strong hydrogen bonding to the solvent. In the gas phase, this stabilization does not exist and ring protonation sometimes can lead to more stable ions. In order to examine these possibilities, the basicities of naphthalene and 1-aminonaphthalene were also determined. It will be shown that by comparisons of the gas-phase basicities of different amino-substituted aromatic compounds, one can determine the site of protonation.

.7.2   Experimental

The measurements of the equilibrium constants for the proton transfer reactions were carried out in a manner similar to that described in chapter II. However, some changes in the sample preparation were necessary for the measurements involving the diaminonaphthalenes. The gaseous samples were generally prepared by injecting a solution of the two bases in $CHCl_3$ into the 5 liter sample bulb containing 120 torr of a major gas at 170°C. Only 120 torr instead of the usual 700 torr of the major gas was used in order to obtain larger relative concentrations of the bases as compared to the major gas, while still maintaining the pressure of the naphthalenes in the bulb below their saturation vapor pressures at 170°C. The diaminonaphthalenes are relatively nonvolatile and their vapor pressures are not known. Although the partial pressure of given bases in the bulb were always below 1

torr, tests were made to ascertain that the samples were completely evaporated. This was done by admitting samples of diaminonaphthalenes directly into the bulb through a solid inlet port and observing whether complete evaporation occurred at 170°C.

In previous measurements, methane was used as a major gas. The final ions obtained on electron bombardment of pure methane are CH_5^+ and $C_2H_5^+$ in a ratio of 6:5. Both CH_5^+ and $C_2H_5^+$ are stronger acids than the conjugate acids of the bases investigated and can protonate most bases B. However, for the diaminonaphthalenes, methane proved to be unsuitable as the major gas since with methane, in addition to BH^+, the production of the parent ion B^+, was also observed. The intensity of B^+ was somewhat smaller but nearly equal to that of BH^+. This suggested that $C_2H_5^+$, instead of engaging in the protonation reaction 7.1 was

$$C_2H_5^+ + B = C_2H_4 + BH^+ \tag{7.1}$$
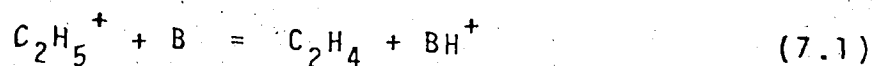
involved mostly in the charge transfer reaction 7.2.

$$C_2H_5^+ + B = C_2H_5 + B^+ \tag{7.2}$$
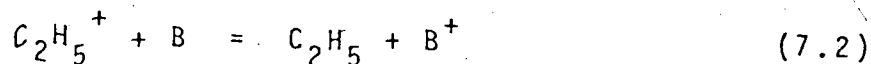
The ionization potential of the ethyl radical is 8.38 eV (81). The ionization potentials of the diaminonaphthalenes are not known. However, IP(aniline) = 7.69 eV (145). The aminonaphthalenes are expected to have even lower ionization potentials because of their extended aromatic structures. Therefore, the charge transfer reaction 7.2 is

strongly exothermic and its occurrence is very probable. Since both BH^+ and B^+ are of high mass (~ 200), where the resolution of our quadrupole mass spectrometer was not quite sufficient to separate the two adjacent ions completely, the presence of B^+ was undesirable. The BH^+ could be produced cleanly by using $t-C_4H_9^+$ as the reactant ion. The ionization potential of tert-butyl radical is 6.7 eV (82). This is probably lower than IP(B) so that charge transfer is endothermic and therefore slow. The tert-butyl cation is essentially the only final ion in electron irradiated isobutane (146). It was shown by Field et al. (147) that the $t-C_4H_9^+$ ion is formed by hydride-transfer (reaction 7.3) from isobutane to the $C_3H_7^+$ ion which is the major primary ion from isobutane on electron

$$C_3H_7^+ + i-C_4H_{10} = t-C_4H_9^+ + C_3H_8 \qquad (7.3)$$
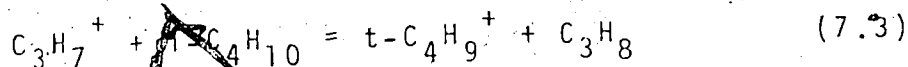
impact. We have found that isobutene also produces $t-C_4H_9^+$ as the major ion, the only other ion being $C_4H_9 \cdot C_4H_8^+$. Equilibrium measurements with isobutane or isobutene as the major gas were performed and the results were identical. Therefore, either isobutane or isobutene was used as a major gas in the measurements. Although $t-C_4H_9^+$ is a weaker acid than CH_5^+ or $C_2H_5^+$, it is still much stronger than the conjugate acids of the diaminonaphthalenes and therefore can protonate the diaminonaphthalenes, B, by the reaction 7.4. With $t-C_4H_9^+$ as the reactant ion,
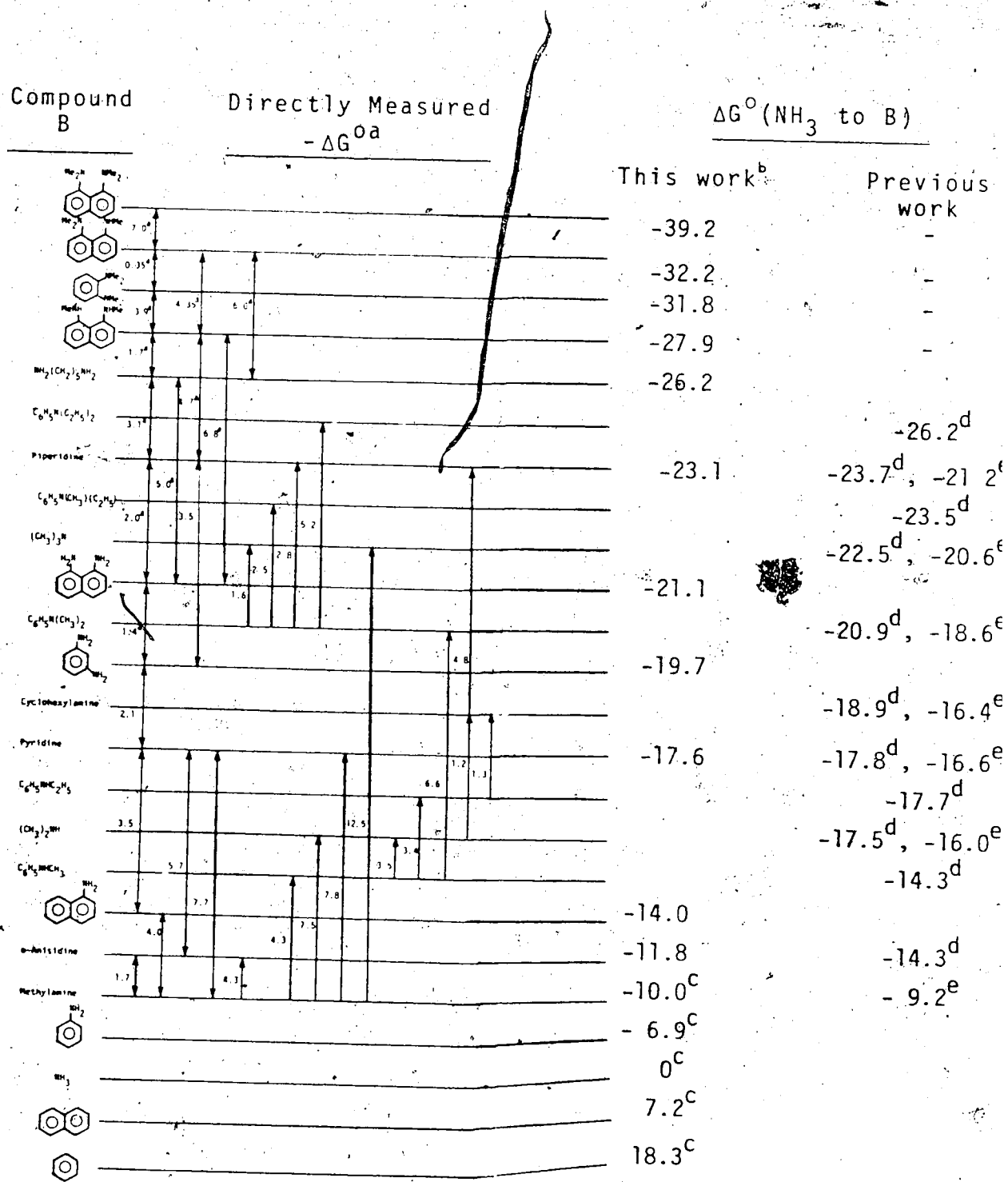
$$t-C_4H_9^+ + B = i-C_4H_8 + BH^+ \tag{7.4}$$
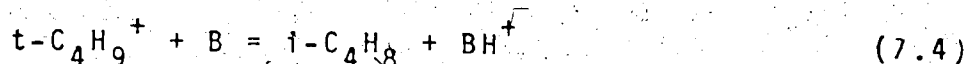
only the formation of BH^+ was observed in most cases. The parent ion, B^+, if present, was formed only in a very insignificant amounts.

Some problems were encountered in obtaining a good total ion intensity when the diaminonaphthalenes were used at 600°K. It was found that by lowering the ion source temperature, a large improvement in total ion intensity was obtained. The problem at higher temperatures may be caused by the deposit of some pyrolysed product in the ion source. This deposit could be generating a non-uniform electric field in the ion source. Tests showed that this difficulty disappeared at the lower temperatures. Consequently, measurements with diaminonaphthalenes were carried out at 460°K.

7.3 Basicity Scale from Methylamine to 1,8-Bis(dimethyl-amino)naphthalene.

Since the diaminonaphthalenes have very high basicities, several bases of gradually diminishing basicities had to be used in order to connect the diaminonaphthalenes to methylamine which has the highest basicity so far determined in the present work. The results are shown in table 7.1 which is extracted from the complete ladder shown in table 3.1. The relative basicities of different bases B with respect to ammonia are given in table 7.1 as the $\Delta G^o(NH_3$ to B) values, corresponding to the ΔG^o of reaction 3.1.

Table 7.1   Free Energy Changes of Proton Transfer Reactions

Compound B	Directly Measured $-\Delta G^{oa}$	$\Delta G^{O}(NH_3$ to B)	
		This work[b]	Previous work
		-39.2	-
		-32.2	-
		-31.8	-
		-27.9	-
$NH_2(CH_2)_5NH_2$		-26.2	
$C_6H_5N(C_2H_5)_2$			-26.2[d]
Piperidine		-23.1	-23.7[d], -21.2[e]
$C_6H_5N(CH_3)(C_2H_5)$			-23.5[d]
$(CH_3)_3N$			-22.5[d], -20.6[e]
		-21.1	
$C_6H_5N(CH_3)_2$			-20.9[d], -18.6[e]
		-19.7	
Cyclohexylamine			-18.9[d], -16.4[e]
Pyridine		-17.6	-17.8[d], -16.6[e]
$C_6H_5NC_2H_5$			-17.7[d]
$(CH_3)_2NH$			-17.5[d], -16.0[e]
$C_6H_5NCH_3$			-14.3[d]
		-14.0	
o-Anisidine		-11.8	-14.3[d]
Methylamine		-10.0[c]	- 9.2[e]
		- 6.9[c]	
NH_3		0[c]	
		7.2[c]	
		18.3[c]	

(a) All values in kcal/mole. Values with superscript (a) were done
     at 460°K, the rest at 500°K. $-\Delta G^{O}$ values refer to the reaction:
 $B_1H^+ + B_2 = B_1 + B_2H^+$ where B_1 is less basic (lower in the

column) than B_2. Double arrows correspond to present measurements , single arrows on the right side correspond to previous results from this laboratory.[d]

(b) For reaction: $NH_4^+ + B = NH_3 + BH^+$. Assume $\Delta G_{460}^o = \Delta G_{600}^o$ for above measurements.

(c) See table 3.1.

(d) R. Yamdagni and P. Kebarle, J. Am. Chem. Soc. 95, 3504 (1973). Based on present value for methylamine.

(e) Values at 300°K. Taft, R. W., "Proton Transfer Reactions" E. F. Caldin and V. Gold Ed., Chapaman and Hall, London, 1975.

$$NH_4^+ + B = NH_3 + BH^+ \qquad (3.1)$$
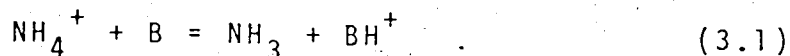
Previous results from this laboratory (1,2) on compounds having basicities higher than that of methylamines are also shown in table 7.1. They are all based on the present value of ΔG^O(NH$_3$ to CH$_3$NH$_2$) = -10.0 kcal/mole (600°K) since the earlier result (1) of ΔG^O(NH$_3$ to CH$_3$NH$_2$) = -10.8 kcal/mole (600°K) is considered to be less accurate (see section 4.1). The basicities of piperidine and pyridine were determined in both investigations. The agreement with the present results is within 0.6 kcal/mole for piperidine and 0.2 kcal/mole for pyridine. Included in table 7.1 are the determinations from Beauchamp's and Taft's (30) laboratories whenever available. On the whole, their ΔG^O(NH$_3$ to B) values are about 2 kcal/mole lower than the values from this laboratory. Part of the difference must be due to the different temperatures used. Taft's determinations are at 300°K while results from this laboratory are for 460°K and more often for 600°K. More appropriate comparison can be made after the entropy corrections. For example, by only considering the changes in rotational symmetry numbers σ, the entropy change for reaction 3.1 can be written as $\Delta S^O = R\ln(\sigma_{NH_4^+}\sigma_B/\sigma_{NH_3}\sigma_{BH^+}) = R\ln(4 \times \sigma_B/\sigma_{BH^+})$. With pyridine as the base, $\sigma_B/\sigma_{BH^+} = 1$. This leads to a $\Delta S^O = 2.7$ cal/degmole. For a temperature difference of $\Delta T = 300°K$, a corresponding $\Delta\Delta G^O = -0.8$
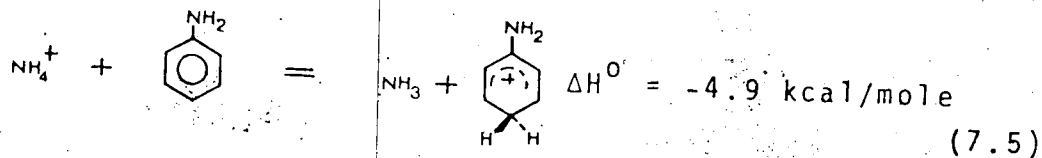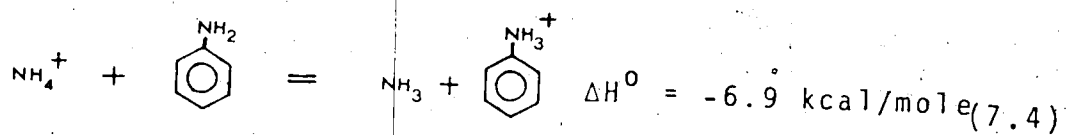
kcal/mole may be calculated. Thus the ΔG^O(NH$_3$ to pyridine) = -16.6 kcal/mole (300°K) observed by Taft when corrected to 600°K, becomes -17.4 kcal/mole, which is very close to the value of -17.5 kcal/mole obtained in the present work.

The enthalpy change for the proton transfer reaction 3.1 may be obtained after making the appropriate entropy corrections, $\Delta H^O = \Delta G^O + T\Delta S^O$. The proton affinities of compounds in table 7.1 may then be calculated by using the reference PA(NH$_3$) = 207.6 kcal/mole (section 3.2). Approximate proton affinities can be obtained by neglecting the $T\Delta S^O$ term, which is probably in the 1-2 kcal/mole range. For example, 1,8-bis(dimethylamino)naphthalene has a ΔG^O(NH$_3$ to B) value of -39.2 kcal/mole. Thus, PA(1,8-bis(dimethylamino)naphthalene) $\approx$ 207.6 + 39.2 = 246.8 kcal/mole. This is the highest proton affinity for a neutral organic base reported so far.

## 7.4 Sites of Protonation of Some Amino-Substituted Aromatic Compounds

The possible sites of protonation of the diaminonaphthalenes should be considered before discussing their relative gas-phase basicities. In the study of the substituent effects on the gas-phase basicity of benzene (chapter 6), the correlation between the relative proton affinity of para-substituted benzenes with the corresponding substituent constants, based on solution experiments, indicated that the proton affinity of aniline

for ring protonation para to NH$_2$ must be similar to that for protonation on the nitrogen. This suggests that amino-substituted aromatic compounds could be ring-protonated or nitrogen-protonated in the gas phase. Taft, Hehre et al. (140) reported the STO-3G calculation of ΔE, the energy change in isodesmic proton transfer reactions involving aniline. They showed that the proton affinities for nitrogen and ring protonation were the same within the error of the estimate. Subsequent considerations on the relative gas-phase basicities involving a second substituent led these authors (140) to conclude that the proton affinity for nitrogen protonation is 1-3 kcal/mole higher than that for ring protonation. If one accepts that N-protonated aniline is 2 kcal/mole more stable than the ring-protonated aniline, one may obtain the energetics for the following reactions by assuming $\Delta G^O = \Delta H^O$ from table 3.1 (the assumption will be used throughout this section):

$$NH_4^+ + \bigcirc NH_2 = NH_3 + \bigcirc NH_3^+ \qquad \Delta H^O = -6.9 \text{ kcal/mole} \quad (7.4)$$

$$NH_4^+ + \bigcirc NH_2 = NH_3 + \bigcirc NH_2 \qquad \Delta H^O = -4.9 \text{ kcal/mole} \quad (7.5)$$

The possible sites of protonation for 1-aminonaphthalene can now be considered. The relative gas-phase basicities of naphthalene and 1-aminonaphthalene are shown in table 7.1. Reaction 7.4 shows that the substitution of a phenyl group for hydrogen increases the proton affinity by 6.9

kcal/mole. This is mostly due to charge stabilization of
the ion by the polarizability provided by the phenyl group.
It is expected that further expansion of the aromatic sys-
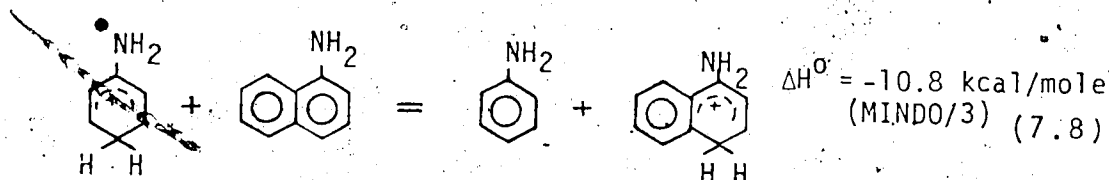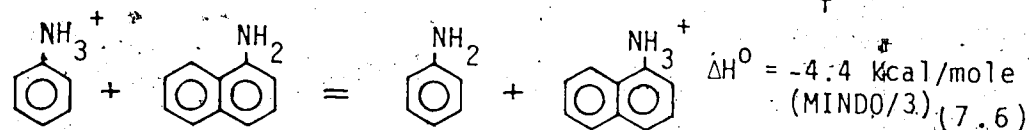tem as in the reaction 7.6 should have a smaller effect

$$(7.6)$$
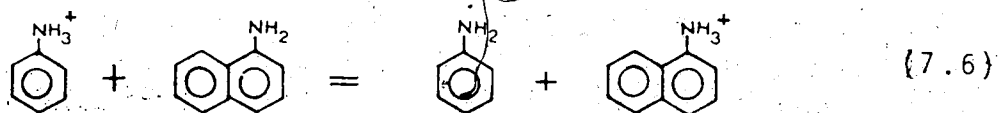
i.e. the exothermicity of reaction 7.6 should be considerably
smaller than that of reaction 7.4. An experimental value
of ΔH^o = 7.1 kcal/mole was obtained for the reaction 7.7


$$(7.7)$$
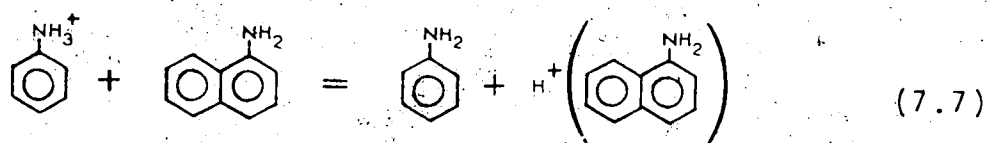
(see table 7.1), which is even more exothermic than reaction
7.4. This "discrepancy" indicates that N-protonation of
the naphthylamine is not the favored process and that in-
stead ring protonation occurs. Theoretical calculations
with the MINDO/3 methods were performed by Mesa-Höjer from
this laboratory (148) on the heats of formation of all
reactants entering reaction 7.7. The results on the
heats of formation obtained were: aniline 18.1 kcal/mole,
N-protonated aniline 165.7 kcal/mole, ring-protonated
aniline 162.0 kcal/mole, 1-aminonaphthalene 47.9 kcal/mole,
N-protonated 1-aminonaphthalene 191.1 kcal/mole, and
ring-protonated 1-aminonaphthalene 181.0 kcal/mole.
Evaluations of the ΔH^o values for the following isodesmic

reactions could be made from these calculated ΔH^o_f values:

$$\Delta H^o = -4.4 \text{ kcal/mole}$$
$$\text{(MINDO/3)} \quad (7.6)$$

$$\Delta H^o = -10.8 \text{ kcal/mole}$$
$$\text{(MINDO/3)} \quad (7.8)$$

The result that ΔH^o = -4.4 kcal/mole for reaction 7.6 is less exothermic than ΔH^o for reaction 7.4 (-6.9 kcal/mole) is in line with the expected stabilization effects by the further expansion of the aromatic ring. The ΔH^o for reaction 7.8 may be compared with that of the experimentally observed reaction 7.7.
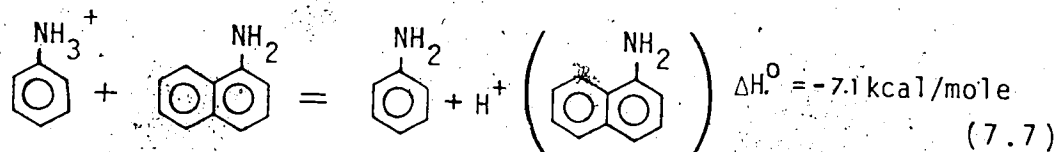

$$\Delta H^o = -7.1 \text{ kcal/mole}$$
$$(7.7)$$

By considering reaction 7.7 together with reaction 7.9 one

$$\Delta H^o = -2 \text{ kcal/mole}$$
$$\text{(estimated (140))}$$
$$(7.9)$$
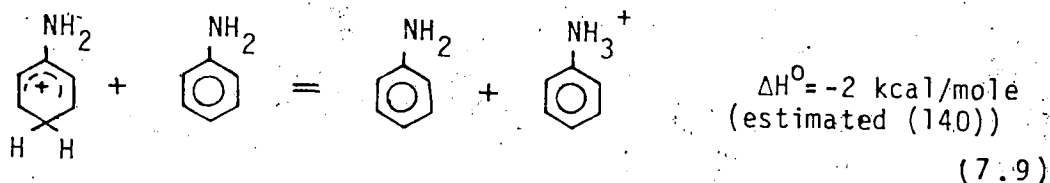
obtains a value of ΔH^o = -9.1 kcal/mole for reaction 7.8, in agreement with the MINDO/3 calculated ΔH^o = -10.8 kcal/mole. This supports the conclusion that the observed protonated 1-aminonaphthalene has indeed the ring-proton- ated structure. By comparing the energetics for the re- actions 7.6 and 7.7 one can estimate that the ring-

protonated 1-aminonaphthalene is about 3-4 kcal/mole more stable than its N-protonated ion. The MINDO/3 calculated heat of formation for the ring-protonated 1-aminonaphthalene is 10 kcal/mole lower than that of its nitrogen-protonated ion. It is believed that direct comparisons of the MINDO/3 calculated ΔH_f^O values are not as accurate as the ΔH^O value derived through isodesmic processes 7.6 and 7.7. This is because the uncertainties in goemetry optimizations for species in an isodesmic reaction tend to cancel each other, whereas in comparing species of different geometric structures, the uncertainties may be additive. The substituent effects of the amino group on ring-protonation in benzene and naphthalene can be determined from the following reactions (ΔH^O values from table 7.1):

$$\Delta H^O = -25.2 + 2 = -23.2 \text{ kcal/mole} \quad (7.10)$$


$$\Delta H^O = -21.2 \text{ kcal/mole} \quad (7.11)$$
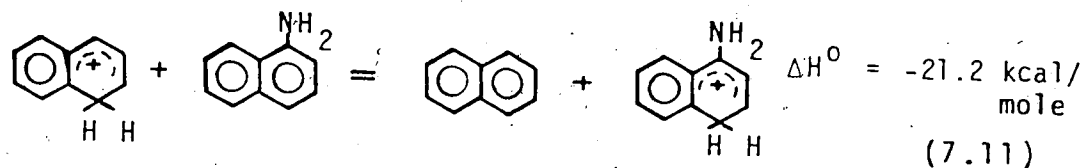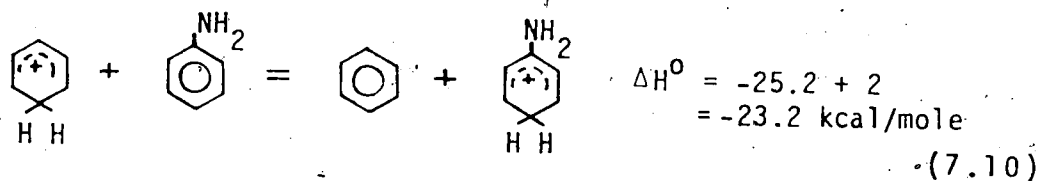
The exothermicity of reaction 7.11 is similar but slightly smaller than that of reaction 7.10. This is the expected result as the charge stabilization through resonance in protonated naphthalene is better than that in protonated benzene. Further addition of an amino group would have a

slightly less resonance stabilizing effect in protonated naphthalene than in protonated benzene. As the aromatic structure grows bigger, the amino group substituent effects for ring protonation would decrease.

The above conclusions that aniline is N-protonated and 1-aminonaphthalene is ring-protonated in the gas phase lead to the question as to whether 1,8-diaminonaphthalene is ring protonated or N-protonated. An experimental ΔG^o value of -7.1 kcal/mole was determined for the following proton transfer reaction (from table 7.1):


$$\Delta G^o = -7.1 \text{ kcal/mole}$$
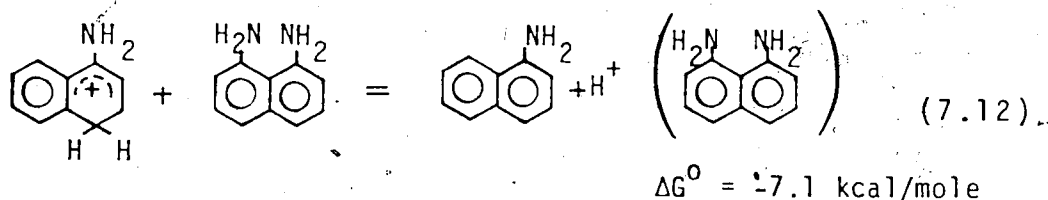
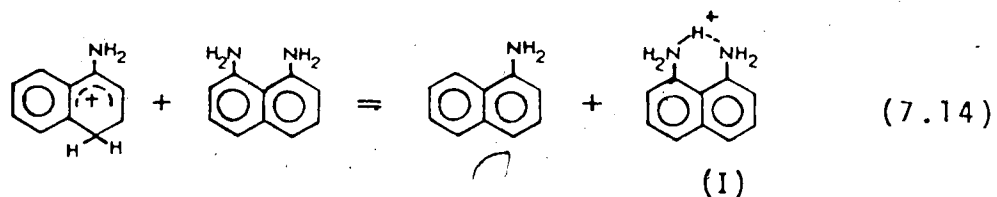If the 1,8-diaminonaphthalene is ring-protonated, reaction 7.12 could be written as:
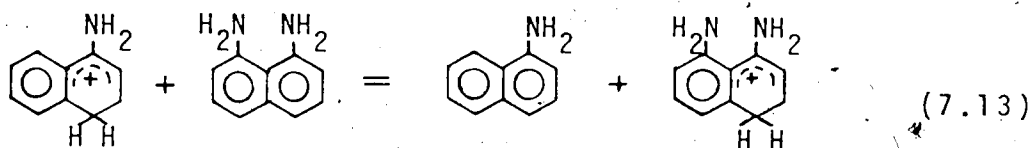
Reaction 7.13 is expected to be exothermic. The magnitude of its ΔG^o value would depend on the substitutent effects of the second amino group introduced in the 8-position of the naphthalene ring. The expected ΔG^o value for reaction 7.13 would be much less than that of reaction 7.11 (ΔG^o = -21.2 kcal/mole) in which the first amino group is introduced to

the 1-position in the naphthalene ring. This follows from the general observations of substituent effects in naphthalene. When a π interacting substituent goes on the ring not carrying the functional group, its effect is very small (149, p.1047). For example, with the ring-protonated 1,8-diaminonaphthalene, the following resonance structures are possible:
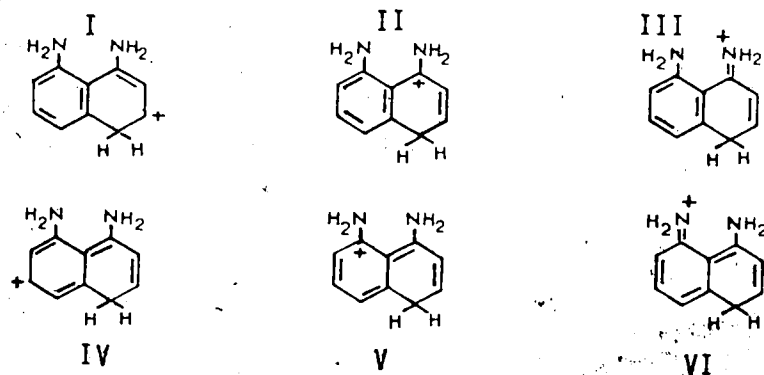
Protonation at the 4-position is preferred because it is much more stable than protonation at the 3-position which does not have the more stable resonance structure similar to III. It is also more stable than protonation at the 2-position because of less steric hindrance. The resonance structure III is the most stable one among all six possible structures. Structures I-III have one completely intact aromatic ring while structures IV-VI have both aromatic rings disturbed. Therefore, the contribution of the latter resonance structures are small compared with that of the former structures, I-III. Consequently, the substituent effects of the amino group on the ring not being attacked by the proton would be very small. Dewar and Grisdale (150),

in a study of the substituent effects on the ionization of 1-naphthoic acid determined the Hammett substituent constant values, $\sigma_4 = -0.72$ and $\sigma_5 = -0.13$, for the effect of an amino group in the 4 or 5 position. Although these values were obtained in aqueous solution, they should have some validity in the gas phase since linear relationship between gas-phase and aqueous properties in similar systems has been obtained for substituted benzene (section 6.4) and substituted aniline (151). Using the experimental value of $\Delta G^0 = -21.1$ kcal/mole for reaction 7.11, and assuming that the σ values are additive for double substitution, one obtains an estimate of ΔG^0 for reaction 7.13, $\Delta G^0 = -21.1 \times \sigma_5/\sigma_4 = -3.8$ kcal/mole. This value is much smaller than the value of -7.1 kcal/mole, which is the experimental proton affinity difference between 1-aminonaphthalene and 1,8-diaminonaphthalene. The result is that substituent protonation as in reaction 7.14 occurs.

$$(7.14)$$

$$(I)$$

The occurrence of this protonation is further supported by the following argument. The two amino groups in the 1,8-diaminonaphthalene are at a distance which is fairly suitable for N-H$^+$---N hydrogen bonding involving the proton and the two nitrogen lone pairs (see structure I in re-

action 7.14). Thus the distance between N-N centers in 1,8-diaminonaphthalene is about 2.5 Å as reported by Einspahr et al. (152) in their X-ray crystallographic study. This distance can be compared with 2.7 Å for the distance between the nitrogens in the N-H$^+$---N bond in $H_3NHNH_3^+$ obtained from SCF-MO calculations by Peyerimhoff et al. (153). The bond energy $D(NH_4^+ - NH_3) = 25$ kcal/mole was previously measured by Payzant et al. in this laboratory (46). The lone pairs on the amino groups in 1,8-diaminonaphthalene are not properly orientated in a straight line. Therefore, the N-H$^+$---H bond in the protonated diaminonaphthalene species cannot be linear and is expected to be weaker. Assuming that the strain reduces the bond energy to 50-70% of the energy of a linear bond and taking $D(NH_4^+-NH_3) =$ 25 kcal/mole as a representative for such linear bond, one obtains 10-15 kcal/mole as the stabilization energy due to the formation of H-bonding in structure I. In considering the standard free energy change in the proton transfer reaction 7.14, one must include not only the favorable stabilization energy, but also the energy required to move the proton from the ring to the N-protonated position and some adverse TΔS change due to the loss of restricted internal rotations of the amino groups on N-protonation. It was estimated earlier in this section that ring-protonation is more stable than N-protonation by 3-4 kcal/mole in 1-aminonaphthalene. This energy will be lost in moving the proton from the ring to the N-protonated posi-

tion. The $T\Delta S$ loss due to the freezing of the restricted internal rotation of the amino group may be expected to be a few kilocalories per mole. Therefore, the ΔG^O for reaction 7.14 should probably amount to less than -10 kcal/mole. The experimental value of $\Delta G^O = -7.1$ kcal/mole for reaction 7.14 is thus of the expected magnitude. It is concluded that 1,8-diaminonaphthalene is nitrogen protonated and its higher proton affinity is due to the hydrogen-bond bridged structure I. By comparing the experimental $\Delta G^O = -7.1$ kcal/mole for reaction 7.14 and the estimated $\Delta G^O = -3.8$ kcal/mole for reaction 7.13, one can estimate that N-protonated 1,8-diaminonaphthalene is more stable than its ring-protonated counterpart by 3.3 kcal/mole.

The conclusion that 1,8-diaminonaphthalene is nitrogen protonated implies that the other N-methylated diamino-naphthalenes are also nitrogen protonated, since the N-methyl substituents will have larger enhancing effect on the nitrogen basicity than on the aromatic ring basicity.

The basicity of o-phenylenediamine was considered of interest for the purpose of comparing it with the basicity of 1,8-diaminonaphthalene. Therefore, attempts were made to determine the gas-phase basicities of o-, m- and p-phenylenediamine. Unfortunately, the measurements of proton-transfer equilibria involving o- and p-phenylene-diamine were not successful. The protonated diamines

were found to rapidly decompose to an ion of molecular weight
two mass units less than that of the protonated ion. Con-
sequently, no equilibrium was reached. No decomposition
problem was encountered in the determinations involving m-
phenylenediamine. The results of the measurements are shown
in table 7.1. The basicity of m-phenylenediamine in itself
is interesting. In a study of possible sites of protonation
for substituted anilines by comparing the gas-phase and
aqueous basicities, Taft, Hehre et al. (151) concluded
that in the gas phase, ring protonation is favored over N-
protonation whenever an electron-donating group such as
CH_3, OCH_3 or NH_2 is introduced to the meta position of the
aniline although N-protonation is more favorable for aniline.
As pointed out by these authors (151), the difference in
stabilities between the ring-protonated and N-protonated
ions would be very large in m-phenylendiamine. Their
attempts to determine the proton affinity of m-phenylene-
diamine by ICR measured proton transfer equilibria had
been unsuccessful, but they had estimated from the results
of the theoretical STO-3G calculations that carbon proton
affinity of m-phenylendiamine is some 17 kcal/mole higher
than that of nitrogen (151). Unfortunately, Taft and Hehre
(151) did not report the actual STO-3G deduced proton
affinity for ring and N-protonated m-phenylenediamine.
Therefore, no direct comparison with the present results
can be made. Indirect estimates on the nitrogen proton

affinity of m-phenylendiamine can be made by using the linear relationship established by Taft, Hehre et al (151) between aqueous basicities and gas-phase proton affinities of N-protonated substituted anilines. With the literature aqueous basicity values (154) for aniline (pK_a = 4.6) and m-phenylenediamine (pK_a = 4.9), one could predict a proton affinity for N-protonated m-phenylenediamine which is about 2.1 kcal/mole higher than that of aniline. The present experimental results show that the proton affinity of m-phenylenediamine is 12.8 kcal/mole higher than that of aniline (see table 7.1). This shows that m-phenylenediamine is indeed ring-protonated in the gas phase, and the estimated proton affinity difference between ring-protonation and N-protonation in m-phenylenediamine is 21.8 - 2.1 = 10.7 kcal/mole. This value is somewhat smaller than the STO-3G calculated difference of 17 kcal/mole but still of similar magnitude. The fact that m-phenylenediamine is a nitrogen base in aqueous solution even though its carbon proton affinity is some 10 kcal/mole higher than its nitrogen proton affinity illustrates the much poorer solvation of the charge-delocalized benzenium ion as compared to the anilinium ion which is capable of forming strong hydrogen bonding with the solvent.
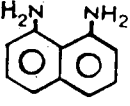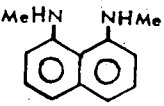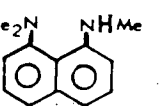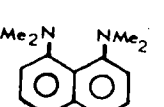
7.5 Gas-Phase and Aqueous Basicities of N-Methyl Substituted 1,8-Diaminonaphthalenes.

The gas-phase basicities of a series of N-methylated 1,8-diaminonaphthalenes were determined in the present

study (see table 7.1). Their corresponding aqueous basici-
ties had been reported by Alder et al (144). These are sum-
marized in table 7.2. The discussion on the gas-phase and
aqueous basicities of N-methylated 1,8-diaminonaphthalenes
should include a comparison with the methyl substituent
effects on the basicities of ammonia and aniline. There-
fore, the standard free energy changes for proton transfer
in the gas phase and in aqueous solution for the two series
are also given in table 7.2.

In the ammonia series, methyl substitution increases
the gas-phase basicity substantially in a regular pattern.
The increase in gas-phase basicity is due to the electron-
donating effect and higher polarizability of the methyl
group relative to that of hydrogen. The observed gas-
phase basicity of amines increases in the order of NH_3 <
$MeNH_2$ < Me_2NH < Me_3N. The enhancing effect of the methyl
substituent on the gas-phase basicity attenuates on suc-
cessive methyl substitution with a regular fall-off factor
of around 70% (see table 7.2). For example, $MeNH_2$ is more
basic than NH_3 by 10 kcal/mole, while Me_2NH is more basic
than $MeNH_2$ by 7.5 kcal/mole $\approx$ 10 kcal/mole x 70%. No
such orderly pattern is observed in aqueous solution. It may
be seen in table 7.2 that the methyl substituent effect is
much smaller in aqueous solution and the effect even be-
comes reversed on progressive substitution.. This results
in the anomalous order of the aqueous basicity for amines:

Table 7.2   Standard Free Energy Changes for Proton Transfer

Reactions.[a]   (Increasing negative value indicates increasing base strength)

I	III	IV	V
H_2N NH_2	$MeHN$ $NHMe$	Me_2N $NHMe$	Me_2N NMe_2

	I		III		IV		V
$\Delta G^{o}(g)$	-6.8			-4.3		-7.0	
$\Delta G^{o}(aq)$	-1.4			-1.1		-8.1	

NH_3	$\longrightarrow$	NH_2Me	$\longrightarrow$	$NHMe_2$	$\longrightarrow$	NMe_3

$\Delta G^{o}(g)$	-10.0		-7.5		-5.0	
$\Delta G^{o}(aq)$	-1.9		-0.2		+1.3	

NH_2	$\longrightarrow$	$NHMe$	$\longrightarrow$	NMe_2

|				
$\Delta G^{o}(g)$	-7.4		-6.6	
$\Delta G^{o}(aq)$	-0.4		-0.3	

a) All values in kcal/mole. ΔG^{o} for $B_1 \rightarrow B_2$ corresponds to the proton transfer reaction $B_1H^+ + B_2 = B_1 + B_2H^+$. $\Delta G^{o}(g)$ values at 460°K or 600°K (see table 7.1), $\Delta G^{o}(aq)$ values at 298°K. $\Delta G^{o}(aq)$ values for ammonia and aniline series are from tabulations by Taft and Arnett in "Proton Transfer Reactions", E. F. Caldin and V. Gold, Ed., Chapman and Hall, London, 1975, p.40 and p.84. Since the temperature dependence for ΔG^{o} in these reactions are small, it may be assumed that $\Delta G^{o}_{298} \simeq \Delta G^{o}_{600}$.

NH_3 < Me_3N < $MeNH_2$ $\lesssim$ Me_2NH. The irregularity in the aqueous basicity order is due mainly to the progressively worsening solvation of the ammonium ions with successive replacement of hydrogen by the methyl group (155). The methyl substituents decrease the solvation stability of the ammonium ion not just by removing the possible H-bonding positions, but also by reducing the strength of interactions between the remaining H-bonding positions and water molecules. The weakening of the strength of the specific hydrogen-bonding solvation on methyl substitution is due to the better delocalization of the charge in the methyl substituted ammonium ion. Consequently, the charge density on the remaining acidic hydrogen becomes less.

'Turning to the aniline series, it may be seen in table 7.2 that methyl substitution also increases the gas-phase basicity of aniline substantially. The effect of the second methyl substituent does not attenuate as much as in the aliphatic amines, indicating that it has a larger effect in the nitrogen-ring conjugation system. The effect of methyl substitution on the aqueous basicity of aniline is very much attenuated, although the aqueous basicity of aniline does increase progressively on successive methyl substitution.

Based on the above observations, it would be expected that N-methyl substitutions would increase the gas-phase basicity of 1,8-diaminonaphthalene, and their effects on

the corresponding aqueous basicity would be much smaller.
The experimental values of 6.8 kcal/mole for gas-phase
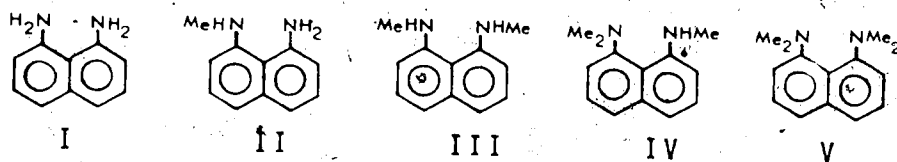
basicity difference and 1.4 kcal/mole for the aqueous basi-
city difference between 1,8-diaminonaphthalene (I) and N,N'-
dimethyl-1,8-diaminonaphthalene (III) are in accord with
the prediction. Unfortunately, the N-methyl-1,8-diamino-
naphthalene (II) was not available and the effect of a
single methyl substitution was not measured directly. It
is fair to presume that the 6.8 kcal/mole difference in
gas-phase basicity between the unsubstituted and the N,N'-
dimethyl substituted 1,8-diaminonaphthalenes should be split
unevenly, say 5 kcal/mole and 1.8 kcal/mole for the first
and second methyl substitution on different nitrogen atoms
respectively. The first methyl substituent is expected to
have the usual enhancing effect. But for going from $(II)H^+ +$
III $\longrightarrow$ II $+ (III)H^+$, one would expect the effect of the
second methyl group on the other nitrogen to be much
smaller. Presumably the proton in $(II)H^+$ is bound mainly
to the nitrogen bearing the methyl group, and the other
nitrogen is only acting as a H-bond acceptor. The intro-
duction of the second methyl group on the other nitrogen
thus only acts to increase the H-bond interaction. The
differential methyl substitution effects may be explained

in analogy with the calculations by Peyerimhoff (153) that
there is a double minimum in the potential energy for the
proton motion between the two nitrogens in the case of
$H_3NH^+NH_3$. The protonated 1,8-diaminonaphthalene is expected
to have a similar double minimum in potential energy. The
energy barrier between the two minima in $H_2NH^+NH_3$, when the
two nitrogens are kept at the equilibrium positions, was
calculated to be 3.5 kcal/mole (153). Similar or even
slightly larger barrier may be assumed for the protonated
1,8-diaminonaphthalene which has a bent H-bond since the
lone pairs on the nitrogens are not properly oriented
Because of the presence of the energy barrier, one would
expect the second methyl substituent would not interact
as a direct substituent but only as a substituent to in-
crease the H-bond interaction. The estimated magnitude of
5 kcal/mole for the first methyl substitution is arrived
at from the observation that the proton affinity difference
between the N-methyl-N'-dimethyl-1,8-diaminonaphthalene (IV)
and the N,N'-dimethyl-1,8-diaminonaphthalene (III) is 4.3
kcal/mole. For this case, the new methyl substitution is
on the nitrogen with which the proton is associated. It
is expected that the introduction of the first methyl group
to a nitrogen atom would enhance the gas-phase basicity
of 1,8-diaminonaphthalene to a similar or even slightly
larger extent.

Everything being equal, the above argument leads

to the generalization that in 1,8-diaminonaphthalene, each methyl substitution on the nitrogen which is going to bear the proton would increase its gas-phase basicity by about 4-5 kcal/mole, whereas each methyl substitution on the nitrogen opposite to that would only increase its gas-phase basicity by about 1-2 kcal/mole. This generalization is in complete disagreement with the experimental results when the gas-phase basicities of trimethylaminonaphthalene (IV) and tetramethylaminonaphthalene (V) are compared. Going from $(IV)H^+ + V \longrightarrow IV + (V)H^+$, the addition of the last methyl group is to be associated with the nitrogen not holding the proton, therefore, the predicted proton affinity difference between V and IV would be just some 1-2 kcal/mole. However, an experimental value of 7.0 kcal/mole was observed (see table 7.2). The remarkably high gas-phase basicity of the 1,8-bis(dimethylamino)-naphthalene (V) is in accord with the explanation offered by Alder et al (144) on the unexpectedly high aqueous basicity of V. The high basicity of compound V is due mostly to the destabilization of the neutral base. Alder et al. (144) pointed out that the tetramethylamino-naphthalene (V) is a highly strained molecule due to steric and coulombic repulsions among the four methyl groups and the two lone pairs on the nitrogen atoms. The tremendous strain on this compound is best appre-hended by considering its X-ray crystal structure, as

reported by Einspahr et al. (152), which showed that the naphthalene ring is twisted at carbons 9 and 10 to allow an increase in distance between the two opposing methylamino groups.
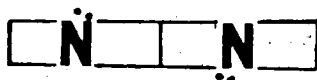

I.
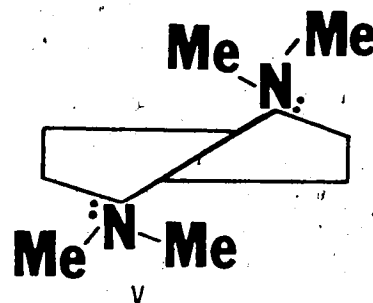
V

As a result, the 1,8-bis(dimethylamino)naphthalene (V) is with a conformation in which there is an out-of-plane distortion of the naphthalene ring. The two nitrogens are not in the plane of the naphthalene ring. There are also small distortions of bond angles and bond stretchings as compared to I. The N---N distance is increased from 2.5 Å to 2.8 Å. Protonation allows the two nitrogen lone pairs to align and the naphthalene ring to become planar, thus effectively removes the strain. The effectiveness of strain removal on protonation of V was confirmed by the crystal structures of the complex Cu(II) salt and complex Mg salts of monoprotonated 1,8-bis(dimethylamino)naphthalene. The results of the X-ray crystallographic studies by Truter and Vickery (156) showed that in the cation, all atoms are approximately coplanar except for the methyl carbon atoms and the hydrogen atoms in these groups. The N---N distance is 2.6 Å which can be compared with the N---N distance of 2.7 Å in $H_3NH^+NH_3$. The bond angle

N-H$^+$-N is about 170° so the N-H$^+$---N bond formed is just slightly, bent. The conformation of the protonated 1,8-bis(dimethylamino)naphthalene therefore does not have the strain that is present in the neutral base. The relieved strain energy thus shows up as an increase of proton affinity.

One might ask oneself whether similar strain is also present in the trimethylaminonaphthalene (IV), causing it to have a higher basicity than normal. It is expected that such strain, if present, must be to a much lesser extent, since compound (IV) may be stabilized by intra-molecular hydrogen bonding between the lone pair on the nitrogen and the available hydrogen as in compound I.


IV
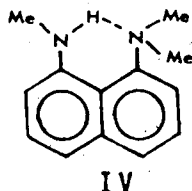
Similar stabilization is, of course, not possible with the tetramethylaminonaphthalene.

Turning to the basicities of these compounds in aqueous solution, it can be seen in table 7.3 that the effect of methyl substitution is much strongly attenuated when compared with that in the gas phase up to trimethyl-aminonaphthalene (IV). The attenuation should have the same cause as that in the ammonia and the aniline series. It should be recalled that the aqueous basicity of a base is a combined effects of its intrinsic basicity

and the solvation stability of the protonated ion. Methyl substitution, while increasing the intrinsic basicity by stabilizing the protonated ion on one hand, also reduces the solvation stability of the ion by decreasing the number of H-bond forming positions and weakening the remaining H-bond interactions. The differential solvation of the cations results in a strong attenuation on the effect of the methyl substitution on the aqueous basicities of the N-methylated diaminonaphthalenes.
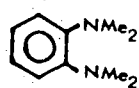
The most interesting point in the aqueous basicities of this series is the large increase in aqueous basicities from trimethylaminonaphthalene (IV) to tetramethylaminonaphthalene (V). The aqueous basicity difference between compounds V and IV, $-\Delta G^o$(aq) for reaction 7.15, had
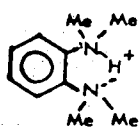

$$(7.15)$$
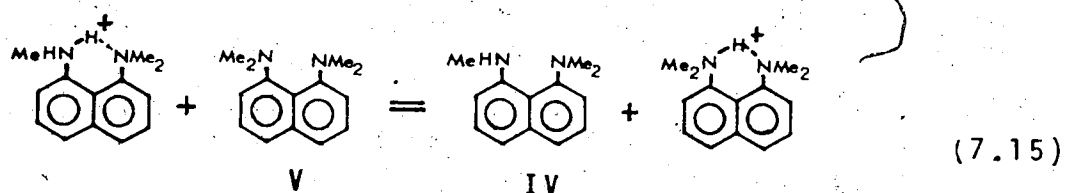
been measured by Alder (144) to be 8.1 kcal/mole. This value is as large as (actually slightly larger than) the corresponding $-\Delta G^o$(g) value (7.0 kcal/mole) measured in the present study. Since the main driving force for reaction 7.15 is the relief of strain energy in V and the strain removal does not affect the solvation of the protonated ion, the basicity change in aqueous solution and in gas phase should be similar. This is indeed what

was observed experimentally. It is noted that the proton-
ated IV has one more possible hydrogen bonding position
than the protonated V, and one would expect the former
is more favorably solvated than the latter. If that is
the case, the gas-phase basicity change from IV to V should
be slightly larger than the aqueous basicity change. It
is not clear why experimental measurements give the reverse
result. However, the cause of the small difference is
probably unimportant. It is also fair to conclude that
both protonated ions of IV and V are poorly solvated due
to the steric hindrance of the possible H-bonding sites.
As a result, there is only little differential cationic
solvation between the two protonated ions.

The gas-phase basicity of o-dimethylaminobenzene (VI)
was also determined as shown in table 7.1. The basicity
can be compared with that of tetramethylaminonaphthalene (V).
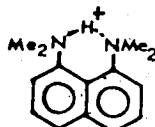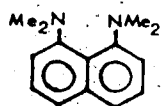

Steric models show that the amino groups in VI are much
less constrained than those in V. Consequently, there
is not much relief of strain energy on protonation of
VI. The protonated VI is stabilized by a similar H-bond
bridged structure as in the protonated V. One would ex-

pect that the gas-phase basicity of VI is lower than that of V by approximately the amount of the strain energy relieved on the protonation of VI, i.e. about 6 kcal/mole. Experimental results show that the gas-phase basicity of tetramethylaminobenzene (VI) is lower than that of 1,8-bis-(dimethylamino)naphthalene (V) by 7.4 kcal/mole, which is in line with the above prediction. The slightly higher experimental value (7.4 kcal/mole) than the predicted value (6 kcal/mole) probably reflects a decrease in the stability of the protonated VI ion relative to the protonated V ion due to the more highly bent H-bond in the protonated VI and the difference between the benzene and the naphthalene ring.

The hydration of the protonated trimethylamino-naphthalene (IV) and the protonated tetramethylamino-naphthalene (V) in which the proton is sterically hindered may be compared with the hydration of other poorly solvated protonated ions due to the absence of the exposed atomic sites with appreciable positive charge. Because of the lack of suitable sites for proper specific H-bonding with the solvent, these systems would only experience physical solvation. If they are of roughly similar size, their hydration energies would be similar. In other words, essentially no solvent effect would be observed for these bases, B, in the proton transfer reaction 1.13,

$$B_1H^+ + B_2 = B_1 + B_2H^+ \qquad (1.13)$$
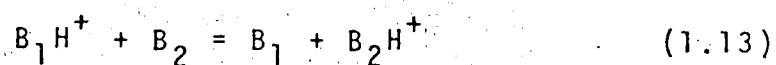
and therefore $\Delta G^O(g) \approx \Delta G^O(aq)$, for the reaction. Using ammonia as the reference base, Taft et al. (157) have determined the standard free energy changes in the gas phase for the proton transfer reaction 3.1 from the ammonium ion to bases B, which on protonation, leads to the formation of BH^+ ions of the above type. A comparison

$$NH_4^+ + B = NH_3 + BH^+ \qquad (3.1)$$
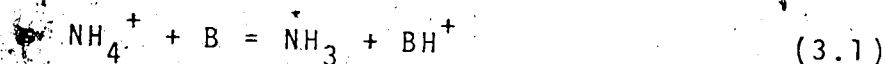
of the $\Delta G^O(g)$ values with the corresponding $\Delta G^O(aq)$ values for reaction 3.1 indicates a nearly constant difference Δ, of $\Delta G^O(aq) - \Delta G^O(g) \approx 35 \pm 1$ kcal/mole for these systems. Some examples of the bases, B, which fit into this relationship are: 2,6-di-tert-butylpyridine (Δ = 34.1 kcal/ mole), hexamethylbenzene (Δ = 35.2 kcal/mole) and 1,1,-di- phenylethylene (Δ = 34.7 kcal/mole). As pointed out by Taft (157), the tert-butyl groups in the first example are ex- pected to have completely blocked out the possible specific hydrogen-bonding sites of the NH^+ group in BH^+ and the N: atom in B, a situation similar to the case with trimethyl- aminonaphthalene (IV) and tetramethylaminonaphthalene (V). In the last two examples, the extensive delocalization of the positive charge throughout the relatively large cation gives the resulting protonated ions a very poor solvating ability. Since the ion hydration energy is the dominant term in Δ, a large positive Δ value reflects that the NH_4^+ is much better solvated than BH^+. A nearly constant Δ for

different bases B implies that the ionic solvation for different BH^+ is similar. Similar Δ values can be calculated for compounds IV and V. The $\Delta G^o(g)$ values for reaction 3.1 were determined to be -39.2 kcal/mole with tetramethylaminonaphthalene (V) and -31.8 kcal/mole with trimethylaminonaphthalene (IV) as the base B (see table 7.1). The $\Delta G^o(aq)$ for reaction 3.1 may be calculated from the relationship

$$\Delta G^o(aq) = -2.303 \ RT[pK_a(BH^+) - pK_a(NH_4^+)] \quad (7.16)$$

With the following literature pK_a values for the conjugate acids BH^+ of bases, B: ammonia, 9.24 (158); trimethylaminonaphthalene (IV), 6.43; and tetramethylaminonaphthalene (V) 12.34 (144), the $\Delta G^o(aq)$ values for reaction 3.1 at 298°K are calculated to be +3.83 kcal/mole and -4.23 kcal/mole for compounds IV and V respectively. Neglecting the temperature effect on the ΔG^o values (which should be within 1 kcal/mole), the calculated Δ $(\Delta G^o(aq) - \Delta G^o(g))$ for diaminonaphthalenes (IV) and (V) are 35.6 kcal/mole and 35.0 kcal/mole. The fact that compounds IV and V also fit into the above mentioned relationship suggests that their protonated ions are poorly solvated and their ionic hydration energies are similar to those BH^+ which do not have favorable specific H-bonding sites available for solvation. This is in agreement with the conclusions drawn previously.

ION EQUILIBRIA STUDIES OF THE SOLVATION OF THE PROTON BY DIMETHYL SULFOXIDE (DMSO) AND ACETONE IN THE GAS PHASE

CHAPTER VIII

8.1 Introduction

In the determination of the proton affinity of dimethyl sulfoxide (DMSO), it was observed that even at 600°K and with DMSO partial pressure of 1 mtorr in the ion source, the formation of the protonated DMSO dimer was still significant. The strong tendency to form the protonated dimers even at such high temperature was only observed with molecules like water where the protonated species can form a strong hydrogen bond with another neutral molecule. It was decided that it would be interesting to study the solvation of the proton by DMSO in

$$H^+(DMSO)_{n-1} + DMSO = H^+(DMSO)_n \qquad (8.1)$$
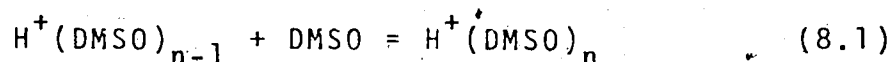
the gas phase. The determination of equilibrium constants, $K_{n-1,n}$ for reaction 8.1 at different temperatures allows the evaluation of the thermodynamic quantities $\Delta G^o_{n-1,n}$, $\Delta H^o_{n-1,n}$ and $\Delta S^o_{n-1,n}$ for different n. With n = 1, reaction 8.1 refers to the definition of the proton affinity.

$$H^+ + DMSO = H^+(DMSO) \qquad \Delta H^o_{0,1} \qquad (8.2)$$

Therefore, $\Delta H^o_{0,1}$ = -PA(DMSO). In the present study, reaction 8.1 was studied for n = 2 and 3. High pressure mass spectrometry has proven to be a very suitable method

for the study of gas-phase solvation (41). Reaction 8.1
is exothermic and requires a third-body for thermalization.
At pressure below ~10 torr, clustering reactions like 8.1
are usually third order (41). Consequently, the forward
and reverse reaction rates are usually too slow and do not
lead to equilibrium when techniques such as ICR are used
in which the total pressure is only around 10^{-6} torr. The
solvation of the hydrogen ion by water, methanol and di-
methyl ether in the gas phase was studied by Grimsrud and
Kebarle (47) in this laboratory some time ago. The marked
difference in the solvation of the protonated H_3O^+, $CH_3OH_2^+$
and $(CH_3)_2OH^+$ by respective molecules was shown to be
mostly due to the blocking of hydrogen bonding sites in
the protonated ion by successively replacing the hydrogen
atom with the methyl group. By comparing the solvation
of the hydrogen ion by DMSO with that by H_2O and $(CH_3)_2O$,
one could determine whether or not hydrogen bonding is
the only important factor in the association of DMSO
molecules with the proton.

The solvation of the hydrogen ion by acetone was
also investigated. Acetone has a molecular structure
that bears some resemblance to that of DMSO. The
equilibrium 8.3 was studied for n = 2 and 3. These

$$H^+(acetone)_{n-1} + acetone = H^+(acetone)_n \qquad (8.3)$$
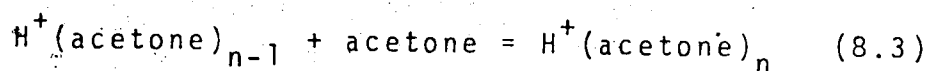
results will also be presented in this chapter.

8.2 Experimental.

The equilibrium constant, $K_{n-1,n}$, for the reaction:

$$H^+(DMSO)_{n-1} + DMSO = H^+(DMSO)_n \qquad (8.1)$$
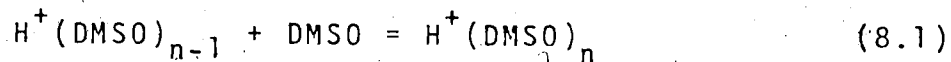
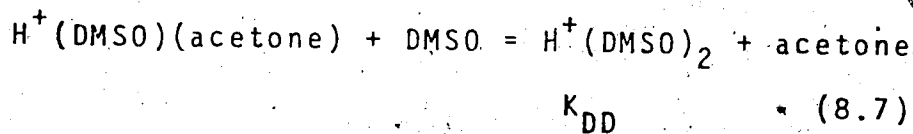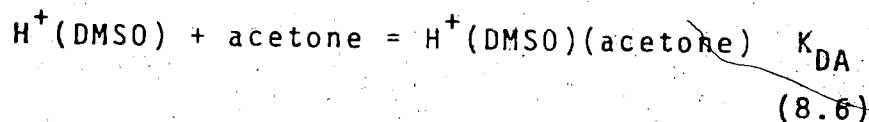was calculated from the expression

$$K_{n-1,n} = \frac{I_n}{I_{n-1}} \times \frac{1}{P_{DMSO}} \qquad (8.4)$$

where I_n/I_{n-1} is the equilibrium ion intensity ratio for the protonated DMSO clusters and P_{DMSO} is the pressure of DMSO in the ion source. The handling and admission of gas mixture to the ion source was very similar to that described previously in Chapter II. Samples were prepared by injecting an appropriate amount of DMSO into the 5 liter glass bulb at 100°C filled with 1 atmosphere of methane buffer gas. The thoroughly mixed gas sample was passed continuously through the thermostated ion source and removed by an exhaust pump. The DMSO concentration (1-150 mtorr) in the ion source was varied by varying the ion source pressure (2-5 torr) and by varying the partial pressures of DMSO in the 5 liter sample bulb. The equilibrium ion ratio, I_n/I_{n-1}, was evaluated in the same way as described in Chapter II. With the known P_{DMSO} in the ion source, $K_{n-1,n}$ can be calculated. In all measurements, conditions were chosen so that the observed ion ratio I_n/I_{n-1} is less than 0.2 if possible. This is to minimize the uncertainties that may result from the possible

decomposition of the higher cluster $H^+(DMSO)_n$, into the lower cluster $H^+(DMSO)_{n-1}$ and DMSO molecule outside the ion source. For example, with a I_n/I_{n-1} ratio of 10, 10% decomposition of the higher cluster would result in a 55% error in the I_n/I_{n-1} ratio, whereas for a I_n/I_{n-1} ratio of 0.2, 10% decomposition would only result in 12% error in the observed I_n/I_{n-1} ratio. For the equil-ibrium constant $K_{1,2}$ corresponding to the association reaction:

$$H^+(DMSO) + DMSO = H^+(DMSO)_2 \qquad (8.5)$$
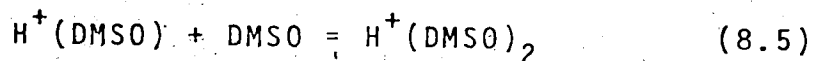
the value of $K_{1,2}$ is very large ($\sim 2 \times 10^3$ torr^{-1}) even at 600°K. Consequently, the criteria that the equilibrium I_n/I_{n-1} ratio <0.2 could not be fulfilled even with a DMSO pressure as low as 1×10^{-3} torr (which gave $I_n/I_{n-1} \sim 2$). Of course, on principle this ratio could be obtained at temperatures above 600°K. However, generally work at such high temperature is difficult as complications often arise from thermal decomposition of the neutral compounds. Therefore the problem was overcome by effectively splitt-ing reaction 8.5 into two steps,

$$H^+(DMSO) + acetone = H^+(DMSO)(acetone) \quad K_{DA}$$
$$(8.6)$$

$$H^+(DMSO)(acetone) + DMSO = H^+(DMSO)_2 + acetone$$
$$K_{DD} \qquad \qquad (8.7)$$

and the two reactions were studied separately. The

equilibrium constant $K_{1,2}$ for reaction 8.5 may then be calculated from the expression: $K_{1,2} = K_{DA}K_{DD}$. Reaction 8.6 is the association reaction of $H^+(DMSO)$ with acetone. The proton affinity of DMSO is 14.9 kcal/mole higher than that of acetone (see table 3.57). Since the stability of a given positive onium ion such as H_3O^+ and NH_4^+ clustering with different bases B 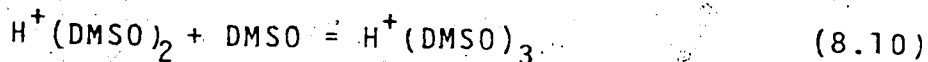decreases with decreasing proton affinity of the bases, it could be expected that $H^+(DMSO)(acetone)$ would be less stable than $H^+(DMSO)_2$. Therefore, reaction 8.6 would be less exothermic than reaction 8.5 and K_{DA} is smaller than $K_{1,2}$ for DMSO at the same temperature. It should be noted that the equilibrium constants K_{DA} do not depend on the partial pressure of DMSO. K_{DA} were measured with traces of DMSO, together with 1-150 mtorr acetone and 2-5 torr methane buffer gas in the ion source. Under such conditions the criteria of $I_{H^+(DMSO)(acetone)}/I_{H^+(DMSO)} < 0.2$ was satisfied. Reaction 8.7 is an exchange reaction measuring the relative stability of the $H^+(DMSO)(acetone)$ ion and the $H^+(DMSO)_2$ ion. Its equilibrium constants, K_{DD}, were determined in a way analogous to that in proton transfer reactions. Since K_{DD} were fairly large (10^3), large ratios of [acetone]/[DMSO] were used in order to minimize the uncertainty in the measurements of the corresponding ion intensity ratios. This was achieved by eliminating the use of methane buffer. When acetone is used as the major gas, the primary ions

formed by electron impact are CH_3CO^+ and $CH_3COCH_3^+$. These react with acetone to give $H^+(CH_3COCH_3)$ as shown in reactions 8.8 and 8.9.

$$CH_3CO^+ + CH_3COCH_3 \longrightarrow H^+(CH_3COCH_3) + CH_2CO \qquad (8.8)$$

$$CH_3COCH_3^+ + CH_3COCH_3 \longrightarrow H^+(CH_3COCH_3) + C_3H_5O \qquad (8.9)$$

The equilibrium constants for the reaction:

$$H^+(DMSO)_2 + DMSO = H^+(DMSO)_3 \qquad (8.10)$$
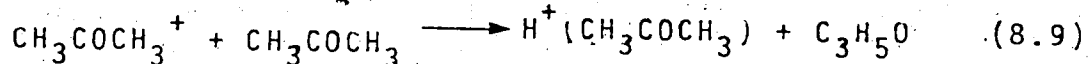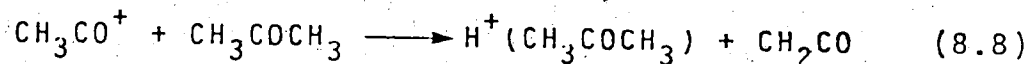
were smaller and therefore these equilibria could be determined directly, i.e. without the mediation of acetone.

8.3 Presentation of Results

The equilibrium constants at different temperatures were determined for the following reactions:

$$H^+(DMSO) + acetone = H^+(DMSO)(acetone) \qquad (8.6)$$

$$H^+(DMSO)(acetone) + DMSO = H^+(DMSO)_2 + acetone \qquad (8.7)$$

$$H^+(DMSO)_2 + DMSO = H^+(DMSO)_3 \qquad (8.10)$$

$$H^+(acetone) + acetone = H^+(acetone)_2 \qquad (8.11)$$

$$H^+(acetone)_2 + DMSO = H^+(DMSO)(acetone) + acetone \qquad (8.12)$$
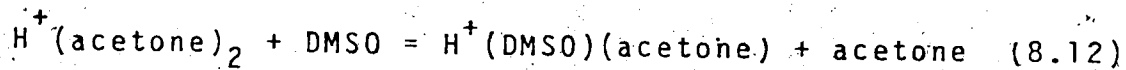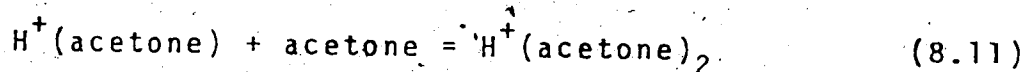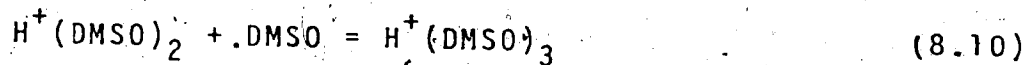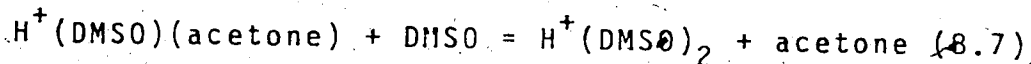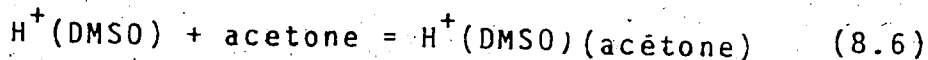
The results showing the invariance of equilibrium constants with the corresponding neutral concentrations are shown in figures 8.1 - 8.4 for reaction 8.6; in table 8.1 for reaction 8.7; in figures 8.5 - 8.7 for reaction 8.10; in
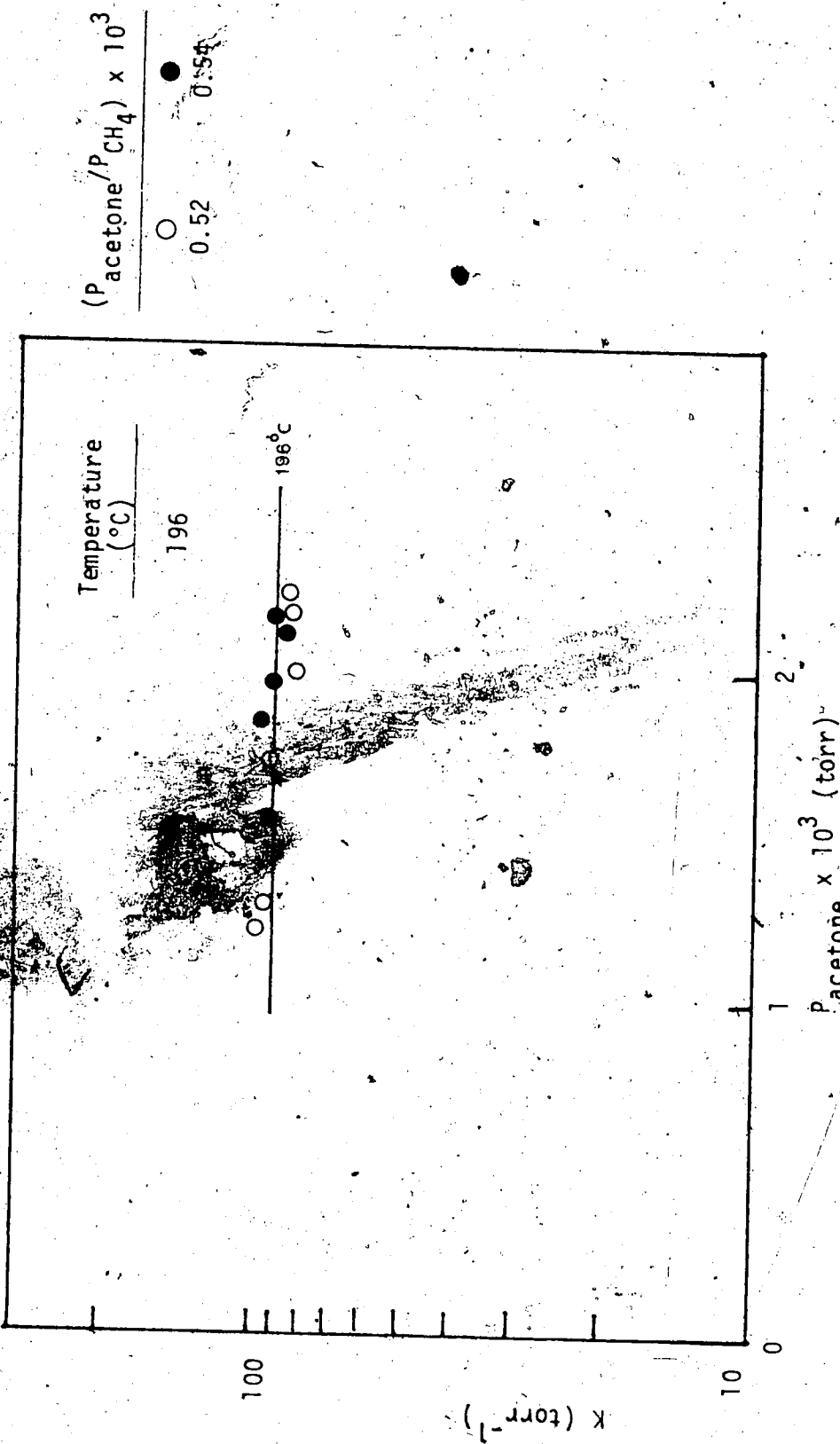
FIGURE 8.1 Equilibrium Constants versus Pressures of Acetone at Various Temperatures for the Reaction:

$$H^+(DMSO) + acetone = H^+(DMSO)(acetone)$$
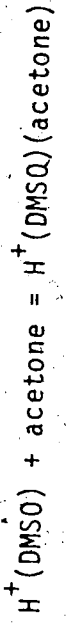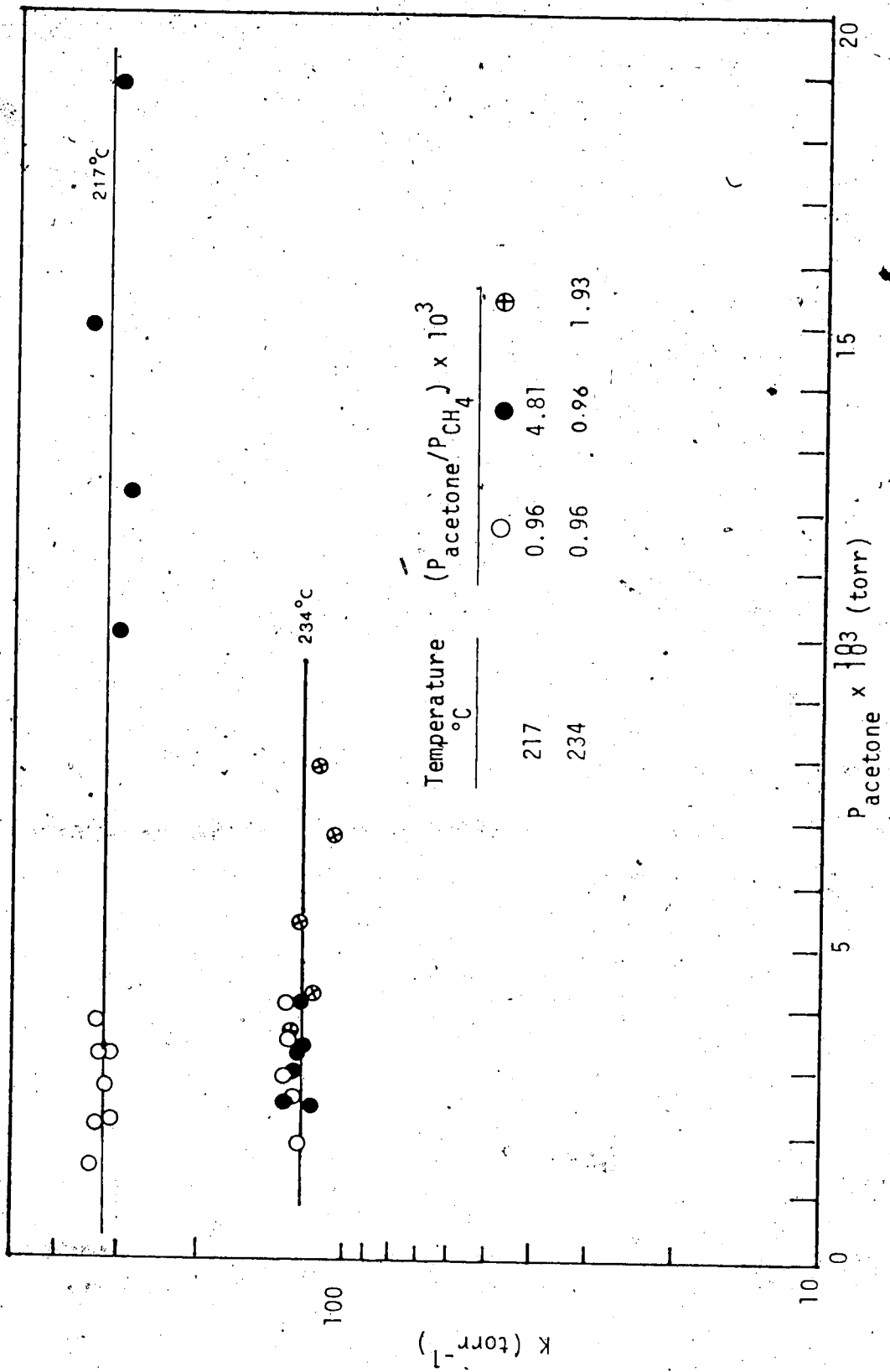
FIGURE 8.2 Equilibrium Constants versus Pressures of Acetone at Various Temperatures for the Reaction: $H^+(DMSO) + acetone = H^+(DMSO)(acetone)$.

369
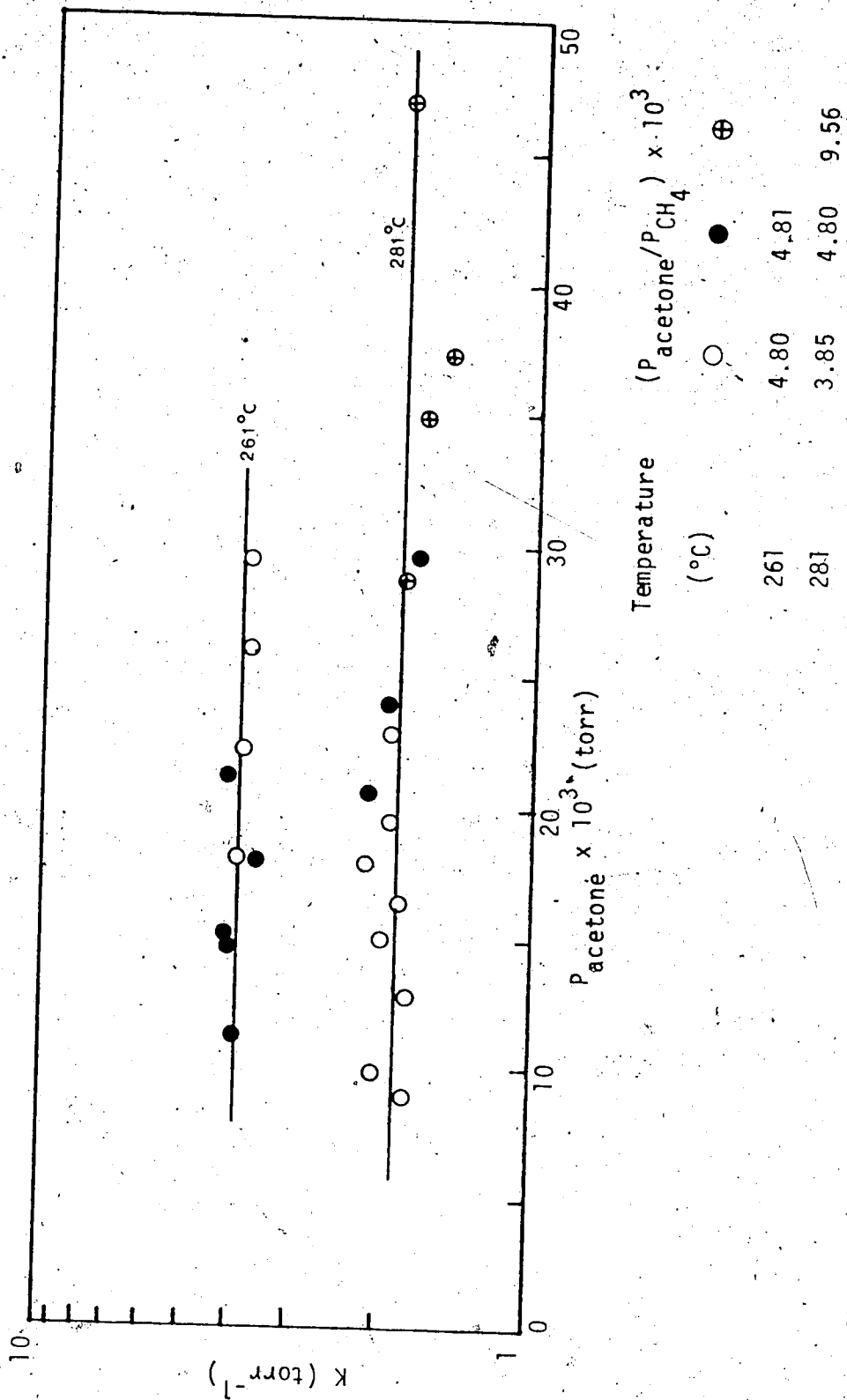
FIGURE 8.3　Equilibrium Constants versus Pressures of Acetone at Various Temperatures for the Reaction: $H^+(DMSO) + acetone = H^+(DMSO)(acetone)$.
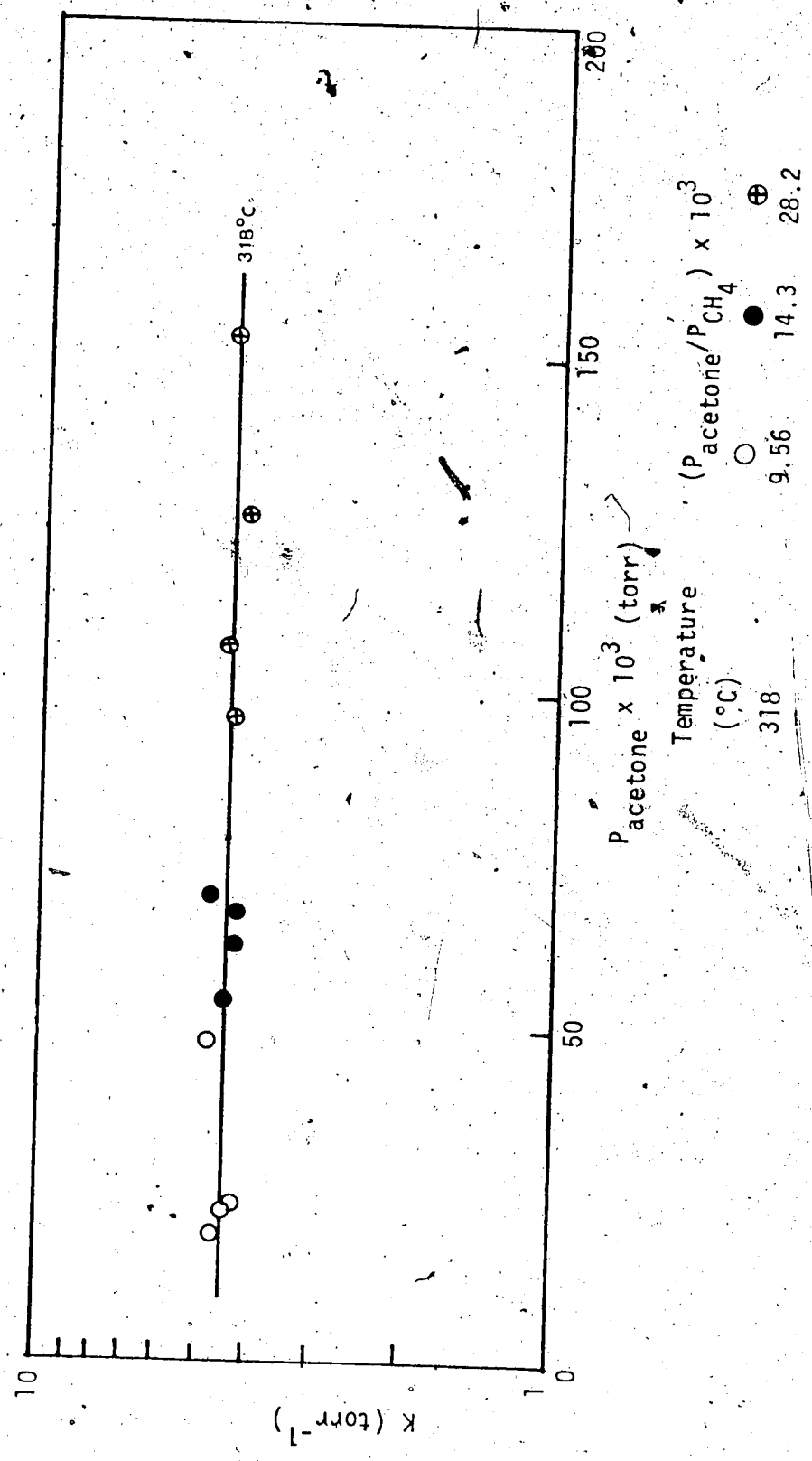
FIGURE 8.4 Equilibrium Constants versus Pressures of Acetone at Various Temperatures for the Reaction $H^+(DMSO)$ + acetone = $H^+(DMSO)(acetone)$.

Table 8.1   Equilibrium Constants at Different Temperatures for the Exchange Reaction:

$$H^+(acetone)(DMSO) + DMSO = H^+(DMSO)_2 + acetone$$

| Temp.	$P_{acetone}$ (mtorr)	P_{DMSO} (mtorr)	$P_{ion\ source}$ (torr)	K	$-\Delta G^0$ (kcal/mole)
318°C	1.40×10^3	4.17	1.40	0.718×10^3	
(591°K)	1.99×10^3	5.96	2.00	0.726×10^3	
	2.69×10^3	8.05	2.70	0.730×10^3	
	3.59×10^3	10.7	3.60	0.705×10^3	
	4.04×10^3	12.1	4.05	0.722×10^3	
			Ave:	0.720×10^3	7.73
280.5°C	2.00×10^3	4.08	2.00	1.03×10^3	
(553.5°K)	2.59×10^3	5.30	2.60	1.06×10^3	
	2.89×10^3	5.92	2.90	1.13×10^3	
	3.69×10^3	7.55	3.70	1.08×10^3	
			Ave:	1.08×10^3	7.68
261°C	1.90×10^3	1.89	1.90	1.16×10^3	
(534°K)	2.35×10^3	2.34	2.35	1.25×10^3	
	2.50×10^3	2.49	2.50	1.38×10^3	
	3.25×10^3	3.23	3.25	1.43×10^3	
	4.20×10^3	4.18	4.20	1.56×10^3	
			Ave:	1.36×10^3	7.66
227.5°C	1.60×10^3	4.77	1.60	2.00×10^3	
(500.5°K)	1.99×10^3	5.96	2.00	1.92×10^3	
	2.39×10^3	7.15	2.40	2.00×10^3	
	2.89×10^3	8.64	2.90	1.88×10^3	
	3.59×10^3	10.7	3.60	1.88×10^3	
	4.29×10^3	12.8	4.30	1.92×10^3	
	1.70×10^3	1.69	1.70	2.19×10^3	

Table 8.1 (continued)

Temp.	$P_{acetone}$ (mtorr)	P_{DMSO} (mtorr)	$P_{ion\ source}$ (torr)	K	$-\Delta G^0$ (kcal/mole)
	2.40×10^3	2.39	2.40	2.13×10^3	
	3.20×10^3	3.18	3.20	2.13×10^3	
			Ave:	2.01×10^3	7.56
208°C	1.45×10^3	4.32	1.45	2.63×10^3	
(481°K)	1.89×10^3	5.66	1.90	2.38×10^3	
	2.59×10^3	7.74	2.60	2.67×10^3	
	3.09×10^3	9.23	3.10	2.68×10^3	
	3.49×10^3	10.4	3.50	2.51×10^3	
	1.40×10^3	1.39	1.40	2.75×10^3	
	1.95×10^3	1.94	1.95	2.75×10^3	
	2.55×10^3	2.54	2.55	2.75×10^3	
	3.40×10^3	3.38	3.40	2.88×10^3	
			Ave:	2.66×10^3	7.54

FIGURE 8.5 Equilibrium Constants versus Pressures of DMSO at Various Temperatures for the

Reaction: $H^+(DMSO)_2 + DMSO \rightleftharpoons H^+(DMSO)_3$

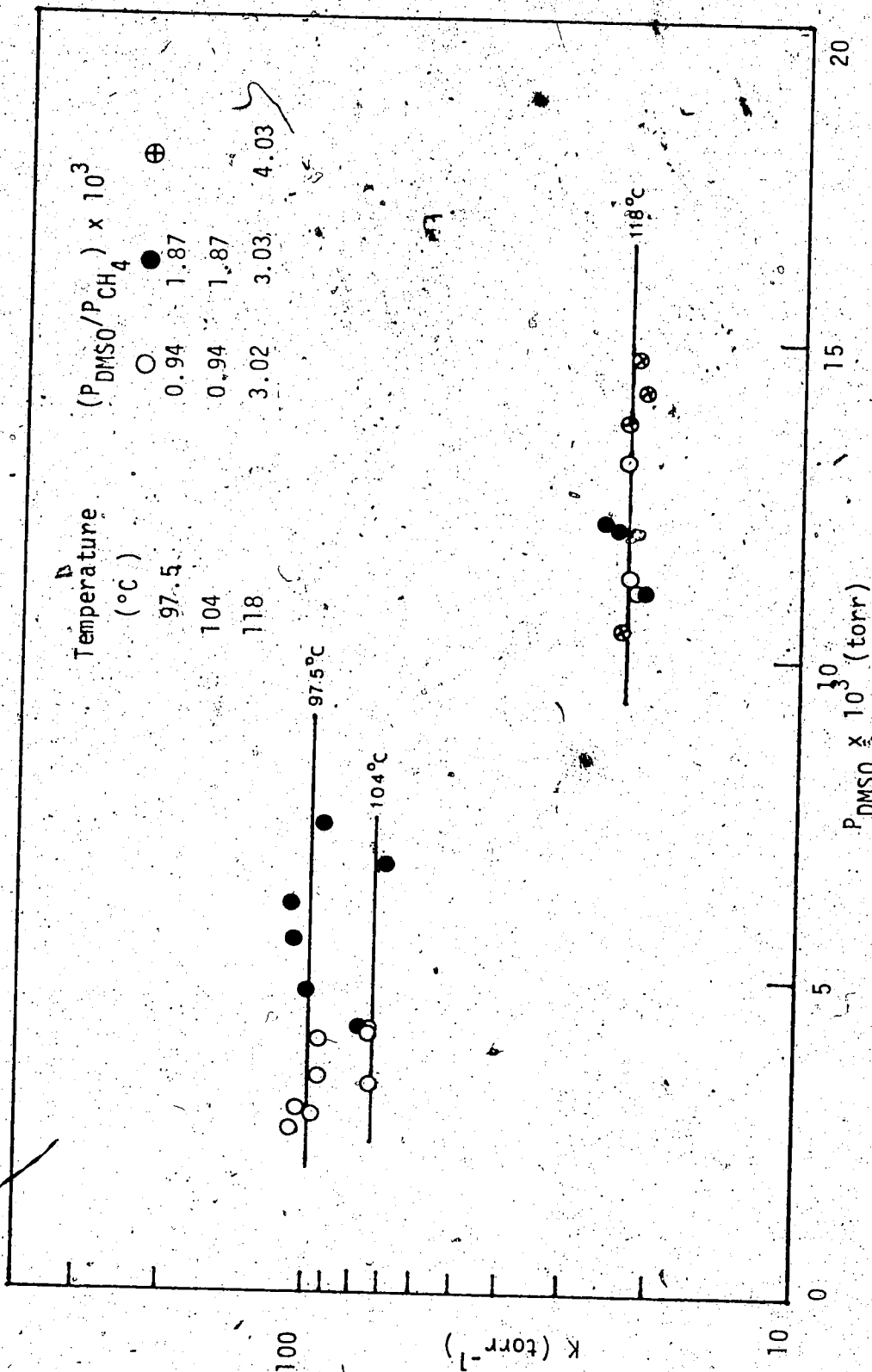FIRGURE 8.6 Equilibrium Constants versus Pressures of DMSO at Various Temperatures for the Reaction:

$$H^+(DMSO)_2 + DMSO = H^+(DMSO)_3$$

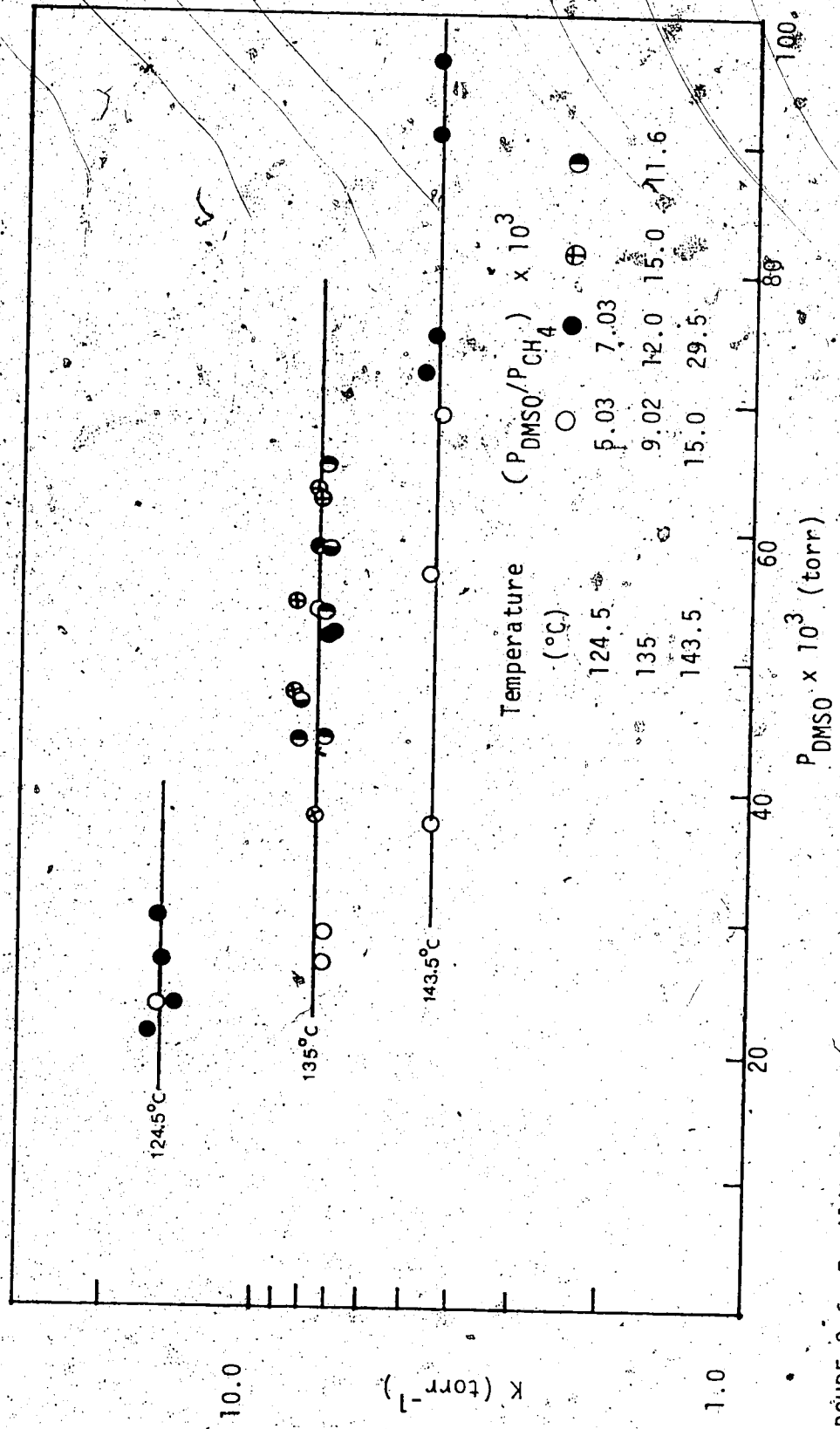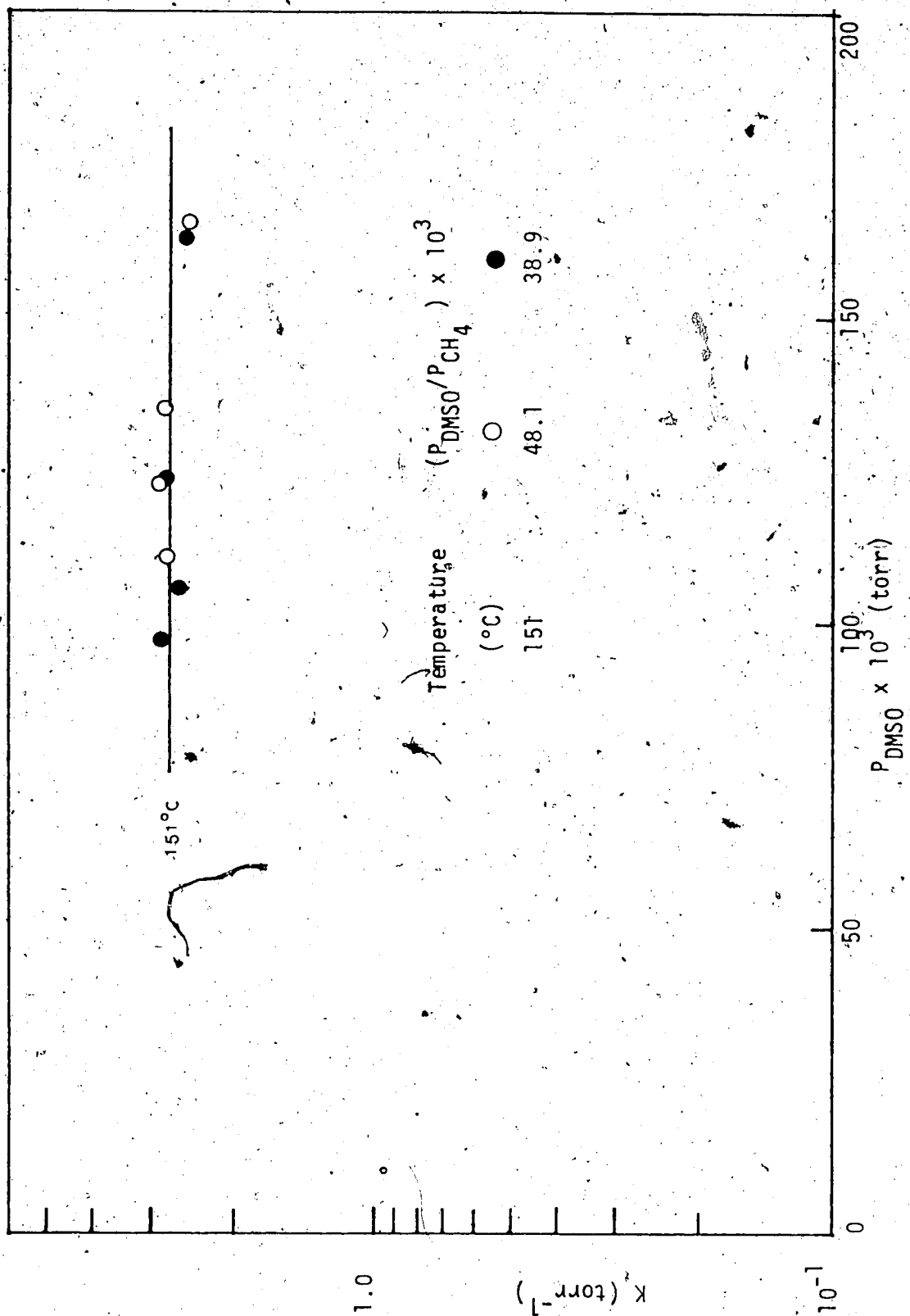FIGURE 8.7 Equilibrium Constants versus Pressures of DMSO at Various Temperatures for the Reaction:

$$H^+(DMSO)_2 + DMSO = H^+(DMSO)_3$$

figures 8.8 - 8.9 for reaction 8.11 and in table 8.2 for
reaction 8.12. The temperature dependence of the equilib-
rium constant K, is shown by plotting the logarithms of K
as a function of 1/T. Such van't Hoff plots for reactions
8.6, 8.7 and 8.10 are shown in figure 8.10. Also shown
in figure 8.10 is the temperature dependence of the equil-
ibrium constant for reaction 8.5 which is calculated from

$$H^+(DMSO) + DMSO = H^+(DMSO)_2 \qquad (8.5)$$
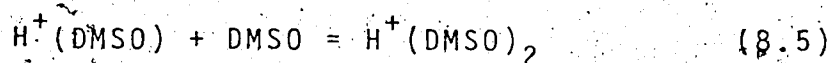
the equilibrium constants of reactions 8.6 and 8.7. The
van't Hoff plots for reactions 8.11 and 8.12 are shown in
figures 8.11 and 8.12, respectively. The standard enthalpy
change, ΔH^O, and the standard entropy change, ΔS^O, for
these reactions were obtained respectively from the slope
and the intercept of the corresponding van't Hoff plot.
The ΔH^O and ΔS^O values derived from the least square
analysis of the data are summarized in table 8.3 together
with their corresponding standard deviations. The ΔG^O_{298}
values for individual reactions obtained by extrapolation
are also shown in table 8.3.

8.4 Solvation of the Hydrogen Ion by DMSO in the Gas Phase.
Comparison with Similar Solvation Processes Involving
Water, Dimethyl Ether and Acetonitrile.

The solvation of the hydrogen ion by DMSO is best dis-
cussed in comparison with that by other protic and aprotic

FIGURE 8.8 Equilibrium Constants _versus_ Pressures of Acetone at Various Temperatures for the Re-

action: H^+(acetone) + acetone = H^+(acetone)$_2$.

FIGURE 8.9 Equilibrium Constants versus Pressures of Acetone at Various Temperatures for the Reaction $H^+(acetone) + acetone = H^+(acetone)_2$

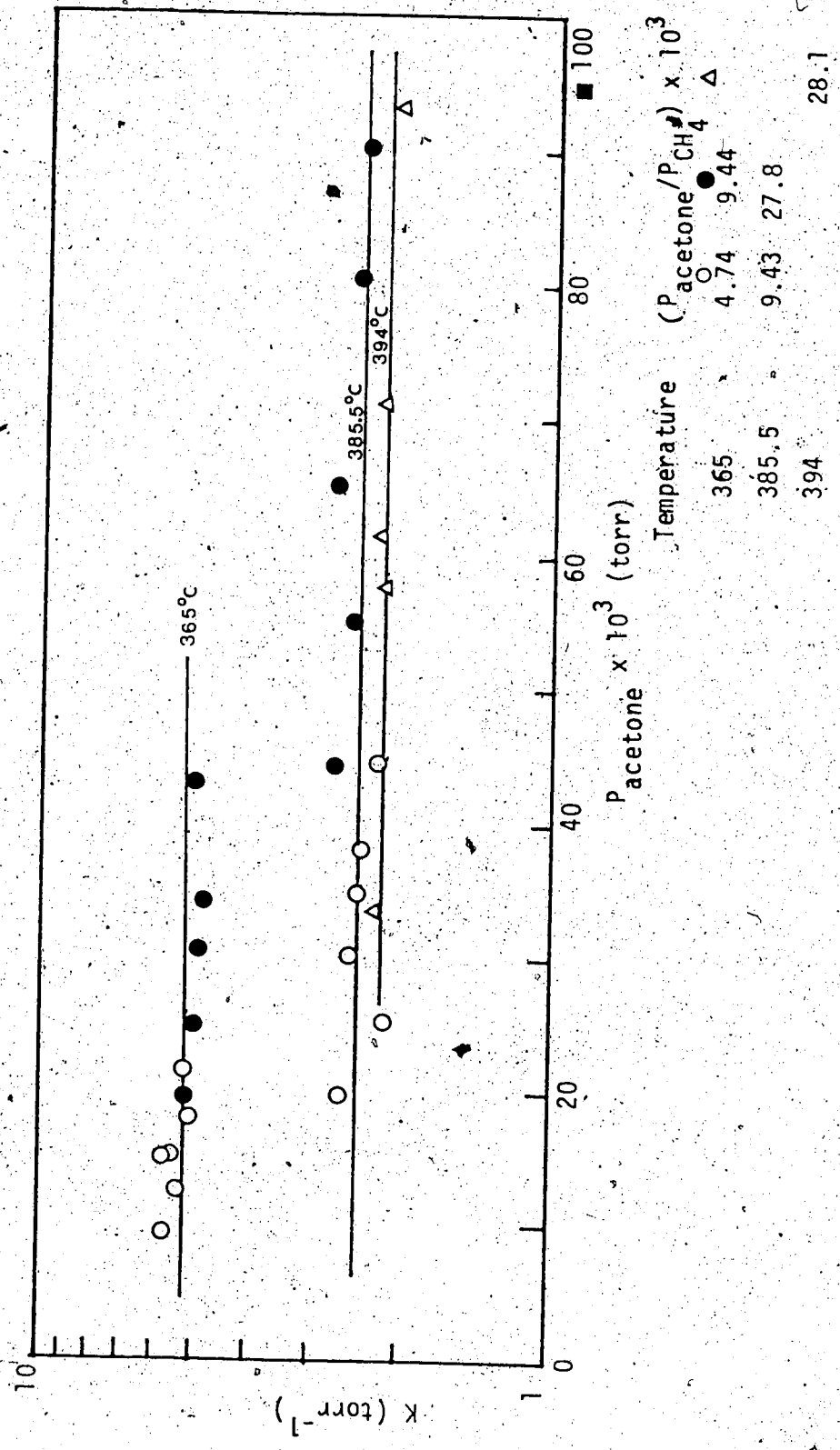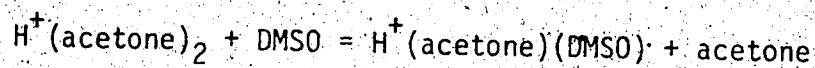Table 8.2   Equilibrium Constants at Different Temperatures for the
Exchange Reaction:

$$H^+(acetone)_2 + DMSO = H^+(acetone)(DMSO) + acetone$$

Temp.	$P_{acetone}$ (mtorr)	P_{DMSO} (mtorr)	P_{ion} source (torr)	K	$-\Delta G^0$ (kcal/mole)
346.5°C	0.90×10^3	1.26	0.90	1.07×10^4	
(619.5°K)	2.50×10^3	3.50	2.50	1.10×10^4	
	3.00×10^3	4.20	3.00	1.07×10^4	
	3.35×10^3	4.69	3.35	1.04×10^4	
	4.00×10^3	5.60	4.00	1.03×10^4	
	1.60×10^3	0.75	1.60	1.04×10^4	
	2.05×10^3	0.96	2.05	1.12×10^4	
	2.75×10^3	1.28	2.75	1.09×10^4	
	3.05×10^3	1.42	3.05	1.06×10^4	
	3.95×10^3	1.84	3.95	1.01×10^4	
			Ave:	1.06×10^4	11.41
332°C	1.44×10^3	2.02	1.44	1.47×10^4	
(605°K)	2.40×10^3	3.36	2.40	1.34×10^4	
	2.45×10^3	3.34	2.45	1.39×10^4	
	2.99×10^3	4.20	3.00	1.43×10^4	
	3.74×10^3	5.25	3.75	1.40×10^4	
	4.24×10^3	5.95	4.25	1.40×10^4	
	1.35×10^3	0.70	1.35	1.39×10^4	
	1.90×10^3	0.98	1.90	1.38×10^4	
	2.65×10^3	1.37	2.65	1.34×10^4	
	3.70×10^3	1.92	3.70	1.39×10^4	
			Ave:	1.39×10^4	11.47
316.5°C	1.30×10^3	1.82	1.30	1.98×10^4	
(589.5°K)	1.85×10^3	2.59	1.85	1.80×10^4	
	2.30×10^3	3.22	2.30	1.99×10^4	
	3.30×10^3	4.62	3.30	1.80×10^4	
	4.10×10^3	5.74	4.10	1.85×10^4	

Table 8.2 (continued)

Temp.	$P_{acetone}$ (mtorr)	P_{DMSO} (mtorr)	P_{ion} source (torr)	K	$-\Delta G^o$ (kcal/mole)
	1.40×10^3	0.70	1.40	1.84×10^4	
	2.50×10^3	1.25	2.50	1.88×10^4	
	3.00×10^3	1.50	3.00	1.85×10^4	
	3.90×10^3	1.95	3.90	1.74×10^4	
			Ave:	1.86×10^4	11.52
300°C	1.87×10^3	2.62	1.87	2.64×10^4	
(573°K)	2.70×10^3	3.78	2.70	2.38×10^4	
	3.35×10^3	4.69	3.35	2.46×10^4	
	4.30×10^3	6.02	4.30	2.46×10^4	
	1.75×10^3	0.83	1.75	2.69×10^4	
	2.15×10^3	1.02	2.15	2.72×10^4	
	2.80×10^3	1.33	2.80	2.67×10^4	
	3.30×10^3	1.57	3.30	2.46×10^4	
	4.10×10^3	1.95	4.10	2.40×10^4	
			Ave:	2.54×10^4	11.55
276°C	1.40×10^3	1.96	1.40	3.47×10^4	
(549°K)	2.40×10^3	3.36	2.40	3.61×10^4	
	3.30×10^3	4.62	3.30	3.92×10^4	
	4.00×10^3	5.60	4.00	3.70×10^4	
	1.65×10^3	0.83	1.65	3.64×10^4	
	2.10×10^3	1.05	2.10	3.62×10^4	
	3.00×10^3	1.50	3.00	3.91×10^4	
	4.00×10^3	2.00	4.00	3.64×10^4	
			Ave:	3.69×10^4	11.47
258°K	2.50×10^3	3.50	2.50	4.89×10^4	
(531°K)	2.70×10^3	3.78	2.70	5.33×10^4	
	3.45×10^3	4.83	3.45	5.05×10^4	
	3.90×10^3	5.46	3.90	4.71×10^4	

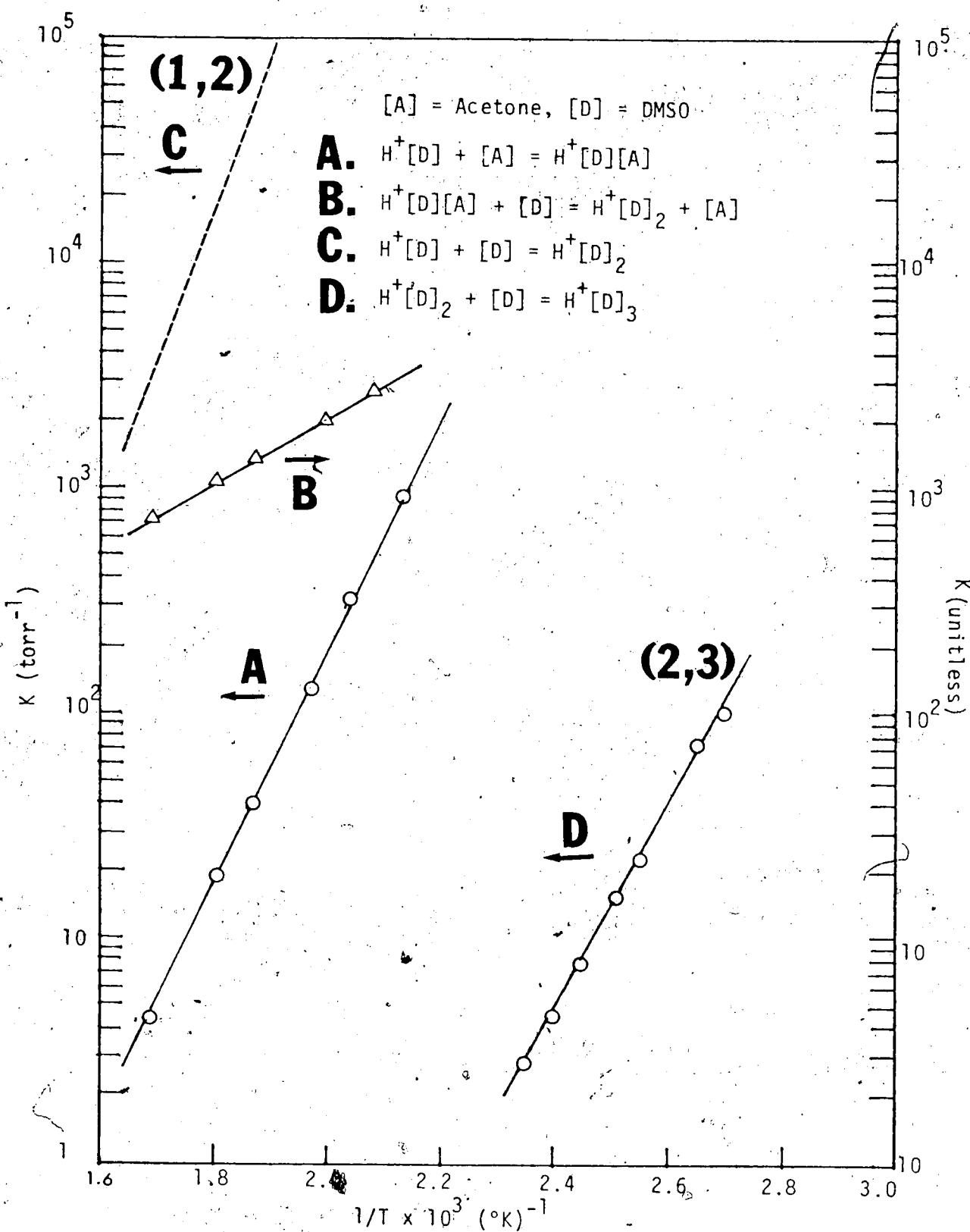| Temp.	$P_{acetone}$ (mtorr)	P_{DMSO} (mtorr)	$P_{ion\ source}$ (torr)	K	$-\Delta G^0$ (kcal/mole)
	4.19×10^3	5.88	4.20	5.01×10^4	
	1.00×10^3	0.50	1.00	5.17×10^4	
	1.90×10^3	0.95	1.90	5.33×10^4	
	2.30×10^3	1.15	2.30	5.06×10^4	
	3.10×10^3	1.55	3.10	5.33×10^4	
	3.50×10^3	1.75	3.50	5.33×10^4	
	4.30×10^3	2.15	4.30	5.28×10^4	
			Ave:	5.12×10^4	11.44
235°C (508°K)	1.80×10^3	0.90	1.80	7.83×10^4	
	2.40×10^3	1.20	2.40	7.99×10^4	
	2.50×10^3	1.25	2.50	7.89×10^4	
	3.30×10^3	1.65	3.30	8.05×10^4	
	4.00×10^3	2.00	4.00	7.99×10^4	
	1.70×10^3	0.35	1.70	7.98×10^4	
	2.30×10^3	0.48	2.30	9.24×10^4	
	2.80×10^3	0.58	2.80	8.88×10^4	
	3.55×10^3	0.73	3.55	9.12×10^4	
			Ave:	8.33×10^4	11.44
204°C (477°K)	3.30×10^3	4.62	3.30	13.5×10^4	
	3.99×10^3	5.60	4.00	14.6×10^4	
	4.19×10^3	5.88	4.20	14.1×10^4	
	2.30×10^3	1.15	2.30	17.1×10^4	
	3.10×10^3	1.55	3.10	18.1×10^4	
	3.30×10^3	1.65	3.30	18.1×10^4	
	4.20×10^3	2.10	4.20	17.3×10^4	
			Ave:	16.1×10^4	11.36

FIGURE 8.10   van't Hoff Plots for Gas-Phase Equilibria:
$H^+(DMSO)_{n-1} + DMSO = H^+(DMSO)_n$
(dashed line calculated from lines A and B).

FIGURE 8.11 van't Hoff Plot for the Reaction:
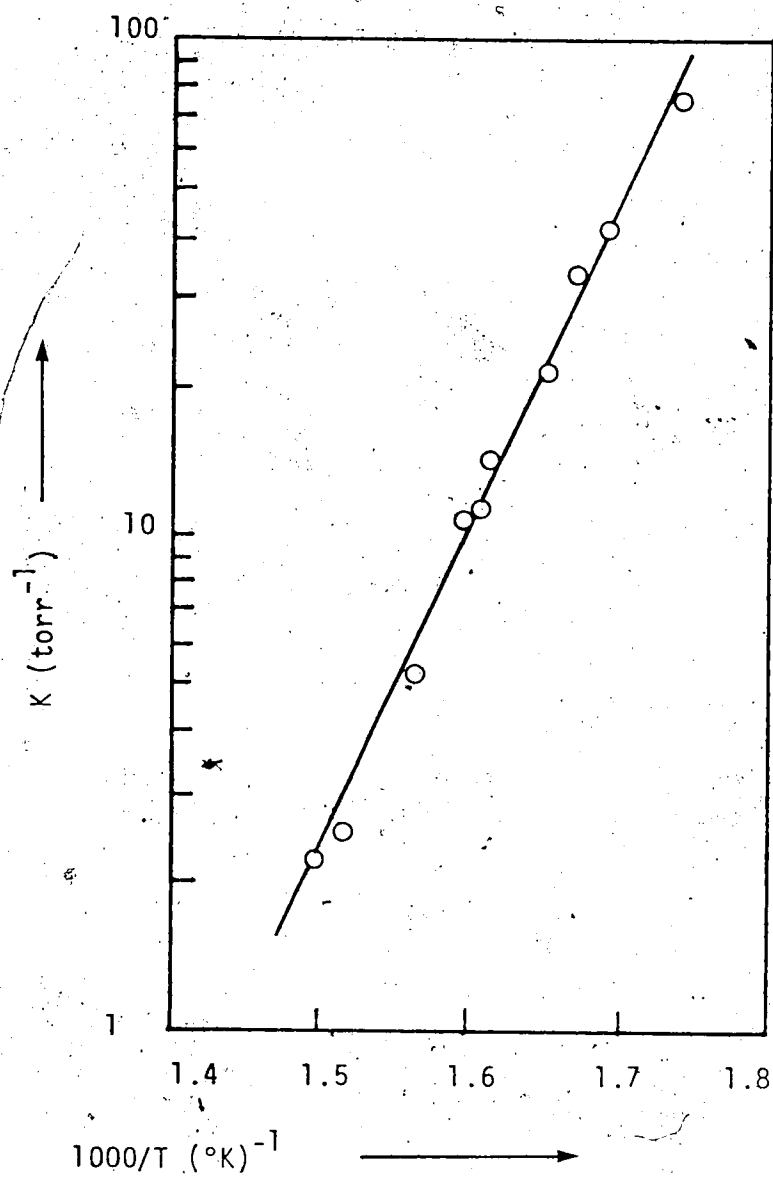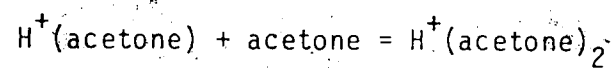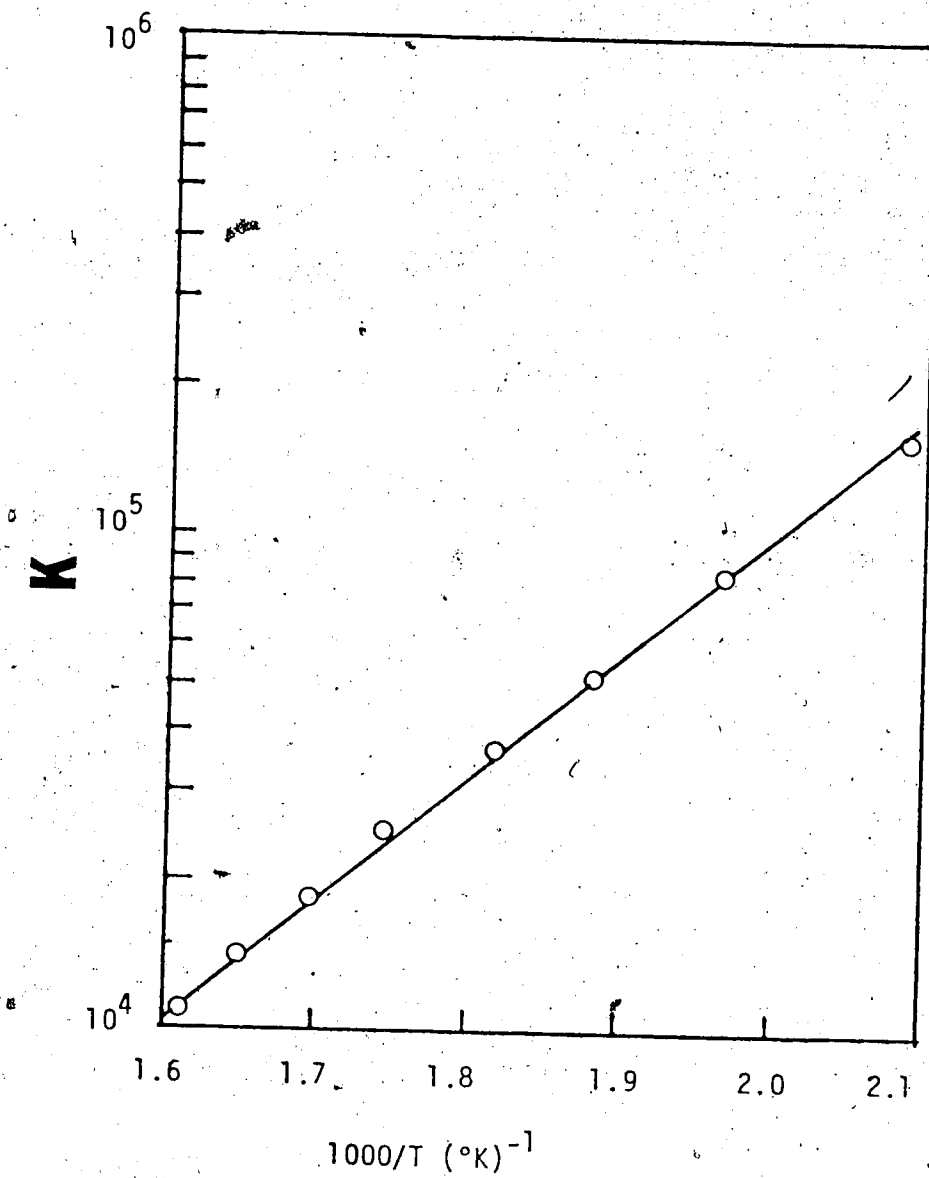
$$H^+(\text{acetone}) + \text{acetone} = H^+(\text{acetone})_2$$

FIGURE 8. 12   van't Hoff Plot for the Reaction:

$H^+(acetone)_2 + DMSO = H^+(acetone)(DMSO) + acet($
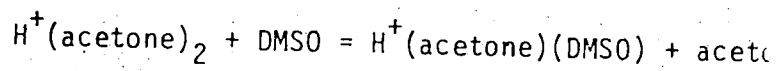
Table 8.3.   Summary of Thermodynamic Data for Protonated Clusters Involving

DMSO and Acetone[a]

Reaction

Association Reactions:

	$-\Delta H^{o}$	$-\Delta G^{o}_{298}$	$-\Delta S^{o}$
(1) $H^{+}(DMSO) + DMSO = H^{+}(DMSO)_2$	30.8 ± 0.3[b]	24.0 ± 0.3[b]	22.9 ± 0.5[b]
(2) $H^{+}(DMSO)_2 + DMSO = H^{+}(DMSO)_3$	21.3 ± 0.4	$10.9 + 0.5$	34.9 ± 1.1
(3) $H^{+}(Acetone) + Acetone = H^{+}(Acetone)_2$	30.1 ± 1.0	21.0 ± 1.2	30.4 ± 1.7
(4) $H^{+}(DMSO) + Acetone = H^{+}(DMSO)(Acetone)$	24.1 ± 0.3	16.8 ± 0.32	24.5 ± 0.5

Exchange Reactions

(5) $H^{+}(DMSO)(Acetone) + DMSO = H^{+}(DMSO)_2 + Acetone$	6.76 ± 0.07	7.25 ± 0.08	1.66 ± 0.13
(6) $H^{+}(Acetone)_2 + DMSO = H^{+}(Acetone)(DMSO) + Acetone$	11.0 ± 0.2	11.3 ± 0.3	-0.80 ± 0.44

a ΔH^{o} and ΔG^{o} values are in kcal/mole, ΔS^{o} in cal/mole °K; standard state 1 atm.

b Values calculated from those for reactions (4) and (5). All others are from directly measured equilibria as shown.

molecules. Protic molecules like H_2O have one or more acidic hydrogen capable of hydrogen-bonding with molecules which are electron-donors. Molecules like $(CH_3)_2O$, $(CH_3)_2SO$ and CH_3CN which do not have any easily dissociable acidic hydrogen are classified as aprotic molecules. Due to the presence of large permanent dipoles in molecules like $(CH_3)_2SO$ and CH_3CN, these molecules are called dipolar aprotic molecules in distinction from other aprotic molecules like $(CH_3)_2O$ which have smaller permanent dipoles. The solvation of the hydrogen ion by water and dimethyl ether has been studied by Grimsrud and Kebarle (47) from this laboratory. Recently, a similar study with acetonitrile has been reported by Meot-Ner (159). A comparison of the thermodynamic data obtained from these studies with the present results obtained with DMSO is given in table 8.4. Comparative van't Hoff plots of these results are illustrated in figure 8.13.

The $-\Delta H^0$ of the 0,1 interactions for the solvation reaction refers to the proton affinities of different sol-

$$H^+(M)_{n-1} + M = H^+(M)_n \qquad (n-1,n) \qquad (8.13)$$
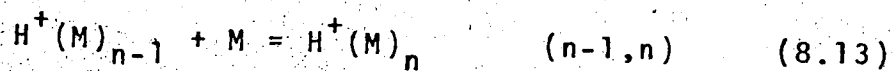
vent molecules, M. It may be seen in table 8.4 that although the proton affinity values differ by as much as 42.7 kcal/mole (PA difference between DMSO and H_2O), the $-\Delta H^0$ of the 1,2 interactions for these molecules are very similar, i.e. ~30.5 kcal/mole (see table 8.4),

Table 8.4 Comparison of Thermodynamic Data on the Solvation of the Hydrogen Ion by Different Solvent Molecules.[a]

$$H^+(M)_{n-1} + M = H^+(M)_n \quad (n-1,n)$$

n-1,n	M = H$_2$O[b]			M = (CH$_3$)$_2$O[b]			M =(CH$_3$)$_2$SO			M = CH$_3$CN[c]			M = (CH$_3$)$_2$CO		
	-ΔH°	-ΔG°	-ΔS°	-ΔH°	-ΔG°	-ΔS°	-ΔH°	-ΔG°	-ΔS°	-ΔH°	-ΔG°	-ΔS°	-ΔH°	-ΔG°	-ΔS°
0,1[d]	171.7			192.3			214.4			191.5			198.6		
1,2	31.6	24.3	24.3	30.7	21.9	29.6	30.8	24.0	22.9	30.2	21.6	29	30.1	21.0	30.4
2,3	19.5	13.0	21.9	10.1	1.9	27.6	21.3	10.9	34.9	9.3	3.6	19			
3,4	17.5	9.3	27.3												
4,5	15.3	5.5	32.6												
5,6	13.0	3.9	30.3												
6,7	11.7	2.8	29.6												
7,8	10.3	2.2	27.0												

a All values in kcal/mole except ΔS° in eu; standard state 1 atm; ΔG° values at 298°K.

b From E. P. Grimsrud and P. Kebarle, J. Am. Chem. Soc., 95, 7939 (1973).

c From M. Meot-Ner. J. Am. Chem. Soc., 100, 4694 (1978).

d PA(CH$_3$)$_2$O from R. Yamdagni and P. Kebarle, J. Am. Chem. Soc., 98, 1320 (1976); others from table 3.1. These values have been corrected for rotational symmetry: standard PA(NH$_3$) = 207.6 kcal/mole.

FIGURE 8.13 van't Hoff Plots for Gas-Phase Equilibria:

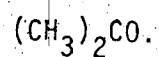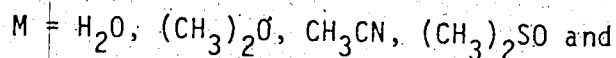$H^+(M)_{n-1} + M = H^+(M)_n$ with n. = 2, 3 and

$M = H_2O$, $(CH_3)_2O$, CH_3CN, $(CH_3)_2SO$ and

$(CH_3)_2CO$.

(-------) M = H_2O;

(—►◄—) M = CH_3CN;

(•••••••) M = $(CH_3)_2CO$

(—·—) M = $(CH_3)_2O$

(———) M = $(CH_3)_3SO$
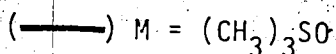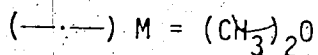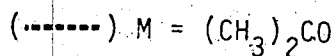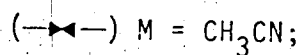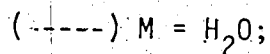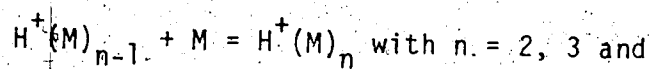
(The 2,3 plot for acetone is shown from estimate only, it is

probably inaccurate. The error bars indicate the variations

observed in the experiments, see section 8.7).
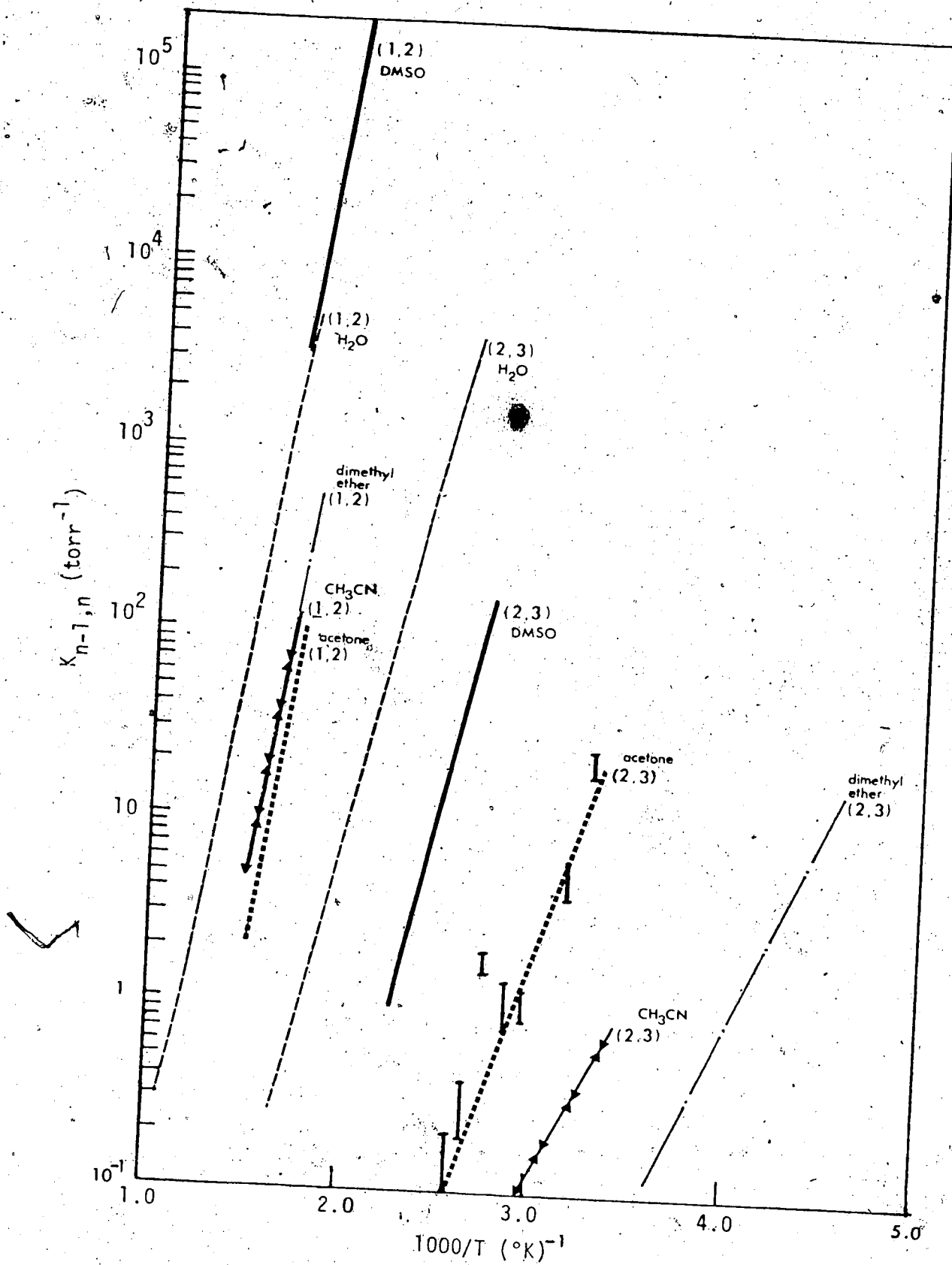
If one examines the structures of the following protonated clusters resulting from the 1,2 interaction:

$H^+(H_2O)_2$ $\qquad$ $H^+((CH_3)_2O)_2$ $\qquad$ $H^+((CH_3)_2SO)_2$ $\qquad$ $H^+(CH_3CN)_2$
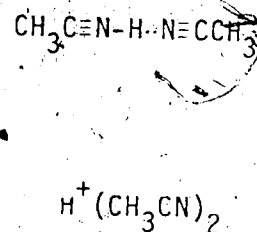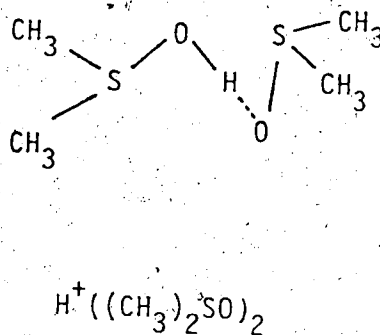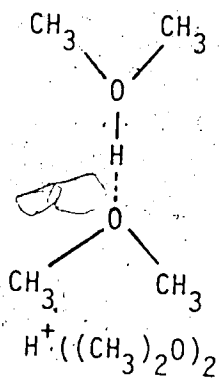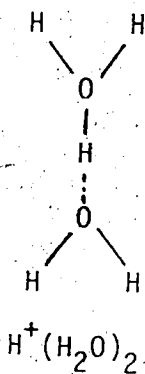
one would see that all four protonated dimers are stabilized by hydrogen bonding. The observation that the 1,2 interactions are similar for water, dimethyl ether, DMSO and acetonitrile may be explained by saying that the strength of hydrogen bonding in these protonated clusters are similar. Since the strength of the ionic hydrogen bond depends on tha partial positive charge of the participating hydrogen on the ion and the availability of the lone-pair electron from the additional molecule, one may hasten to draw the conclusion that the partial positive charges on the hydrogens in all four protonated monomers are similar. This is not necessarily so, the dipole moments (160) of DMSO (3.96D) and acetonitrile (3.92D) are much larger than those of water (1.85D) and dimethyl ether (1.30D). The resulting ionic hydrogen bonds within the $H^+(DMSO)_2$ and $H^+(CH_3CN)_2$ clusters are strengthened more by the ion-dipolar interactions. This effect may be visualized as the

better availability of the electron lone-pair from the oxygen of DMSO and the nitrogen of acetonitrile, since a large fraction of the permanent dipoles of DMSO and acetonitrile are located in the SO and CN group, respectively. This may suggest that while the partial positive charge on the hydrogen is similar in the protonated water and the protonated dimethyl ether, it is probably less in the protonated DMSO and the protonated acetonitrile. It may be interesting to point out here that, from the results of studies by Yamdagni and Kebarle (2), the strength of bonding in the nitrogen bases $R_3N---H^+---NR_3$ does not depend much on the substituents R, and it is lower than that of the $R_2O---H^+---OR_2$ system. Thus, the nature of the basic atom O or N in the bases seems decisive in determining the stabilities of the protonated symmetric dimers.

Very drastic differences are observed among the 2,3 interactions for water, dimethyl ether, DMSO and acetonitrile. The $\Delta H^0_{2,3}$ values for the four solvent molecules may be roughly divided into two groups. H_2O and DMSO have higher $-\Delta H^0_{2,3}$ values (~20 kcal/mole) indicating the presence of stronger external stabilization. The $-\Delta H^0_{2,3}$ for dimethyl ether and acetonitrile are lower and of similar magnitude (~10 kcal/mole). The explanation offered by Kebarle (47) for the difference in $-\Delta H^0_{2,3}$ values for water and dimethyl ether is the absence of hydrogen bonding in the 2,3 interaction for dimethyl

ether. This is very reasonable if one examines the structures of the following protonated clusters:

$$H^+(H_2O)_3 \qquad\qquad H^+((CH_3)_2O)_3$$
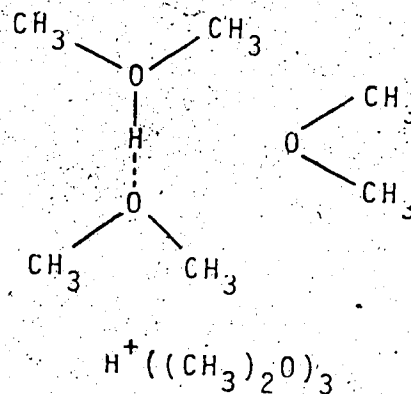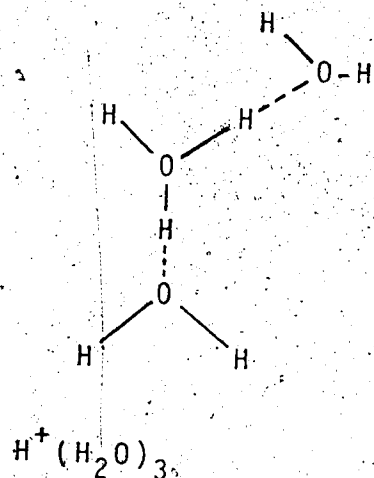
The addition of the third H_2O molecule to the $H^+(H_2O)_2$ ion can still be stabilized by a strong hydrogen bond although the strength of the H-bond would be a little weaker than the first one because the partial positive charge on the hydrogen of the $H^+(H_2O)_2$ is less than that of H_3O^+. But for $H^+(CH_3OCH_3)_2$, due to the complete blockage of H-bonding sites by the methyl groups, the only stabilization for a further addition of $(CH_3)_2O$ molecule is the ion-dipolar interactions. The significance of hydrobeng bonding in the stability of the protonated clusters may be illustrated by the results that $-\Delta H^0_{2,3}$ value for water is higher than that for dimethyl ether by 9.4 kcal/mole. The same reasoning was used by Meot-Ner (159) in explaining the lower $-\Delta H^0_{2,3}$ value for CH_3CN relative to that for H_2O, since only ion-dipolar forces are operative in the association of $H^+(CH_3CN)_2$ with the

third CH_3CN molecule.

According to the reasoning given above, it would be expected that the 2,3 interaction for DMSO should be similar to those of dimethyl ether and acetonitrile. The inner solvation "shell" of H^+ is completely filled by the addition of two DMSO molecules. Further addition of a DMSO molecule, if it goes to the next solvation "shell" of the H^+ ion, would be stabilized just by "physical" solvation between the ion and the neutral molecule, the same as in the case of dimethyl ether and acetonitrile. The present results (see table 8.4) show that the $-\Delta H^0_{2,3}$ value for DMSO is 21.3 kcal/mole, much higher than those for dimethyl ether and acetonitrile (~10 kcal/mole). This suggests that the stabilization forces for the $H^+(DMSO)_3$ cluster are different from those for the $H^+(CH_3OCH_3)_3$ and the $H^+(CH_3CN)_3$ clusters. Since H-bonding is not possible in the 2,3 interactions for all three cases, the higher $-\Delta H^0_{2,3}$ value for DMSO probably comes from higher ion-dipolar stabilization. The higher ion-dipolar stabilization cannot be explained simply on the basis that DMSO has a large permanent dipole in the SO group. If the permanent dipole of the solvent molecule is the only governing factor, the 2,3 interactions for DMSO and acetonitrile would be similar, since the dipole moment of acetonitrile (3.92D) is as large as that of DMSO (3.96D). This leads to the suggestion that the

higher ion-dipolar interactions between $H^+(DMSO)_2$ and DMSO is a result of the alignment of the permanent dipole in DMSO with a specific site in the $H^+(DMSO)_2$ ion which carries a large partial positive charge. It may be expected that considerable partial positive charge would locate in the sulfur atom in the protonated DMSO. As DMSO has a pyramidal structure I (161), the alignment for such ion dipolar inter-
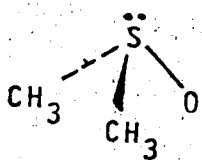
(I)

action resulting in a chain like structure II for $H^+(DMSO)_3$ has little steric hindrance.
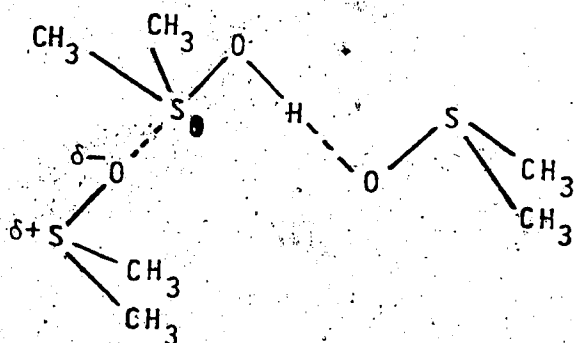
(II)

The reason for the weaker 2,3 interactions in acetonitrile even though it has a large permanent dipole probably lies in the fact that no strong partial positive charge is localized on the unsaturated carbon atom in the protonated acetonitrile. This results in much weaker ion-dipolar interaction similar to the case of $H^+(CH_3OCH_3)_3$.

The above explanation is supported by the experimental $\Delta S^0_{2,3}$ value for DMSO. In comparing the $\Delta S^0_{n-1,n}$ values for H_2O, $(CH_3)_2O$, $(CH_3)_2SO$ and CH_3CN in table 8.4, it is observed that there is a steady decrease going from $-\Delta S^0_{1,2}$ to $-\Delta S^0_{2,3}$ ($\Delta = -\Delta S^0_{1,2} + \Delta S^0_{2,3}$) in water ($\Delta = 2.4$ eu), dimethyl ether ($\Delta = 2.0$ eu) and acetonitrile ($\Delta = 10$ eu), but for DMSO, the $-\Delta S^0_{2,3}$ is much higher than $-\Delta S^0_{1,2}$, $\Delta = -12$ eu. The decrease in the entropy change probably reflects the tightening of the $H^+(DMSO)_3$ cluster through the alignment of all three DMSO molecules around the proton. The entropy change of a clustering reaction such as reaction 8.10 may be represented as the sum of contributions from
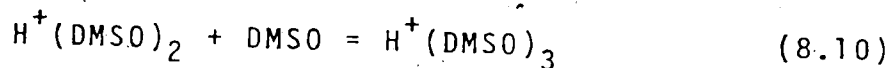
$$H^+(DMSO)_2 + DMSO = H^+(DMSO)_3 \qquad (8.10)$$

translational, rotational and vibrational entropy changes:

$$\Delta S^0 = \Delta S^0_{trans} + \Delta S^0_{rot} + \Delta S^0_{vib} \qquad (8.14)$$

The contribution of ΔS^0_{trans} is the predominant term and is always negative in magnitude due to the loss of freedom in associating a molecule to the growing cluster. The sum of ΔS^0_{rot} and ΔS^0_{vib} is usually much smaller and it tends to be positive due to the increase of the moments of inertia and the increase of vibrational modes in the larger cluster. Therefore, $-\Delta S^0_{trans}$ may be used as the maximum limit of $-\Delta S^0$ for comparing with the experimental $-\Delta S^0$ for clustering reaction. The translational entropy of a

molecule with molecular weight M is given by the Sackur-
Tetrode equation (162):

$$S^o_{trans} = 3/2 R \ln M + \frac{5}{2} R \ln T - 2.311 \qquad (8.15)$$

It follows that for the association reaction 8.10, the
translational entropy change could be written as:

$$\Delta S^o_{trans} = \frac{3}{2} R \ln \frac{M_{H^+(DMSO)_3}}{M_{H^+(DMSO)_2} M_{DMSO}} - \frac{5}{2} R \ln T + 2.311 \qquad (8.16)$$

where M are the corresponding molecular weights. Equation
8.16 gives a value of $\Delta S^o_{trans}(298°K) = -37.8$ cal $°K^{-1}$
mole^{-1}. Comparing with the experimental $\Delta S^o = -34.9$ cal
$°K^{-1}$ mole^{-1}, the increase in rotational and vibrational
entropies of the 2,3 interaction for DMSO is just 2.9 cal
$°K^{-1}$ mole^{-1}. Similar calculation for dimethyl ether
yields $\Delta S^o_{trans}(298°K) = -36.3$ cal $°K^{-1}$ mole^{-1}. Comparing
with the corresponding experimental $\Delta S^o = -27.6$ cal $°K^{-1}$
mole^{-1}, the difference is 8.9 cal $°K^{-1}$ mole^{-1}. The rela-
tively small increase in rotational and vibrational entro-
pies is expected for reaction 8.10, since the proposed
rigid structure of $H^+(DMSO)_3$ is more tightly bound than
the corresponding $H^+(CH_3OCH_3)_3$ ion.

It is interesting to note that the $-\Delta H^o_{2,3}$ value for
DMSO (21.3 kcal/mole) is even slightly higher than that
for H_2O (19.5 kcal/mole). It shows that under favorable
conditions, the ion-dipolar interactions can be as effec-

tive as hydrogen bonding in the stabilization of the pro-
tonated clusters. In passing, it should also be mentioned
that in solution, the strong molecular association of DMSO
by dipole-dipole interactions is also comparable with
that of water which owes its highly associative properties
to strong hydrogen bonding. This is evident from the
ΔH^0_{evap} values (163) of DMSO (12.6 kcal/mole) and H_2O
(10.5 kcal/mole).

8.5   Single Ion Solvation in the Gas Phase and in the
       Liquid Phase.

The solvation of the hydrogen ion by DMSO in the
gas phase and the liquid phase may be considered in the
following manner. The enthalpy of ion solvation measured
in the gas phase, $\Delta H^\circ_{0,n}$, as shown in reaction 8.17, can

$$H^+(DMSO)_{n-1} + DMSO = H^+(DMSO)_n \quad \Delta H^0_{n-1,n} \quad (8.17)$$
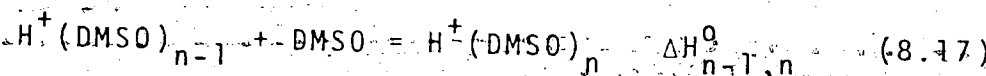
$$\Delta H^0_{0,n} = \sum_1^n \Delta H^0_{n-1,n} \quad (8.18)$$

be expressed in terms of successive values of $\Delta H^0_{n-1,n}$.
The enthalpy of ion solvation in the liquid phase,
$\Delta H_{tr}{}^{g \to DMSO}(H^+)$, is conventionally expressed as that cor-
responding to putting the ion into the bulk liquid as
illustrated in figure 8.14A. (i.e. H^+ is dipped into
liquid DMSO). An alternate process leading to
$\Delta H_{tr}{}^{g \to DMSO}(H^+)$ would be to evaporate DMSO molecules from

(A)

$\Delta H_{tr}^{g \rightarrow DMSO} (H^+)$
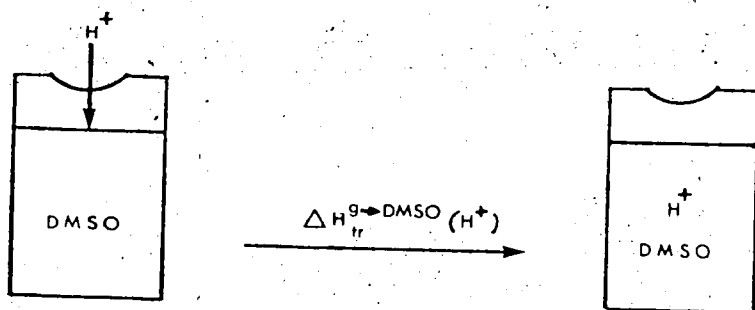
Conventional Representation
Ion is dipped into the
liquid

(B)
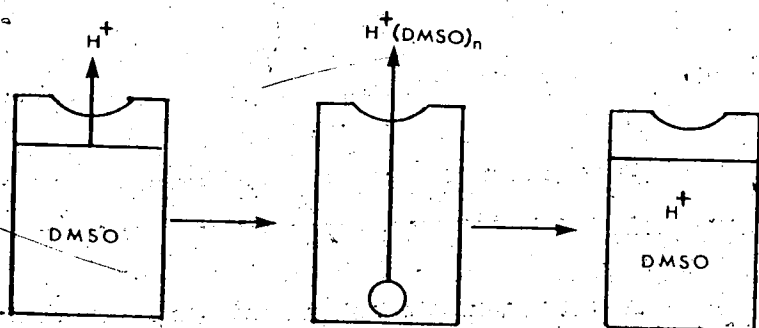
Equivalent Representation
DMSO molecules are
evaporated from liquid
DMSO and added to the
ion, the process is
continued until all DMSO
molecules in the bulk
liquid have been trans-
ferred to the ion.

$$\Delta H_{tr}^{g \rightarrow DMSO} = \sum_{2}^{n} \Delta H_{n,n-1}^{o} (DMSO)_n + \sum_{1}^{n} \Delta H_{n-1,n}^{o} (H^+(DMSO)_n)$$

$$= \sum_{2}^{n} \Delta H_{n,n-1}^{o} (DMSO)_n - \sum_{1}^{n} \Delta H_{n,n-1}^{o} (H^+(DMSO)_n)$$

<u>FIGURE 8.14</u>   Single Ion Solvation in Liquid

liquid DMSO and add them to the hydrogen ion until all DMSO molecules in the bulk liquid have been transferred to the ion. This process is pictorially illustrated in figure 8.14B. Based on the latter representation, the ion solvation enthalpy in the liquid phase, $\Delta H_{tr}^{g \rightarrow DMSO}(H^+)$, may be expressed as the sum of two terms: (a) the summation of the enthalpy change corresponding to splitting one DMSO molecule from n DMSO molecules, $\sum_{2}^{n} \Delta H_{n-1,n}^{o}$ $(DMSO)_n$; (b) the summation of the enthalpy changes of stepwise additions of DMSO molecules to the hydrogen ion, $\sum_{1}^{n} \Delta H_{n-1,n}^{o}(H^+(DMSO)_n)$.

$$\Delta H_{tr}^{g \rightarrow DMSO}(H^+) = \sum_{2}^{n} \Delta H_{n,n-1}^{o}(DMSO)_n - \sum_{1}^{n} \Delta H_{n,n-1}^{o}(H^+(DMSO)_n) \quad (8.19)$$

The first term in equation 8.19 deserves some comments. The value of $\Delta H_{n,n-1}^{o}(DMSO)_n$ is equal to the heat of vaporation of DMSO, $\Delta H_{vap}^{o}(DMSO)$, only when n is very large (DMSO as bulk liquid). When n is small, $\Delta H_{n,n-1}^{o}(DMSO)_n < \Delta H_{vap}^{o}(DMSO)$. This may be visualized from the fact that it is much easier to separate one DMSO molecule from two DMSO molecules than from a large number of DMSO molecules. Therefore, equation 8.20 always holds. On examining the two components in the

$$\sum_{2}^{n} \Delta H_{n,n-1}^{o}(DMSO)_n < (n-1) \Delta H_{vap}^{o}(DMSO) \quad (8.20)$$

right-hand side of equation 8.19, it is noted that, when

n is small, $\Delta H^{o}_{n,n-1}(H^{+}(DMSO)_n)$ is much greater than

$\Delta H^{o}_{n,n-1}(DMSO)$. When n is very large (i.e. $(DMSO)_n$ and

$H^{+}(DMSO)_n$ exist as a large liquid droplet), both

$\Delta H^{o}_{n,n-1}(DMSO)$ and $\Delta H^{o}_{n,n-1}(H^{+}(DMSO)_n)$ approach the value

of $\Delta H^{o}_{vap}(DMSO)$. This is because as n increases to a

very large number, the ionic charge in the resulting cluster

$H^{+}(DMSO)_n$ is shielded more and more by the DMSO mole-

cules. Eventually, the cluster $H^{+}(DMSO)_n$ would approach

a large liquid droplet and the presence of the ionic

charge has minimal effects on the removal or the addi-

tion of one DMSO molecule from or to the DMSO liquid

droplet (164). Thus, further addition of DMSO molecule

has little effect on the $\Delta H_{tr}^{g \rightarrow DMSO}(H^{+})$ value, and it

becomes constant theoretically when n = ∞.

The solvation energy of hydrogen ion in liquid

DMSO was studied by Benoit (165). A value $\Delta H_{tr}^{g \rightarrow DMSO}$

(H^{+}) = -276.1 kcal/mole was reported. Direct quantita-

tive comparisons between $\Delta H_{tr}^{g \rightarrow DMSO}(H^{+})$ and $\Delta H^{o}_{0,n}(H^{+}$

$(DMSO)_n)$ in this case are not possible. This is be-

cause the $\Delta H^{o}_{n,n-1}(H^{+}(DMSO)_n)$ values were only deter-

mined up to n = 3 in the present study. The ion trans-

mission efficiency of the present quadrupole mass

spectrometer starts to drop tremendously for ions with

m/e > 250 (see figures 2.10 and 2.11), leading to

insufficient sensitivity for the detection of ions

with higher masses (m/e for $H^+(DMSO)_4$ = 313). But qualitative comparison can be made by observing that the second term in equation 8.19 is the dominating term relative to the first term (i.e. $\Delta H^o_{vap}(DMSO)$ = -12.6 kcal/mole (163)). By comparing the present value $\sum_{n=1}^{3} \Delta H^o_{n,n-1}$ $(H^+(DMSO)_n)$ = -266.5 kcal/mole (table 8.4) with the value $\Delta H_{tr}^{g \rightarrow DMSO}(H^+)$ = -276.1 kcal/mole, it is justified to say that a large part of $\Delta H_{tr}^{g \rightarrow DMSO}(H^+)$ can be accounted for by the association of the hydrogen ion with a few DMSO molecules. It may be expected that the solvation of an ion by liquid solvent can be qualitatively studied with models based on the interactions of the ion with only a few solvent molecules.

8.6 Proton Affinity Difference Between DMSO and Acetone.

The gas-phase basicity difference between DMSO and acetone has been determined earlier from the multicycles of proton transfer reactions (see table 3.1). A value of $-\Delta G^o_{600}$ = 15.0 kcal/mole was obtained for the reaction 8.21. The enthalpy change of the reaction

$$H^+(acetone) + DMSO = acetone + H^+(DMSO) \qquad (8.21)$$
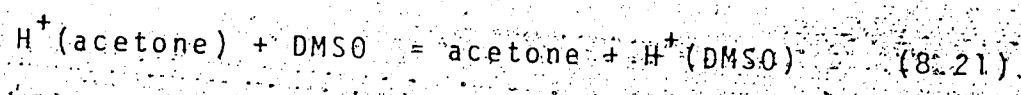
may be calculated by correcting for the entropy term, $T\Delta S^o$, of the reaction. An estimate of $T\Delta S^o_{rot.s}$ = $RT\ln(\frac{1}{2})$ = 0.8 kcal/mole is obtained by considering the changes in rotational symmetry number for reaction 8.21.

This leads to $-\Delta H^O = 15.8$ kcal/mole for the reaction, i.e. the proton affinity difference between DMSO and acetone is 15.8 kcal/mole.

The proton affinity difference between DMSO and acetone may also be obtained indirectly from the results of present determinations through the following thermodynamic cycle:

$$H^+(acetone) + acetone = H^+(acetone)_2 \qquad (8.11)$$
$$H^+(acetone)_2 + DMSO = H^+(acetone)(DMSO) + acetone \qquad (8.12)$$
$$H^+(acetone)(DMSO) = H^+(DMSO) + acetone \qquad (8.6)$$

$$\overline{\qquad\qquad\qquad\qquad\qquad\qquad\qquad\qquad\qquad\qquad}$$

$$H^+(acetone) + DMSO = acetone + H^+(DMSO) \qquad (8.21)$$
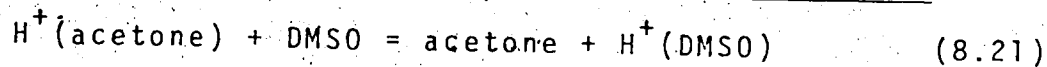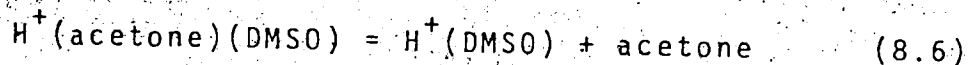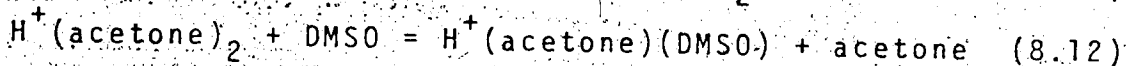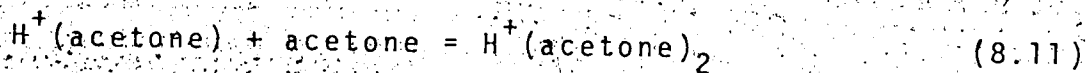
The thermodynamic data for reactions 8.11, 8.12 and 8.6 were tabulated in table 8.3 and are illustrated in figure 8.15. The results of the above thermodynamic cycle lead to the values of $-\Delta H^O = 17.0 \pm 1.1$ kcal/mole, $-\Delta G^O_{298} = 15.5 \pm 1.3$ kcal/mole and $-\Delta S^O = 5.1 \pm 1.8$ eu for reaction 8.21. The good agreement in the proton affinity difference between DMSO and acetone as determined from solvation study (17.0 $\pm$ 1.1 kcal/mole) and by direct proton-transfer reactions (15.8 $\pm$ 0.2 kcal/mole) may be taken as a proof of the thermodynamic consistency of the results obtained from studies of ion-molecule reactions by the high pressure mass spectrometric method in this laboratory. The standard entropy change for

FIGURE 8.15 - Thermodynamic Data for Addition and Exchange Reactions of Protonated Clusters Involving DMSO and Acetone.[a]

Enthalpy Changes ($-\Delta H^o$ are shown)
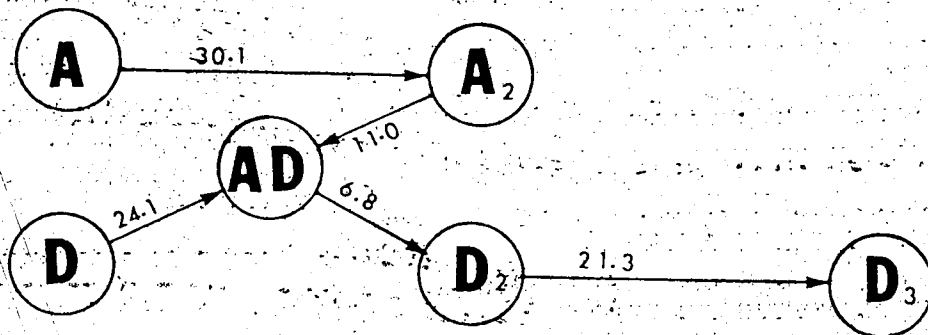
Free Energy Changes ($-\Delta G^o_{298}$ are shown)
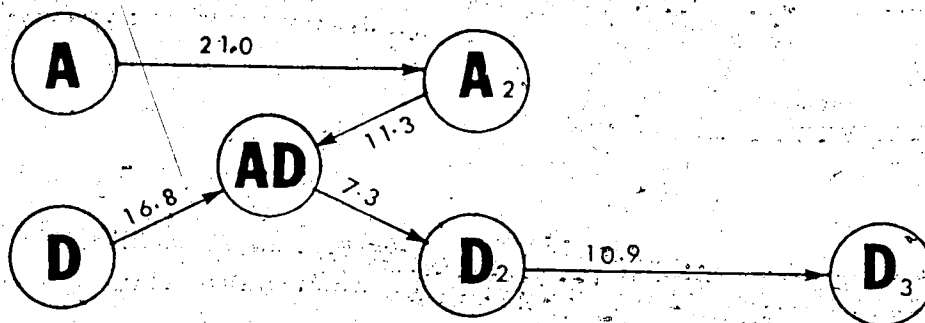
Entropy Changes ($-\Delta S^o$ are shown)
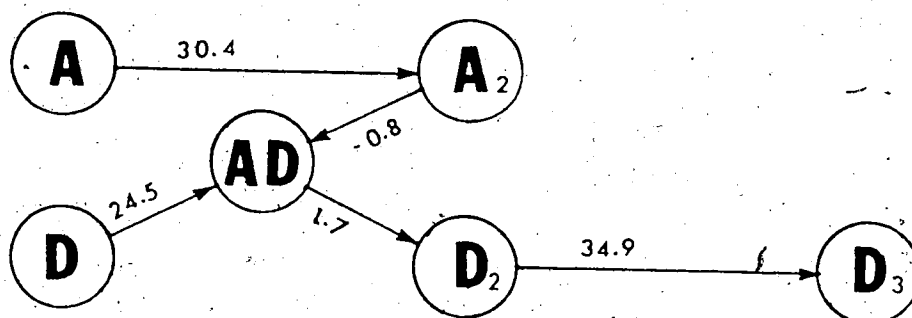
[a] A = acetone, D = DMSO; the proton is omitted from the clusters. Example: A → A_2 refers to the reaction $H^+(A) + A = H^+(A)_2$. ΔG^o and ΔH^o values are in kcal/mole, ΔS^o in eu, standard state 1 atm.

reaction 8.21 as obtained from the thermodynamic cycle ($\Delta S^0 = -5.1 + 1.8$ eu) is somewhat more negative than that estimated from rotational symmetry numbers ($\Delta S^0_{rot} = -1.4$ eu). Part of the difference must be due to the larger uncertainty imparted on the values of ΔS^0 for the clustering reactions. Very often, the extrapolations from narrow temperature ranges in the van't Hoff plots limit the accuracy of the experimental ΔS^0 values. Further, the ΔS^0 for reaction 8.21 obtained from the thermodynamic cycle (reactions 8.10, 8.12 and 8.6) may include cumulative errors of the experimental determinations. Therefore, the $\Delta S^0 = -5.1$ eu for reaction 8.21 from the cycle needs not be more accurate than the estimated value based on rotational entropy changes alone.

8.7 The Elimination of Water from H^+ (Acetone)$_3$

The 2,3 interaction for acetone relating to the equilibrium:

$$H^+(acetone)_2 + acetone = H^+(acetone)_3 \qquad (8.22)$$
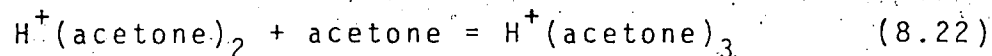
was also investigated. Unfortunately, attempts to measure the equilibrium constants for reaction 8.22 were not successful. The system was studied in the temperature range of 30°C-140°C with the appropriate acetone concentrations (40×10^{-3} torr - 3 torr) necessary for an observed equilibrium ion ratio of $[H^+(acetone)_3] / [H^+(acetone)_2] < 0.2$. It was observed that although

"apparent" stationary ion ratios of $[H^+(acetone)_3]/$ $[H^+(acetone)_2]$ were obtained in individual runs, the equilibrium constants calculated from these ion ratios decreased with an increase of ion source pressure. In some cases, the calculated equilibrium constants decreased by a factor of about 3 when the ion source pressure was increased from 1 torr to 4 torr. A summary of the results are presented in a van't Hoff plot in figure 8.13. A $\Delta H^\circ_{2,3} \simeq -12$ kcal/mole was estimated for reaction 8.22. The results probably are inaccurate, and it is presented only for the purpose of showing where the equilibrium constants at different temperatures are approximately located. It was also noted that under the conditions of the present experiments, ions of m/e ratio equal to 157 and 131 were presented in significant amounts besides the two major ions of interest: $H^+(acetone)_3$, m/e = 175 and $H^+(acetone)_2$, m/e = 117. The ion of m/e = 157 probably corresponds to the ion formed by the elimination of a water molecule from $H^+(acetone)_3$, while m/e = 131 may be due to $CH_3^+(acetone)_2$. Futrell and MacNeil (166) in the study of the ion-molecule reactions of gaseous acetone, reported the formation of $H^+(CH_3COCH_3)_n$, $CH_3^+(CH_3COCH_3)_n$, $CH_3CO^+(CH_3COCH_3)_n$ and $H^+(CH_3COCH_3)_n-H_2O$ as second-order or higher order ions formed with an ion source pressure of 10^{-2} torr - 0.6 torr acetone. Unfortunately, little

information was given regarding to the formation of these species.

It is interesting to note that under the present high ion source pressure conditions, the water elimination from $H^+(acetone)_2$ was not observed in any significant extent even though the equilibrium 8.11 was studied at

$$H^+(acetone) + acetone = H^+(acetone)_2 \qquad (8.11)$$
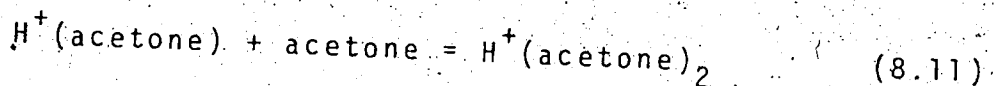
a higher temperature. The observation of the elimination of water from $H^+(acetone)_3$ as in reaction 8.23 suggests

$$H^+(CH_3COCH_3)_3 = C_9H_{17}O_2^+ + H_2O \qquad (8.23)$$
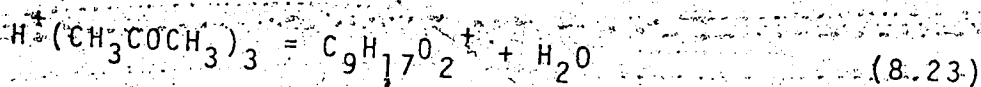
that the third acetone molecule may be necessary for the mechanism for the water elimination in the dilute gas phase. In aqueous solution, similar dehydration reaction is known to occur following the acid catalyzed aldol condensation reaction involving two acetone molecules. A mechanism for the dehydration of protonated acetone clusters in the gas phase analogous to that in solution given by Streitwieser and Heathcock (149, p.553) may be written as follows:

Step 1 Protonation of acetone

$$CH_3-\overset{\overset{\displaystyle O}{\|}}{C}-CH_3 + H^+ = CH_3-\overset{\overset{\displaystyle +OH}{\|}}{C}-CH_3 \longleftrightarrow CH_3-\overset{\overset{\displaystyle H}{\overset{\displaystyle O}{|}}}{\underset{\displaystyle +}{C}}-CH_3 \qquad (8.24)$$
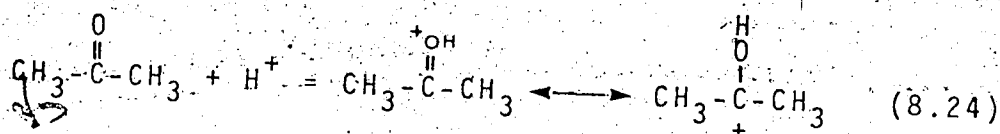
Step 2   Proton transfer to another acetone (acid cata-
lyzed formation of enol from keto form)

$$\underset{CH_3}{\overset{CH_3}{>}}C=\ddot{O} \;+\; H-CH_2-\underset{+}{\overset{\overset{H}{\overset{|}{O}}}{C}}-CH_3 \;=\; \underset{CH_3}{\overset{CH_3}{>}}C=OH^+ \;+\; CH_2=\overset{\overset{H}{\overset{|}{O}}}{C}-CH_3 \qquad (8.25)$$
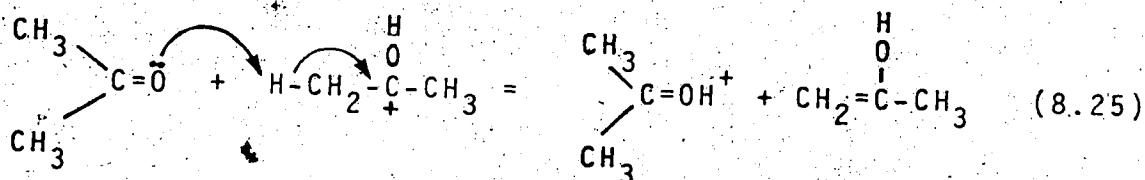
Step 3   Addition of acetone in enol form to another
protonated acetone

$$\underset{\underset{CH_3}{\overset{|}{}}\;\;\underset{CH_3}{\overset{|}{}}}{\overset{\overset{+}{\overset{|}{OH}}}{\underset{}{C}}} \;+\; \overset{\overset{:OH}{\overset{||}{}}}{CH_2=C-CH_3} \;=\; CH_3-\underset{\overset{|}{CH_3}}{\overset{\overset{OH}{\overset{|}{}}}{C}}-CH_2-\overset{\overset{+OH}{\overset{|}{}}}{C}-CH_3 \qquad (8.26)$$

$$(I)$$
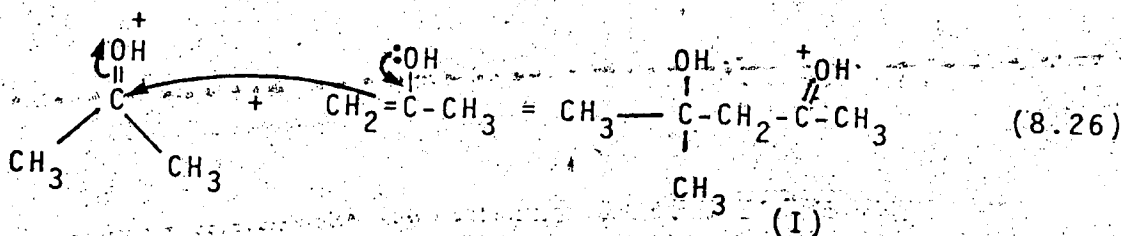
Step 4   Abstract of the proton by a BASE to give the
enol form of diacetone alcohol

$$CH_3-\underset{\overset{|}{CH_3}}{\overset{\overset{OH}{\overset{|}{}}}{C}}-CH_2-\overset{\overset{+OH}{\overset{||}{}}}{C}-CH_3 \;\rightleftharpoons\; CH_3-\underset{\overset{|}{CH_3}}{\overset{\overset{OH}{\overset{|}{}}}{C}}-CH=\overset{\overset{OH}{\overset{|}{}}}{C}-CH_3 \;+\; H^+ \qquad (8.27)$$

$$(I) \qquad\qquad\qquad (II)$$
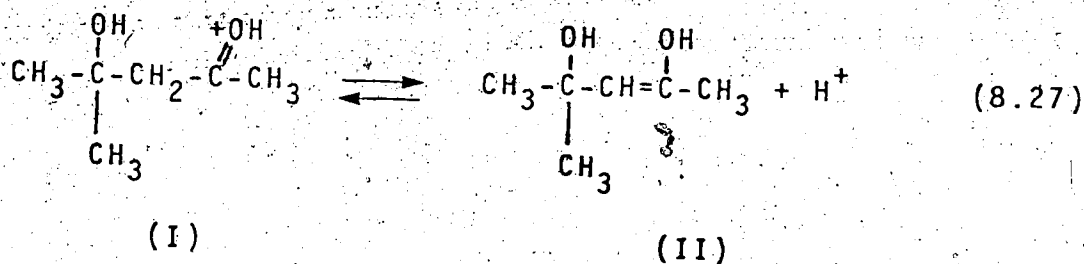
Step 5   Protonation of the tert-OH group followed by
water elimination, resulting in an oxonium ion
(III) which is resonance stabilized.

$$CH_3-\underset{\underset{CH_3}{|}}{\overset{\overset{OH}{|}}{C}}-CH=\overset{\overset{OH}{|}}{C}-CH_3 + H^+ \;=\; CH_3-\underset{\underset{CH_3}{|}}{\overset{\overset{+OH_2}{|}}{C}}-CH=\overset{\overset{OH}{|}}{C}-CH_3$$

(II) (III) (8.28)

$$CH_3-\underset{\underset{CH_3}{|}}{C}=CH-\overset{\overset{+OH}{\parallel}}{C}-CH_3 + H_2O$$

(IV)
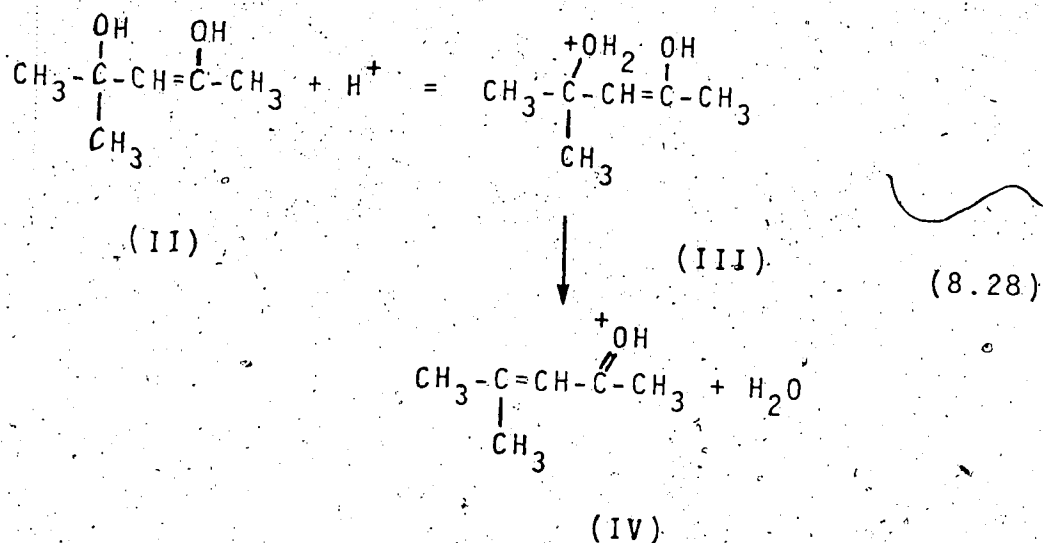
The formation of the protonated aldol condensation product (structure I) involves the addition of the enol form of acetone to another protonated acetone (step 3). It is interesting to note that in this classical physical organic mechanism, the elimination of water is achieved by having a base B as an intermediate in steps 4 and 5. The base B abstracts the proton from the methylene group of I in step 4, forming BH^+ and II. In step 5, BH^+ protonates the tertiary OH group of II forming III. It is followed by the dehydration of III yielding the ion IV which is resonance stabilized. In solution, H_2O serves as the base B for the above reactions. In the dilute gas phase where the solvent is absent, a third acetone "buffer" molecule serving as the base B might be necessary for the elimination of water molecule from the protonated acetone clusters.

Another possible explanation for the absence of dehydration from the protonated acetone dimer in the

gas phase is that $H^+(acetone)_2$ probably has the structure V rather than I in the absence of solvation effects,

$$CH_3 \quad\quad\quad\quad\quad\quad\quad\quad CH_3$$
$$\diagdown\diagup$$
$$C=O---H^+---O=C$$
$$\diagup\diagdown$$
$$CH_3 \quad\quad\quad\quad\quad\quad\quad\quad CH_2$$

(V)
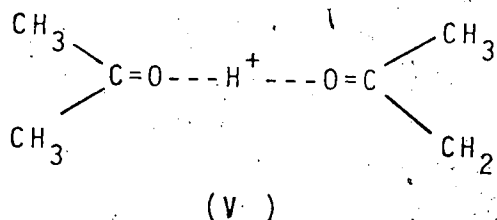
taking the advantages of the strong hydrogen bonds thus formed. As for $H^+(acetone)_3$, since there is no additional H-bonding site for the third incoming acetone molecule, the stabilization of the 2,3 interaction may be by "physical" ion-dipolar solvation or the interaction between the third acetone molecule with the acidic hydrogens of a methyl group in $H^+(acetone)_2$. The observation of the dehydration of $H^+(acetone)_3$ suggests the latter interaction is probably operative:

(8.29)

(VI)
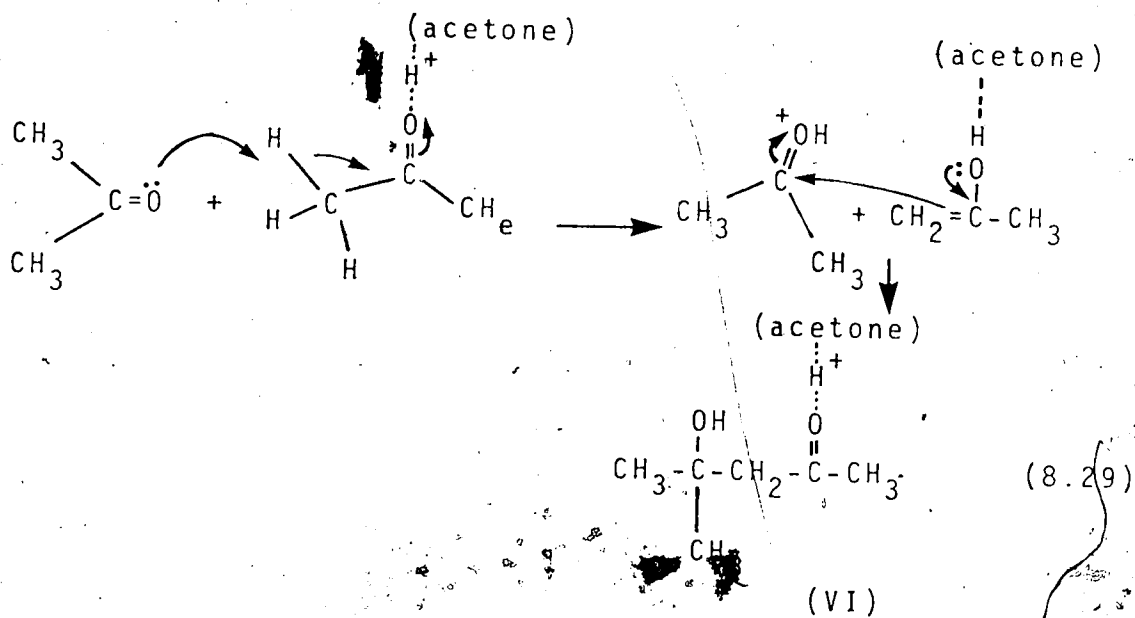
The resulting $H^+(acetone)_3$ with structure VI in analogy to I is capable of undergoing dehydration since a "buffer" acetone molecule within the ion can serve as the intermediate base required in step 4 of the proposed mechanism (reaction 8.27).

The interaction with the acidic hydrogens (reaction 8.29) has to be energetically more favorable than the ion-dipolar interaction in $H^+(acetone)_3$ in order for it to occur. It may then be expected that the $-\Delta H^0_{2,3}$ for acetone would be higher than that for CH_3OCH_3 $(-\Delta H^0_{2,3} = 10.1$ kcal/mole) and for CH_3CN $(-\Delta H^0_{2,3} = 9.3$ kcal/mole) where ion-dipolar interaction was thought to be predominant. The present estimate of $-\Delta H^0_{2,3} \approx 12$ kcal/mole may be in line with the above reasoning. Since the uncertainties in the present estimate are large, a firm conclusion can only be drawn after a more accurate $\Delta H^0_{2,3}$ value is determined for acetone.

In order to be able to measure the equilibrium constant for reaction 8.22 directly, the rates of other

$$H^+(acetone)_2 + acetone = H^+(acetone)_3 \qquad (8.22)$$
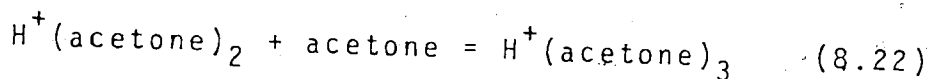
competitive reactions have to be slow relative to those of the forward and reverse reaction 8.20. Reaction 8.23

$$H^+(CH_3COCH_3)_3 = C_9H_{17}O_2^+ + H_2O \qquad (8.23)$$
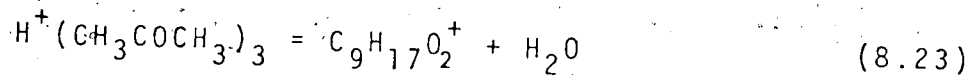
leading to the elimination of water from $H^+(acetone)_3$

probably requires some activation energies since scramb-
ling of atoms within the complex is required. If the
free energy of activation of the decomposition reaction
is larger than that of the reverse reaction 8.22, this
could probably be achieved by lowering the temperature.
Unfortunately, the present ion source does not have the
provisions for lowering its temperature below room tem-
perature. It is possible that with a low-temperature
ion source whose temperature can be regulated by a
circulating coolant, the equilibrium 8.22 could be
studied without the interference of the decomposition
reaction.

SUGGESTIONS FOR FURTHER WORK

CHAPTER IX

Most of the present equilibrium measurements for proton transfer reactions were carried out at a single temperature (600°K). This allowed the tabulation of a relative gas-phase basicity scale as expressed by the ΔG^0_{600} values of the proton transfer reactions (see table 3.1). The proton affinities of different compounds were obtained by choosing the external standard, PA(isobutane) = 198.2 kcal/mole (see table 3.55) and converting ΔG^0 to ΔH^0 with the assumption that ΔS^0 for proton transfer reaction can be estimated entirely on the basis of rotational symmetry numbers. Recently, it was suggested by Lias and Ausloos (167-171) that a more accurate estimation of the entropy change for ion-molecule equilibria should also take into account the effect of intermolecular forces experienced by the ions and molecules which undergo reaction. Lias and Ausloos (167-171) showed that the intermolecular contribution to entropy change, $\Delta S^0_{intermolecular}$, may be estimated from the expression:

$$\Delta S^0_{intermolecular} = R \ln Z_f / Z_r \qquad (9.1)$$

where Z_f and Z_r are the forward and reverse ion-molecule

collision rate constants. For non-polar molecules, the ion-molecule collision rate constant Z may be estimated approximately by the Langevin-Gromousis-Stevenson formation 1.6 (13), where q is the charge on the electron,

$$Z = 2\pi q \left(\frac{\alpha}{\mu}\right)^{\frac{1}{2}} \qquad (1.6)$$

α the polarizability of the molecule and μ the reduced mass of the colliding pair. For reactions involving molecules having a permanent dipole moment μ_D, an estimate of Z may be obtained from the Average Dipole Orientation (ADO) theory derived by Bower and Su (172):

$$Z = \frac{2\pi q}{\mu^{\frac{1}{2}}}\left[\alpha^{\frac{1}{2}} + c\mu_D \left(\frac{2}{\pi kT}\right)^{\frac{1}{2}}\right] \qquad (9.2)$$

where c is a parameter having values between 0 and 1 which is a function of $\mu_D/(\alpha)^{\frac{1}{2}}$. Although it has been pointed out by Ausloss and Lias (167) that the ΔS^o intermolecular term is usually small (<3 eu) for proton transfer reactions, it would be interesting to find out if the inclusion of ΔS^o intermolecular in the entropy correction as in equation 9.3 would give a more

$$\Delta S^o \text{(proton transfer)} \simeq \Delta S^o_{rot.s.} + \Delta S^o \text{ intermolecular} \qquad (9.3)$$

accurate prediction of the experimental ΔS^o for proton transfer reactions. At present, most of the supporting experimental ΔS^o results were determined within a small temperature range (300-400°K) by ICR method (171). As mentioned in chapter III, the experi-

mental determinations of small ΔS^o values over a limited temperature range may have large uncertainties. Unfortunately, measurements of proton transfer equilibria by high pressure mass spectrometers at lower temperatures were often hindered by the formation of protonated dimers. Since the stabilities of these protonated dimers are mostly due to the formation of strong hydrogen bonds within the protonated clusters (e.g. $H^+(H_2O)_2$), it may be expected that for proton transfer reactions involving compounds whose protonated dimers do not allow the formation of strong hydrogen bond, the equilibrium measurements may be carried out with high pressure mass spectrometers even at lower temperatures ($\sim300°K$) without the interference from the formation of the protonated dimers. The present study of the temperature dependence of equilibrium constants involving benzene and halobenzenes is a prime example (table 3.53). Two other classes of compounds which may be studied over a large temperature range are the sulfides and phosphines. Due to the low electronegativities of the sulfur and phosphorous atoms, the partial positive charge on the hydrogens of the protonated sulfides R_2SH^+ and protonated phosphines R_3PH^+ is expected to be much smaller than that on the hydrogen of the protonated oxygen - or nitrogen-containing compounds involved in the present study. For example, Meot-Ner and Field (173) have calculated the

partial positive charge on the hydrogens of H_3O^+, NH_4^+, H_3S^+ and PH_4^+ to be 0.25, 0.18, 0.004 and 0.0, respectively. As a result, only relatively weak hydrogen bonding would be operative in the $(R_2S)_2H^+$ and $(R_3P)_2H^+$ clusters, and the tendency to form such dimers would not be high even at lower temperatures. The determination of equilibrium constants over a temperature range 600–300°K for the reactions 9.4 and 9.5 should enable a

$$(R_2S)H^+ + R_2'S = R_2S + (R_2'S)H^+$$

$$R,R': \text{H or alkyl} \quad (9.4)$$

$$(R_3P)H^+ + R_3'P = R_3P + (R_3'P)H^+$$
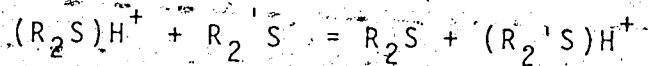
$$R,R': \text{H or alkyl} \quad (9.5)$$

direct comparison of the experimental ΔS^0 with the calculated $\Delta S^0_{intermolecular}$ since $\Delta S^0_{rot.s.} = 0$ for both reactions 9.4 and 9.5.

If the $\Delta S^0_{intermolecular}$ does prove to be a valid entropy correction for proton transfer reactions, it would be useful in improving the quality of the proton affinity values and the ΔH^0_f values of the protonated ions. Unfortunately, at the time of writing, the error limit associated with these absolute values from the external standard PA(isobutene) is relatively large (~3 kcal/mole) compared with the magnitudes of the corrections. Nevertheless, the internal accuracy and precision of the relative

proton affinity scale do depend on the good entropy corrections in all equilibrium measurements. It is hoped that the availability of better experimental ΔS^o values would lead to better theoretical considerations on the ΔS^o for proton transfer equilibria.

The present gas-phase basicity ladder (table 3.1) could be further extended to include compounds with basicities lower than that of water ($PA(H_2O) = 171.7$ kcal/mole from table 3.57). The relative proton affinities of simple molecules such as H_2, O_2, N_2, rare gases, CH_4 and C_2H_6 have been determined by Bohme and co-workers using the flowing afterglow technique (33,40). With the external standard $PA(H_2) = 101$ kcal/mole which is based on a theoretical calculation of the total energy of H_3^+ by Duben and Lowe (174), $PA(CH_4) = 128.2$ kcal/mole and $PA(C_2H_6) = 140.4$ kcal/mole were reported (40). Three groups of compounds which have proton affinities between those of C_2H_6 and H_2O are the hydrogen halides, the alkyl halides and the paraffins. The proton affinities of alkanes higher than ethane have not been determined by proton transfer because the protonated ions are unstable and decompose to alkyl ions and H_2 or alkanes. No equilibrium measurements have been made for the determinations of proton affinities of hydrogen halides and alkyl halides, but estimated proton affinity values based on the "occurrence-nonoccurrence" technique or

the appearance potential method can be found in the tabu-
lations by Beauchamp (175,176). It would be useful to
determine the relative proton affinities of hydrogen hal-
ides and alkyl halides by equilibrium measurements so as to
connect the gas-phase basicity gap between C_2H_6 and H_2O.
The results from such studies would also enable the
determination of more accurate ΔH_f^o values for the cor-
responding protonated ions. This is important in the
investigations of gas-phase ion chemistry of alkyl halides.

R E F E R E N C E S

1. J. P. Briggs, R. Yamdagni and P. Kebarle, J. Am. Chem. Soc., 94, 5128 (1972).

2. R. Yamdagni and P. Kebarle, J. Am. Chem. Soc., 95, 3504 (1973).

3. R. Yamdagni and P. Kebarle, J. Am. Chem. Soc., 98, 1320 (1976).

4. J. J. Thompson, Phil. Mag., 24, 209 (1912).

5. A. J. Dempster, Phil. Mag., 31, 438 (1916).

6. T. P. Hogness and E. G. Lunn, Phys. Rev., 26, 44 (1925).

7. H. D. Symth, Phys. Rev., 25, 452 (1925).

8. D. P. Stevenson and D. O. Schissler, J. Chem. Phys., 23, 1353 (1955).

9. D. P. Stevenson and D. O. Schissler, J. Chem. Phys., 29, 282 (1958).

10. V. L. Tal'rose and A. K. Lyubimova, Doklady Akad. Navk. SSSR, 86, 909 (1952), per Chem. Abstracts, 47, 2590 (1953).

11. F. H. Field, J. L. Franklin and F. W. Lampe, J. Am. Chem. Soc., 78, 5697 (1956).

12. F. H. Field, J. L. Franklin and F. W. Lampe, J. Am. Chem. Soc., 79, 6132 (1957).

13. G. Gioumousis and D. P. Stevenson, J. Chem. Phys., 29, 294 (1958).

14. V. L. Tal'rose and E. L. Frankevich, Russian J. Phys. Chem., 34, 1275 (1960).

15. V. L. Tal'rose, Pure Appl. Chem., $\underline{5}$, 454 (1962).

16. K. R. Ryan and J. H. Futrell, J. Chem. Phys., $\underline{42}$, 824 (1965).

17. K. R. Ryan and J. H. Futrell, J. Chem. Phys., $\underline{43}$, 3009 (1965).

18. T. W. Shannon, F. Meyer and A. G. Harrison, Can. J. Chem., $\underline{43}$, 159 (1965).

19. F. H. Field, J. Am. Chem. Soc., $\underline{83}$, 1523 (1961).

20. F. H. Field, J. L. Franklin and M. S. B. Munson, J. Am. Chem. Soc., $\underline{85}$, 3575 (1963).

21. F. H. Field and M. S. B. Munson, J. Am. Chem. Soc., $\underline{87}$, 3289 (1965).

22. H. E. Horning, M. G. Horning, D. I. Carroll, I. Dzidic and R. N. Stillwell, Anal. Chem., $\underline{45}$, 936 (1973).

23. F. H. Field and M. S. B. Munson, J. Am. Chem. Soc., $\underline{87}$, 3294 (1965).

24. F. H. Field, Accounts. Chem. Res., $\underline{1}$, 42 (1968).

25. F. H. Field in "Ion-Molecule Reactions," J. L. Franklin, Ed., Plenum Press, New York (1972).

26. B. Munson in "Interactions Between Ions and Molecules," P. Ausloos, Ed., Plenum Press, New York (1975).

27. J. J. Solomon and F. H. Field, J. Am. Chem. Soc., $\underline{97}$, 2625 (1975).

28. R. T. McIver, Rev. Sci. Inst., $\underline{41}$, 555 (1970).

29. B. D. Baldeschwieler, Science, $\underline{159}$, 263 (1968).

30. R. W. Taft in "Proton-Transfer Reactions," E. F. Caldin and V. Gold, Eds., Chapman and Hall, London (1963).

31. J. Wolf, R. H. Staley, I. Koppel, M. Taagepera, R. T. McIver, Jr., J. L. Beauchamp and R. W. Taft, J. Am. Chem. Soc., 99, 5417 (1977).

32. E. E. Ferguson, F. C. Fehsenfeld and A. L. Schmeltekopf, Advan. Atomic and Mol. Phys., 5, 1 (1969).

33. D. K. Bohme in "Interactions Between Ions and Molecules," P. Ausloos, Ed., Plenum Press, New York (1975).

34. N. Davidson, "Statistical Mechanics", McGraw-Hill, New York (1962), p.125.

35. M. S.B. Munson, J. Am. Chem. Soc., 87, 2332 (1965).

36. M. T. Bowers, D. H. Aue, H. M. Webb and R. T. McIver, Jr., J. Am. Chem. Soc., 93, 4314 (1971).

37. P. F. Fennelly, R. S. Hemsworth, H. I. Schiff and D. K. Bohme, J. Chem. Phys., 59, 6405 (1973).

38. D. K. Bohme, R.S. Hemsworth, H. W. Randle and H. I. Schiff, J. Chem. Phys., 58, 3504 (1973).

39. R. S. Hemsworth, H. W. Randle, D. K. Bohme, H. I. Schiff, D. B. Dunkin and F. C. Fehsenfeld, J. Chem. Phys., 59, 61 (1973).

40. J. D. Payzant, H. I. Schiff and D. K. Bohme, J. Chem. Phys., 63, 149 (1975).

41. P. Kebarle, Ann. Rev. Phys. Chem., 28, 445 (1977).

42. A. Good, A. Durden and P. Kebarle, J. Chem. Phys., 52, 222 (1969).

43. R.F. Porter in "Interactions Between Ions and Molecules," P. Ausloos, Ed., Plenum Press, New York (1975).

44. A. J. Cunningham, J. D. Payzant and P. Kebarle, J. Am. Chem. Soc., 94, 7627 (1972).

45. P. Kebarle, S. K. Searles, A. Zolla, J. Scarborough and M. Arshadi, J. Am. Chem. Soc., 89, 6393 (1967).

46. J. D. Payzant, A. J. Cunningham and P. Kebarle, Can. J. Chem., 51, 3242 (1973).

47. E. P. Grimsrud and P. Kebarle, J. Am. Chem. Soc., 95, 7939 (1973).

48. K. Hiraoka, E. P. Grimsrud and P. Kebarle, J. Am. Chem. Soc., 96, 3359 (1974).

49. M. S.B. Munson and J. L. Franklin, J. Phys. Chem., 68, 3191 (1964).

50. A. G. Harrison, A. Irko and D. VanRaalte, Can. J. Chem., 44, 1625 (1966).

51. K. M. A. Refaey and W.A. Chupka, J. Chem. Phys., 48, 5205 (1968).

52. M. A. Haney and J. L. Franklin, J. Chem. Phys., 48, 4093 (1968).

53. M. A. Haney and J. L. Franklin, J. Chem. Phys., 50, 2028 (1969).

54. D. A. Durden, Ph.D. Thesis, University of Alberta (1969).

55. S. Dushman, "Scientific Foundations of Vacuum Technique", John Wiley and Sons, Inc., New York (1958).

56. P. Kebarle in "Interactions Between Ions and Molecules," P. Ausloos, Ed., Plenum Press, New York (1975).

57. "Handbook of Chemistry and Physics, 52nd Edition", Chemical Rubber Company Press, Cleveland (1971) p. F-45.

58. W. Paul and H. Steinwedd, Z. Naturforsch, 8A, 448 (1953)

59. W. Paul and M. Raether, Z. Physik, 140, 262 (1955).

60. W. Paul and H. P. Reinhard and U. von Zahn, Z. Physik, 152, 143 (1958).

61. W. E. Austin, A. E. Holme and J. H. Leck in "Quadrupole Mass Spectrometry and Its Application," P. H. Dawson, Ed., Elsevier Scientific Publishing Company, Amsterdam (1976), p.123.

62. U. von Zahn, Thesis, University of Bonn (1956).

63. "Instruction Manual for Quadrupole Power Supply Model 011-1", Extranuclear Laboratories Inc., Pittsburgh, Pennsylvania (1969), p. II-2.

64. P. H. Dawson, J. Vac. Sci. Technol., 9, 487 (1972).

65. W. M. Brubaker, Advan. Mass Spectrom., 4, 293 (1968).

66. W. M. Brubaker, J. Vac. Sci. Technol., 10, 291 (1973).

67. W. E. Potter and K. Mauersberger, Rev. Sci. Instrum., 43, 1327 (1972).

68. E. W. McDaniel, "Collisional Phenomena in Ionized Gases", John Wiley and Sons, New York, (1964), pp. 512-513.

69. G. M. Barrow, "Physical Chemistry", McGraw-Hill, New York, (1961), p.44.

70. S. G. Lias and P. Ausloos, "Ion-Molecule Reactions", American Chemical Society, Washington, D. C. (1975), p. 442.

71. L. J. Kieffer, Atomic Data, Vol. 1, Part I, 58 (1969).

72. S. C. Lind, "Radiation Chemistry", Reinhold, New York (1961), p.25.

73. R. W. Taft, private communication.

74. B. S. Freiser and J. L. Beauchamp, J. Am. Chem. Soc., 98, 265 (1976).

75. W. J. Hehre, R. T. McIver, Jr., J. A. Pople and P.v. R. Schleyer, J. Am. Chem. Soc., 96, 7162 (1974).

76. J. L. Franklin, G. J. Dillard, H. M. Rosenstock, J. T. Herron, K. Draxl and F. H. Field, "Ionization Potentials, Appearance Potentials and Heats of Formation of Gaseous Positive Ions", Nat. Stand. Ref. Data Series, Nat. Bur. Stand. (U.S.) 26, (1969).

77. D. D. Wagman, W. H. Evans, V. B. Parker, I. Halow, S. M. Bailey and R. H. Schumm, "Selected Values of Chemical Thermodynamic Properties", NBS Technical Note 270-3 (1968).

78. W. Tsang, J. Phys. Chem., 76, 143 (1972).

79. W. Tsang, Int. J. Chem. Kinet., 10, 821 (1978).

80. D. Parkes and C. P. Quinn, J.C.S. Faraday I, 72, 1935 (1976).

81. F. P. Lossing and G. P. Semeluk, Can. J. Chem., 48, 955 (1970).

82. F. A. Houle and J. L. Beauchamp, "Photoelectron Spectroscopy of Methyl, Ethyl, Isopropyl and te- Butyl Radicals. Implementations for the Thermo-Chemistry and Structures of the Radicals and their Corresponding Carbonium Ions," to be

published in J. Am. Chem. Soc.(1979)

83. Y. K. Lau and P. Kebarle, J. Am. Chem. Soc., $\underline{98}$, 7452 (1976).

84. F. T. Wall, "Chemical Thermodynamics", W. H. Freeman and Company, San Francisco (1965), chapter 13.

85. S. W. Benson, "Thermochemical Kinetics", Wiley, New York, (1968), p.35.

86. K. S. Pitzer, "Quantum Chemistry", Prentice-Hall, New York (1954), p.498.

87. K. S. Pitzer, J. Chem. Phys., $\underline{14}$, 329 (1946).

88. R. T. Morrison and R. N. Boyd, "Organic Chemistry", Allen and Bacon, Inc., Boston (1969), p.94.

89. G. Herzberg, "Infrared and Raman Spectra", Van Nostrand New York (1945), p.195.

90. M. A. Haney and J. L. Franklin, J. Phys. Chem., $\underline{73}$, 4328 (1969).

91. G. H. F. Diercksen, W. P. Kraemer and B. O. Ross, Theoret. Chim. Acta., $\underline{36}$, 249 (1975).

92. G. A. Olah and A. M. White, J. Am. Chem. Soc., $\underline{89}$, 3591 (1967).

93. G. A. Olah and A. M. White, J. Am. Chem. Soc., $\underline{89}$, 7072 (1967).

94. W. R. Davidson, Y. K. Lau and P. Kebarle, Can. J. Chem., $\underline{56}$, 1016 (1978).

95. K. Tanaka, G. I. Mackay and D. K. Bohme, Can. J. Chem., $\underline{56}$, 193 (1978).

96. J. March, "Advanced Organic Chemistry : Reactions, Mechanisms and Structure", McGraw-Hill, New York (1968), p.753.

97. K. Hiraoka and P. Kebarle, J. Am. Chem. Soc., 99, 360 (1977).

98. J. H. S. Green, Q. Rev., Chem. Soc., 15, 125 (1961).

99. R. W. Taft, M. Taagepera, J. L. M. Abboud, J. F. Wolf, D. J. DeFrees, W. J. Hehre, J. E. Bartmess and R. T. McIver, Jr., J. Am. Chem. Soc., 100, 7765 (1978).

100. D. P. Beggs and F. H. Field, J. Am. Chem. Soc., 93, 1576 (1976).

101. C. R. Noller, "Chemistry of Organic Compounds", 3rd Ed.; W. B. Saunders, Philadelphia and London (1966), p.990.

102. E. M. Arnett and G. Scorrano, Advan. Phys. Org. Chem., 13, 83 (1976), tables 10, 17 and 18.

103. R. W. Taft, J. F. Wolf, J. L. Beauchamp, G. Scorrano and E. M. Arnett, J. Am. Chem. Soc., 100, 1240 (1978).

104. "Selected Values of Physical and Thermodynamic Properties," Nat. Bur. Stand., Cir. No. 500, U. S. Govt. Printing Office, Washington, D.C. (1952); $\Delta H_h^o(H_2O) = -\Delta H_v^o(H_2O)$.

105. J. M. Corkill, J. F. Goodman and J. R. Tate. ns. Faraday Soc., 65, 1742 (1969); and W. S. Mac. gor, Ann. N.Y. Acad. Sci., 141, 3 (1967). The former

gives $\Delta H_V^O(DMSO) = 12.6$ kcal/mole and the latter $\Delta H_S^O(aq)(DMSO) = -4.5$ kcal/mole. $\Delta H_h^O(DMSO) = -\Delta H_V^O(DMSO) + \Delta H_S^O(aq)(DMSO)$.

106. J. Long and B. Munson, J. Am. Chem. Soc., <u>95</u>, 2427 (1973).

107. D. Murad and M. Inghram, J. Chem. Phys., <u>40</u>, 3263 (1964).

108. E. Murad and M. Inghram, J. Chem. Phys., <u>41</u>, 404 (1964).

109. R. H. Staley, R. D. Wieting and J. L. Beauchamp, J. Am. Chem. Soc., <u>99</u>, 5964 (1977).

110. J. D. Cox and G. Pitcher, "Thermochemistry of Organic and Organometallic Compounds", Academic Press, New York (1970).

111. R. L. Nuttall, A. H. Laufer and M. V. Kilday, J. Chem. Thermodynamics, <u>3</u>, 167 (1971).

112. P. Ausloos and S. G. Lias, Chem. Phys. Letters, <u>51</u>, 53 (1977).

113. J. Vogt, A. D. Williamson and J. L. Beauchamp, J. Am. Chem. Soc., <u>100</u>, 3478 (1978).

114. J. W. Williams and C. D. Hurd, J. Org. Chem., <u>5</u>, 122 (1940).

115. PA(acetic acid) is derived from a combination of the present results and the results reported in reference 3.

116. A. C. Hopkinson, J. Chem. Soc., Perkin Trans. II, 795 (1975).

117.   D. Y. Yarkony and H. F. Schaefer III, J. Chem. Phys., 63, 4317 (1975).

118.   G. A. Olah, K. Dunne, Y. K. Mo and P. Szilaggyi, J. Am. Chem. Soc., 94, 4200 (1974).

119.   J. Hine, "Structural Effects on Equilibria in Organic Chemistry", Wiley, New York (1975).

120.   L. P. Hammett, "Physical Organic Chemistry", McGraw-Hill, New York (1940), p. 185.

121.   B. S. Freiser, R. L. Woodin and J. L. Beauchamp, J. Am. Chem. Soc., 97, 6893 (1975).

122.   D. P. Martin and S. E. Buttrill, Jr., Org. Mass Spectrom., 11, 762 (1976).

123.   R. G. Cavell and D. A. Allison, J. Am. Chem. Soc., 99, 4203 (1977).

124.   D. M. Brouwer, E. L. Mackor and C. MacLean in "Carbonium Ions, Volume 2," G. A. Olah and P. v. R. Schleyer, Eds., Wiley-Interscience, New York (1970), Chapter 20.

125.   T. Birchall and R. J. Gillespie, Can. J. Chem., 42, 502 (1964).

126.   H. Köhler and G. Scheibe, Z. Anorg. Allgem. Chem., 285, 221 (1956).

127.   L. P. Hammett, Chem. Rev., 17, 125 (1935).

128.   G. A. Olah, R. H. Schlosberg, R. D. Porter, Y. K. Mo, D. P. Kelly and G. D. Mateescu, J. Am. Chem. Soc., 94, 2034 (1972).

129. J. M. McKelvey, S. Alexandratos, A. Streitwieser, Jr., J.-L. M. Abboud and W. J. Hehre, J. Am. Chem. Soc., 98, 244 (1976).

130. W. J. Hehre, R. Ditchfield, L. Random and J. A. Pople, J. Am. Chem. Soc., 92, 4796 (1970).

131. H. C. Brown and Y. Okamoto, J. Am. Chem. Soc., 79, 1913 (1957).

132. A. G. Harrison, P. Kebarle and F. P. Lossing, J. Am. Chem. Soc., 83, 777 (1961).

133. H. C. Brown and Y. Okamoto, J. Am. Chem. Soc., 80, 4979 (1958).

134. E. M. Arnett and J. W. Larsen, J. Am. Chem. Soc., 91, 1438 (1969).

135. W. M. Schubert and W. A. Sweeney, J. Org. Chem., 21, 119 (1956).

136. D. H. Aue, H. M. Webb and M. T. Bowers, J. Am. Chem. Soc., 98, 311 (1976).

137. (a) J. I. Braumen and L. K. Blair, J. Am. Chem. Soc., 90, 6561 (1968); (b) J. I. Braumen and L. K. Blair, ibid., 92, 5987 (1970).

138. H. H. Jaffe, Chem. Rev., 53, 191 (1953).

139. M. Liler in "Advances in Physical Organic Chemistry, Volume 11," V. Gold and D. Bethell, Eds., Academic Press, New York (1975), p.267.

140. S. K. Pollack, J. L. Devlin III, K. D. Summerhays, R. W. Taft and W. T. Hehre, J. Am. Chem. Soc., 99, 4583 (1977).

141. R. L. Martin and D. A. Shirley, J. Am. Chem. Soc., 96, 5299 (1973).

142. E. M. Benoit and A. G. Harrison, J. Am. Chem. Soc., 99, 3980 (1977).

143. D. F. Hunt, C. N. McEwen and R. A. Upham, Anal. Chem., 44, 1292 (1972).

144. R. W. Alder, P. S. Bowaman, W. R. S. Steele and D. R. Winterman, Chem. Commun., 723 (1978).

145. F. I. Vilesov and A. N. Terenin, Dokl. Akad. Nauk. SSSR, 115, 744 (1957).

146. F. H. Field, J. Am. Chem. Soc., 91, 2827 (1969).

147. M. S. B. Munson, J. L. Franklin and F. H. Field, J. Phys. Chem., 68, 3098 (1964).

148. Y. K. Lau, P. P. S. Saluja, P. Kebarle and R. W. Alder, J. Am. Chem. Soc., 100, 7328 (1978).

149. A. Streitwieser, Jr. and C. H. Heathcock, "Introduction to Organic Chemistry", Mcmillan Publishing Co. Inc., New York, (1976).

150. M. J. S. Dewar and P. J. Grisdale, J. Am. Chem. Soc., 84, 3546 (1962).

151. K. D. Summerhays, S. K. Pollack, R.W. Taft and N. J. Hehre, J. Am. Chem. Soc., 99, 4585 (1977).

152. H. Einspahr, J. B. Robert, R. E. Marsh and J. D. Roberts, Acta Crystalogr., Sect. B, 29, 1611 (1973).

153. P. Merlet, S. D. Peyerimhoff and R. J. Buenker, J. Am. Chem. Soc., 94, 8301 (1972).

154. D. D. Perkin, "Dissociation Constants of Organic

Bases in Aqueous Solution", Butterworths, London (1965), p.58 and p. 61.

155. E. M. Arnett in "Proton Transfer Reactions," E. F. Caldin and V. Gold, Eds., Chapman and Hall, London (1975).

156. M. R. Truter and B. L. Vickery, J. Chem. Soc. Dalton, 395 (1972).

157. J. F. Wolf, P. G. Harch and R. W. Taft, J. Am. Chem. Soc., 97, 2904 (1975).

158. E. M. Arnett, Accounts Chem. Res., 6, 404 (1973).

159. M. Meot-Ner, J. Am. Chem. Soc., 100, 4694 (1978).

160. R. D. Nelson, Jr., D. R. Lide, Jr., and A. A. Maryott, "Selected Values of Electric Dipole Moments for Molecules in the Gas Phase", Nat. Stand. Ref. Data Series, Nat. Bur. Stand. (U.S.) 10, (1967).

161. H. H. Szmant in "Dimethyl Sulfoxide, Volume 1," S. W. Jacob, E. E. Rosenbaum and D. C. Wood, Eds., Marcel Dekker, Inc., New York (1971).

162. S. Glasstone, "Textbook of Physical Chemistry", D. Van Norstrand Co. Inc., New York (1964), Chapter 11.

163. S. Ahrland in "The Chemistry of Nonaqueous Solvents, Volume VA," J. J. Lagowski, Ed., Academic Press, New York (1978), p.10.

164. I. Dzidic and P. Kebarle, J. Phys. Chem., 74, 1466 (1970).

165. R. Domain, M. Rinfret and R. L. Benoit, Can. J.

Chem., 54, 2101 (1976).

166. K. A. G. MacNeil and J. H. Futrell, J. Phys. Chem., 76, 409 (1972).

167. S. G. Lias and P. Ausloos, J. Am. Chem. Soc., 99, 4831 (1977).

168. P. Ausloos and S. G. Lias, J. Am. Chem. Soc., 100, 1953 (1978).

169. K. G. Hartman and S. G. Lias, Int. J. Mass Spectrom. Ion Phys., 28, 213 (1978).

170. S. G. Lias in "Lecture Notes in Chemistry; Ion Cyclotron Resonance Spectrometry," H. Hartmann and K.-P. Wanczek, Eds., Springer-Verlag, Berlin, Heidelberg, New York (1978).

171. S. G. Lias in "Kinetics of Ion-Molecule Reactions," P. Ausloos, Ed., Plenum Publishing Corp., New York (1979).

172. T. Su and M. T. Bowers, J. Am. Chem. Soc., 95, 1370 (1973).

173. M. Meot and F. H. Field, J. Am. Chem. Soc., 99, 998 (1977).

174. A. J. Duben and J. P. Lowe, J. Chem. Phys., 55, 4270 (1971).

175. J. L. Beauchamp in "Interactions Between Ions and Molecules," P. Ausloos, Ed., Plenum Press, New York (1975), p.415.

176 B. J. Blint, T. B. McMahon and J. L. Beauchamp, J. Am. Chem. Soc., 96, 1269 (1974).